A Multi-Analytical Investigation of the Hydrogel Phase

SEHAM JUMAH FAYADH ALANAZI

Submitted in accordance with the requirements for the degree of
Doctor of Philosophy

The University of Leeds
School of Chemistry

June 2022

The candidate confirms that the work submitted is her own and that appropriate credit has been given where reference has been made to the work of others, except where work which has formed part of jointly-authored publications has been included. The contribution of the candidate and the other authors to this work has been explicitly indicated below. The candidate confirms that appropriate credit has been given within the thesis where reference has been made to the work of others. *Further details of the jointly-authored publications and the contributions of the candidate and the other authors to the work are included below this statement.*

Reference for Jointly Authored Publication

Seham Alanazi, Hind Aluqmani, Kamal Albdeery and Terence P. Kee, Self-Assembly of Amphiphiles in Mineral Hydrogel Media. Implications for Abiogenesis, *Life*, to be submitted for publication, September 2022.

- This paper contains material from Chapters 2 and 3 of this thesis. Particularly, it consists of some results obtained for SHG by cryo-scanning electron microscopy, EDX analysis, BET measurements, and critical micelle concentration of SDS presence of salts in aqueous an SHG phase.

Seham Alanazi and Terence P. Kee, Effects of Inorganic Salts and Organic Alcohols on Molecular Self-Assembly in the Silica Hydrogel Phase, *Life*, manuscript in preparation.

Seham Alanazi, Hind Aluqmani, Samantha Price, Majed Alsaiaari and Terence P. Kee, Light Scattering as a tool to Probe Hydrogel Behavior, *Life*, manuscript in preparation

Acknowledgemets

In the name of Allah, the Most Gracious, the Most Merciful praises and thanks are for Allah, Lord of the world, and prayers and peace be upon the most honorable of the prophets and messengers.

First and foremost, I would like to praise and thank God, the Almighty, who has granted countless blessings, knowledge, and opportunity to the writer so that I have been finally able to accomplish the thesis.

I would like to take this opportunity to express my heartfelt gratitude to everyone who has supported and assisted me during this journey:

I would want to express my heartfelt thanks to my supervisor, Dr. Terence Kee, for providing me with the chance to work with him, as well as for his support, inspiration, and encouragement at every step of the way toward completing my work.

I would like to thank my parents for their love, prayers, and support. Without them, this day would not have been possible. I would also like to thank my entire siblings, especially Mohammad, Abdul Aziz, and Ahlam, for their assistance and advice.

My heartfelt gratitude goes to my family, especially my husband, Mohammed. Since the beginning, he has been with me on this journey, supporting, advising, inspiring, and helping me in everything; without him, achievement would not have been possible. My beloved children, Deema, Danah, Abdullah, Lana, and Abdul Aziz, you have made me stronger, better, and more fulfilled than I could have ever imagined. I love you to the moon and back.

I would like to express my thanks and appreciation to my co-supervisor Dr Paul Thornton. Many thanks to my colleague Kamal Albdeery for his valuable time monitoring and guiding me throughout this period of time. I would like to thank Natalia Sergeeva, my assessor for her valuable feedback and corrections on my transfer, second and third reports.

I would like to thank my group researchers Dr. Ian Gorrell, Majed Alsaiaari for their useful comments and advice. Special thanks to Hind Alharbi for her helping, supporting, advising, and motivating. Also, I want to thank Mansour Alsarrani who has helped me with the software program.

Many thanks to Martin Fuller (critical point drying), Dave Fogarty (UV/vis), Dr Alexander Kulak (SEM/ EDX, and BET measurements), Stuart Micklethwaite (cryo-SEM) for their technical work, Dr. Andrew Booth (training of epifluorescence microscopy), Dr Ruth Hughes (Imaging of Confocal fluorescence microscopy) visualising and analysing images.

I would like to thank Mrs A. Luty and all staff members at the University of Leeds.

Thanks to the Ministry of Higher Education in Saudi Arabia and King Saud University for their financial support, and The Saudi Cultural Bureau in London for their support during my research time.

Abstract

In this thesis are discussed aspects in which certain chemical and physical behaviour of relevance to abiogenesis, the origins of life, changes when compared between the aqueous phase and a mineral hydrogel phase. The significance of this work is based on observations that the cytosolic medium within all biological cells is better thought of as a hydrogel rather than aqueous.

Chapter 1 provides an introduction to the fundamental principles of interest to this work, discusses hydrogels, their synthesis, properties and especially their potential role in abiogenesis. Also discussed are the concepts of amphiphilic self-assembly which is an important process examined in this thesis, and then concludes with some discussion of the analytical techniques used within the project.

Chapter 2 describes the surface analysis of two different concentrations of silica hydrogels along with methods for isolating the silica matrix and surface analyses using electron microscopy (SEM) and associated techniques (BET, EDX).

Chapter 3 outlines critical micelle concentration (CMC) measurements of the model amphiphile, sodium dodecyl sulfate (SDS) in both the aqueous and silica hydrogel phases in the presence of various salts. Included in this salt list are simulated seawater, NaCl, Na_2CO_3, Na_2HPO_4, Na_2SiO_3, Na_2SO_4 and $MgCl_2$. Colorimetric methods were used employing a colorimetric reporter dye (pinacyanol chloride) by UV-Vis spectrophotometry.

Chapter 4 outlines related CMC measurements of SDS-alcohol mixtures (C_2-OH, C_6-OH, C_8-OH, C_{10}-OH, C_{12}-OH) again in both the aqueous and silica hydrogel phase using the same method.

Chapter 5 Outlines the possibility of vesicle formation of SDS-Alcoholic composites in Silica Hydrogels.

Chapter 6 examines the use of two different methods to explore the gelation process within silica hydrogels and any influence of inorganic and organic additives by UV-Vis light scattering, and turbidity meter measurements.

Chapter 7 contains experimental details and sample preparation from Chapters 2 to Chapter 6.

Chapter 8 offers a summary, conclusion, and future work perspective on the studies reported in this thesis.

Table of Contents

List of Figures

List of Tables

Abbreviations

°C	Degrees Celsius
ϵ	The molar absorptivity coefficient
λ_{max}	Wavelength of Maximum Absorbance
µL	Microliter
µm	Micrometer
nm	Nanometer
3D	Three dimensions
Abs	Absorbance
BET	Brunauer-Emmett-Teller (surface area analysis)
CMC	Critical Micelle Concentration
CPD	Critical Point Drying
Cryo-SEM	Cryo-Scanning Electron Microscopy
DLVO	Derjaguin, Landau, Vervey, and Overbeek
DTAB	Dodecyltrimethylammonium bromide

eV	Electron volts
EDL	Electrical Double Layer
EDX	Energy Dispersive X-ray
FTIR	Fourier Transform Infrared Spectroscopy
GAA	Glacial Acetic Acid
GUV	Giant unilamellar vesicle
Hrs	Hours
Hz	Hertz
I	Intensity
I.S.	Ionic strength
K	Kelvin
LUV	Large unilamellar vesicles
LEMAS	Leeds Electron Microscopy and Spectroscopy Centre
M	Moles per litre
Min	Minute
Mm	Millimoles per litre
mS	Milli Siemens
MLV	Multilamellar vesicle
MVV	Multi-vesicular vesicle
NIR	Near-Infrared
NR	Nile Red
NTU	Nephelometric Turbidity Unit
P	phosphorus
PIC	Pinacyanol Chloride
PGS	Glyceryl Silicate
Ppm	Part per million
SAXS	Small Angle X-ray Scattering

SCA	Single Chain Amphiphile
LPD	Liquid Phase Deposition
SDS	Sodium Dodecyl Sulfate
SEM	Scanning Electron Microscopy
SHGs	Silica Hydrogels
ST.Dev	Standard Deviation
SUV	Small unilamellar vesicles
TEM	Transmission Electron Microscopy
UV-Vis	Ultra Violet-Visible
WAXS	Wide Angle X-ray Scattering
Yrs	years

Chapter 1 Introduction and Background

The purpose of this chapter is to discuss the structural concept of silica hydrogels as well as their significance in abiogenesis research as a reaction environment that was most likely present during the Hadean period. The later section of this chapter subsequently focuses on the procedures and instruments used during the studies reported in this thesis, along with the appropriate theory that underpins them.

1.1 Hydrogels

A hydrogel is a polymer with a three-dimension network, that can swell to a very large degree in water due to cross-linking of the individual polymer molecules (Fig. 1-1.a, b), thus trapping a significant body of water within the polymer matrix [1, 2].

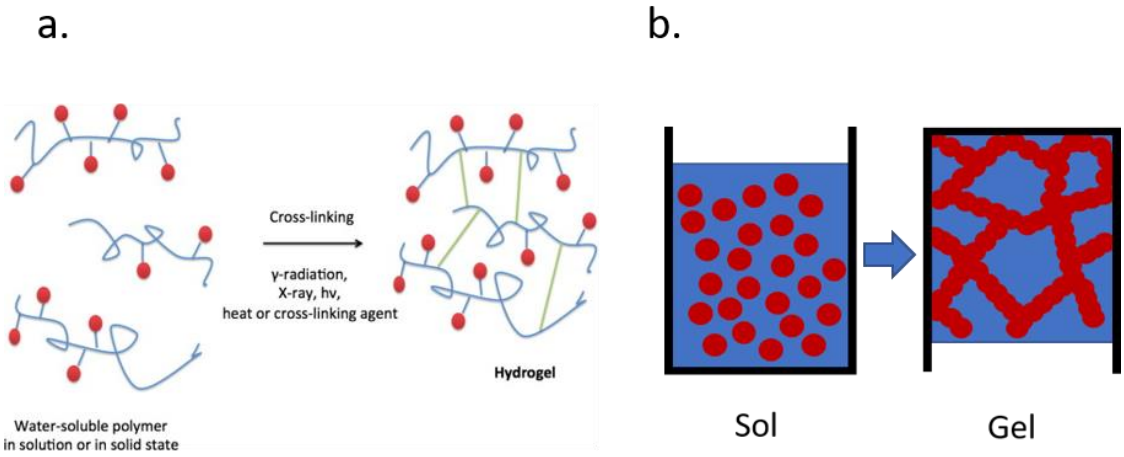

Figure 1-1: Network in the hydrogel: a) the formation of hydrogel by cross linking [3], b) The transition of sol to gel phase [4].

Hydrogels have become very popular materials because of the significance of their properties such as biocompatibility, high content of water, reversibility, and physical flexibility [3, 5]. Natural and synthetic hydrophilic polymers can be cross-linked by physical or chemical agents to produce hydrogels. Recently, synthetic hydrogels can be accurately used for many applications. Their resemblance to living tissue opens up many opportunities for applications in biomedical areas [3],

such as drug delivery [6, 7], contact lenses [8, 9], sealing [10], bio-medical applications [11], tissue engineering [12, 13], food additives [14], pharmaceuticals [15], regenerative medicines [16], wound dressing [17, 18], separation of biomolecules or cells [19], agriculture [20], barrier materials to regulate biological adhesions [21], and biosensors [22]. Also, sol-gel hybrid coatings are used in automotive topcoat applications because they can produce hyper-branched polymers used widely as protective layers due to their features such as lower viscosity in solution, high solubility, and molten state [23].

1.2 Hydrogels and Abiogenesis

Striving to understand how life began on earth remains a considerable challenge to scientists and philosophers and has long been a topic of interest to the general public alike. From the scientific perspective, scientists are trying to understand how the first primitive cellular life forms could have emerged on the early Hadean earth (ca 4.5-4.0 billion yrs ago). This includes many factors such as the requirements of physical and chemical conditions, suitable environments for the growth and division of the first such cellular organisms, and the implication of mineral surfaces or deep oceanic vents [24-30]. An implicit assumption has developed that a biological cell, is fundamentally an aqueous suspension of solutes. Hence, it is typically considered that pre-cellular environments would also correspond to an aqueous suspension either by itself or in close proximity to a mineral surface with the potential to behave as a catalyst/partitioning material [31]. Therefore, the aqueous environments such as (i) freshwater, (ii) saltwater, (iii) wetting-drying cycles, and (iv) the aqueous-mineral interface have been the focus of all prebiotic chemical research.

However, when we recognise that the aqueous-based environment (the cytoplasm) of a biological cell is better described as a hydrogel, we then realise that it appears logical that the results obtained through prebiotic experiments in gel-phase media might differ from those conducted in purely aqueous media [31]. Moreover, prebiotic experiments in gel-phase media are still very few in number and nature [32].

The benefits of hydrogels can easily be seen when compared with aqueous media. As an example, diffusion is responsible for the mechanism of ion transport [33]. Furthermore, a hydrogel medium has the ability to change convection heat

flow as molecules have different diffusional behaviour within the gel phase [34]. As an example, gels maintain their integrity due to variances in natural density or viscosity. Hence, even though they do not have any membranes, they are able to maintain a separation from their immediate aqueous environment. Due to the presence of a cross-linked molecular structure, hydrogel media are able to hold a significant amount of water, gas bubbles, and oily hydrocarbons [35] as well as protect nucleic acid molecules [36]. Synthesised hydrogels, for delivery drug, are able to respond to various physiological stimuli such as temperature, pH, and ionic strength, all of which are present in the body [37]. They are also capable of providing stable environments for various activities such as the accretion of polymeric mass and the division and evolution of the subsequent cell [24]. An oily water mixture may have constituted the most primitive and original geological gel environment [24] reached through the capturing of essential nutrients from the surrounding environment, such prebiotic gels may have transitioned into something resembling a biofilm. This would have facilitated the first incorporated chemical machines from which life emerged [35]. This is further justified when considering that the cells of contemporary biology are themselves made from molecularly crowded gel environments consisting of large macromolecules and internal compartments. Trevors et al. also stated that since hydrogels provide a phase boundary to the external aqueous environment and are able to implement many tasks, there is no need for a formal membrane [24]. Large quantities of water or biological fluids, including biological tissue, are easily absorbed due to the presence of three-dimensional networks and hydrophilic material within hydrogels [37].

In abiogenesis, few studies have used hydrogel as the working medium [32]. This approach was initially put forward as a theoretical hypothesis in the mid-2000's. In 2005, Trevors and Pollack reported that "*a primitive hydrogel was a more suitable environment for the assembly of pre-cells, and ultimately cells capable of growth and division*" *[24].* Pohorille and Deamer proposed that "*The origin of cellular life occurred when self-assembled membranes captured catalytic/informational polymers capable of growth and replication*" [38]. Therefore, tracking amphiphile and polymer emergence can lead to understanding the molecular evolutionary process (Fig. 1-2) relevant to the emergence of life [38].

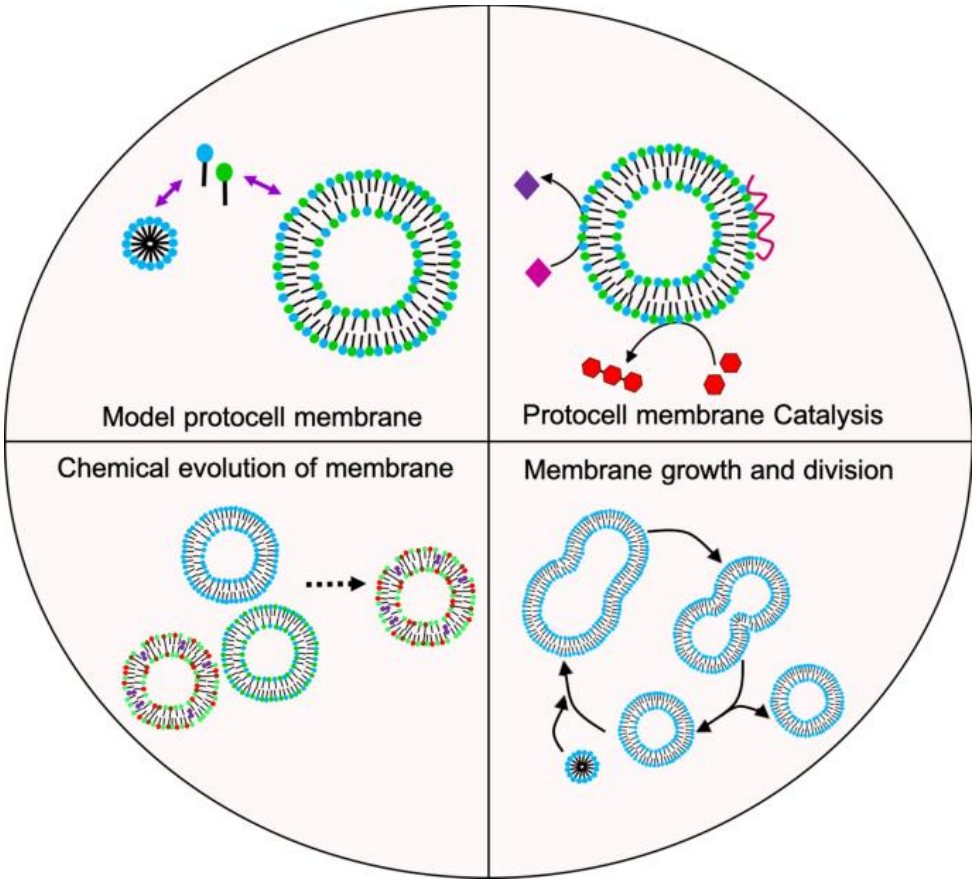

Figure 1-2: The molecular evolutionary process relevant to the emergence of life [39].

1.3 Formation and the Structure of Silica Hydrogels

The synthesis of sol-gel has been used widely because it is simple, room temperature, scalable, efficient energy, and controllable [40, 41]. Solution species undergo a series of hydrolysis and condensation steps during the sol-gel process, resulting in the formation of a sol which is a solid/liquid dispersed system. The sol phase can be formed by particles dispersed in the liquid phase, while the condensation process leads to a semi-rigid structure containing a large quantity of solvent, which is called a gel because the particles react with each other to form a cross-linked 3D network [42]. Elimination of the trapped solvent results in the formation of a rigid structure which is called a xerogel [43, 44]. Silica hydrogels are well recognised as appropriate matrices for biomaterial development. Therefore, it is very important to evaluate the mechanical

properties of the silica hydrogel in order to examine whether the silica hydrogels will be able to maintain their physical structure at the site of application.

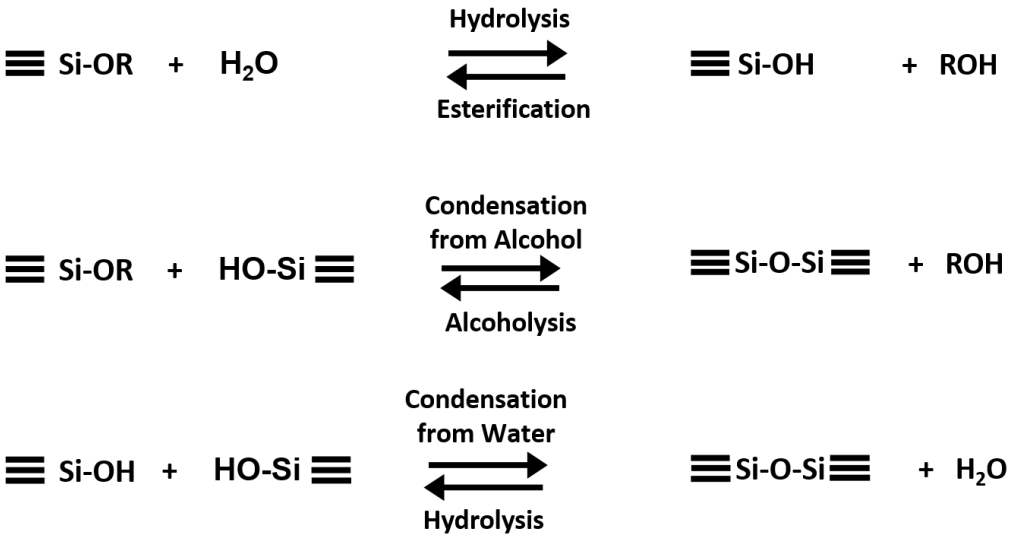

Figure 1-3: Sequence of chemical reactions in the sol-gel process of forming silica hydrogels [45].

Researchers have extensively worked by using different analytical methods to determine the internal microenvironment of silica hydrogels. One of these studies, reported by Nedelčev et al. [45] used FTIR and dynamic light-scattering measurements together to characterise the results of silica hydrogel matrix formation *via* sol-gel processing as shown in Fig.1 -3. This study revealed that visible vibrational bands were observed and could be assigned to (Si–O) vibrations of the Si-OEt groups, which appeared at 1,079, 1,100 and 969 cm^{-1}. However, during the sol-gel process, it was observed that the intensities of all these bands decreased as hydrolysis proceeded to afford silicic acid, which then condensed to silica. The intermediate Si–OH moieties of the silicic acid groups were observed at 1,049 cm^{-1} and Si–O–Si at 1,086 cm^{-1} groups. The FTIR spectra showed that the formation of Si–OH occurs after one min of mixing all the components, whereas vibrations associated with the presence of Si–O–Si bonds are observed after a longer period of gestation, 14 min. One h from the start of the sol-gel process, the signals associated with the Si–OEt groups disappear, and there are no subsequent differences in their intensities. This demonstrated that the ethoxy groups were eliminated from silicon and most if not all silicon was incorporated into a silica matrix. In this system, Si–O–Si bands are not observed in the FTIR spectra after one minute. However, light-scattering measurements were used, and the calculation of the average hydrodynamic particle diameter

(DA) showed the presence of Si–O–Si bonds because of the growth of the particles, which corresponds to a quick process of hydrolysis of the Si–OEt groups, with the formation of the Si–O–Si groups.

The same group's research [46] indicated a precise and simple tool for characterising the formation and aging of silica hydrogel that was prepared from poly(glyceryl silicate) (PGS) sol (Fig. 1-4).

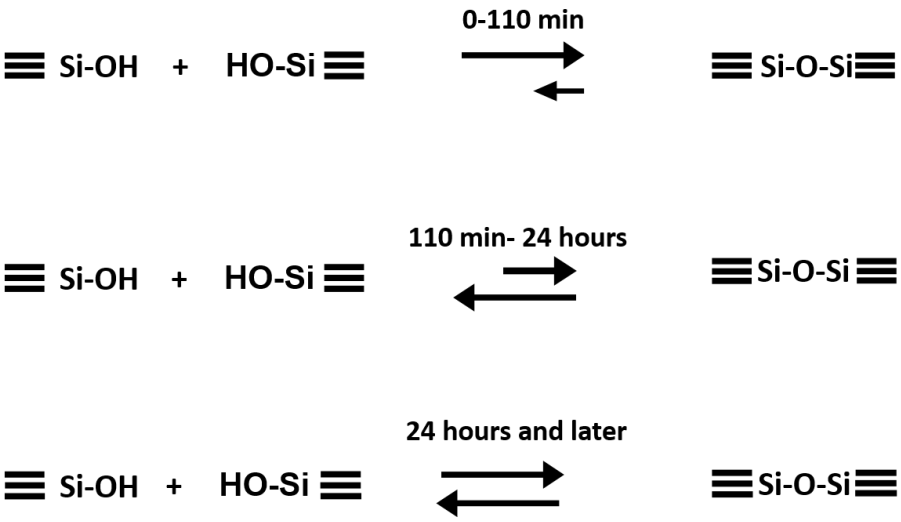

Figure 1-4: Timing of chemical reactions in the sol-gel process of forming silica hydrogels. The equilibrium state of the reaction within PGS hydrogel ageing [46].

Nedelčev used fluorescent probes including pyrene (Py), di(1 pyrenylmethyl) ether (DiPyM) and 2,3-bis-[4-(1- pyrenemethoxy) methylphenyl] butane (DiPyS). This technique can define the chemical transition of Si-OH to Si-O-Si, which is considered the principal reaction is inducing changes in local polarity of the microenvironment of pyrene(Py)-based with the two mentioned pyrene structures. The formation of a network can reduce the probability of forming the dynamic excimer of Py-based probes. In the first stage of the formation of the hydrogel, the polarity of the hydrogel matrix estimated by pyrene probes decreases during the sol-gel transition. After 2 hours, the polarity increases gradually until a constant level is reached; after 24 hours, the sol-gel process is used to prepare silica hydrogel in two steps, including hydrolysis and condensation.

Beside that, many studies have reported significant features in diagnostic hydrogel structure to explain the mechanisms of silica hydrogels formation and

how they can retain large amounts of water. Cammarata et al. [47] conducted a study using X-ray scattering and the dielectric spectroscopy method of optical transparent SHGs, which illustrated water restricted within the 3D structure. SHGs were prepared by sol-gel methods, and the measurements were conducted on samples after they had experienced different aging times. The results of this study were then compared with another result gained by using near-infrared (NIR) absorption spectroscopy. The X-ray scattering results estimated the size and structure of the pores within the SHG structure and showed the irregular distribution of water molecules around the SHG.

Both WAXS (Wide Angle X-ray Scattering) and SAXS (Small Angle X-ray Scattering) techniques, as well as dielectric relaxation spectroscopy techniques, present the structure and dynamic studies of water molecules trapped in the cross-linked structure of SHGs [48]. This study was also compared with the Cammarata study by NIR spectroscopy. The result obtained from the dielectric spectroscopy technique provides information on water dynamics within the 3D structure. It illustrates a disordered SHG structure and irregular distribution of water molecules within cavities of the matrix of SHG. It also shows how the disorder of the water molecule increases as the age of the gel increases. This can be explained by the effect of the constraints forced by the gel matrix on trapped water molecules, increasing with increasing sample age [47].

Different formations of hydrogel include neutral catalysed aerogels and colloidal SHG. These patterns of gels indicate their tendency to fractal behaviour at a length scale under a crossover length and also show that fractal dimension silica volume and gelation conditions can control the fractal dimension [48]. Chemical reactions of aluminium chloride ($AlCl_3$) and silicon chloride ($SiCl_4$) with a hydroxyl group on the surface of a gel have also been used to investigate the surface structure of SHG [49]. Results obtained show that a higher degree of hydroxyl group residuals have paired with each other even though the SHG surface was strongly dried. This research found that, after drying, more than 95% of hydroxyl groups had undergone a chemical transformation at 400°C, while more than 85%

of the hydroxyl groups were found to have reacted at 600˚C. Fig. 1-5 and 1-6 show the products of these reactions [49].

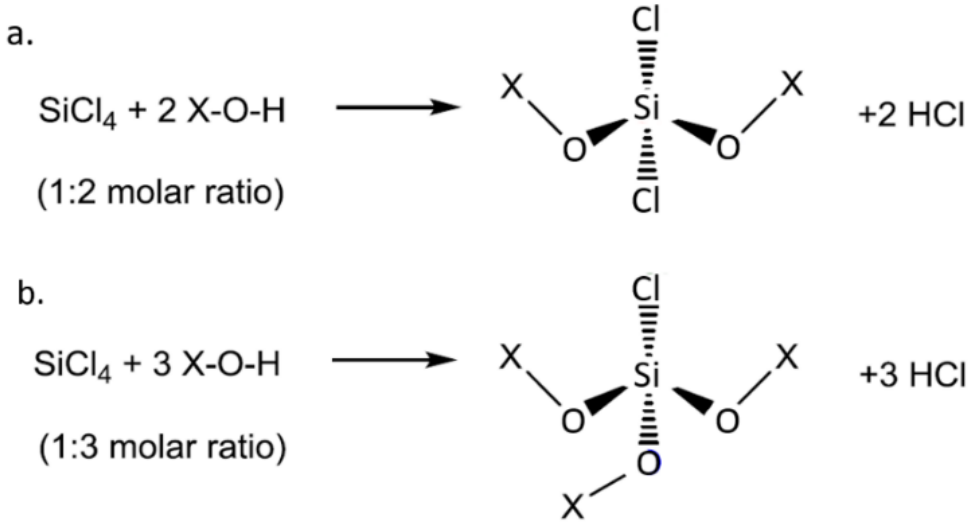

Figure 1-5: Possible reaction between SiCl4 and surface hydroxyl groups (X: Na), with the ratio of reactant in a) (1: 2), b. (1: 3), [49].

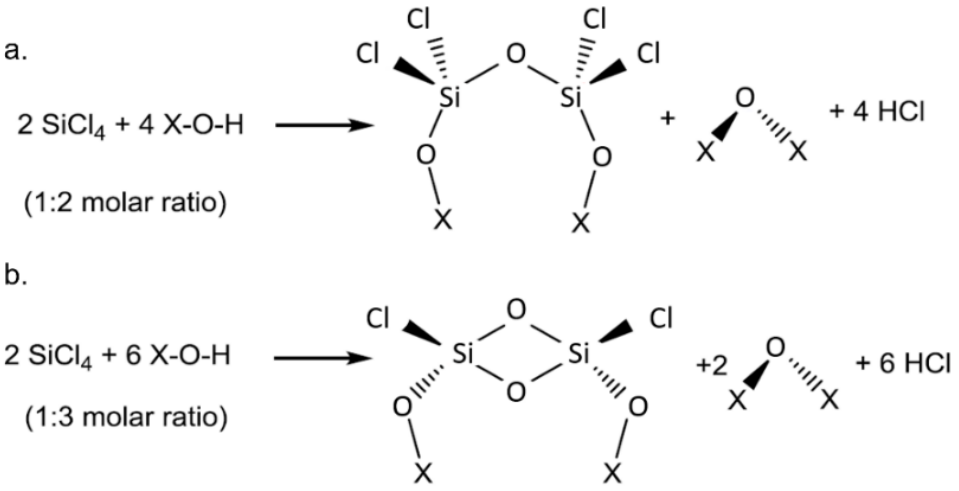

Figure 1-6: Possible reaction between $SiCl_4$ and surface hydroxyl groups (X: Na), each $SiCl_4$ reacts with only one hydroxyl group, and one H_2O was formed by condensation [49].

1.4 Analytical Methods Used in This Project

1.4.1 Critical Point Drying

Critical Point Drying (CPD) is a process of fluid to solid transition which allows water to be removed from fragile samples to reveal any underlying solid materials while minimising the risk of these materials being destroyed [50]. It is considered

an important step in producing powdered silica, for example, and is commonly recognised as a milder drying procedure than evaporation or lyophilisation [51]. In order to examine a structure of a sample, some microscopes are designed to image dehydrated samples which can be obtained by CPD.

The CPD technique (Fig. 1-7) was introduced by Anderson more than half a century ago to prepare samples for observation in conventional microscopes [52]. It is commonly used as a dehydrating method for sensitive or delicate biological or medical samples to preserve the sample morphology, which could otherwise be damaged due to surface tension changes upon transitioning from the liquid to the gaseous state [53]. In traditional drying, the sample to be dried is heated until the liquid contained within it converts to a gas, thus creating pore spaces within the retained solid matrix.

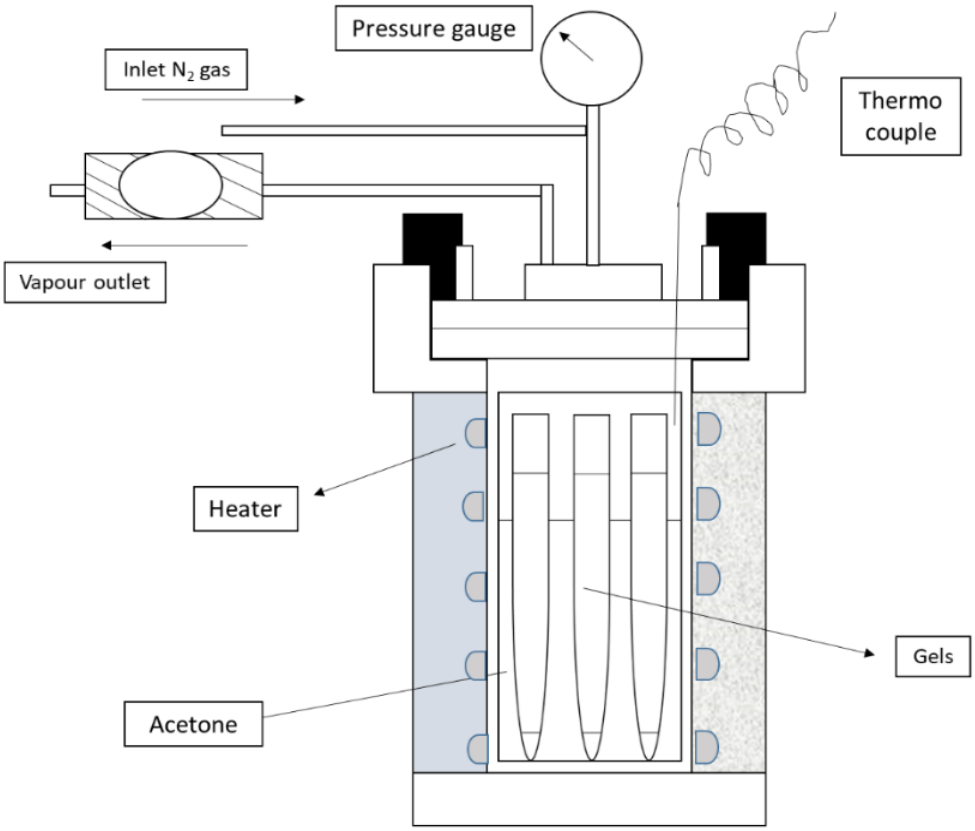

Figure 1-7: The schematic diagram of critical point drying process (modified from [54]).

The shape of the pore depends upon the surface tension of the liquid to be removed; too high a surface tension can lead to capillary stress on the pore wall during liquid removal. However, in critical point drying, the liquid (which is water in the case of a hydrogel) is first replaced by a second liquid with far lower surface tension. This, in turn, is replaced by supercritical fluid, which has lower surface tension. Consequently, the supercritical fluid can leave the pore space without extending capillary stress, hence preserving any delicate solid matrix. By using critical point dryers, water (374 °C and 229 bar) can be replaced by liquid carbon dioxide (31 °C and 74 bar), which has a lower critical point. However, using CO_2 as a transitional fluid has the disadvantage of not being miscible with water. Therefore, acetone, which is miscible in both water and liquid CO_2, is used. The liquid CO_2 at its critical point converts to the gaseous phase by decreasing the pressure at a constant critical point temperature. This allows compounds to transform to the liquid or gaseous phase without crossing the interfaces between liquid and gaseous, thus avoiding damaging effects because the densities of liquid and gas are equal at this point (Fig. 1-8) [55].

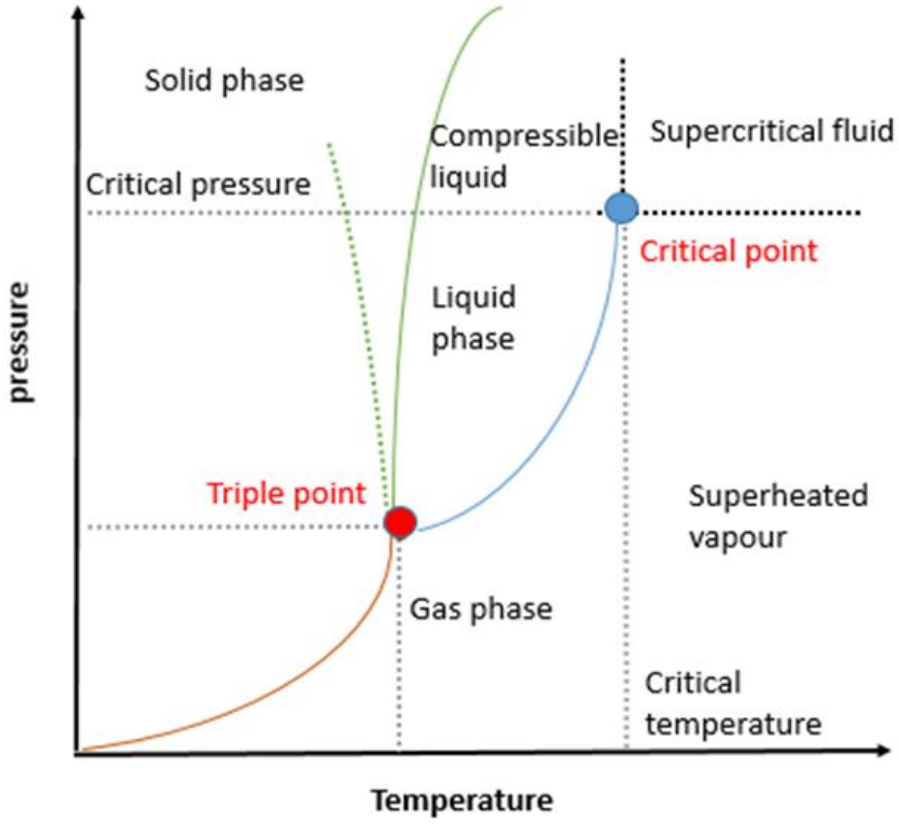

Figure 1-8: Schematic diagram of critical point drying [56].

1.4.2 Freeze Drying (Lyophilisation)

Freeze drying is another possible technique for avoiding phase boundaries between the liquid and the gas phase during drying. This is the process of removing the ice or frozen solvent from the sample under vacuum by sublimation, followed by desorption [57, 58]. That makes the ice change directly from solid state to vapour phase without passing through a liquid phase [59]. Lyophilisation is conducted below the triple point (Fig. 1-9) of the temperature and pressure conditions, to allow sublimation.

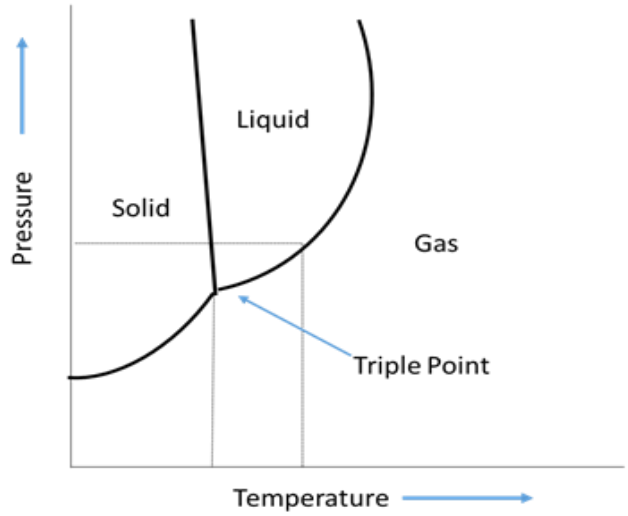

Figure 1-9: Phase diagram illustrating the triple point of water [57] .

This technique is considered a significant procedure for colloidal systems that have the ability to transport active molecules while maintaining their stability and solubility as well as reducing their side effects including chemical reactions; for example: oxidation, hydrolysis, crosslinking and aggregation in aqueous solution, and disulphide rearrangements [58, 60]. These reactions lead to destabilisation of the colloidal system in the short or long term [60].

Figure 1-10: Lyophilisation steps [57].

The freeze-drying procedure (Fig. 1-10) starts with the preparation of the sample, followed by freezing, primary drying and secondary drying to get the final dried product [61]. During the primary drying, the gaseous pressure of water rises with

a rise in temperature. In this phase, the temperature of the primary drying must be kept as high as possible. Also, the temperature should be below the critical process temperature to prevent structural collapse. This is because the critical process temperature leads to the ‘meltback’ or ‘collapse’ phenomenon [62]. On primary freezing, the ice crystals will start to separate until the solution converts to concentrated material, whereas on secondary drying, the phase of ice crystal separation is completed [61].

1.4.3 Dialysis

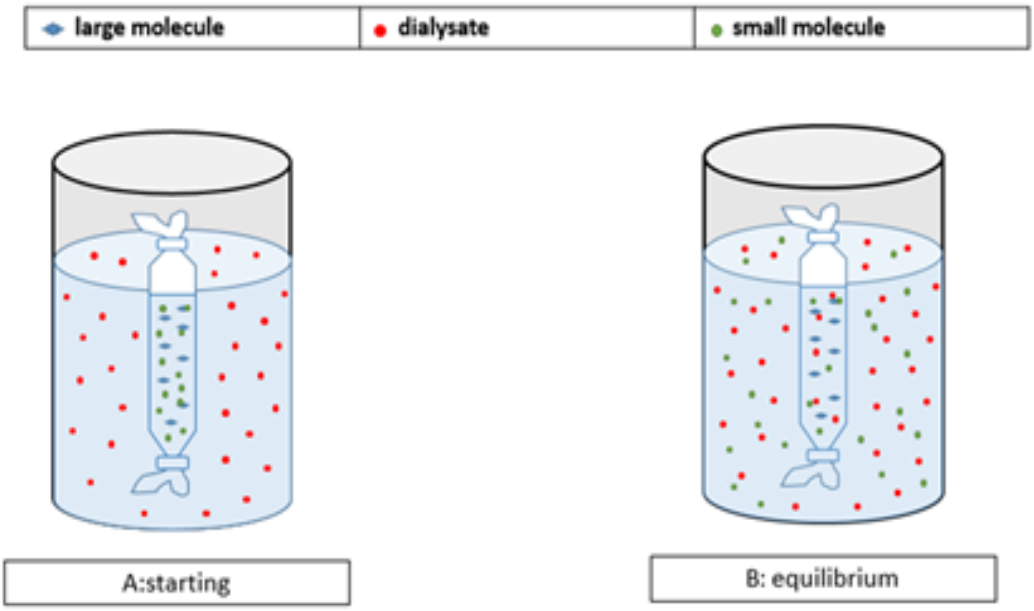

Figure 1-11: Dialysis process at A:the starting and B: the equilibrium point [63].

Dialysis is one of the membrane operations (Fig. 1-11) that are used widely because it can minimise the denaturation, deactivation, and/or degradation of the macromolecules [64]. It is a process based on selective diffusion of molecules through a semi-permeable membrane material. This technique is used to separate molecules depending on concentration gradients [65]. This process has beneficial value over other methods like electrodialysis and reverses osmosis. It offers the advantages of being of relatively low-cost, simple, and environmentally friendly [66].

This method consists of a sample and dialysate placed on opposite sides of a semi-permeable membrane that permits the passage of water (or solvent) but not molecules or ions (solutes). When equilibrium is reached, the molecules which

are smaller than the pores can transit through the membrane, whereas large molecules are retained on the sample side. Consequently, the concentration of the small molecules will be reduced. In extreme cases, if the external compartment is continually replenished with fresh water, it is possible to remove all the soluble or smaller components from the larger and/or fixed insoluble materials.

1.4.4 Scanning Electron Microscopy(SEM) and Energy Dispersive X-Ray Spectroscopy (EDX)

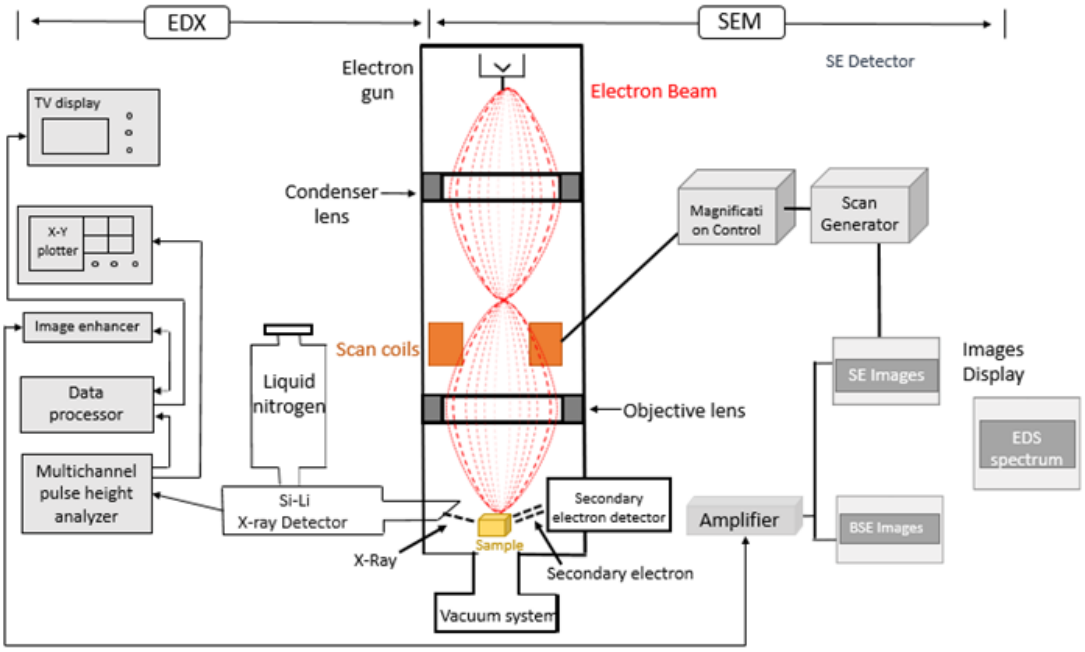

Figure 1-12: Schematic of Scanning electron microscopy and Energy Dispersive X-ray Spectroscopy (EDX). (Modified from [67]).

Scanning Electron Microscopy (SEM) (Fig. 1-12) is considered an effective technique to distinguish the 3D morphology and high-resolution images of a sample at the nano and micro-scales [68]. It enables one to investigate the surface analysis of matrices with powerful magnification; since it provides information on morphology and size distribution when coupled with other porosity and surface area methods [69, 70].

The operation of electron microscopy starts by accelerating electrons produced under a high vacuum by applying a high voltage across a tungsten filament. By using electromagnetic lenses, the accelerated electrons are concentrated in a very small beam with a very high intensity. That results in Interactions between the sample and electron beam which produces different radiative forms like

backscatter electrons, secondary electron, and characteristic X-ray at the same time. Backscatter electrons and secondary electrons are emitted at or near the specimen surface. This is followed by using a special detector to collect the secondary electrons to form an image of the specimen's surface topography. Back-scattered electrons, which represent the beam electrons reflected from the sample, originating deeper sites within the specimen. Then, electronic amplifiers of various types used to amplify the signals, which are shown as variations in brightness on a computer screen [67].

Inelastic electron interactions with the sample include an energy transfer between the incident electron and the target atoms. If this transferred energy is above a certain threshold, it may eject an electron from the inner shell of a target atom. After such an electron has been so ejected from the inner shell, an outer shell electron will transfer to the hole, releasing energy in the form of specific X-ray emissions. The released X-ray energy can then be used to distinguish the materials' qualities (characteristic peak positions) and quantity (relative peak area). In particular, when the EDX detector is connected with SEM, they can identify the types and amount of the elements in a specific region of a sample.

1.4.5 Cryo-Scanning Electron Microscopy(Cryo-SEM)

Cryo-Scanning Electron Microscopy (cryo-SEM), which combines scanning electron microscopy (SEM) with a cryogenic technique for sample preparation, enables scientists to examine structures and materials in their hydrated phase with high image resolution [71]. Current advancements in speed, imaging performance, and ease of use have transformed cryo-SEM from a highly particular discipline to an available technique in labs with wide-ranging applications in materials sciences [71].

1.4.5.1 Sample Preparation for cryo-SEM

Cryo-scanning electron microscopy is an effective way to get better images of samples containing moisture without risking the collapse of the sample's surface by removing the solvent phase, so the main aim of cryo-SEM is to preserve the structure of the hydrated material [72]. The sample is attached to a stand with a layer of added carbon-rich conductive glue for allowing the discharge of electrons to prevent causing interference into SEM imaging or analysis. It is then quickly frozen with liquid nitrogen, and the stand with the frozen material is placed under liquid nitrogen to be coupled to a rod and pulled back into a small cylindrical container. This is achieved by locating the sample within the freezing unit with a high vacuum and preventing severe contamination of the gas molecules while slipping the sample into the freezer chamber. The freezer camper is prepared with a knife that can be controlled from the outside to fracture the sample. Then the sample's moisture is sublimated, and a thin layer of gold-palladium is sputtered on the sample to apply a good electrical conductivity [73]. Finally, the fractioned sample is inserted into the observation chamber using a rod. Fig 1-13 shows the important steps for the preparation of sample, which then becomes ready for SEM analysis.

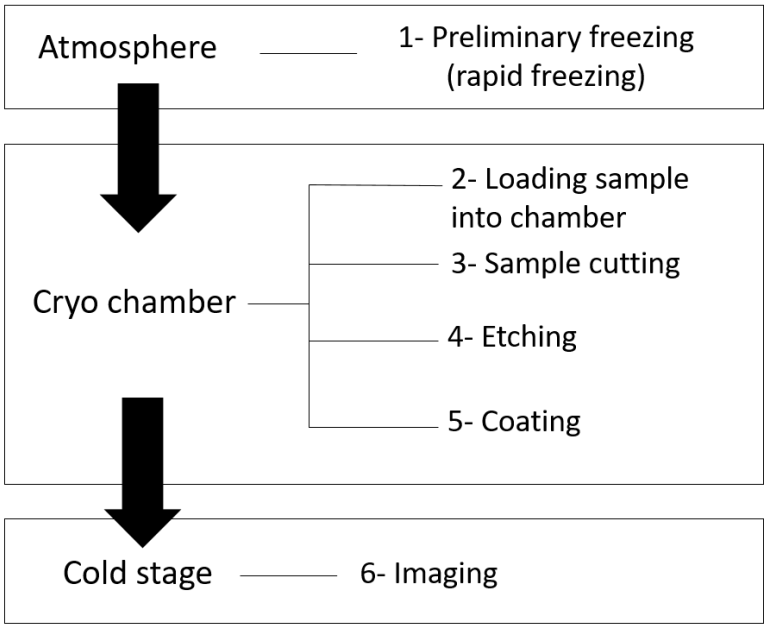

Figure 1-13: Procedure of sample preparation for cryo-SEM.

1.5 Amphiphile Self-Assembly

Amphiphilic compounds relevant to biology, are synthetic or natural molecules, defined chemically as molecules that possess both non-polar and polar components that are covalently bonded together in the same molecule. The non-polar part is a hydrophobic hydrocarbon chain, whereas the hydrophilic polar part is ionic (anionic or cationic), non-ionic, or zwitterion amphiphile as shown in Fig. 1-14 [74].

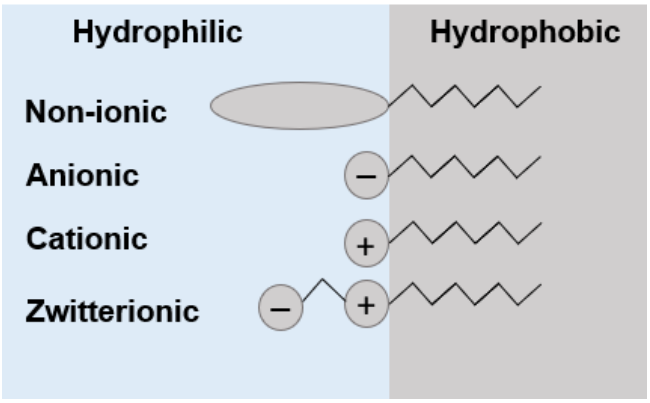

Figure 1-14: General structures of the different types of amphiphile (modified from [74])

This leads to the physical property of being surface-active, which can reduce the surface tension; therefore, it is called a surfactant. Because of their surface activity (amphiphilicity) in a liquid, there will be an interaction between the polar head group of the amphiphile and the polar part in the liquid, while The non-polar hydrophobic chain prefers energetically to occupy regions at the interface (in the air or non-polar liquid) [75]. These amphiphilic molecules are able to self-assemble via spontaneous, non-covalent interaction processes. Spontaneous processes form ordered aggregates (Fig. 1-15), such as micelles, vesicles, and lamella materials [76].

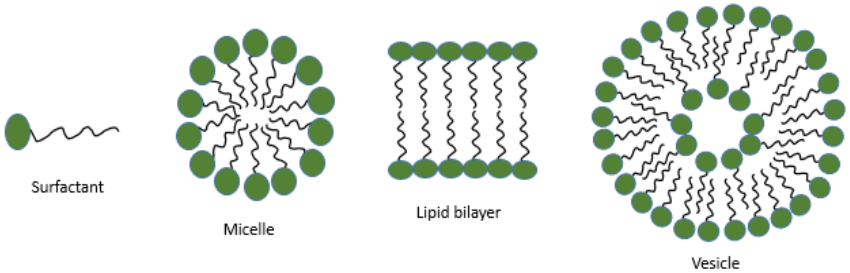

Figure 1-15: Different shapes for self-assembly of amphiphilic components (modified from [74]).

Self-assembled amphiphiles have weak individual forces, but they produce an overall effect of weak interactions that are strong enough to connect various amphiphile molecules together and make sure that they are stable in the solution. Stability in the solution of the amphiphiles self-assembly results in the hydration of the hydrophilic head and the insertion of the hydrophobic tail in the solvent [74]. Furthermore, weak forces contribute to making the structure more flexible to resist minor disruption while maintaining the reversibility of the ordered aggregates structure [74]. The weak forces of the amphiphilic self-assembly include hydrogen bonding, van der Waals forces, hydrophobic effects, and electrostatic interactions to form the micellar structure based on the force balance between these forces, both increasing the hydrophobicity and reducing the opposing hydrophilic interactions have the same trend in lowing the CMC [69].

The hydrophobic effect is one of the main driving forces of amphiphile self-assembly into various supramolecular structures. When surfactants are dissolved in water, an apolar group makes a disruption in the hydrogen bond of the water structure, which raises the free energy of the system. Hence, surfactants migrate to the interfaces and orientate the hydrophobic groups towards the air, which can contribute to the reduction of the free energy of the solution. Another way that can reduce the free energy of the solution is the micellar formation . In this process, non-polar groups tend to create a cavity to accommodate the hydrophobic molecules, which orientate to the interior of the micelles reducing the disruption of water by the self-assembly of the surfactants, and their polar groups orientate to the water (Fig. 1-16).

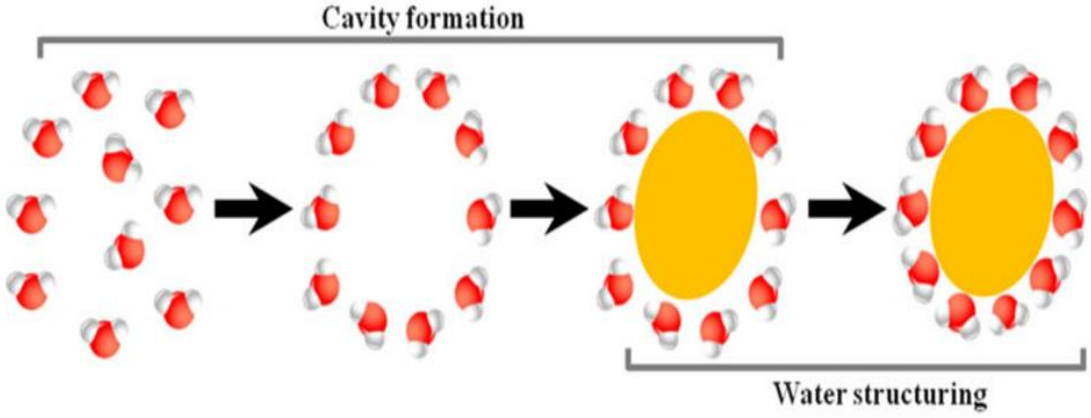

Figure 1-16: Scheme of the cavity formation and water structuring [77].

Another important interaction is described by the Derjaguin, Landau, Vervey, and Overbeek (DLVO) theory of charged colloids [78]. This interaction is mainly relevant to the ionic surfactants for self-assembling and colloidal stability interactions in the solution. DLVO explains the aggregation behaviour of charged surfactants at interfaces in the solution. The theory supposes that the interaction in the solution between the charged colloids consists of two main interactions, the van der Waals and double layer interactions [79]. Van der Waals interactions consist of the two short-range electrostatic forces, one repulsive and one attractive , called London dispersion forces originated by a temporary dipole that is induced by a polarisation of the electron distribution of an adjacent atom. In addition to that, the electrical double layer (EDL) also contributes to micellization. EDL interaction originates from the adsorption of charged molecules on the surface of the micellar structure from the solution.

Fig.1-17 illustrates the principal layers of EDL that are composed of both immobile and diffuse layers. The ions of the immobile layer are strongly connected to the charged surface (Stern layer ,a mono-layer), and the second layer consists of the adjacent region of loosely associated mobile ions. The total electrical double layer, due to the formation of counterion layers, results in the electrostatic screening of the micelle charge and therefore reduces the Gibbs free energy of EDL formation [74]

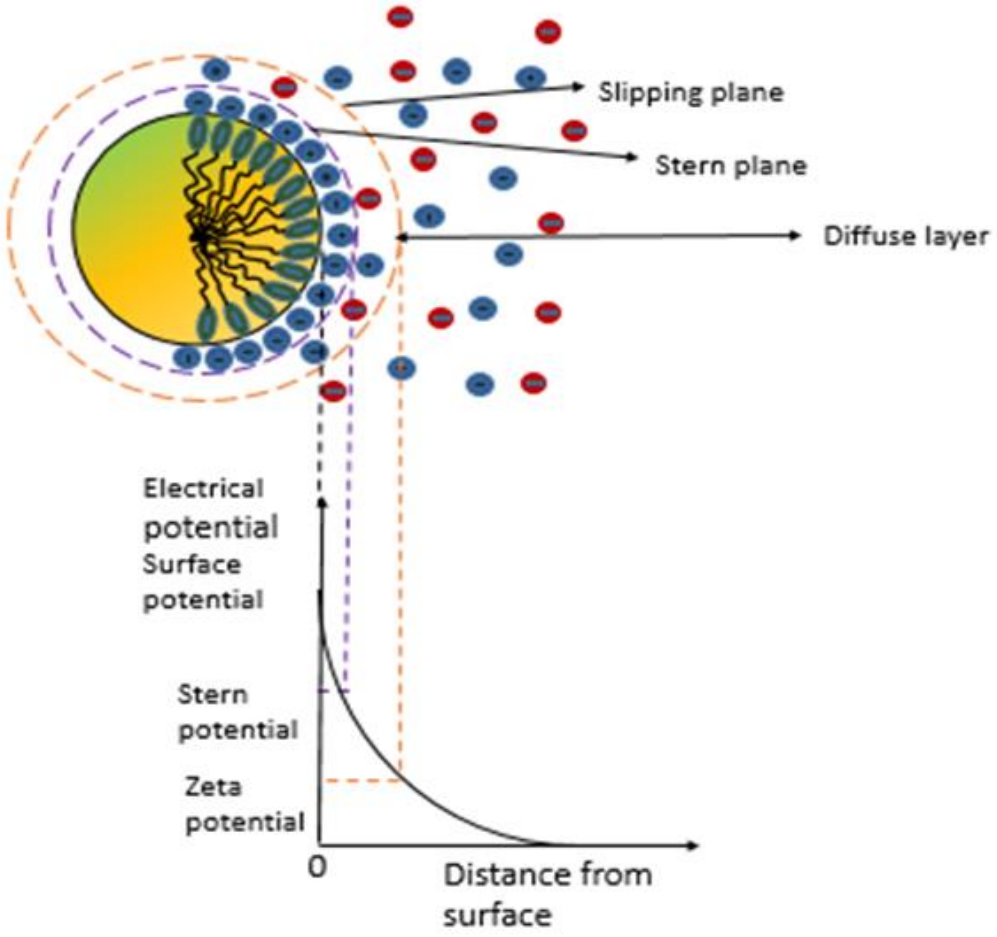

Figure 1-17: Scheme of the Electrical Double Layer of self-assembly of charged surfactants. (modified from [74]).

The shape and size of the aggregation of an amphiphile into a self-assembled structure is influenced by the molecular geometry of the surfactant molecule, ionic strength, and the surfactant concentration [76]. The study of physical models of self-assembly can assist in understanding both natural and advanced technology [80]. The self-assembly of amphiphilic molecules can provide new opportunities in nanotechnology to fabricate novel substances in various applications [81]. In addition to that self-assembly is thought to be one of the most important of the driving forces behind origin of life and would have been influenced by the environment circumstance in the early earth [82, 83]. Therefore, self-assembly is considered as an important step in the formation of membranous compartments, which seem to be formed from small single-chain amphiphiles [82].

1.5.1 Micellar Formation

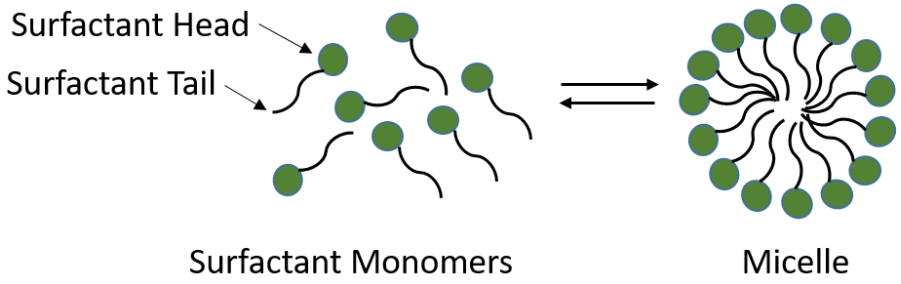

Figure 1-18: Micelle formation of surfactant (modified from [84]).

Micellar formation (Fig 1-18) is one of important self-assembly motif of amphiphiles [74]. An important parameter in the context of micelle self-assembly is the critical micelle concentration (CMC). This is the concentration of surfactant in bulk at which micelles first appear in the solution [85]. Above the CMC, amphiphilic molecules can form aggregates in equilibrium of distinct size with single molecules in solution [83].

In this study, sodium dodecyl sulphate (SDS), ionic detergent surfactant, Fig. 1-19, is selected due to the feature of its structure which possesses sulphate as a head group and a long chain of the hydrophobic dodecyl group that can form micellar structure for mimicking the phospholipid molecules of a biological membrane [86].

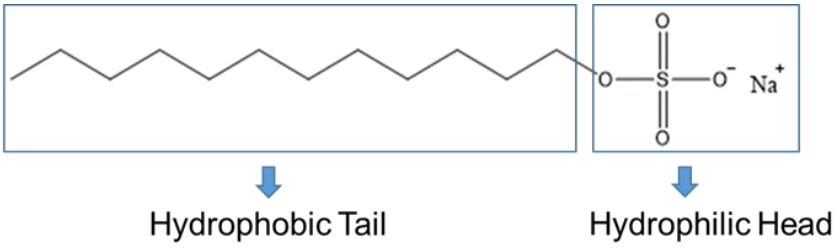

Figure 1-19: Sodium dodecyl sulphate structure (hydrophilic head and hydrophobic tail).

It is worth stating here though that our choice of SDS has been made not on any belief that it may have played an active role in the emergence of biological life but rather that it may act as a suitable and well-studied model. It may however, bear some functional resemblance to other anionic amphiphilic molecules, such as long chain carboxylate salts, known to be present on the early earth through, for example, meteoritic impacts [87].

1.5.2 Vesicle Formation

Beside micelle formation, amphiphiles also can be self-assembly to a vesicle, which is considered as a micelle stretched in two dimensions, and it appears when the amphiphile' concentration in solution is increased and the micelles become unstable then start to fuse. This results in formation of structure composed of bilayers, which is then called a vesicle [83].

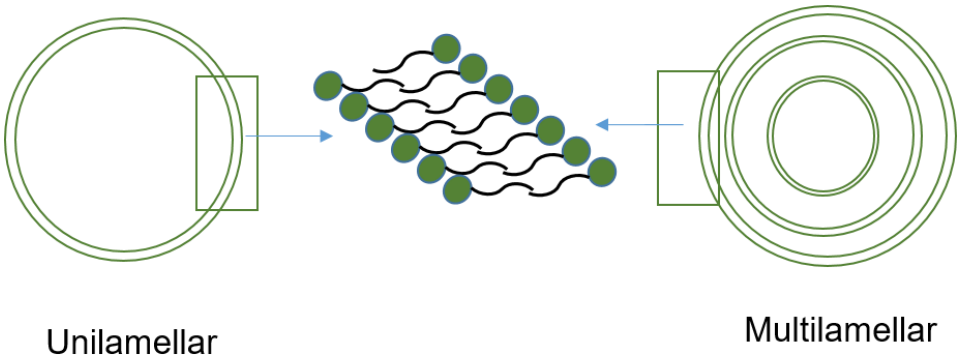

Figure 1-20: The morphologies of different vesicle bilayer. Green circles represent the hydrophilic head, and squiggly lines represent the hydrophobic tail [88].

Vesicles are closed structures (Fig. 1-20) that are composed of bilayers of amphiphilic molecules and act to separate an interiors side aqueous compartment from the outside aqueous medium [89]. Vesicle formation starts from single-chain amphiphile (SCA) molecules [90]. The presence of complex head groups like glycerol ,amine, and sulphate in the mixture of (SCA) allows to form stable vesicles with a wide range of pH range and temperatures, at lower amphiphile concentrations, and higher salt tolerance [91]. For example, sodium dodecyl sulphate can produce a vesicular membrane structure upon being mixed with dodecyl alcohol. This is because that dodecyl alcohol can form a H-bond interaction between hydrogen and the sulphate oxygen, which resulting in vesicles formation [83]. Also, within the context of biological emergence, adding 1-alkanols could be seen as valuable within early earth environments, because they can stabilise vesicles formation at the high pH's found in alkaline vents, these kinds of environments being frequently quoted as cradles for biology [92].

1.5.3 Factors Influencing Critical Micelle Concentration (CMC)

The formation of micelles occurs at the critical micelle concentration (CMC). Many factors can have an effect on the CMC including temperature [93, 94], buffer

solution [95, 96], adding organic modifiers [97], ionic strength of the aqueous solution [93], adding additives [98] and adding electrolytes [97, 98].

The change in the CMC value by adding salt can be explained by the fact that the formation of the micelle can be affected by electrolytes. When the electrolyte is added, the negative charge at the micelle surface is partially neutralised by the cation of the added electrolyte (Fig. 1-21). This can decrease the thickness of the ionic environment around the head of the ionic surfactant [99]. Therefore, the electrostatic repulsions between the surfactant and electrolyte decrease, and consequently the value of CMC decreases [85].

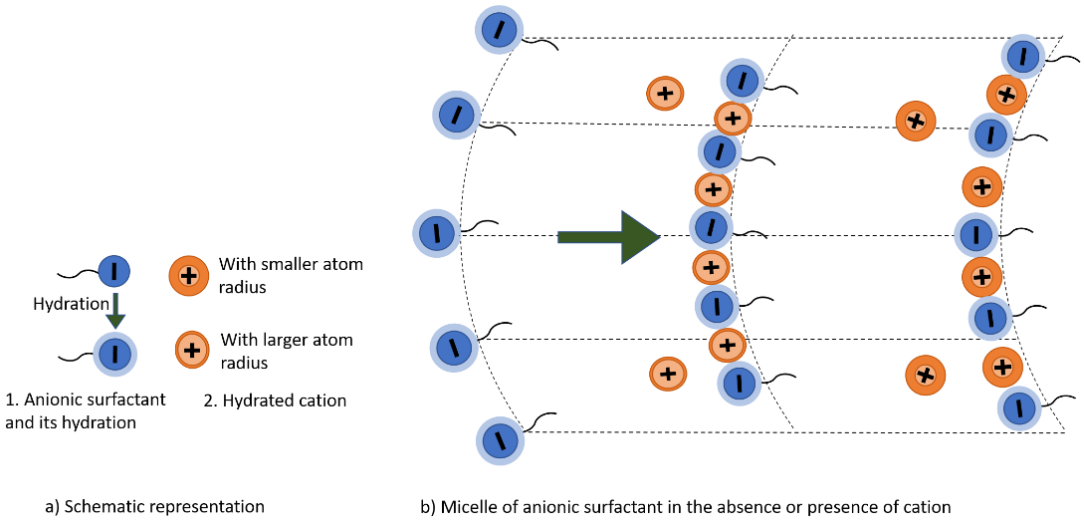

Figure 1-21: Micelle structure of anionic surfactant in the absence or presence of different counterion (modified from [100]) .

Another driving force to self-assembly is the hydrophobic effect of apolar group of dissolved surfactants in water which makes a disruption in the hydrogen-bond of the water structure that raises the free energy of the system. Hence, apolar groups orientate to the interior of the micelles, and their polar groups orientate to the water to reduce the disruption of water by the self-assembly of the surfactants into micelles, which can reduce the free energy of the solution (Fig. 1-22) [74].

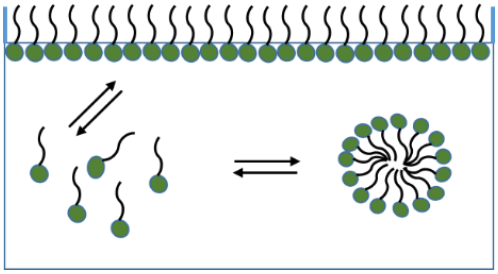

Figure 1-22: Schematic representation of the surfactant molecules in water.

1.5.4 Measurement of Critical Micelle Concentration

Critical Micelle Concentrations (CMCs) can be estimated from the inflection point in the plot of a physical property of the solution as a function of the surfactant concentration [85]. It has been investigated by many techniques in order to estimate the critical micelle concentration in different media. The following sections describe the important methods commonly used in various fields: the UV-vis spectrum [101], the fluorescence emission spectrum [102], electrical conductivity [103], surface tension and viscosity [104].

1.5.4.1 UV-Vis Spectrophotometry

Spectrometer devices are used to measure the absorbance of a system at a specific wavelength of electromagnetic radiation, most commonly in the visible and ultraviolet (UV) ranges.

The main elements of the UV-Vis Spectrophotometer (Fig. 1-23) are: UV-visible light source, two cells, and a detector to measure the intensity of light passing across the cells. The light in the double-beam UV-Vis spectrophotometer is divided into two parallel beams. Every beam passes through a cell; one cell containing a solvent, and the other cell containing the sample that is dissolved in the solvent. Then, the detector measures the intensity of the light transmitted through the solvent (reference), which is represented (I_o), and the intensity of light transmitted through the sample cell, which is represented (I); the detector shows their ratio in real-time.

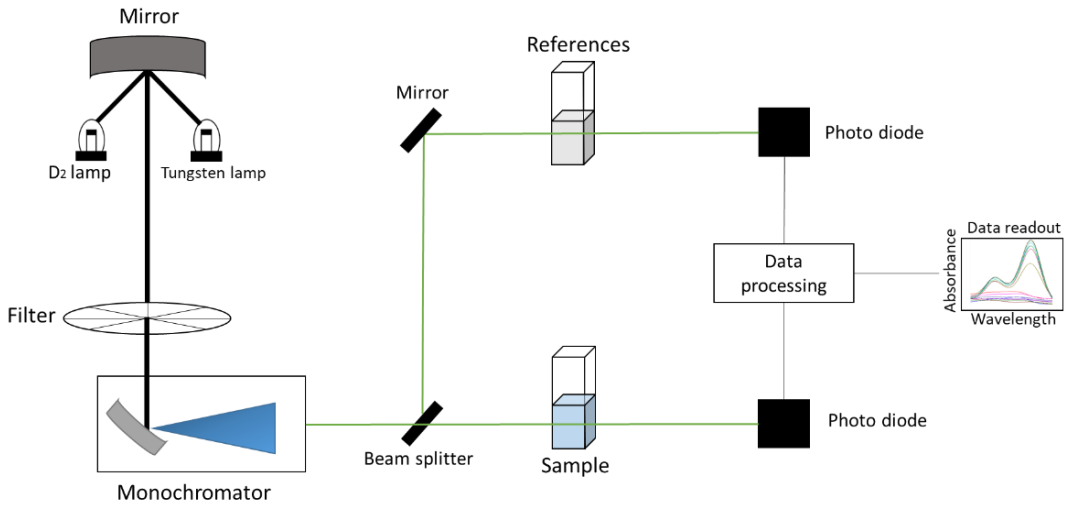

Figure 1-23: Schematic system of UV/Vis (modified from [105]).

The absorbance, Abs, is calculated by the following equation, which shows the relationship between the two transmitted light sources [106].

$$A = \log \frac{I_\circ}{I} \qquad \text{Equ.1-1}$$

The Beer-Lambert Law indicates the absorbance and concentration of the sample. As a result, Beer's Law can be applied when there is a linear relationship only; it is written as:

$$A = \epsilon \, l \, c \qquad \text{Equ. 1-2}$$

where A is the absorbance, ϵ is the molar absorptivity coefficient having units of L mol^{-1} cm^{-1}, l is the length of the bath with cm, and c represents the concentration with the unit of mol/L.

Using the UV-Vis method to estimate CMC values of amphiphiles relies on using a probe molecule which can be easily incorporated into the micelles and which has a physicochemical property which changes when so incorporated. Many studies have investigated dye–surfactant interactions and the mimicking of various biological processes taking place between the biomembranes and organic molecules [107]. The study of dye–surfactant interaction is considered to provide significant knowledge with which to understand the mechanisms, chemical equilibria, and kinetics of surfactant-sensitised colour [108]. Among the most common techniques, spectrophotometry has been used widely to investigate the complexation equilibria between dyes and surfactants in solutions [108]. Many researchers have emphasised that surfactant and dye can interact with two types, depending on the chemical structure of both dye and surfactant. The formation of the complex between the dye and surfactant will be observed by decreasing the absorbance value, with the appearance of a new band below the critical micelle concentration (CMC), while the incorporation of dye to micelle will be observed by increasing the absorption coefficient at high concentration of micelles as it shown in Fig. 1-24 [101, 109].

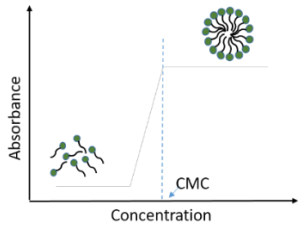

Figure 1-24: Schematic representation of critical micelle concentration.

For applying the colorimetric method for determining the CMC value, it is essential to select the dye that does not interact with another material and has suitable spectral features, which should be modified by interaction with the surfactant. Also, surfactant interactions can be strong enough to modify the degree of binding of the surfactant reagent to the dye.

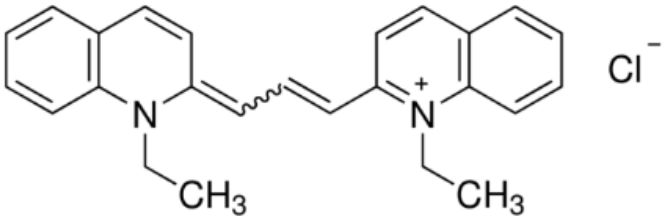

Figure 1-25: The structure of pinacyanol chloride.

In this project, pinacyanol chloride, Fig.1-25, which is considered a cationic dye, was selected to estimate CMC of SDS, depending on the absorption shift of pinacyanol chloride, by using the UV-vis absorption in the micellar media [97]. Khouri et al. [110] reported many results showing the absorbance of pinacyanol chloride that dissolved in pure ethanol with different concentrations, such as the results: 2.3×10^{-6} M of pinacyanol chloride with absorbance 0.499, and 9.7×10^{-6} M with absorbance 1.771 at wavelength 601 nm. By the Beer-Lambert Law, the absorbance was directly proportional to the concentration, so the concentration between them was chosen to get reasonable absorbance. Selected concentration 5×10^{-6} M of pinacyanol chloride gives the value of absorbance under one value, with a slight difference at the wavelength (608 nm).

1.5.5 UV/Vis Spectrophotometry for Measuring Light Scattering

Light interacts with matter in different ways. One of them is light scattering which provides information on the system being probed. That can be achieved by monitoring the time-dependent optical density of a solution to investigate the kinetics of silica hydrogel formation [111]. The interaction of the light with a sample can be attenuated its intensity because of the absorption by the sample, which is described by its absorbance density, α, and scattering by particles within the sample which is described by its turbidity, T. The attenuation of intensity as a function of distance x through a sample is given by:

$$-dI_\lambda(x) = (\alpha_\lambda + T_\lambda)\, I_\lambda(x)\, dx. \quad (1)$$

Absorbance and turbidity make separate contributions to the loss of light. If multiple species are present in the solution, with different concentrations c_j, the absorbance density and turbidity are a sum of the contributions of each:

$$\alpha_\lambda = \sum c_j \varepsilon_{j,\lambda} \, , \; \tau_\lambda = \sum c_j \sigma_{j,\lambda} \, . \qquad (2)$$

Where ε_λ is the extinction coefficient which represent a function of the electronic structure of the species and relates to the strength of electronic transitions as a function of wavelength, and σ_λ is the scattering cross-section which depends on many factors including particle geometry, size and refractive index.

Integrating Eq. (1) reveals that the intensity of light at a distance x through the sample decreases exponentially with absorbance density and turbidity:

$$I_\lambda(x) = I_{\lambda,0}(x)\, e^{-(\alpha\lambda+T\lambda)\, x} \, . \qquad (3)$$

In this study, spectrophotometer was used to determine the attenuation of light intensity by silica hydrogel. The detector in this device records the transmitted light through the sample, T, relative to a reference sample (a blank cuvette):

$$T(\lambda) \equiv I(\lambda) / I_0(\lambda). \qquad (4)$$

Where, I(λ) is the intensity of light of wavelength λ transmitted through the sample when a light of intensity $I_0(\lambda)$ is incident on it [112].

This project focused on measuring light scattering. In the sol−gel process, the number of particles increases during oligomerisation, and their size increases with polymerisation. As a result, the scattered intensity increases over the process, which proves to be an effective alternative for determining gelation times from the scattering profiles.

1.6 Fluorescence microscopy

Fluorescence microscopy technique uses light emission from a substance to discover its structure and morphology. This highly sensitive technique has the ability to gather information, an advantage that makes it an excellent candidate for elucidation of the structure of polymers and nanomaterials [113]. Indeed, the concept of fluorescence is similar to the method of optical separation using filters, but the design of the microscope is different, as it depends on the resolution of images [114].

1.6.1 Principle of Fluorescent Molecules

The advantage of the use of fluorescent molecules (fluorophore) lies in their ability to respond to light distinctly. When a photon of excitation light is absorbed by an electron of the fluorescent molecule, this electron jumps from its outer shell to the next orbital shell, causing a molecular energy change from ground state level to excitation state level (short wavelength)) (Fig. 1-26). After a few nanoseconds, the molecule releases the photon of light and returns to the ground state again to become more stable. This means that the molecule loses some of its energy (high wavelength) and emits light which presents the fluorescence light [114]. Fluorescent molecule can offer easier, cheaper and little amount comparing with other technique like a large panel of chromatography approaches such as high-pressure liquid chromatography and gas chromatography coupled with mass spectrometry that require heavy and expensive tools and take up working time of qualified experts [115]. Fluorescent molecule binds to the compounds and offers a quick response for the detection of intracellular lipid by fluorescence microscopy by stains [116].

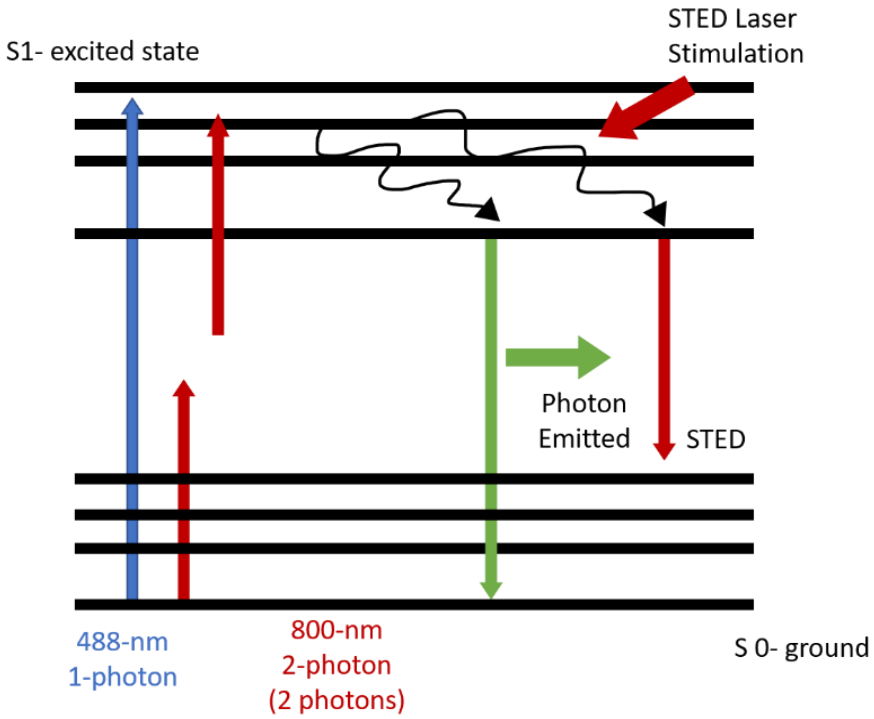

Figure 1-26: Fluorescence energy diagram modified from [117].

In This study, Nile Red (NR) (Fig. 1-27) was used because it offers several advantageous characteristics such as fast screening of oleaginous microalgae, semi-quantitative techniques, quantifying lipid levels [118]. Also, it is considered one of the important dyes that displays large shifts from hydrophobic solvents to hydrophilic solvents in excitation and emission maxima [119].

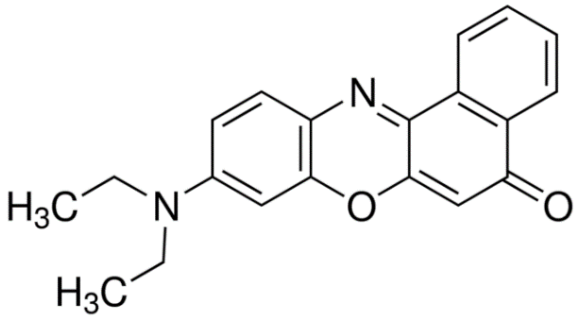

Figure 1-27: Structure of Nile red.

1.6.2 Epifluorescence Fluorescence Microscopy

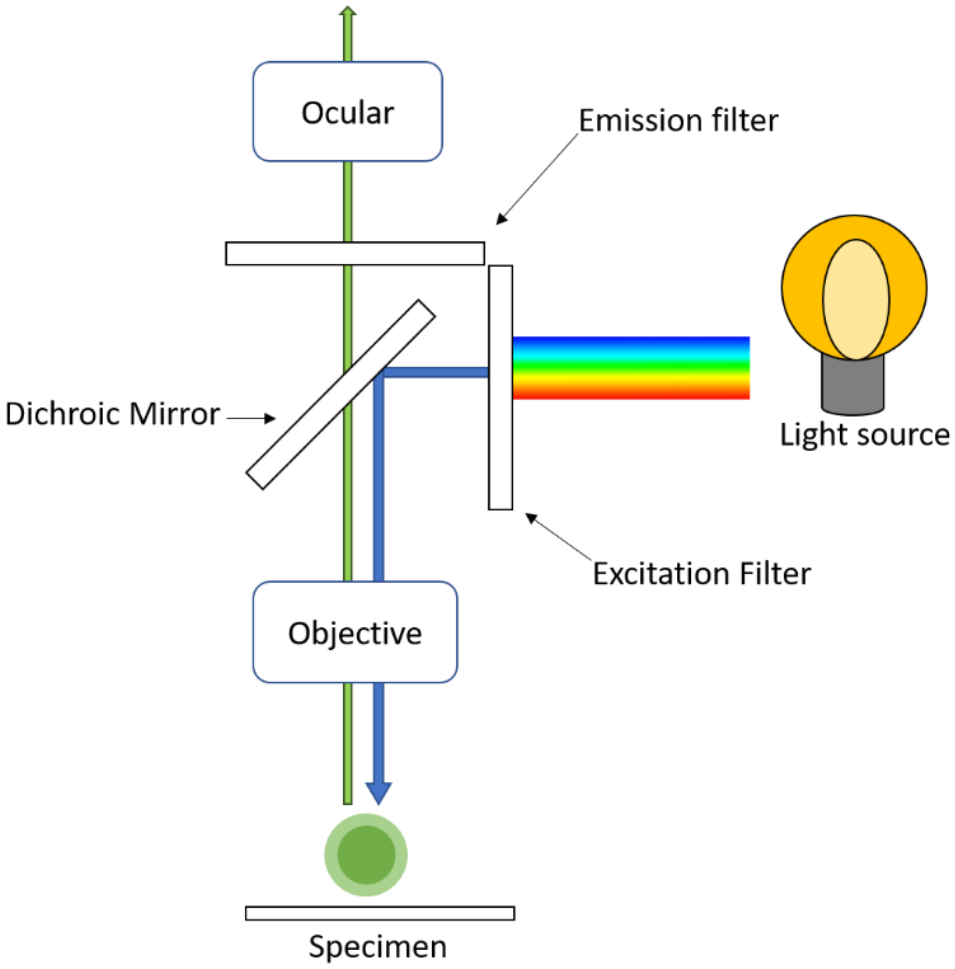

Figure 1-28: Schematic illustration of epifluorescence fluorescence microscopy modified from [120].

The design of epifluorescence (Fig. 1-28) incorporates a source of light that excites an electron of the specimen at a specific wavelength of the objective lens. Then, the specimen emits the fluorescence that is focused on the detector, using the same objective lens that excited the specimen. Therefore, the excitation light that is transmitted through the specimen, and the emitted light, reach the objective together, giving a high signal-to-noise ratio. To solve this, a dichroic beamsplitter is used, which acts as a wavelength specific filter to allow the transmitting fluorescence light to pass to the detector and reflect any remaining excitation light [120].

1.6.3 Confocal Fluorescence Microscopy

The use of confocal microscopy can offer several advantages over traditional widefield optical microscopy because of its spatial filtering techniques. These provide the ability to control depth of substance, reduce background information from the focal plane which can cause image degradation, and collect serial optical sections in thick specimens [121].

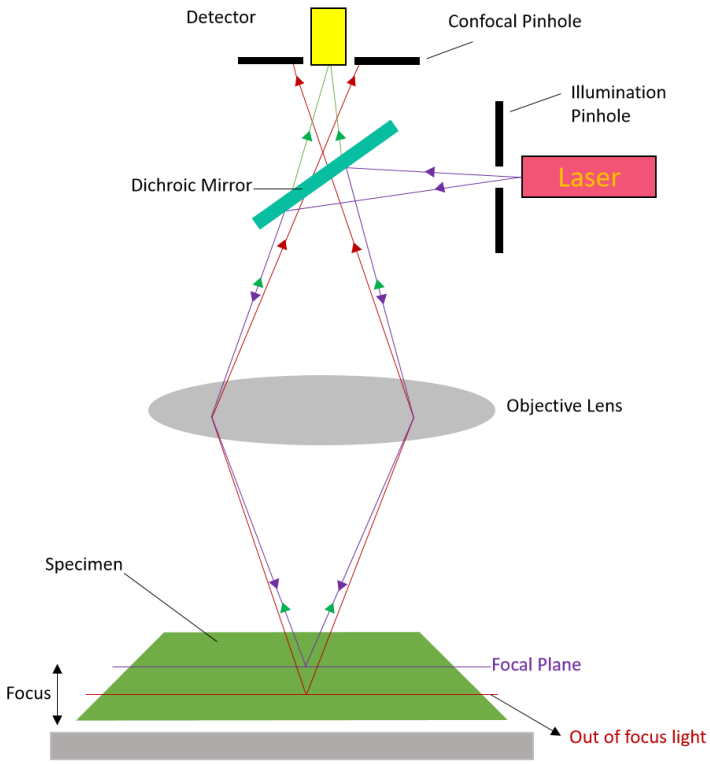

Figure 1-29: Schematic illustration of confocal fluorescence microscopy, (modified from [122]) .

The confocal fluorescence microscopy (Fig. 1-29) technique uses a laser source for exciting light at a specific wavelength as well as a specific fluorophore. The process starts when the excitation laser hits the specimen, generating high intensity fluorescence at a focal point. Then the laser light and the emission fluorescence pass through a dichroic mirror that is used to reflect the laser light with higher-energy (shorter-wavelength) and only allows fluorescent light with lower-energy (higher-wavelength) to reach the light detector. In this technique, the pinhole is also used to remove scattering light, resulting in the collection of lights from a focal point to obtain high resolution images of the scanned specimen [123].

1.7 Aims and Objectives of the Project

The aims of this project are to examine and compare certain fundamental aspects of molecular behaviour in both the aqueous and silica hydrogel phases. Hydrogels have multiple applications and, in most cases, their value in such applications lies in the way in which properties are modified on transiting from the aqueous to gel phase.

As outlined in Section 1.1, hydrogels could have been an extremely important phase or environmental condition in terms of the emergence of biological cells. Therefore, in order to more closely align our work with questions in this field, we have chosen to explore molecular behaviours of self-assembly. In the first instance our early work has and will focus on self-assembly, using sodium dodecylsulfate (SDS) as a probe amphiphile and silica hydorgels as a representative geologically relevant hydrogel.

The key objectives of of this project are:

1. To examine silica hydrogels with a view to characterising the surface morphology of the matrix silica.
2. To examine the effects of salts (concentration and identity) on the critical micelle concentration of amphiphiles in water and the hydrogel phase.
3. To examine the effects of SDS-Alcohol (C_2-OH, C_4-OH, C_6-OH, C_8-OH, C_{10}-OH, C_{12}-OH) on the CMCs in aqueous and hydrogel phase.
4. To examine vesicle formation of SDS-Alcoholic composites in silica hydrogels by fluorescent microscopy technique.

5. To estimate gelation time by using two different methods of light scattering by UV-Vis and turbidity measurements.

Chapter 2 Surface Analysis of Silica Hydrogels Matrices

The main objective of this section is to present a standard operating protocol for the formation of silica hydrogels preparation at two different concentration (0.5 and 0.75 M). Following this outline, studies of the surface morphologies are described for the prepared silica hydrogels at both concentrations.

Firstly, for the (0.75 M) silica hydrogel, the matrices was prepared by Critical Point Drying (CPD) and then examined by Scanning Electron Microscopy (SEM), Energy Dispersive X-ray spectroscopy (EDX) surface and area porosity measurements (BET). To probe the effects of salts present, samples of silica hydrogels were treated by dialysis for 48 h and 96 h respectively, followed by freeze drying of each of them prior to analysis. Subsequently, SEM, EDX and BET measurement were repeated and compared to data prior to treatment. In addition to normal scanning electron microscopy, a sample of the 0.5 M silica hydrogel was also examined using cryo-Scanning Electron Microscopy (cryo-SEM) which did not entail having to remove water prior to microscopic examination. This allowed us to provide an additional view of the silica matrix without any water-removal methodology having to be applied. In addition, Energy Dispersive X-ray spectroscopy (EDX) and surface and area porosity measurements (BET) were carried out on matrices prepared by freeze drying. Also, the undesirable salts was removed by dialysis process for 96 h, followed by freeze drying to prepare the matrices for SEM-EDX and BET measurement again. Finally, the main features of silica matrices, at both concentrations studied, were reported, discussed and supported by images and diagrams obtained via the technique used in this section.

2.1 Standard Operating Procedure for the Production of Silica Hydrogels

The procedure used by Barge et al. [34], a sol-gel synthesis method, has been followed in this work. The sol-gel has been preferred by researcher because it is simple, room temperature, scalable, efficient energy, and controllable [40]. Solution species undergo a series of hydrolysis and condensation steps, during the sol–gel process, resulting in the formation of a sol which is solid/liquid dispersed system. The sol phase can be formed by particles that are dispersed in the liquid phase, while the condensation process leads to a semi-rigid structure

containing a large quantity of solvent which is called a gel. The particles react with each other to form a cross linked 3D network that trapped solvent. Elimination of the trapped solvent results in the formation of a rigid structure called a xerogel [43].

This method, which we refer to as the Barge method, was slightly modified in the used concentration of sodium silicate to prepare different concentrations of silica hydrogels (SHGs), including 1.0, 0.75 and 0.5 M SHGs. This method was based on using Glacial Acetic Acid (GAA) as a protonation agent to acidify an alkaline solution of sodium silicate. Two solutions were prepared, Solution A was composed of sodium silicate solution (1.25 mL) which contains (≥ 27% of silicate) and (≥10 sodium hydroxide) mixed with deionised water (6.75 mL), and Solution B which comprised GAA (360 µL) in deionised water (7.6 mL). Upon the addition of Solution A to Solution B in a test tube, the combined mixture was inverted 2-3 times very slowly and with care to make sure that the components are mixed effectively, and also to prevent air bubble formation which may be caused by shaking the test tube. Subsequently, the mixture was left to stand for up to 24 hours without disturbance in order for the gelation process to be completed. The formation of silica hydrogel can be easily noticed by the naked eye, becoming solid and homogenous and cloudy matrix. Also, hydrogel formation is confirmed by inversion of the tube whereupon the contents are seen to be fixed in place.
This method consists of two stages chemical reaction, hydrolysis and condensation:

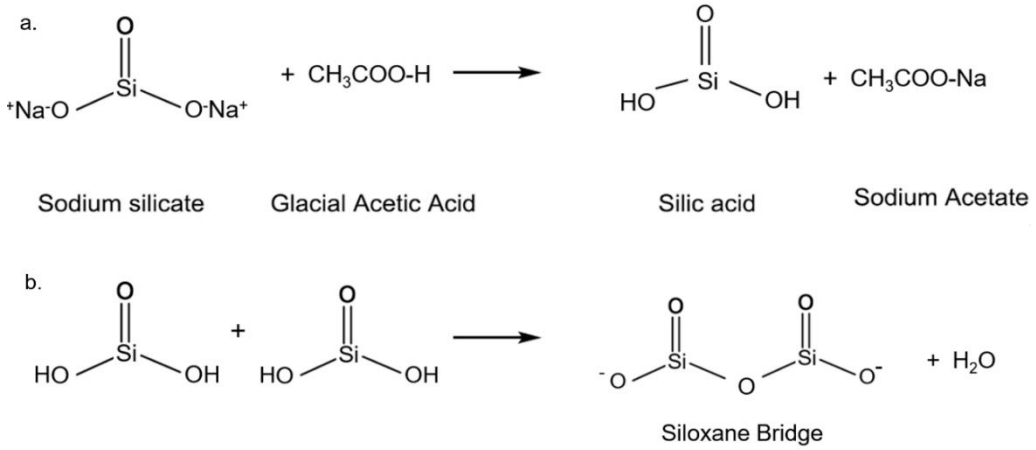

Figure 2-1: The two stages reaction (a) protonation, (b) condensation for the formation SHGs [124].

The protonation represents the hydrolysis stage of sodium silicate by GAA, resulting in the formation of silanol (Fig. 2-1.a). The following condensation stage (Fig. 2-1.b) involves a reaction between two silanol groups to form a siloxane bridge while extruding water.

It is worth mentioning that this process produces homogeneous, optically clear gels in a consistent manner with minimum precipitation, most notably when silicate concentration of 0.5 M is used.

2.1.1 Calculation for Preparation of Silica Hydrogels

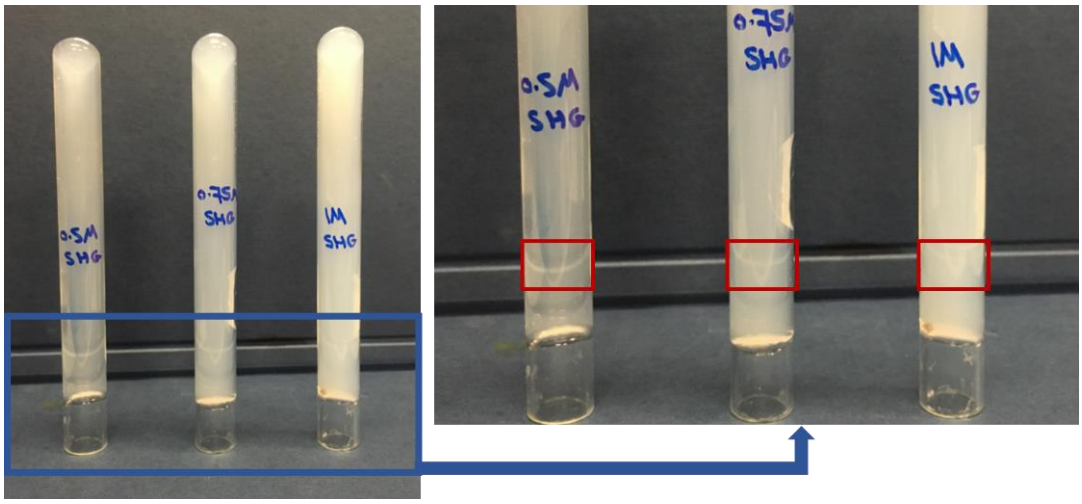

Figure 2-2: Preparing of silica hydrogel by Barge method with three different concentrations of 0.5, 0.75, and 1M.

The Barge method was used to prepare three different “concentrations” of hydrogels which we label as 0.5, 0.75, and 1.0 M (Fig. 2-2) based on the amount of silica present. The following is the calculation we used in our recent publication on the subject which explains how these labels are arrived at:

We have chosen to name our gel formulations as either 0.5 M, 0.75 M, or 1.0 M with SiO_2 on the basis of the following calculations:

The silicate solution that we use is graded at ≤ 27% SiO_2. Thus, this translates to ≤ 27 g in 100 g of the solution; which is 27/60.08 =0.45 moles. Therefore, as the density of the silicate solution we use is 1.39 g/mL, 100 g of silicate solution constitutes 72 mL of solution. Consequently, a solution which contains 0.45 moles in 72 mL of solution translates to a concentration of 6.25 M. Thus, as our silica hydrogel (SHG) formulations require diluting 1283, 1924, and 2565 µL respectively of this stock solution to 16 mL; dilution factors of 0.08, 0.12 and

0.16 ,respectively; these three formulations contain silica concentrations at 0.5 M, 0.75 M, and 1.0 M respectively.

2.2 SEM/EDX for Surface Analysis of Silica Hydrogels

For successful analysis of the surface of silica hydrogel matrix material, it is essential to have a dry sample, but the drying processes need to be performed in such a way as to prevent collapse or damage to the solid silica matrix. In this study, critical point drying was used to prepare the solid matrix of 0.75 M for both surface area (BET) and microscopy. The silica hydrogel matrix mineral was examined *via* BET and SEM under three sets of conditions: (i) post-CPD, (ii) post-CPD and dialysis for two days and (iii) post-CPD and dialysis for four days. The reasons for this selection are outlined below.

2.2.1 Critical Point Drying (CPD) Preparation

Silica hydrogels were prepared (in triplicate) with the 0.75 M. Over a period of three hours, the water in the hydrogels was replaced with acetone which was followed by treatment with liquid carbon dioxide with heating to 35°C. The final step involves an increase of pressure in the system to 1200 psi to evaborate carbon dioxide. This process produced a dried powder of silica hydrogel suitable for SEM/EDX analysis.

2.2.2 Freeze-Drying

After each dialysis process, the silica hydrogel was frozen and lyophilised in order to prepare them for SEM/EDX again. This is an essential operation to reduce the presence of undesirable salt such as sodium hydroxide. The lyophilisation process took a long time in this experiment because of the high content of water that was used to dissolve dried silica hydrogel. Freeze drying produced dried silica hydrogel as is shown in Fig. 2-3. 0.75 M silica hydrogel after freeze-drying process.

Figure 2-3: 0.75 M silica hydrogel after freeze-drying process.

2.3 Scanning Electron Microscopy

A Scanning Electron Microscopy (SEM) study has been conducted for our 0.75 M silica hydrogel sample. This analysis was performed on the 0.75 M silica samples after (i) critical point drying (CPD) with no further processing, (ii) CPD followed by dialysis into deionised water for 48 h and (iii) CPD followed by dialysis into deionised water for a period of 4 days. Analysis of the SEM results on the sample (i) revealed small but reproducible amounts of sodium and phosphorus in the sample. The presence of sodium is not unexpected as there is sodium hydroxide (NaOH) present in the starting water-glass silicate preparation. The presence of phosphorus, presumably as phosphate, is more perplexing and may be due to some form of contamination as other members of the group have been exploring phosphate retention in SHG's. In order to remove these salt from the surface, dialysis was performed, a well-established process for removing salts from insoluble matrices. This process was performed twice, once for a period of 2 days and, when SEM-EDX analysis revealed that the samples still contained salts, a second round of dialysis was performed for a longer period of time, four days, which results in salt removal.

2.3.1 SEM/EDX Analysis of 0.75 M Silica Hydrogel

2.3.1.1 After Critical Point Drying (CPD)

Fig. 2-4 are reproduced SEM images at four levels of magnification. The first, lowest magnification image (200 µm scale), reveals a fractured surficial material. Upon increasing the magnification from 200 µm down to 5 µm, the rough surface, greater porosity and granularity of the sample is shown.

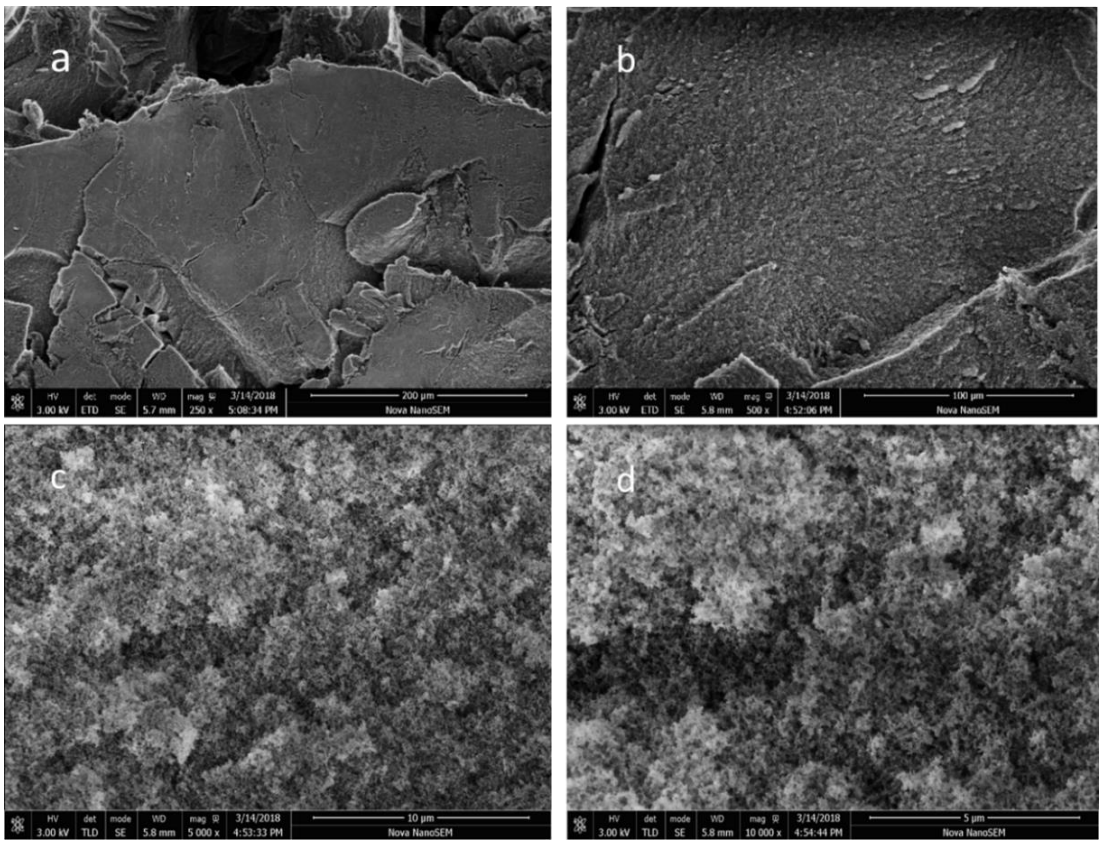

Figure 2-4: 0.75 M silica hydrogel after critical point drying. a. 200 µm, b.100 µm, c 10 µm, d. 5 µm.

However, EDX analysis reveals, in addition to the expected silicon and oxygen, that both sodium and phosphorus are also present (Fig.2-5).

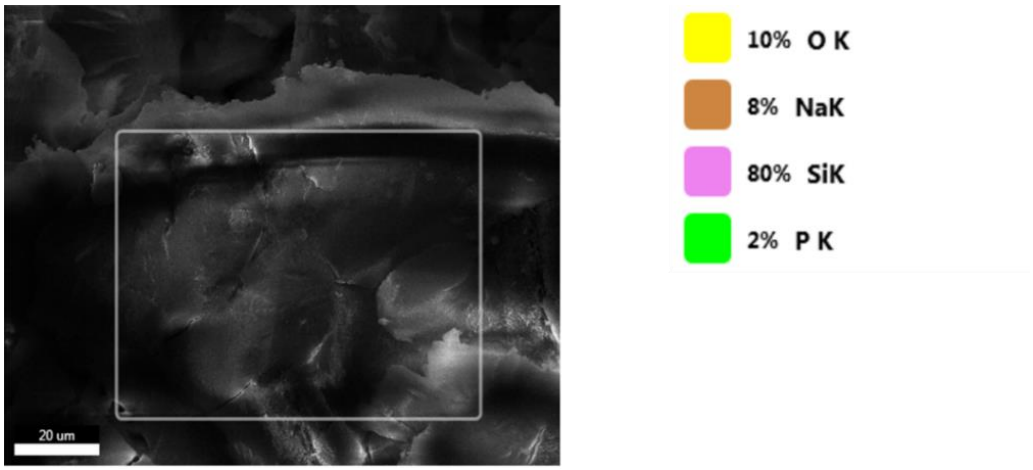

Figure 2-5: Mineral analysis by EDX of 0.75 M silica hydrogel shown the percentages of each element.

Sodium is to be expected as the silicate solution used to formulate the hydrogel also contains sodium hydroxide. The presence of phosphorus (P) is, however, somewhat more puzzling but it is plausible that P could have been introduced via

a contaminated syringe being used by another member in the group. Analysis of the silica matrix, post-CPD, via BET measurements allows us to return a surface area of 344.0713 m^2/g for 0.234 g of the sample with a 0.9999903 correlation coefficient.

2.3.1.2 After Dialysis (48 h)

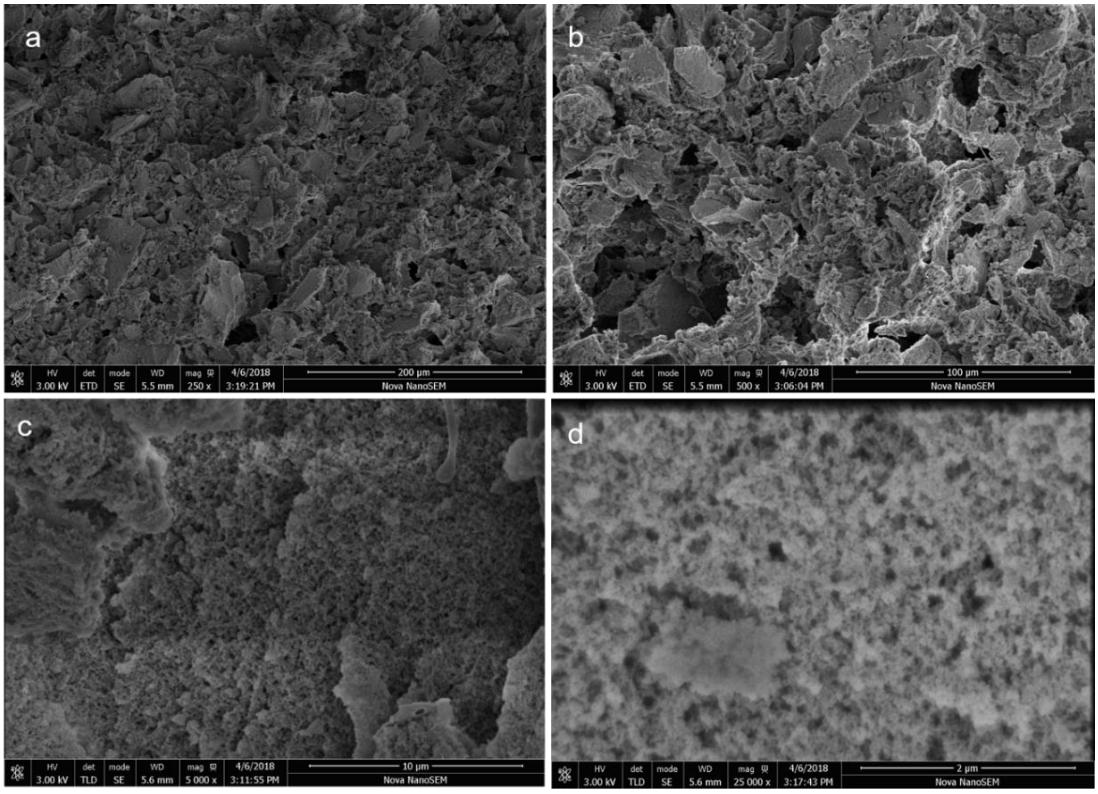

Figure 2-6: SEM analysis of 0.75 M silica hydrogel matrix after 48h dialysis, followed by freeze-drying process, a. 200 µm, b. 100 µm, c. 10 µm, d. 2 µm.

Dialysis is a valuable method for removing soluble components, in this case, salts, from an insoluble matrix. Dialysis was therefore performed on the post-CPD silica matrix for a period of 2 days after which time the matrix sample was freeze-dried and analysed again *via* SEM-EDX. The resulting images (shown in Fig. 2-6) suggest that the matrix structure and morphology are largely unchanged from those observed post-CPD immediately.

EDX analysis (Fig. 2-7) revealed that there was still some sodium salt which remained although it appeared significantly reduced to the post CPD sample.

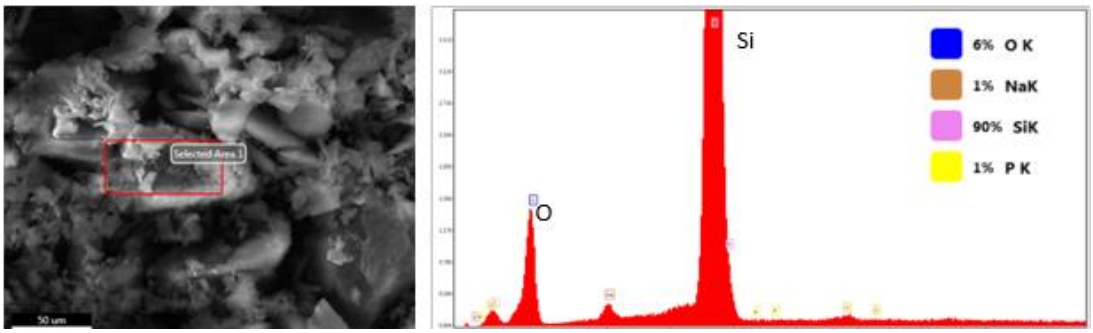

Figure 2-7: EDX mineral analysis of 0.75 M silica hydrogel shown the percentage of mineral present on the selected area red rectangle after short dialysis.

BET measurements were also made again after this first round of dialysis, the characterisation of the silica surface revealed a significant increase in the surface area to 473.202 m^2/g for 0.1679 g of the sample correlation coefficient of 0.9999551, consistent with a reduction in salt content and exposure of porous matrix mineral.

It can be noticed that the weight of the dried silica was slightly less in the second BET measurement, due to a slight loss of the sample mass during recovery from dialysis.

2.3.1.3 After Dialysis (96 h)

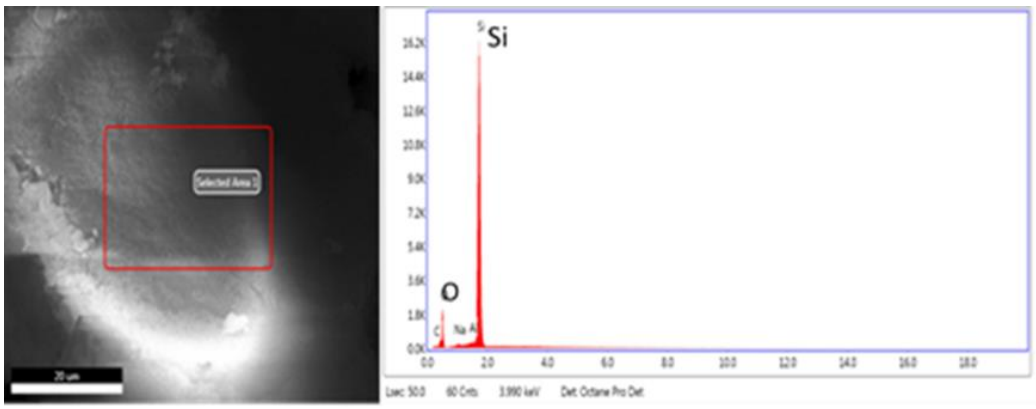

Figure 2-8: EDX mineral analysis of 0.75 M silica hydrogel showing the percentage of mineral present on the selected area red square after long dialysis.

A decision was taken to perform second dialysis procedure but over a longer period of time (4 days, 96 h) in order to remove as much salt as possible. Subsequently, EDX analysis (Fig. 2-8) demonstrated that this was essentially achieved after 96 h, with very low levels of sodium and no phosphorus remaining in the matrix. Morphologically again, there was little change in the structural integrity of the silica matrix (Fig. 2-9).

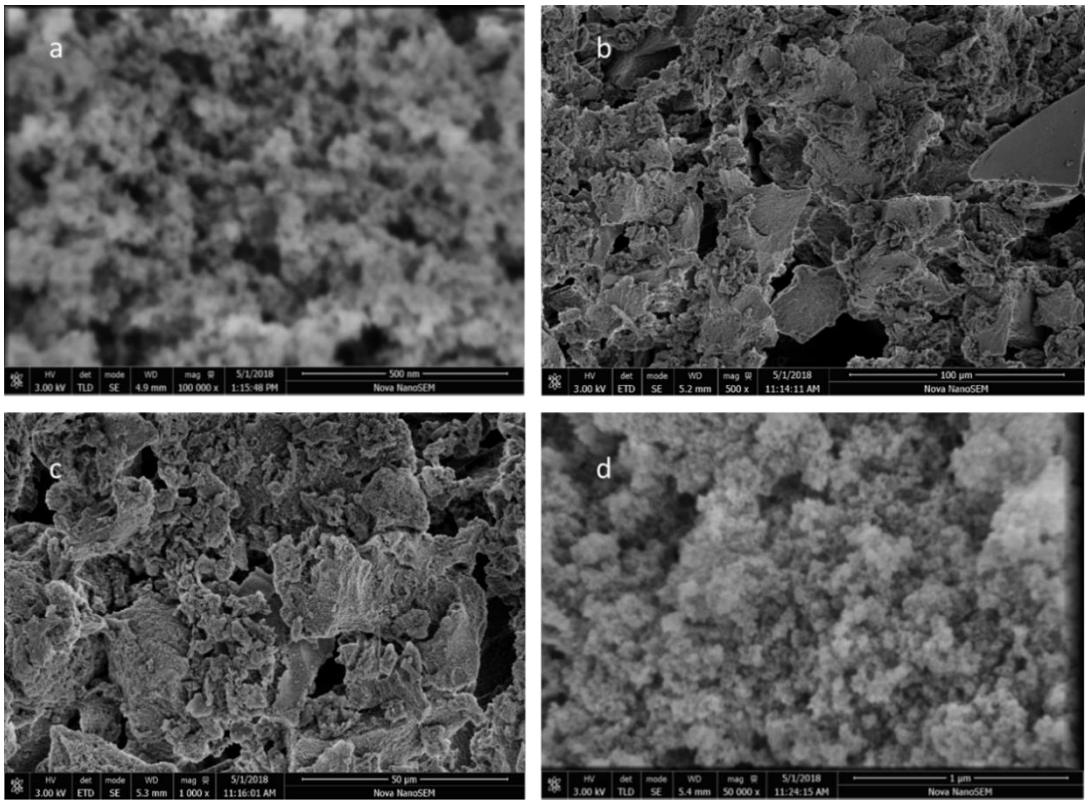

Figure 2-9: 0.75 M silica hydrogel after critical point drying. a. 500 µm, b.100 µm, c. 50 µm, d. 1 nm.

2.3.2 Cryo-SEM for Surface Analysis of 0.5 M Silica Hydrogels

2.3.2.1 Preparation of the 0.5 M Silica Hydrogel for Cryo-SEM

The major goal of cryo-SEM is to retain the structure of the hydrated material [58]. The sample was mounted on a platform with a layer of a carbon-rich conductive adhesive to prevent electron interference in SEM imaging or analysis. The stand holding the frozen item was then placed under liquid nitrogen and brought back into a tiny cylindrical container. This was done to avoid serious contamination of the gas molecules when slipping the sample into the freezer chamber. The freezer camper was prepared using an externally controlled knife. Then a thin coating was deposited on top to improve electrical conductivity. Finally, a rod was used to put the fractioned material into the chamber.

2.3.2.2 Cryo-SEM Analysis of 0.5 M Silica Hydrogel

To observe the morphology of the hydrogel surface, the sample were characterised in cryo-Scanning Electron Microscopy (cryo-SEM) because of its ability for mapping the water distribution within matrix and preserving its structural integrity.

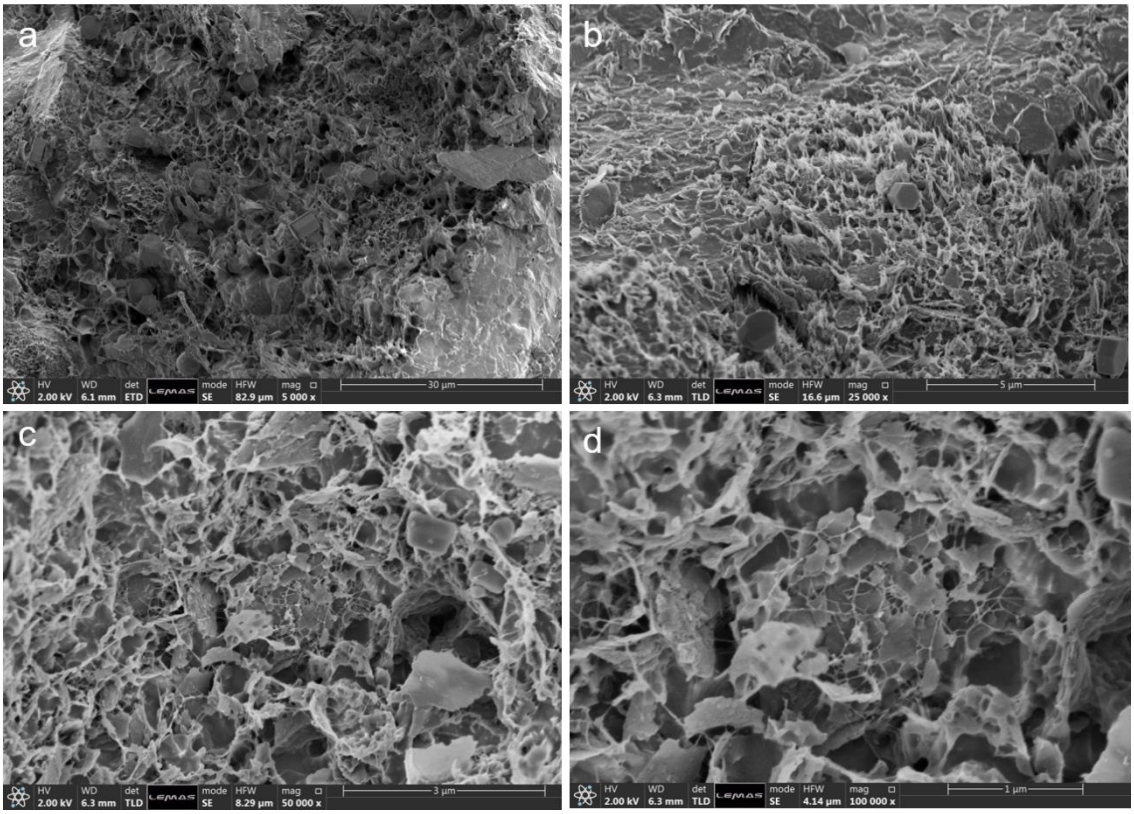

Figure 2-10: Cryo-SEM analysis of 0.5 M silica hydrogel a. 30 µm, b. 5 µm, c. 3 µm, d. 1 µm.

Fig. 2-10 (a to d) shows a series of micrographs with four levels of magnification images. At the lowest magnification including a and b (30, 5 µm scale), the SEM shows a porous material and the presence of ice hexagonal. Upon increasing the magnification from 30 µm down to 1 µm, the greater porosity and the crosslinking of the sample are revealed (d).

It is worth mentioning that the presence of hexagonal ice (Fig. 2-11), indicated by the blue arrows), which forms either in the liquid nitrogen then sticks to the sample when they are plunged, or when it was transferred from the slusher to the SEM. It is virtually impossible to avoid getting any ice on the sample while doing cryo-SEM. Thompson et al. [125] stated that ice contamination weakens the specimen's structural integrity by removing water molecules from the hydration shells or the specimen itself which results in reducing image quality by diffracting

electrons. Hexagonal ice contamination during the freezing process can be reduced by working in humidity controlled conditions and reducing ice contamination in liquid nitrogen.

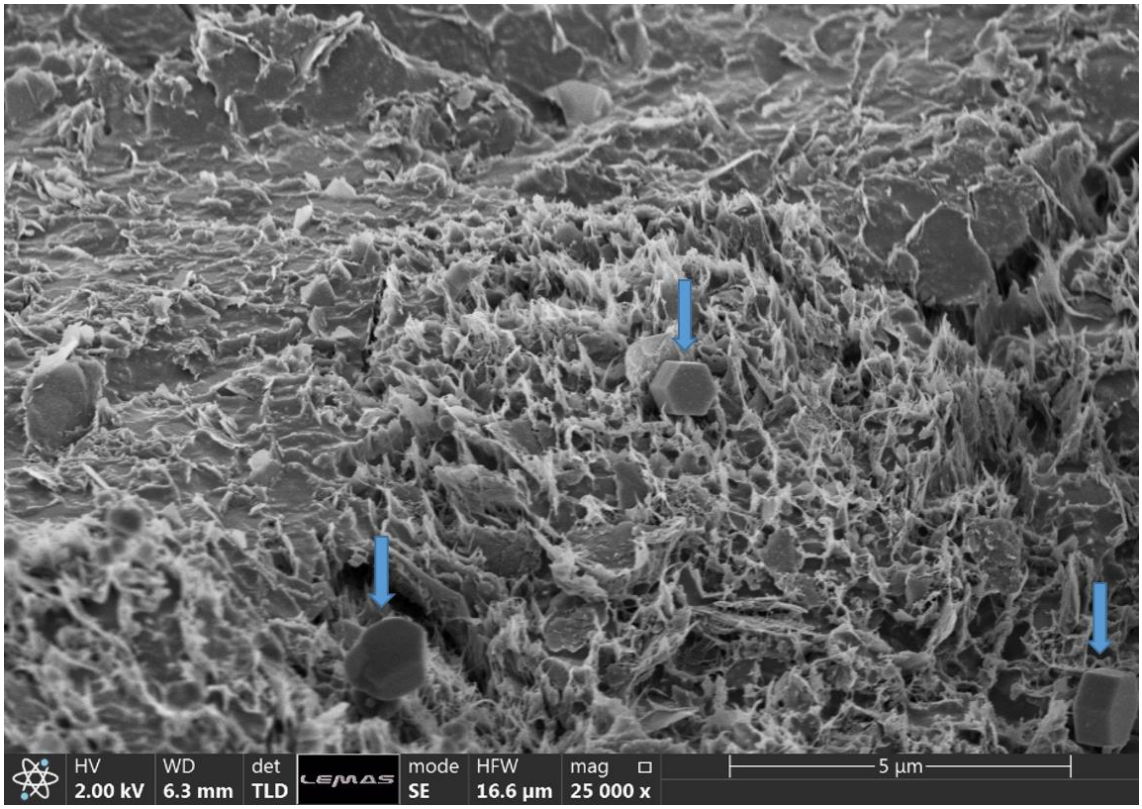

Figure 2-11: Hexagonal ice contamination during the freezing process.

EDX analysis (Fig. 2-12), which was done in collaboration with a Master degree student, Amy Nicholls, reveals the presence of Si and O from the silica hydrogel matrix as expected. Also, the sample contained minor (trace) levels of salt which was expected due to the sodium hydroxide present in the silicate solution and acetic acid used to produce the SHG. In addition to that, the EDX shows signal for boron signal whose presence is less obvious because of its presence in the stock solution. The surface area of the 0.5 SHG sample was determined by BET analysis to be 8.0752 m^2/g of 0.1665 g, with a correlation coefficient of 0.9961224, which could be related to the salt present in the sample, which could explain the decreased surface area.

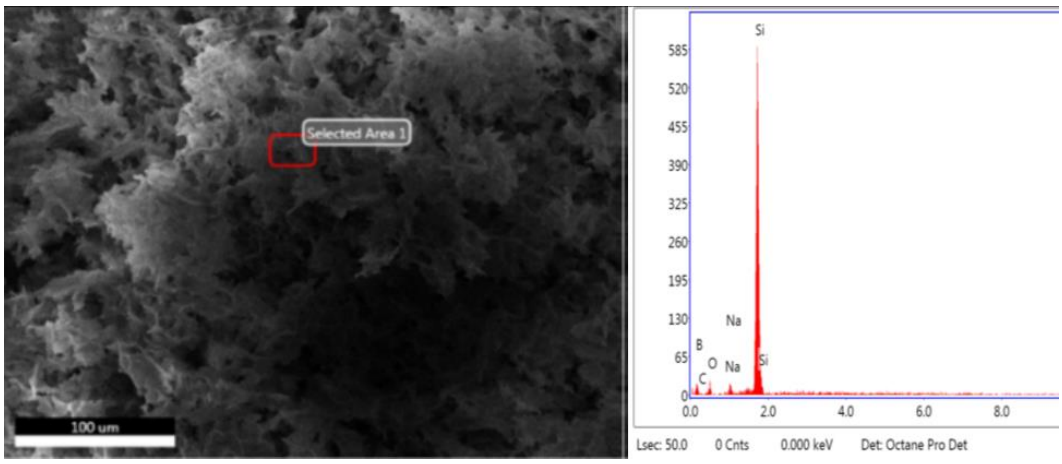

Figure 2-12: EDX mineral analysis of 0.5 M silica hydrogel shown the percentage of mineral present on the selected area red square after four days dialysis.

To remove undesired salts from the original used material to make this hydrogel, dialysis was conducted for four days, followed by lyophilisation, then examined by SEM/EDX and BET measurement.

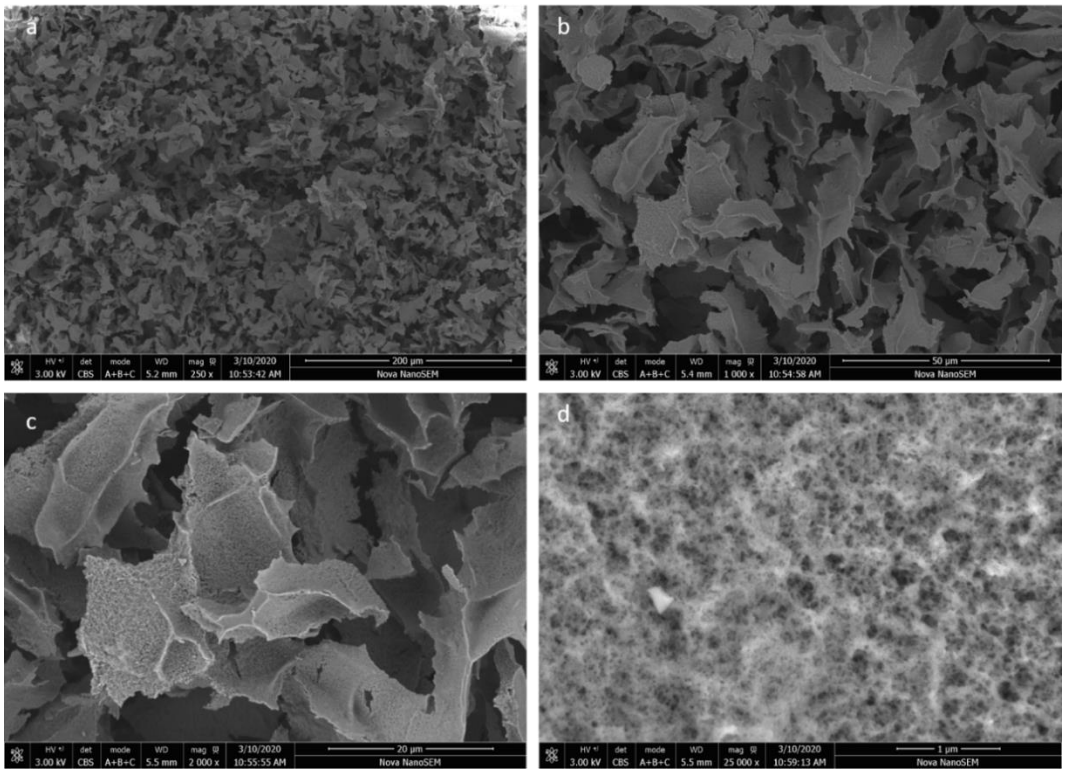

Figure 2-13: SEM analysis of 0.5 M silica hydrogel matrix after four days dialysis, and after freeze-drying process, a. 200 µm, b. 50 µm, c. 20 µm, d.1 µm.

The resulting images reveal greater porosity of the morphology in Fig. 2- 13 (a to d), which can explain the BET measurement of a very high surface area (718.7201m^2/g) of 0.1679 g with a 0.9997575 correlation coefficient.

The EDX analysis for the composite matrix of selected area indicated that the elemental composition of the materials was O and Si with no Sodium Fig. 2-14.

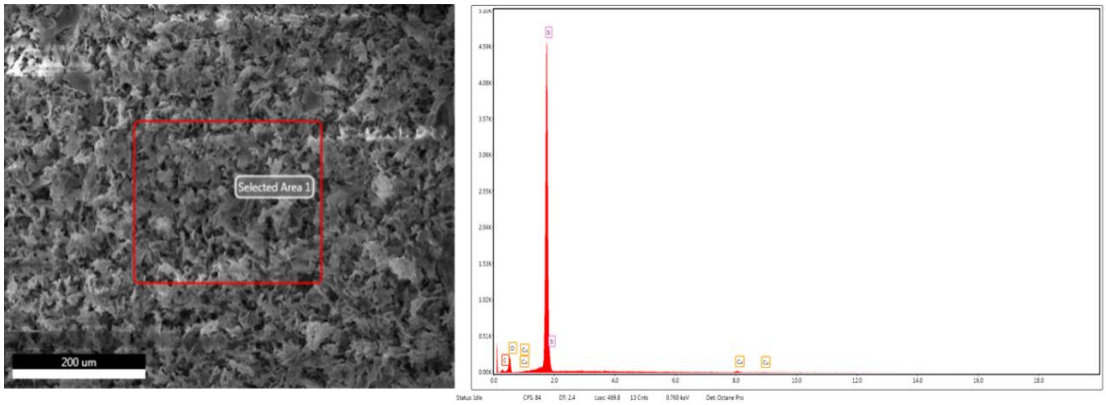

Figure 2-14: EDX mineral analysis of 0.5 M silica hydrogel shown the presence of O and Si present on the selected area red rectangle after four days dialysis.

Depending on the previous analyses of 0.75 and 0.5 M SHG using SEM and BET measurements, the 0.5 M SHG images revealed more pore structure than the 0.75 M SHG (Fig. 2-6 and Fig. 2-13), the BET measurement also showed a higher surface area for 0.5 M SHG. Such pore structure can be used to retain the physical properties of the SHG structure.

In addition, of the three concentrations 1, 0.75, and 0.5 M SHG, 0.5 was the most transparent, as easily seen by the naked eye and shown in Fig. 2.2. Its advantage as an optical material makes 0.5 SHG useful as a medium for estimating the CMC of the SDS amphiphile. This feature also makes 0.5 M SHG optimal for determining the self-assembly of the SDS amphiphile.

2.4 Conclusion

Following is a summary of the main points of this chapter's content and main findings.

1. Surface analysis of the matrix of 0.75 M of silica hydrogel by using SEM, EDX, BET was obtained several times, due to the presence of undesirable salts. Critical point drying, freeze-drying and dialysis offer reliable

techniques to illustrate a porous morphology with surface area of 473.202 m^2/g for 0.1679 g of the sample with correlation coefficient of 0.9999551.

2. Surface analysis of the matrix of 0.5 M of silica hydrogel by using cryo-SEM, EDX, BET was conducted to illustrate a porous morphology with surface area of 718.7201 m^2/g of 0.1679 g with a 0.9997575 correlation coefficient.

Chapter 3 Measuring Critical Micelle Concentration of Sodium Dodecyl Sulphate in Aqueous and the Hydrogel Phase in the Presence of Salts

3.1 Aim of this chapter

One of the key aspects of this project is to explore the effects of salts on critical micelle concentrations (CMCs) of the representative amphiphile sodium dodecyl sulphate (SDS) and how such behaviour might differ when the self-assembly process is examined in both aqueous and silica hydrogel phases. Within the context of origin of life studies, self-assembly of simple amphiphiles constitutes one of the fundamental processes available to primitive organisms and any exploration of how such processes might be influenced within a medium more closely related to a biological cellular medium than water, is likely to hold some value. It should be mentioned here that our selection of SDS is not based on any reasoned existence of this specific chemical on the early earth, but rather as an example of chemically simple, mono-chain amphiphiles similar in nature to those that may have been prevalent on the early earth [83].

From previous work performed by Mr Kamal Albdeery in this laboratory, it was demonstrated that the CMC of the anionic amphiphile SDS decreased significantly when moving from the non-salt containing aqueous phase to a silica hydrogel environment. The question we wished to answer is: *to what extent does the change in CMC measurement reflect the presence of salts and is there any dependence on the type of salt present in the SHG phase.* Therefore, in order to address these issues we have constructed four experimental sets:

1. To measure the CMC of SDS in aqueous solution and hydrogel phase in the presence of different concentrations of the following sodium salts (carbonates, silicates, chlorides, sulfates, and phosphates) and magnesium chloride.
2. To measure the CMC of SDS in aqueous solution and hydrogel phase in the presence of a simulated seawater mixture.
3. To measure the CMC of SDS in aqueous phase in the presence of different concentrations of the colorimetric dye pinacyanol chloride, a cationic dye molecule used as a reporter molecule for CMC measurements

It is a widespread view that in prebiotic eras, only the simple processes would

have been capable of occurring [89]. Therefore, one important example of these is ‘spontaneous' activities, such as self-assembly and hydrophobic interactions [89]. Accordingly, self-assembly could be regarded as a first step in developing an organised system that displays molecular complexity and performs a meaningful function [126]. For a model protocell construction in the laboratory, it is very important to understand the self-assembly of different biological materials starting from simple to complex structures for mimicking the pre-biotic environment [83]. It has been proposed that protocells have membranes, but they are not the same as the modern cell membranes [127]. The membrane of a modern cell is composed of nanometer-sized long-chain amphiphilic molecules, such as the mixture of phospholipids and glycolipids with one hydrophilic and two hydrophobic acyl chains (Fig. 3-1.a up) [128]. Another example is Fatty acid (Fig 3-1. a down) which can form different self-assembly structures depending on the pH, such as micelle and vesicle (Fig. 3-1.b) [129].

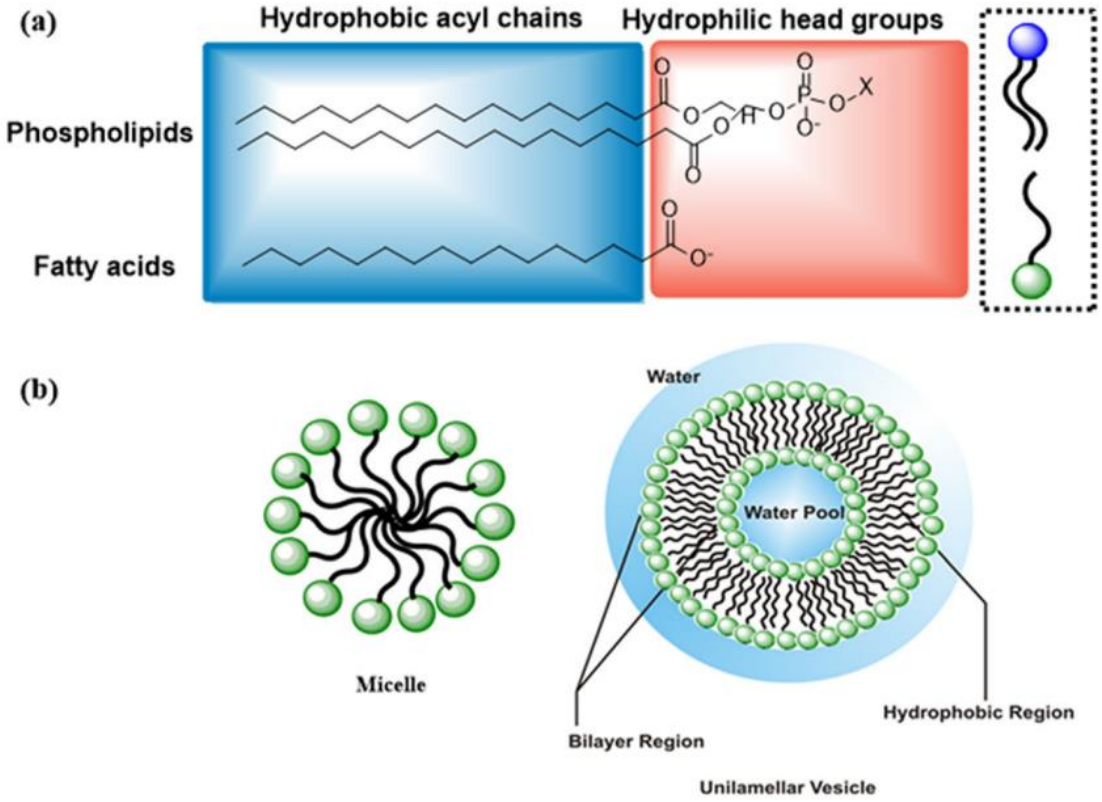

Figure 3-1: a) The structure of phospholipids and fatty Acids. b) Self-assembly of fatty acid with different structures such as micelle and vesicles formed over a wider pH range [127].

On this basis, the idea that compartmentalisation is a critical principle for the origin of life on the earth, as it results in structures which could have evolved into

the first functional cellular units [126]. Early work and research on surfactant assemblies was conducted with micelles and reverse micelles aqueous phase [130]. Therefore, the one that is most relevant to the study presented in this thesis is the effect of transitioning from an aqueous to a hydrogel phase on self-assembly processes and CMCs. To put that into context, biological cell membranes are composed of self-assembled structures that are required for the development of biological activities in live cells and functional organs [131]. These structures originate from a hydrogel-based cellular cytosol substance [24].

In addition to the importance of doing those reactions in hydrogels phase instead of using water as environmental media, the examination of self-assembly in the presence of salts is not less important because a wide range of membranes are likely to require some salt to form. Membranes composed of single chain amphiphiles (SCA) are frequently stable at significantly higher salt concentrations [82]. Also, some mixtures of single-chain amphiphiles in seawater are able to form more stable viscles. Namani and Deamer showed the formation of stable vesicles by a mixture of decanoic acid and decylamine in the presence of seawater [132].

In this chapter, we have started to examine the self-assembly of micelle formation as a first step in the presence of components of artificial seawater: inorganic salts (sodium carbonates, sodium silicates, sodium chlorides, sodium sulfates, sodium phosphates and magnesium chloride) which are the subject of this current chapter, and artificial seawater before examining organic additives (such as alcohols) which will be discussed in Chapter 4.

3.2 Measuring the Critical Micelle Concentration of SDS

Critical micelle concentrations of SDS were measured using spectrophotometry at ambient temperature, using pinacyanol chloride as a reporter molecule as described in experimental section. The particular advantage of this technique over other methods of CMC measurement (e.g. surface tensiometry, fluorescence, solution conductivity…) is that it can be used to estimate the CMC of SDS in both aqueous and hydrogel phase which will form an important part of this study going forward. The same procedure was used in all experiments to measure the absorbance level of different concentrations of SDS between 500 and 650 nm. It was found that the wavelength of maximum absorbance (λ_{max})

was 608 in aqueous phase and 609 nm in the SHG phase, which is in good agreement with that reported by Khouri et al. [110]. Each absorbance at λ_{max} of 608 nm or 609 nm was plotted against the concentration of the SDS surfactant and from the plots of absorbance vs the concentration of SDS, there are discontinuities which represent the transition line from molecular amphiphiles to micelle formation, which is indicated by the intercalation of the pinacyanol cation into the self-assembled structure of the SDS [103]. This results in a rather pronounced change to the self-assembly behaviour of pinacyanol chloride itself and hence to the colorimetric properties of the reporter dye from which CMC measurements can be obtained. All experiments with different salts were performed at least four times.

3.2.1 Measuring the Critical Micelle Concentration of SDS in Deionized Water

In order to be able to examine the influence of salts on the critical micelle concentration of SDS in silica hydrogel media, it was first necessary to explore salt effects in aqueous solution as a control, the CMC of SDS was obtained in deionised water only to see the influence of adding salts on the CMC of SDS values. As a salt-free control, CMC values were first measured in deionised water with salt saturation of 0 M (with a solution conductivity of 6.35 µs).

Depending on the method for estimating CMC of SDS mentioned in Section 3.2, the absorbance level of different concentrations of SDS between 500 and 650 nm was measured. Three independent sets of experiments were performed so that averages and estimated standard deviations (e.s.d) could be reported. The wavelength of maximum absorbance (λ_{max}) was found to be 608 nm. Then, the average of the absorbance of the three runs and the error (estimated standard deviation of sample) concentration of SDS was plotted against the absorbance value at λ_{max} (Fig. 3-2).

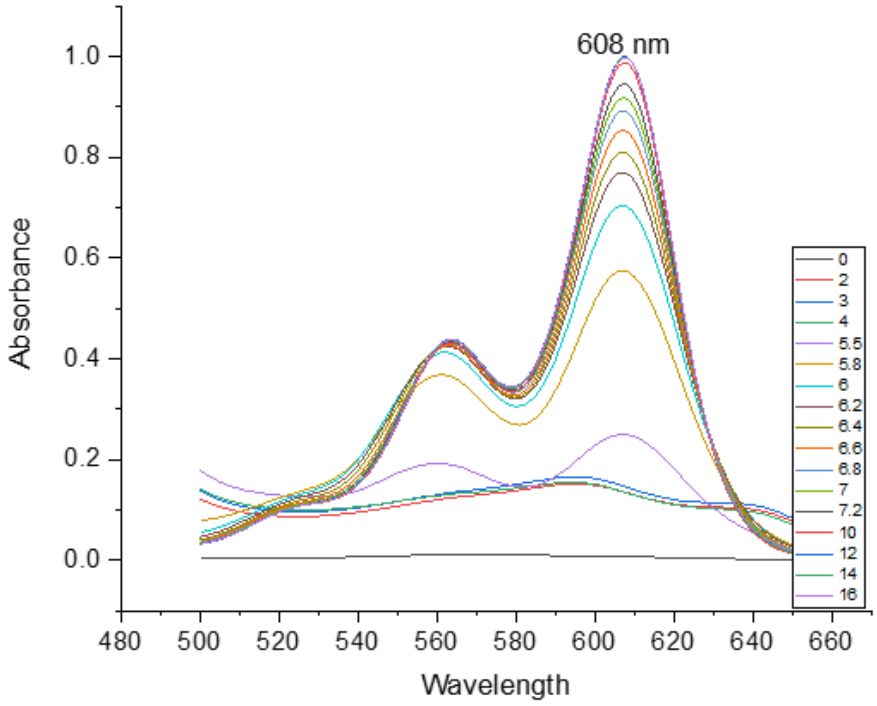

Figure 3-2: The raw data for determining the (λmax) of PIC in aqueous solution in the presence of a range of SDS concentrations from 2 to 16 mM.

Then background correction was applied as shown in Fig. 3-3 by using Origin software. Baseline correction is used as a pre-processing technique to remove background effects.

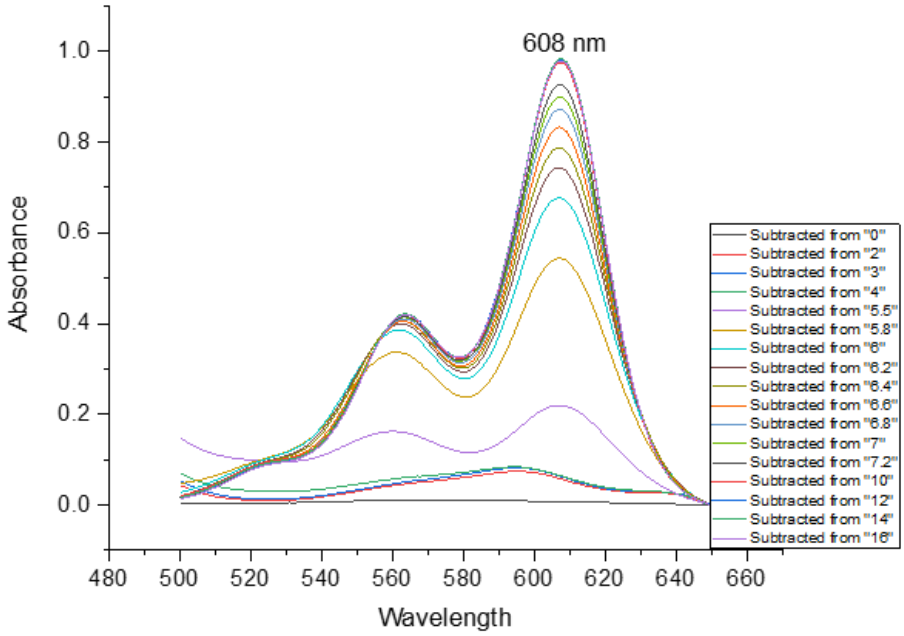

Figure 3-3: Determination of the (λ_{max}) of PIC in aqueous solution in the presence of a range of SDS concentrations from 2 to 16 mM after baseline correction.

After that, each absorbance at λ_{max} of 608 nm was plotted against the concentration of the SDS surfactant and in the plots of absorbance vs the concentration of SDS, there are discontinuities which represent the transition line from molecular amphiphiles to micelle formations, which we presume is a reflection of the intercalation of the pinacyanol cation into the self-assembled structure of the SDS. The average of the three absorbance runs and the standard deviation are collected as an example in Table 3-1.

Table 3-1 The average and standard deviations of the absorption values of different concentrations of SDS samples at 608 nm in the aqueous phase.

[SDS] mM	1st run	2nd run	3rd run	4th run	Average	St. Dev.
0.0	0.0066	0.0056	0.0083	0.0071	0.0069	0.0011
2.0	0.0539	0.0593	0.0559	0.0563	0.0563	0.0022
3.0	0.0582	0.0639	0.0626	0.0621	0.0617	0.0025
4.0	0.0615	0.0651	0.0655	0.0610	0.0633	0.0024
5.5	0.2241	0.2127	0.2171	0.2206	0.2186	0.0049
5.8	0.5445	0.5406	0.5414	0.5438	0.5426	0.0019
6.0	0.6799	0.6710	0.6740	0.6767	0.6754	0.0038
6.2	0.7424	0.7401	0.7438	0.7420	0.7421	0.0015
6.4	0.7872	0.7821	0.7873	0.7880	0.7861	0.0027
6.6	0.8199	0.8376	0.8395	0.8260	0.8308	0.0094
6.8	0.8717	0.8670	0.8746	0.8730	0.8716	0.0033
7.0	0.8868	0.9068	0.9057	0.8908	0.8975	0.0102
7.2	0.9161	0.9356	0.9355	0.9181	0.9263	0.0107
10.0	0.9831	0.9392	1.0116	0.9674	0.9753	0.0303
12.0	0.9759	0.9818	0.9726	0.9927	0.9807	0.0088
14.0	1.0263	0.9870	0.9400	0.9784	0.9829	0.0354
16.0	0.9741	0.9733	0.9818	0.9865	0.9789	0.0063

It is worth reiterating that for a given set of data, we are plotting the same lambda value each time; that this does not represent a variable in each data run. The maximum absorbance of PIC was plotted for each concentration of SDS to give a graph showing the relationship between the SDS concentration in millimolar (mM) in the range 1-16 mM against the average of absorbance values as shown in Fig. 3-4 which reveals a strong change in the absorbance as a function of concentration of SDS of the peak absorbance values around the inflection point. The CMC values of the surfactant SDS is estimated from the graph at 6.7 ± 0.3 with shaded area that represents 95% confidence that was done by Origin software.

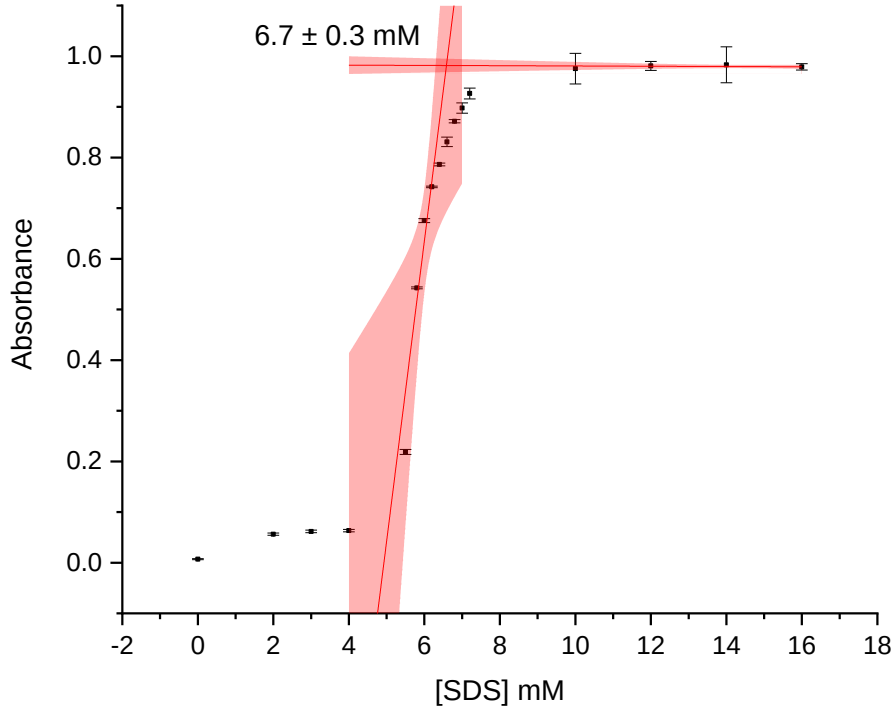

Figure 3-4: Estimation of the CMC values by plotting specific absorbance of SDS versus concentration at the wavelength of 608 nm in deionized water. The shaded line represents the fitting line with 95% confidence.

The value obtained in aqueous medium (6.7 ± 0.3 x 10^{-3} M) is very close to the value found in the literature using the spectrophotometric and conductimetric (8.0 x10^{-3} M) [97], fluorimetric (8 x 10^{-3} M) [102], and conductivity methods (7.8 x 10^{-3} M) [98]. In general, this result is within the practical estimated range reported by Lukanov for CMC of SDS which may vary from 7.6 to 8.3 x 10^{-3} M at 25 °C [133].

All of the figures of estimating the values of the CMC of SDS in different media were drawn using the Fitted Curve Plot Analysis tool on Origin software (2016, 64 Bit). The expression of confidence interval means that the width of the confidence band is proportional to the standard error of the predicted y value (the value of the absorbance in this case).

The fitted curve, as well as its confidence band, are plotted on the Fitted Curves Plot, which can help estimate the value of CMCs. The confidence bands in this case of our experiments is 95 %, showing the limits of all possible fitted lines for the given data, to draw the best-fit line.

The two lines drawn in every figure were determined by the correlation coefficient, and the equation of all fitted lines are as shown in the Appendix (9.1.3), which

also contains all of the following experiments in both deionised and SHG phases.

The procedure of measuring CMC of SDS to manipulate data in the deionized water was followed in all experiments in both aqueous and silica hydrogel media.

3.2.2 Measuring the Critical Micelle Concentration of SDS in the Presence of Salts in Aqueous Phase

The aim of those experiments is to explore the impact of salts on critical micelle concentrations (CMC's) of SDS surfactant and how this might influence such measurements in the gel phase. The question we wished to answer is: *to what extent does the change in CMC measurement reflect the presence of salts and is there any dependence on the type of salt present in the SHG phase.* Several salts have been selected, which are present in artificial seawater with the same cation, namely sodium (silicates, carbonates, chlorides, sulfates, phosphates). In addition to these, some preliminary studies have also been performed using magnesium chloride. Also, the CMC of SDS in the presence of two specific ratios of seawater was examined. Final results in the aqueous phase in the presence of salts represented the lower (1×10^{-6} M) and high concentrations (1×10^{-5} M) of PLC dye.

3.2.2.1 In the Presence of Sodium Silicate Salts

The CMC of SDS has been measured using the same method as described for aqueous solutions above to investigate the effect of sodium silicate on the self-assembly of SDS. A selection of 14 different sodium silicate concentrations were used (0, 0.015, 0.025, 0.04, 0.05, 0.1, 0.15, 0.2, 0.25, 0.35, 0.5, 0.7, 0.9, 1.2, and 1.4 M), in each case these concentrations can only be interpreted as indicative due to the nature of the commercial silicate solutions calibration. Nevertheless, any differences should be systematic.

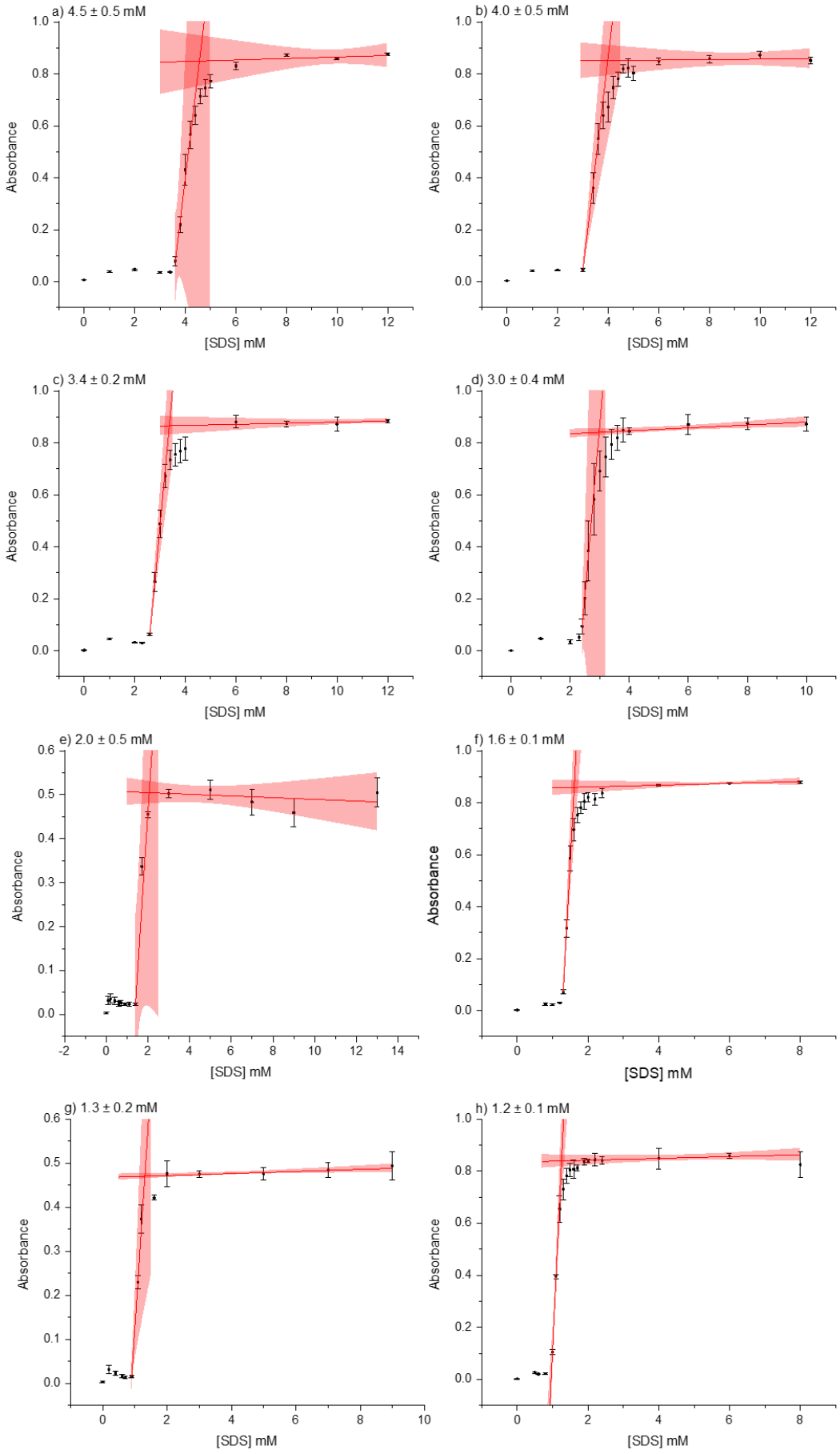
a) 4.5 ± 0.5 mM
b) 4.0 ± 0.5 mM
c) 3.4 ± 0.2 mM
d) 3.0 ± 0.4 mM
e) 2.0 ± 0.5 mM
f) 1.6 ± 0.1 mM
g) 1.3 ± 0.2 mM
h) 1.2 ± 0.1 mM
Absorbance
[SDS] mM

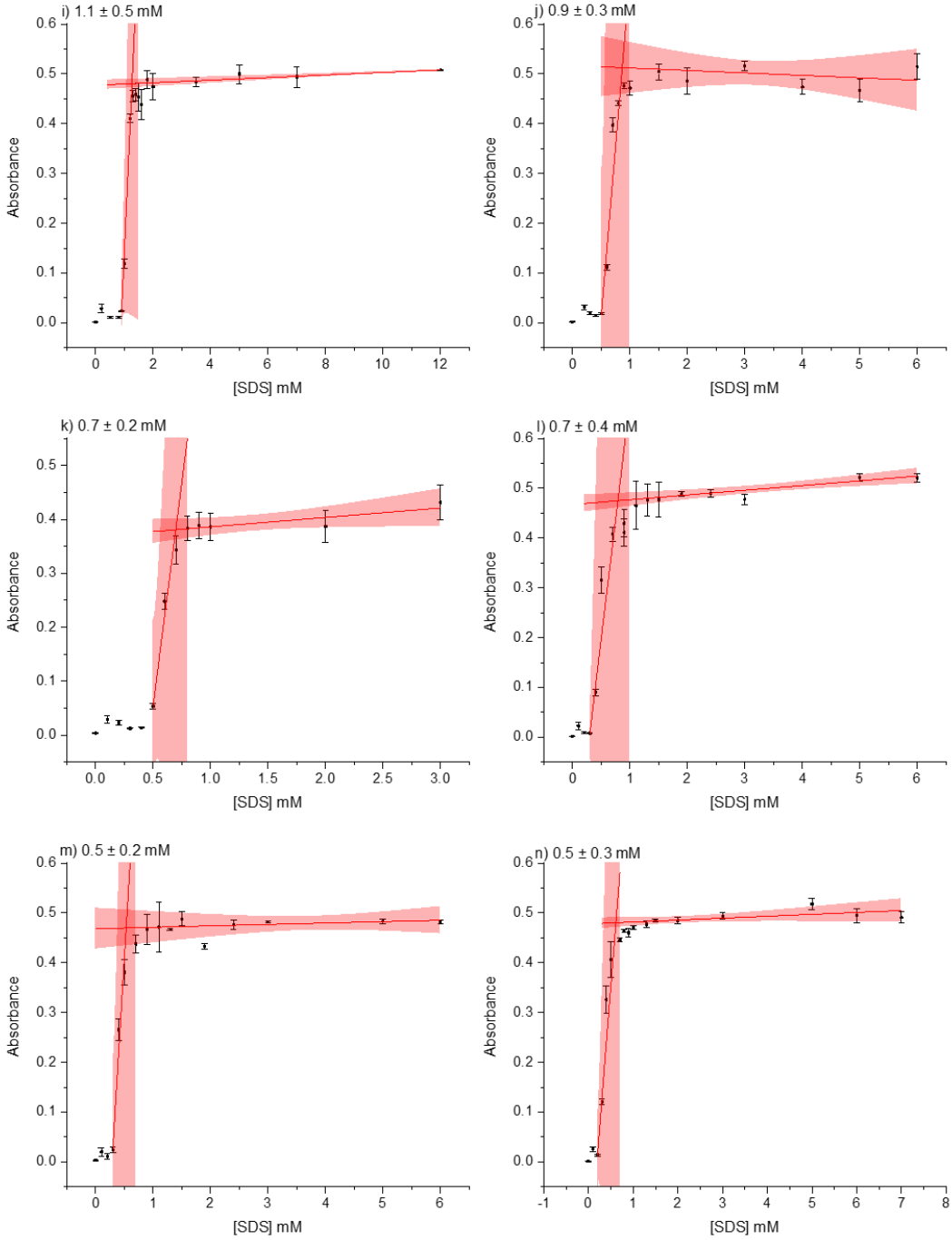

Figure 3-5: Estimation of the CMC values by plotting specific absorbance of SDS versus concentration at the wavelength of 608 nm in silicate solution: a) 0.015 M , b) 0.025 M , c) 0.04 M , d) 0.05 M , e) 0.1 M, f) 0.15 M , g) 0.2 M , h) 0.25 M , i) 0.35 M , j) 0.5 M , k) 0.7 M , l) 0.9 M , m) 1.2 M , n) 1.4 M of silicate. The shaded line represents the fitting line with 95% confidence.

All the graphs for silicate (Fig. 3-5 a to n) show the effect of sodium silicate with the range of the mentioned concentration on the micellar formation of SDS. Indeed, the CMC of SDS is reduced by the presence of a positively charged

cation in the sodium silicate solution. Although it is difficult to find any literature values for comparison, the following values seem reasonable since they follow the rule of adding electrolytes [98, 134-136].

Fig. 3-5 (from a to n) displays the charts of (pinacyanol chloride) absorbance at 608 nm alongside concentration of sodium silicate. From these plots, values of CMC can be extracted which are collected together in Table 3-2 and Fig. 3-6.

Table 3-2 Summary of CMC values (to 95% confidence) of SDS with various concentration of sodium silicate.

$[Na_2SiO_3]$ M	CMC mM of SDS
0	6.7 ± 0.3
0.015	4.5 ± 0.5
0.025	4.0 ± 0.5
0.04	3.4 ± 0.2
0.05	3.0 ± 0.4
0.1	2.0 ± 0.5
0.15	1.6 ± 0.1
0.2	1.3 ± 0.2
0.25	1.2 ± 0.1
0.35	1.1 ± 0.5
0.5	0.9 ± 0.3
0.7	0.7 ± 0.2
0.9	0.7 ± 0.4
1.2	0.5 ± 0.2
1.4	0.5 ± 0.3

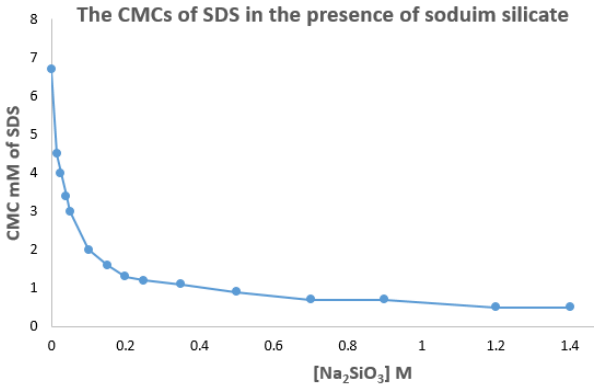

Figure 3-6: The CMCs value of SDS in the presence of sodium silicate

This study shows that above concentration of 0.5 M sodium silicate, there does not appear to be much change in overall CMC, the system having effectively reached a steady state in the context of salt presence. At higher concentrations than 1.4 M, we did begin to observe crystallisation of the salt during measurements. This, therefore, provided a natural limit to our investigations. Indeed, in concentrations of 0.7, 0.9, 1.2, and 1.4 M, the opalescence appeared, or crystals were formed in the samples after measuring the absorbance as stated by Dutkiewicz [99].

3.2.2.2 In the Presence of Sodium Carbonate Salts

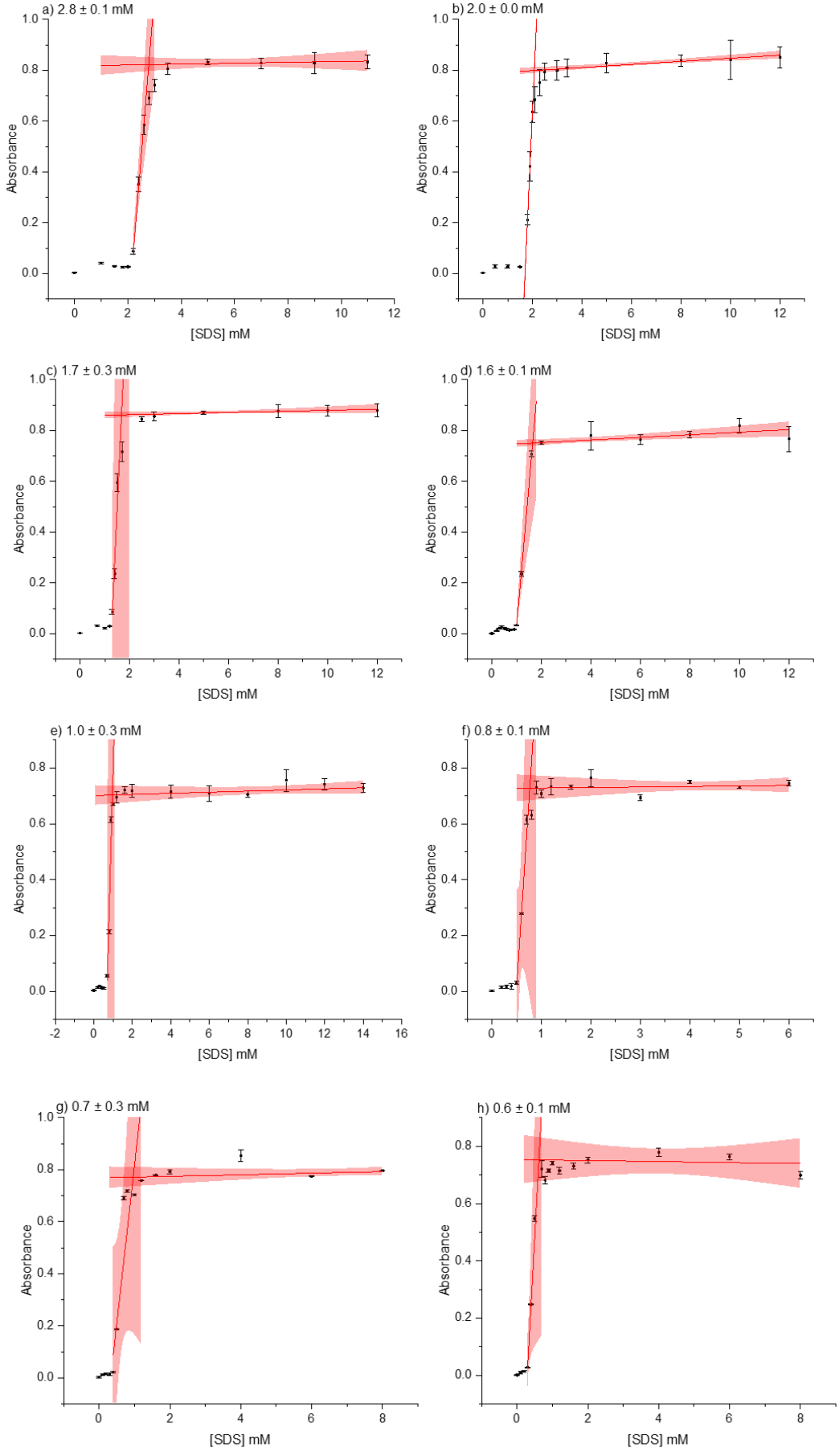

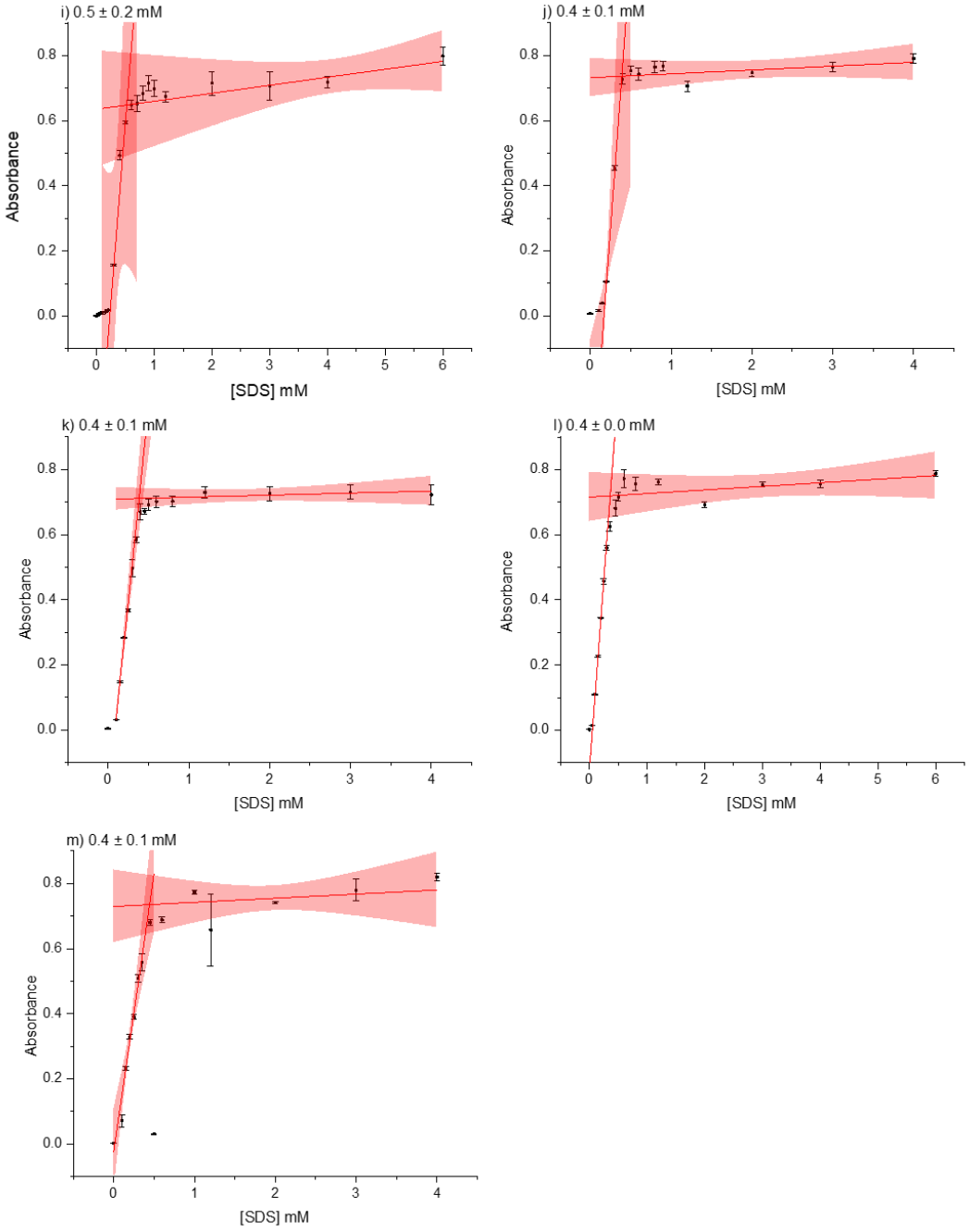

Figure 3-7: Estimation of the CMC values by plotting specific absorbance of SDS versus concentration at the wavelength of 608 nm in carbonate solution: a) 0.015 M , b) 0.025 M , c) 0.04 M , d) 0.05 M , e) 0.1 M, f) 0.15 M , g) 0.2 M , h) 0.25 M , i) 0.35 M , j) 0.5 M , k) 0.7 M , l) 0.9 M , and m) 1.2 M. The shaded line represents the fitting line with 95% confidence.

Fig. 3-7 from a to m shows the effect of carbonate on the CMC of SDS in the presence of sodium carbonate concentrations in the 0.015 M – 1.2 M. Overall, the CMC of SDS is found to decrease in the presence of salt in agreement with Miqan et al. [137].

It is pertinent to note that at carbonate concentrations above 0.5 M, the solutions show a greater degree of opalescence in agreement with observations by Dutkiewicz [99]. In samples where carbonate concentration was 0.7, 0.9 and 1.2 M, crystals formed in the solutions soon after measurements were obtained. The summary of the values of the CMC is recorded in the following Table 3-3 and Fig. 3-8.

Table 3-3 Summary CMC values (to 95% confidence) of SDS with different concentrations of sodium carbonate.

[Na_2CO_3] M	[CMC] mM of SDS
0	6.7 ± 0.3
0.015	2.8 ± 0.1
0.025	2.0 ± 0.0
0.04	1.7 ± 0.3
0.05	1.6 ± 0.1
0.1	1.0 ± 0.3
0.15	0.8 ± 0.1
0.2	0.7 ± 0.3
0.25	0.6 ± 0.1
0.35	0.5 ± 0.2
0.5	0.4 ± 0.0
0.7	0.4 ± 0.1
0.9	0.4 ± 0.0
1.2	0.4 ± 0.1

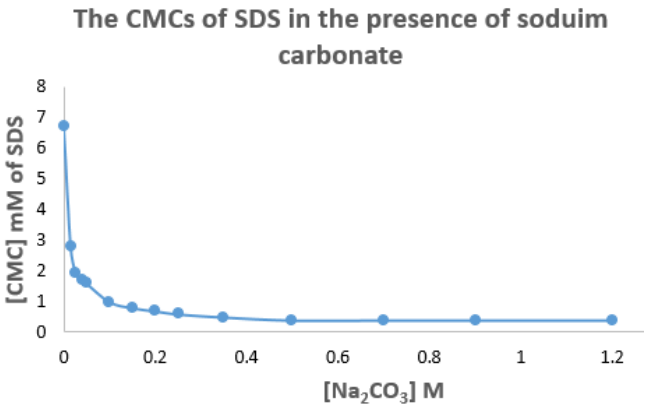

Figure 3-8: The CMCs value of SDS in the presence of sodium carbonate.

3.2.2.3 In the Presence of Sodium Sulfate Salts

The CMC's of SDS were also determined in the presence of add sodium sulfate within the concentration range 0.015 M – 0.5 M sulfate in line with solubility limitations. As expected, adding sodium sulfate causes a decrease in the CMC value. Accordingly, the addition of sodium sulfate facilitates the formation of the micelles by initially causing a decrease in the CMC values. Fig. 3-6 (from a to j) shows the gradual decrease of the CMC's value of SDS as the concentration of sodium sulfate increases.

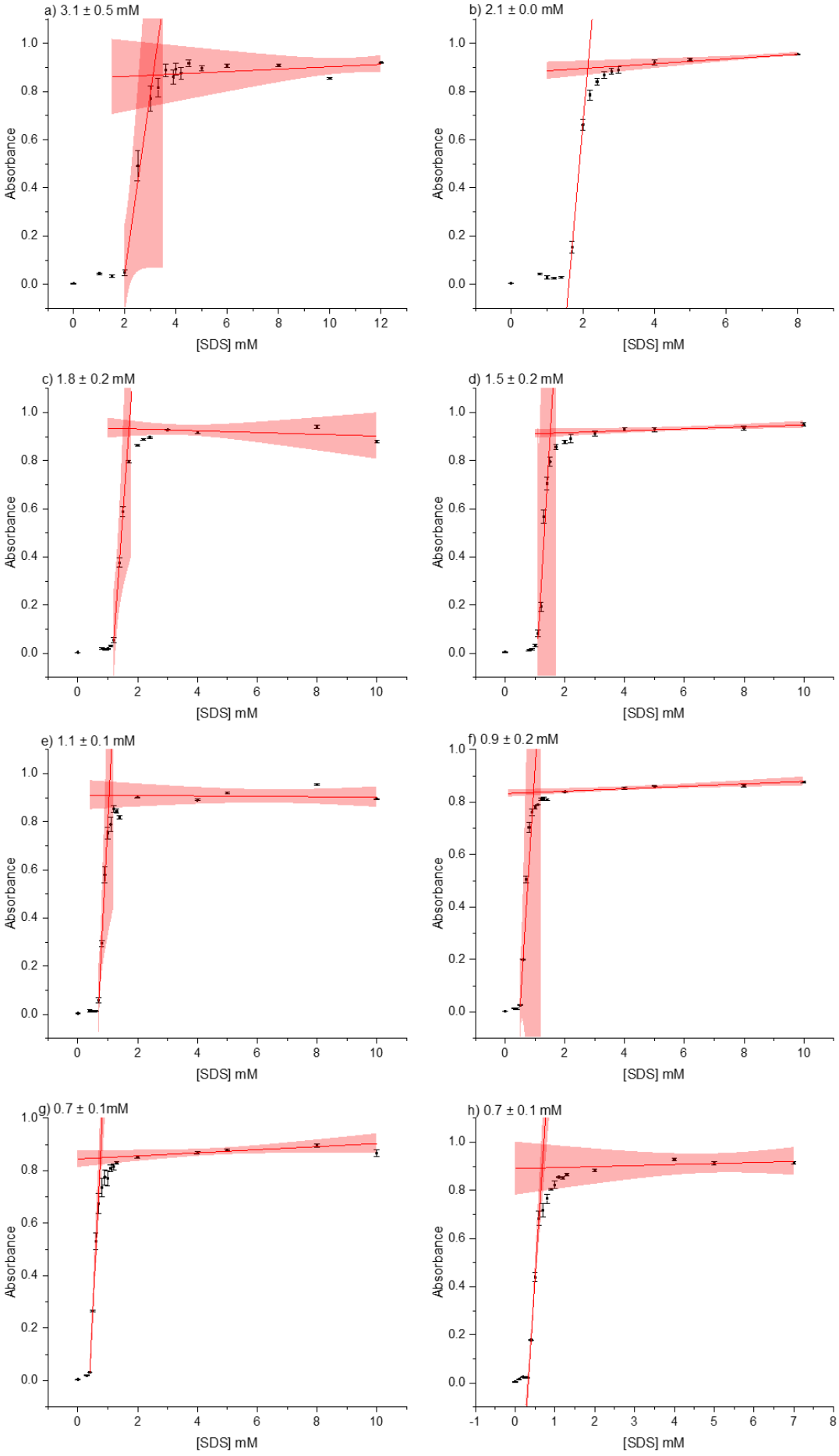
a) 3.1 ± 0.5 mM
b) 2.1 ± 0.0 mM
c) 1.8 ± 0.2 mM
d) 1.5 ± 0.2 mM
e) 1.1 ± 0.1 mM
f) 0.9 ± 0.2 mM
g) 0.7 ± 0.1mM
h) 0.7 ± 0.1 mM
Absorbance
[SDS] mM

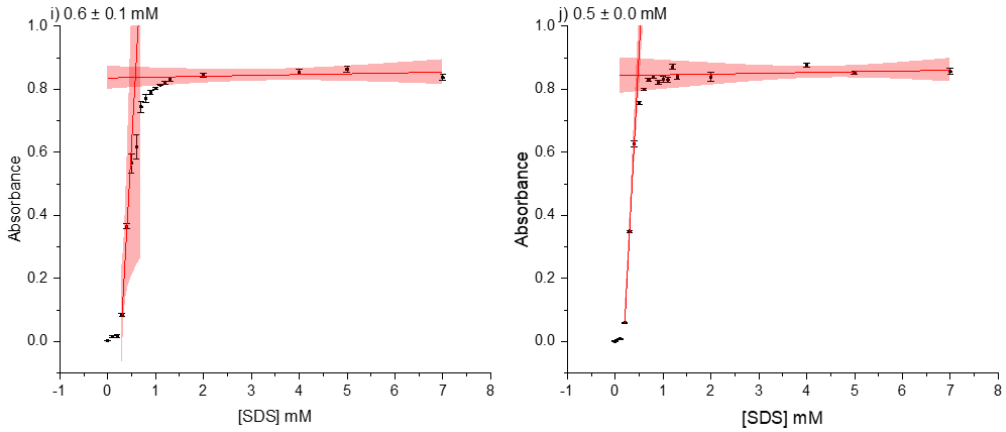

Figure 3-9: Estimation of the CMC values by plotting specific absorbance of SDS versus concentration at the wavelength of 608 nm in sodium sulphate solution: a) 0.015 M , b) 0.025 M , c) 0.04 M , d) 0.05 M , e) 0.1 M, f) 0.15 M , g) 0.2 M , h) 0.25 M , i) 0.35 M , and j) 0.5 M. The shaded line represents the fitting line with 95% confidence.

For sodium sulphate, the summary values of the CMC are recorded in Table 3-4 and Fig. 3-10.

Table 3-4 Summary of CMC values (to 95% confidence) of SDS with different concentrations of sodium sulphate.

$[Na_2SO_4]$ M	[CMC] mM
0	6.7 ± 0.3
0.015	3.1 ± 0.5
0.025	2.1 ± 0.0
0.04	1.8 ± 0.2
0.05	1.5 ± 0.2
0.1	1.1 ± 0.1
0.15	0.9 ± 0.2
0.2	0.7 ± 0.1
0.25	0.7 ± 0.1
0.35	0.6 ± 0.1
0.5	0.5 ± 0.0

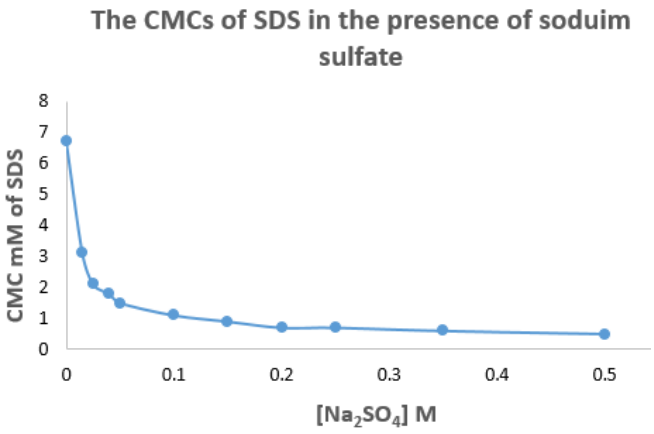

Figure 3-10: The CMCs value of SDS in the presence of sodium sulphate.

3.2.2.4 In the Presence of Sodium Chloride Salts

In line with measurements made on other salts, CMC measurements on SDS in the presence of sodium chloride within the range of 0.015 M – 0.5 M have been performed and relevant results presented in Fig. 3-11.

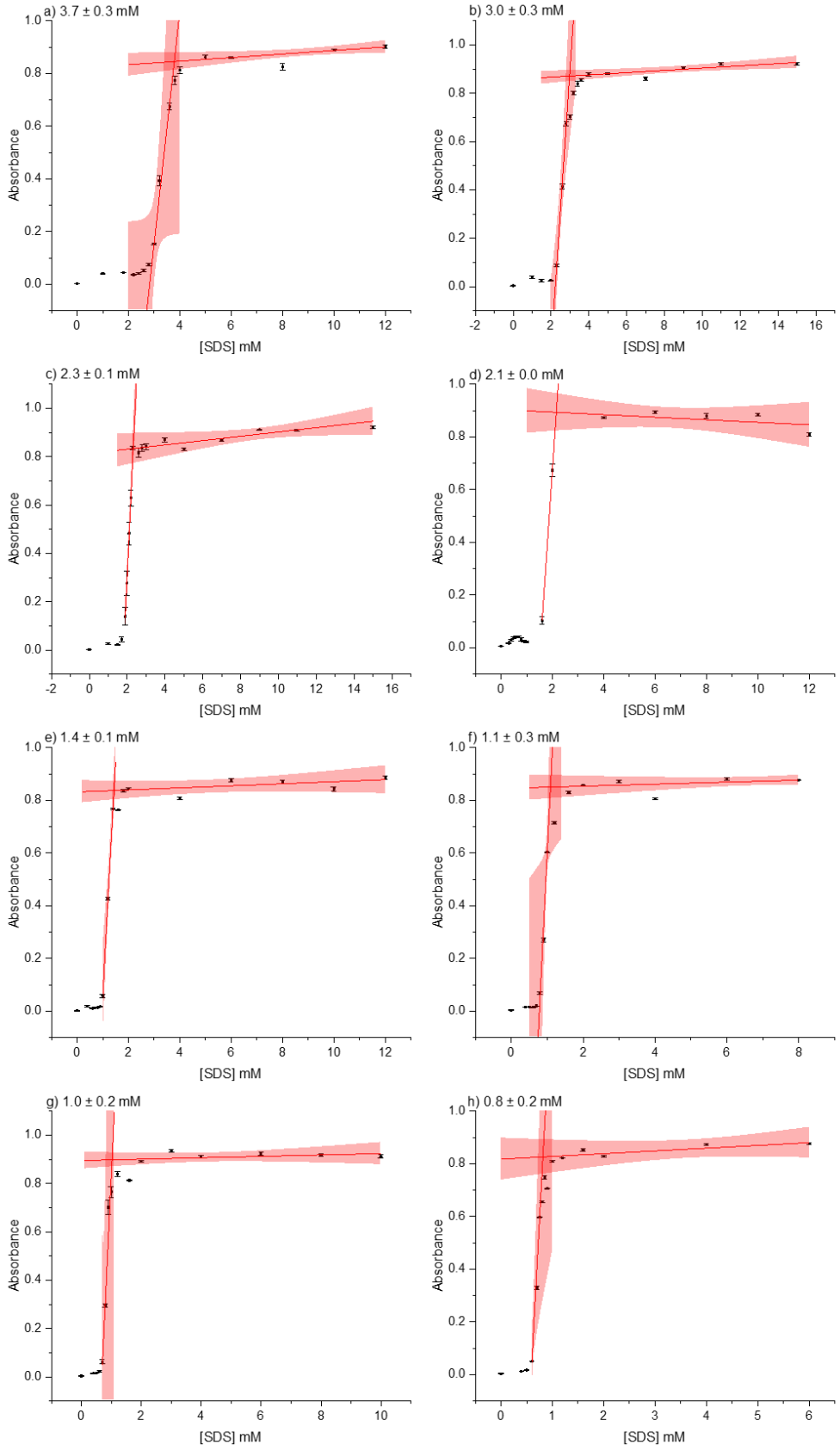

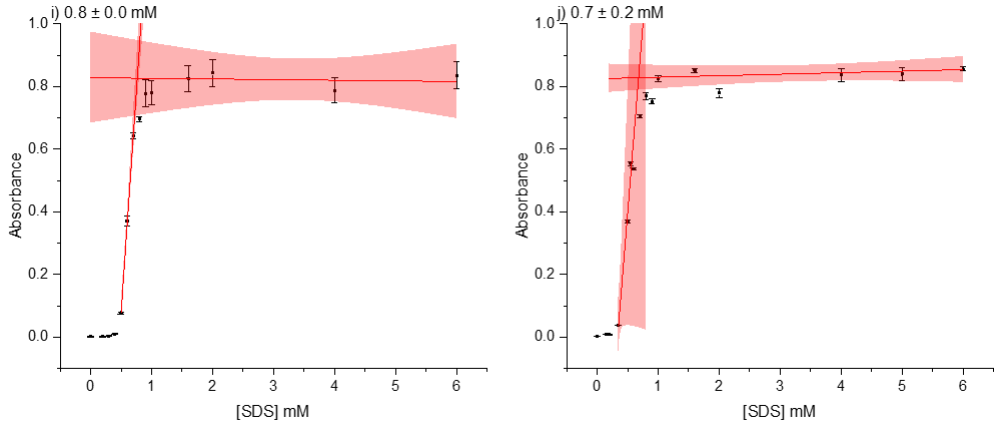

Figure 3-11: Estimation of the CMC values by plotting specific absorbance of SDS versus concentration at the wavelength of 608 nm in chloride solution: a) 0.015 M , b) 0.025 M , c) 0.04 M , d) 0.05 M , e) 0.1 M, f) 0.15 M , g) 0.2 M , h) 0.25 M , i) 0.35 M , and j) 0.5 M. The shaded line represents the fitting line with 95% confidence.

The values of the CMC are summarised and recorded in Table 3-5 and Fig. 3-12 which show the gradual decrease of the CMC's value of SDS as the concentration of sodium chloride increases.

Table 3-5 Summary of CMC values (to 95% confidence) of SDS with different concentration of sodium chloride.

[NaCl] M	[CMC] mM of SDS
0	6.7 ± 0.3
0.015	3.7 ± 0.3
0.025	3.0 ± 0.1
0.04	2.3 ± 0.1
0.05	2.1 ± 0.0
0.1	1.4 ± 0.1
0.15	1.1 ± 0.3
0.2	1.1 ± 0.2
0.25	0.8 ± 0.2
0.35	0.8 ± 0.0
0.5	0.7 ± 0.2

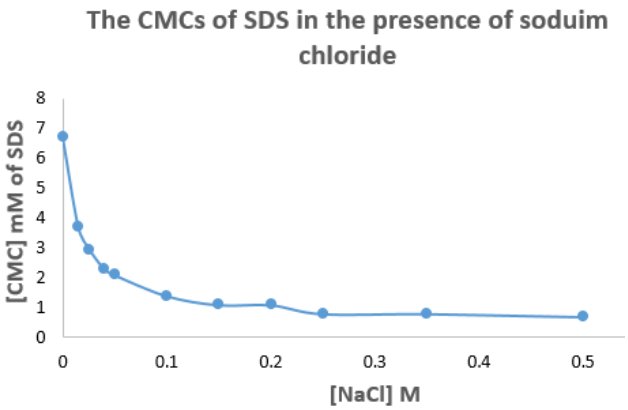

Figure 3-12: The CMCs value of SDS in the presence of sodium chloride.

The CMC's of SDS are determined in the presence of add sodium chloride within the concentration range 0.015 M – 0.5 M chloride in line with solubility limitations. As expected, adding sodium chloride causes a decrease in the CMC value. Accordingly, the addition of sodium chloride facilitates the micelles formation by initially causing a decrease in the CMC values.

Table 3-6 displays the results of this study with the practical estimated range reported by Dutkiewicz et al. [99] for CMC of SDS which gave a good agreement by using conductimetry, which is a different way to measure the CMC of SDS.

Table 3-6 Comparison of the same concentration of practical estimated range between this work and Dutkiewicz's work.

[NaCl] M	[CMC] mM of SDS this work	[CMC] mM of SDS by conductimetry of ref [99]
0.015	3.7 ± 0.3	4.2
0.025	3.0 ± 0.3	3.3
0.04	2.3 ± 0.1	2.6
0.05	2.1 ± 0.0	2.3
0.1	1.4 ± 0.1	1.7
0.15	1.1 ± 0.3	1.4
0.2	1.0 ± 0.2	1.2
0.25	0.8 ± 0.2	1.1

3.2.2.5 In the Presence of Disodium Phosphate Salts

Adding sodium disodium phosphate with different concentrations has been shown to affect the CMC of SDS. Again, the concentration window used in this study was 0.015 M – 0.5 M and CMC measurements are presented in Fig. 3-13 (a - j). Disodium phosphate salts enable the formation of the micelles by decreasing the CMC values.

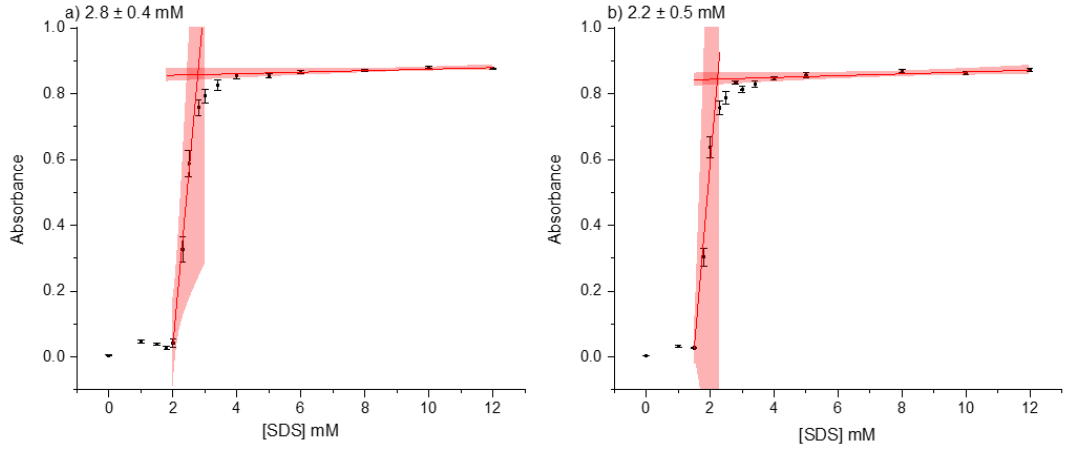

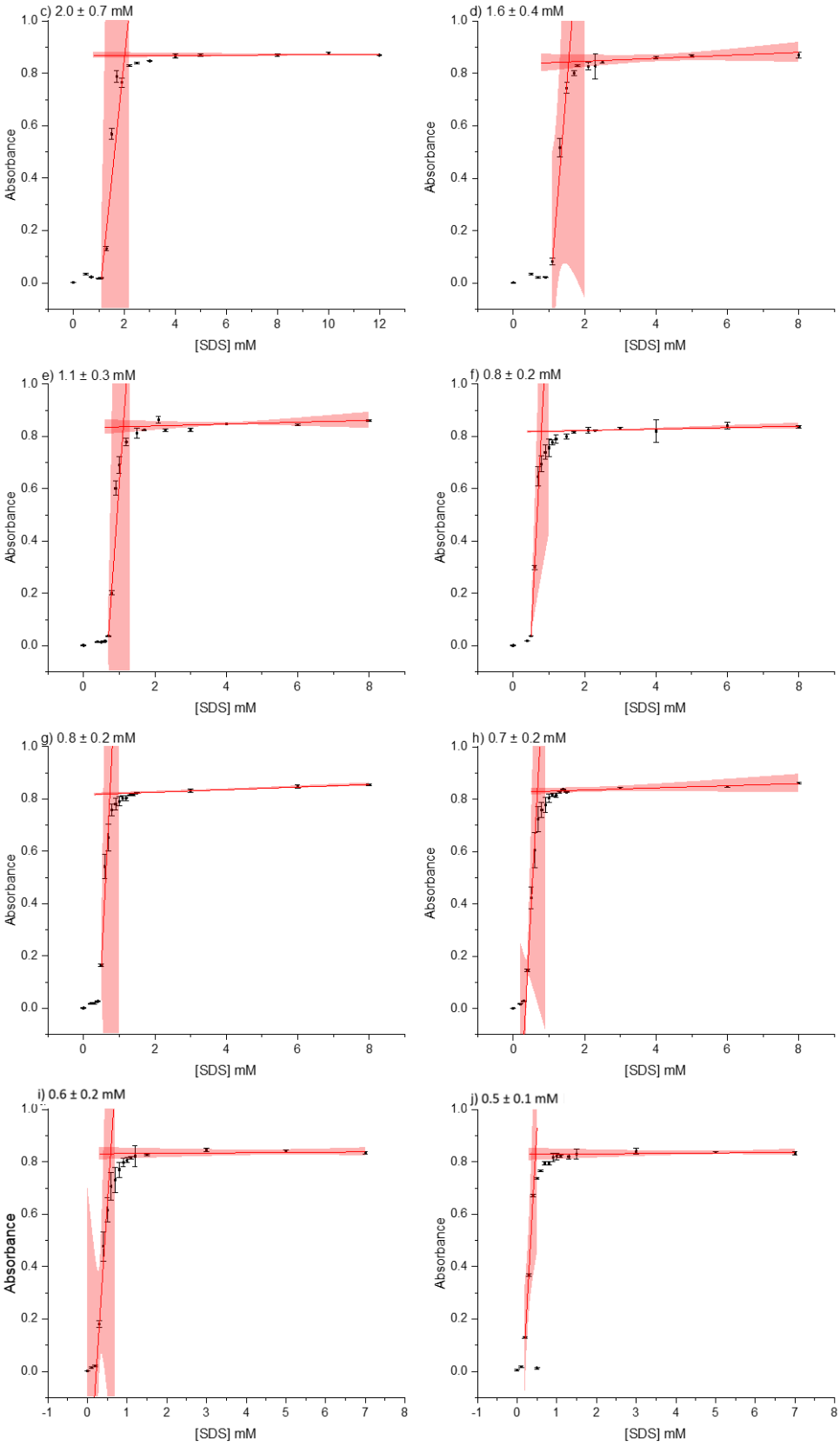

Figure 3-13: Estimation of the CMC values by plotting specific absorbance of SDS versus concentration at the wavelength of 608 nm in phosphate solution: a) 0.015 M , b) 0.025 M , c) 0.04 M , d) 0.05 M , e) 0.1 M, f) 0.15 M , g) 0.2 M , h) 0.25 M , i) 0.35 M , and j) 0.5 M. The shaded line represents the fitting line with 95% confidence.

The values of the CMC of SDS are summarised and recorded in Table 3-7 and Fig. 3-14.

Table 3-7 Summary of CMC values (to 95% confidence) of SDS with different concentrations of disodium phosphate.

[HNa_2PO_3] M	[CMC] Mm of SDS
0	6.7 ± 0.3
0.015	2.8 ± 0.1
0.025	2.2 ± 0.5
0.04	2.0 ± 0.7
0.05	1.6 ± 0.4
0.1	1.1 ± 0.3
0.15	0.8 ± 0.2
0.2	0.8 ± 0.0
0.25	0.7 ± 0.2
0.35	0.6 ± 0.2
0.5	0.5 ± 0.1

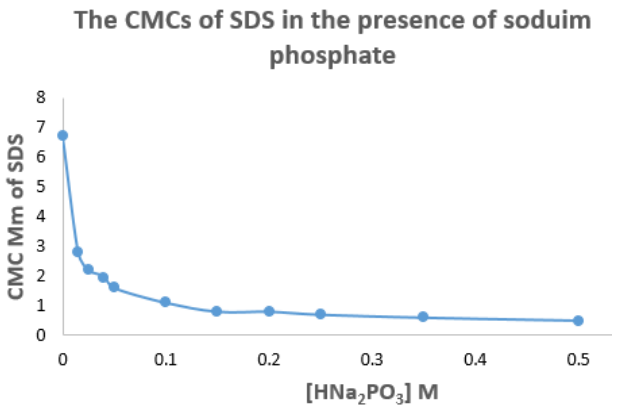

Figure 3-14: The CMCs value of SDS in the presence of sodium phosphate.

3.2.2.6 In the Presence of Magnesium Chloride Salts

The CMC of SDS has been measured using the same method to investigate the effect of magnesium chloride on the self-assembly of SDS. A significant number of concentrations have been done to do this experiment starting from the same concentration that was used with previous salts with sodium. Unfortunately, those concentrations did not work because of precipitation, so one experiment was done by using 0.5 mM of magnesium.

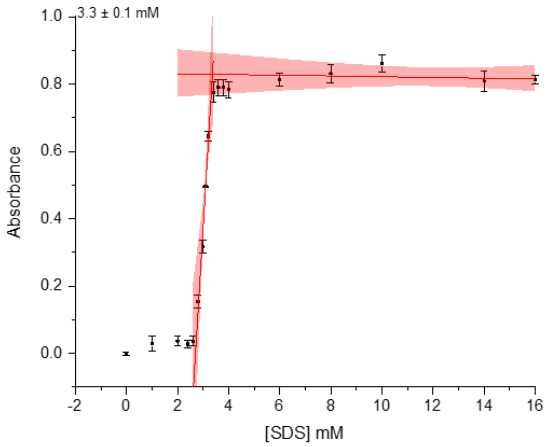

Figure 3-15: Estimation of the CMC values by plotting specific absorbance of SDS versus concentration at the wavelength of 608 nm in 0.5 mM magnesium chloride. The shaded line represents the fitting line with 95% confidence.

Fig. 3-15 shows the significant effect with a very low concentration of magnesium chloride comparing with other selected salts on the micellar formation of SDS. Indeed, the CMC of SDS is reduced by the addition of the positive charge of the magnesium chloride solution which seems reasonable since they follow the rule of adding electrolytes [99].

3.2.2.7 In the Presence of Simulated Seawater

The previous selected salts are some of the component of simulated seawater. Simulated seawater composed of NaCl, Na_2SO_4, KCl, $NaHCO_3$, KBr, $MgCl_2$, H_3BO_4, $SrCl_2$, NaF, $CaCl_2$, and it was prepared by following Kester approach [138].

The possible availability of Freshwater from rain and dew formation was less widespread [87]. Therefore, Fresh freshwater looks unlikely choice in the origin of life because biological cells have a concentrated ionic medium, which is considered an advantage for self-assembly compared to freshwater [82]. Many studies discuss the compatibility of salts in amphiphile with a single chain required for membrane formation [139]. For instance, using fatty acid to form biological membranes does not mention adding NaCl in many experiments. However, they used NaOH to increase pH and then decrease it by adding HCl to form vesicles [140]. The formation of the vesicle is likely because of the increase of the solubility of hydrophobic tails and the neutralisation of the charge of the carboxylate head groups, allowing for the formation of fatty acid membranes [141]. Another study by Namani and Deamer [132] was done successfully to form stable vesicles in the presence of seawater by using mixtures of single-chain amphiphiles including decanoic acid/decylamine. On this basis, it is worth seeing how seawater can affect the CMC of SDS in the aqueous and SHG phase.

Seawater in this study was examined in two ratios, 1:5 and 1:10, in aqueous solution to keep the percentage of seawater constant in every experiment. The result of the CMC values of SDS showed similar values (Fig. 3-16) even though the volume of the seawater was double in the second experiment.

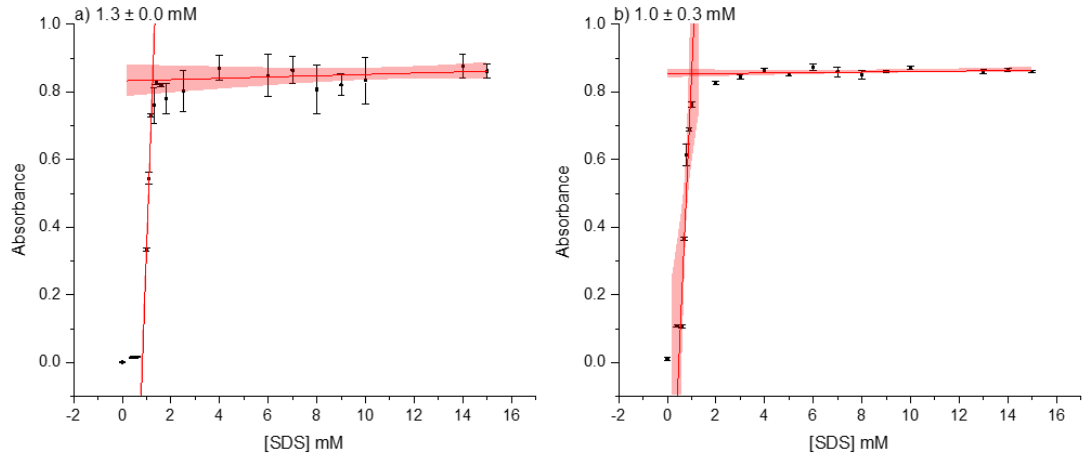

Figure 3-16: Estimation of the CMC values by plotting specific absorbance of SDS versus concentration at the wavelength of 609 nm in seawater : a) 1:10, b). 1:5 ratio of total 8000. The shaded line represents the fitting line with 95% confidence.

The effects of the seawater salt content on the CMC of SDS also showed a significant decrease in the CMC value compared to deionized water for the same reason.

The general conclusion of this section is that the CMC of SDS in the presence of some seawater salts separately or together has been extensively estimated with various concentrations. Their values showed similar general trends reported in other literatures [142-144]. Increasing the salt concentration results in reducing the electrostatic repulsion between the head group of the SDS, which can decrease the CMC of SDS.

3.2.3 Effect of the Concentration of Electrolytes on CMC Values in Aqueous Phase

3.2.3.1 Selected Salts

Fig. 3-17 shows the influence of adding different concentrations of various electrolytes with the same counterion sodium on the micellar formation. Dutkiewicz et al. [99] stated that depending on the type and concentration of the added electrolyte, the cations have more responsibility for decreasing the CMC value than anions which have a much smaller influence on the CMC value for negative micelles. It should be noted that the aforementioned selected electrolytes were all used with deionized water to dissolve them.

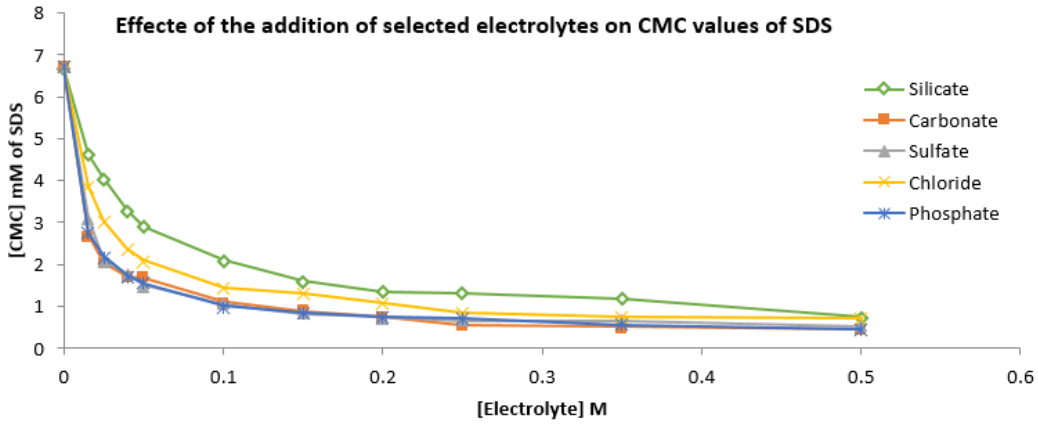

Figure 3-17: CMC values of SDS as a function of electrolytes concentration.

Adding electrolyte causes a decrease of CMC value with the addition of salts [96, 98, 134, 135]. That is because that micellization process of ionic surfactants is controlled by two forces as mentioned in Section 1.4.3. One of these forces is based on the hydrophobic effect, which is responsible for regulating the tendency of hydrophobic chains to undergo self-assembly. As a result, this allows the hydrophobic chains to separate from the hydrophilic water. The other effect is the electrostatic repulsion force between the ionic head group of SDS and the positive charge of salts, which is sodium in this case for all selected salts. The negative charge on the SDS (sulfate ion) is responsible for the electrostatic repulsion of SDS micelles. Adding electrolyte solution reduces the electrostatic repulsion by cationic part (Na^+ in this case). This reduction in the CMC value is due to the electrostatic interaction between the SDS and sodium, which helps neutralise the negative charges on the SDS head group. Therefore, adding salts helps the micellization process of SDS by overcoming the electrostatic repulsion between the head groups of SDS through electrostatic interaction. The degree of reduction in the CMC of SDS with different concentrations of electrolytes was reported with this trend by Dutkiewicz et al.[99] and Naderi et al. [137].

Within the Fig. 3-17 again, almost the same obtained value of CMCs with carbonate, sulphate, and diphosphate compared to chloride can be seen. All these salts were dissolved in deionised water, and have two sodium atoms in their formula structure Na_2An (An = anion).

It is perhaps also worth noting that these electrolytes have different values of pH within the concentration ranges selected (see Appendix). Sodium carbonate and

disodium phosphate are in alkaline media, which means a high value of pH, while sodium sulphate and sodium chloride are close to neutral media. For example, with the concentration of 0.05 M of carbonate, sulfate, and phosphate, the CMC values were 1.6, 1.5, and 1.6 mM respectively. That suggests that anions and/or pH can have a slight influence on the CMC. That can be clearly noticed with other different concentrations of other carbonate, sulphate, and phosphate. The behaviour of SDS in different solutions, such as NaCl, NaF, and $NaClO_4$, with Na^+ cations, displays that the CMC values could have very similar values and trends to those reported by Dutkiewicz in the same study [99]. They indicate that the cations of the added salts are principally responsible for influencing the value of CMC of SDS. However, Bhattarai et al. [98] made an order of selected electrolytes including NaCl, NaBr, KCl, and their research about the micellization process of sodium dodecyl sulphate in presence and absence of alkali metal halides reveals that the order of influence over CMC is as: NaCl> NaBr > KCl with 5.3, 5.0, 2.9 mM, which confirms less impact of anions than cations.

One clear difference between our silicate measurements and those involving other salts is that the silicate solutions also contain sodium hydroxide in addition to the silicate, as mentioned in the experimental section (sodium silicate is analytical grade and contains ≥ 27% of silicate and ≥10% sodium hydroxide). That has to be considered due to its influence on the CMC value of silicate, which caused more electrostatic repulsion than the salts with the same number of Na^+ [145]. For example, with a concentration of 0.025 M of salts, the CMC values of silicate, carbonate, sulfate, and phosphate are 4.0, 2.0, 2.1, and 2.2 mM, respectively. The CMC of SDS of silicate was almost double the CMC values of others. A similar outcome can be seen with other results between the silicate and the mentioned electrolytes that is due to the presence of sodium hydroxide, which provides a more negative environment. The same trend in another study [146] in the CMC of SDS solution is due to the same reason.

Comparing the CMC values with a particular concentration of chloride, which contains one counterion of monovalent salt, with carbonate, sulfate, and phosphate, which have two Na^+, it was noticed that at the concentration of 0.1 M of chloride, carbonate, sulfate, and phosphate, the CMC values were 1.4, 1.0, 1.1, and 1.1 mM, which indicated less effect of NaCl on the CMC of SDS. The same behaviour was noticed with the other concentrations of these salts. That

shows that a greater number of counterions that can bond to the surface of the micelle causes a greater decrease in the CMC values in the aqueous solutions [99].

However, in the higher concentration ranges of sodium silicate and carbonate, namely 0.5, 0.7, 0.9, 1.2, and 1.4 M, the changes in the CMC values appear to plateau, although the influence of adding the low concentration of electrolytes can lead to a significant change (Fig. 3-18)compared to aqueous media [96]. As mentioned in Section 3.2.2.1 and 3.2.2.2, it is worth noting that at silicate and carbonate concentrations above 0.5 M, the solutions show some degree of opalescence in agreement with observations by Dutkiewicz [99].

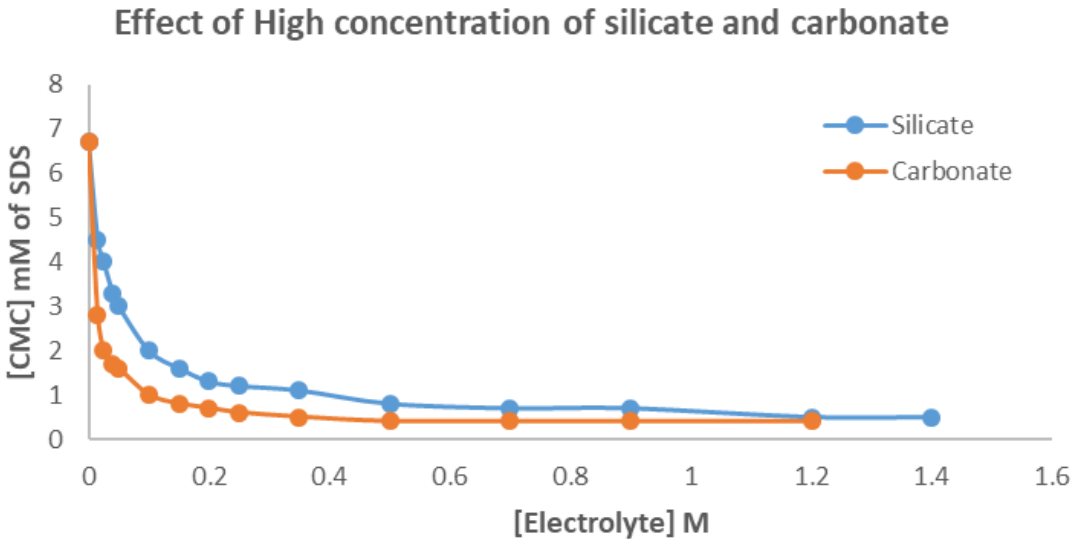

Figure 3-18: Constant values of CMC of SDS with 0.5 M and above of silicate and carbonate salts.

Regarding the magnesium chloride, the result of this experiment shows that the CMC of SDS solution with Mg^{++} counterion which represents a divalent salt follows the behaviour of previous selected salt solutions with Na^{+}. A very significant decrease in CMC of SDS with adding 0.5 mM Mg^{++} solution which is considered a very low concentration comparing with other sodium salt concentration. That could be explained by the stronger interaction of head group of SDS micelles with Mg^{++} than the selected salts with Na^{+}. Indeed, the Mg^{++} counterion can be more hydrated than Na^{+}, therefore, the Mg^{++} ion is more screened than Na^{+}. And also, Mg^{++} has more effective ionic charge which means that it can cause a greater decrease in the CMC comparing with Na^{+} [99]. The same trend of decreasing the CMC of SDS by adding magnesium chloride was obtained by using the conductivity method [147].

3.2.3.2 In the Presence of Seawater

In this manner of study, the effects of seawater with two different volume ratio were measured. Those two different ratio of seawater were used in aqueous solution containing 1:10 (8000:800 µL), and 1:5 (8000:1600 µL) with total volume 8000 µL.

It can be seen clearly from Table 3-8 that the CMC value a significant decreased from 6.7 mM in aqueous solution to around 1.3 ± 0.0 and 1.0 ± 0.3 mM in 1:10 (8000:800 µL), and 1:5 (8000:1600 µL) respectively of seawater.

Simulated seawater, which is composed of NaCl, Na_2SO_4, KCl, $NaHCO_3$, KBr, $MgCl_2$, H_3BO_4, $SrCl_2$, NaF, and $CaCl_2$ has a significant impact on the CMC of SDS. The presence of cationic seawater counterion causes a significant decrease in the CMC of SDS following the rule of adding salts [99]. The seawater contains a large amount of NaCl and divalent metal cations like Ca^{++} and Mg^{++} and it has a tendency to associate with the negative charge of the head group of SDS to generate ion-surfactant assemblies [148].

Table 3-8 CMC of SDS in Seawater

Seawater Volume µL	CMC of SDS Mm
0.0	6.7± 0.3
800	1.3 ± 0.0
1600	1.0 ± 0.3

That can be explained by adding positive charges of seawater to the aqueous solution. The CMC values were reduced due to the electrostatic interaction between the SDS and cationic element in seawater, which helped neutralise the negative charges on the SDS head group. That means that adding seawater helps the micellization process of SDS by overcoming the electrostatic repulsion between the head groups of SDS through electrostatic interaction. It is important to note that increasing the ratio of seawater in aqueous media means greater decrease in the CMCs value. In other words, the degree of reduction in the CMC of SDS with two different ratios of seawater reveals rational results reported by the literatures [96, 99].

3.2.3.3 In the Presence Different Concentrations of PIC Dye

The key thing here is that pinacyanol chloride is a cationic amphiphile, and we wondered if it could be having a positive effect upon amphiphile self-assembly.

Therefore, pinacyanol chloride, which was used in this project as a probe, was tested with two different concentrations; the higher and lower concentrations used in all experiments to measure the CMC of SDS.

Fig. 3-9 shows the CMCs of SDS with two different concentrations including low (1×10^{-6} M), and high concentration (1×10^{-5} M). The values obtained in aqueous media with low and high concentrations of PIC were (6.4 ± 0.6, and 6.9 ± 0.4 mM, respectively, which means that the obtained results did not reveal any significant change in the CMCs of both.

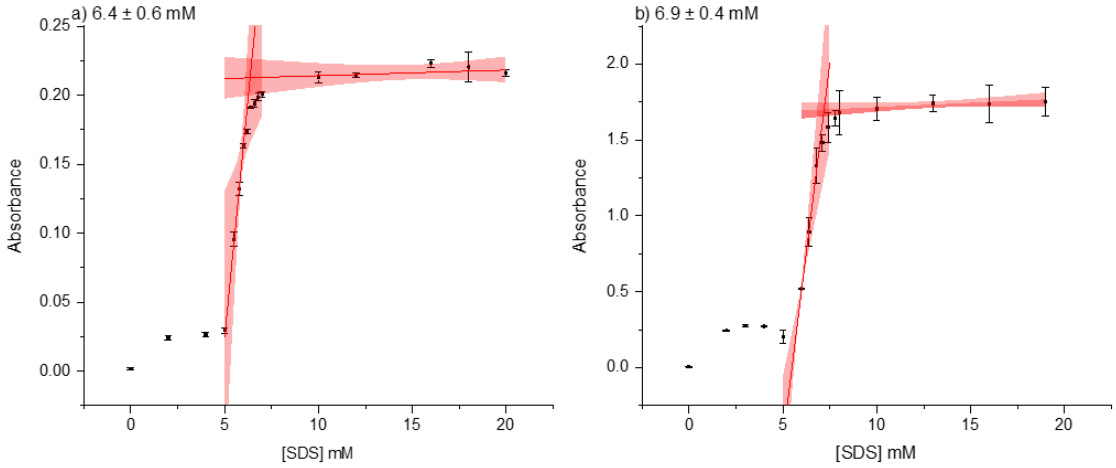

Figure 3-19: Estimation of the CMC values by plotting specific absorbance of SDS versus concentration at the wavelength of 608 nm with different concentration of PIC: a) 1.0 × 10^{-6} M, b) 1×10^{-5} M. The shaded line represents the fitting line with 95% confidence.

Pinacyanol Chloride, as a cationic salt with low concentration, made the absorbance lower than the normal one based on the Beer's Law. Similarly, based on the same law, a high concentration of PIC gave the high value of absorbance, which increases the CMC value slightly.

However, I suspect that we did not see much of a concrete effect because the concentrations of pinacyanol chloride used are ca 1000 times lower than the level of SDS (mM vs. µM).

In general, for applying the colorimetric method for determining the CMC value, it is essential to select the dye that does not interact with another material and has suitable spectral features. Also, surfactant interactions should be strong enough to modify the degree of binding of the surfactant reagent to the dye.

Therefore, the charge and hydrophobicity of analytes will dictate the selection of both the dye and the surfactant reagent [107].

At the end of this part, measuring the CMC of SDS in aqueous phase, it is very important to notice that the CMC for deionised water was measured by using quartz cuvette 8.1 mM (not included in this report), which is more in agreement with other studies compared to using polystyrene cuvette because it can absorb a portion of light resulting in reducing the CMC of deionised water [149]. However, to make this study more compatible, polystyrene cuvette was used in all experiments.

3.2.4 Calculating Ionic strength and its Effect on CMC Values of SDS in the Presence of Selected Salts

To support interpreting the results of the different concentrations of selected salts on the SDS micellar formation, the ionic strength, which is related to the number of charges and the concentration of the counterion, was calculated by equation [150]:

$$I = 1/2\Sigma c_i z^2_i \qquad 4\text{-}1$$

The unit for C_i is mol / L.

The determination of ionic strength contributes to identifying the thickness of the diffusion layer that contains the remaining counter-ions, which extend further into the aqueous phase. The surfactant hydrophobicity can be increased by shielding the electrostatic repulsion between surfactant head groups; in this case, via added cation of the selected salt. The increased hydrophobic interaction among the surfactant monomers enables them to form micelles at a lower concentration, consequently decreasing the CMC [151, 152].

Table 3-9 Calculating ionic strength of the different concentrations of selected salts and the unit of Ci is mol/L.

[Salt] M	I.S of Na_2SiO_3/NaOH	I.S of Na_2CO_3	I.S of H_2SO_4	I.S of Na_2HPO_3	I.S of NaCl	I.S of $MgCl_2$
0.5×10^{-3}	-	-	-	-	-	0.0005
0.015	0.0534	0.045	0.045	0.045	0.015	-
0.025	0.089	0.075	0.075	0.075	0.025	-
0.04	0.1424	0.12	0.12	0.12	0.04	-
0.05	0.178	0.15	0.15	0.15	0.05	-
0.1	0.356	0.3	0.3	0.3	0.1	-
0.15	0.534	0.45	0.45	0.45	0.15	-
0.2	0.712	0.6	0.6	0.6	0.2	-
0.25	0.89	0.75	0.75	0.75	0.25	-

0.35	1.246	1.05	1.05	1.05	0.35	-
0.5	1.78	1.5	1.5	1.5	0.5	-

Table 3-9 shows the gradual increase of ionic strength as salt concentration increases in solutions of carbonate, sulfate, and phosphate (in the dibasic form), which have the same effective stoichiometry, so was the same ionic strength values for all of them expected. For silicate solution, the calculated ionic strength is greater than other mentioned dibasic salts because of the sodium hydroxide present in the original solution. Thus, as the silicate-NaOH solutions have the largest ionic strength, we may have anticipated a correspondingly lowered CMC value for this environment. However, the value of the CMC of sodium silicate is 4.5 mM, whereas those for carbonate, sulfate, and phosphate are 2.8, 3.1, 2.8 mM, respectively, the reverse of what might be expected on ionic strength grounds. One might have thought that pH could have played a role even though the pH values for the silicate solution are in the same region as for the carbonate solutions. Adding alkaline material could increase the solution pH, reducing the number of positively charged sites on the solid surfaces and resulting in stronger repulsion with the negatively charged SDS surfactant leading to lower adsorption [151-153]. Thus, the effects of carbonate, sulfate, and phosphate appear to parallel each other closely in terms of cation effects and ionic strength, as indeed do the results for chloride solution.

According to Mg^{++} ion, the ionic strength of the solutions in the table represents the minimum number because of the low concentration used comparing to other selected salts. Therefore, it is not reasonable to compare it with the others. In general, the CMC values of the SDS was decreased by increasing the ionic strength without adding alkaline material.

3.2.5 Measuring the Critical Micelle Concentration of SDS in the Presence of Salts in Silica Hydrogel Phase

Silica hydrogel as a 3D network has been demonstrated to have a structure that allows self-assembly by surfactants. By adding the surfactants solution to a homopolymer, two types of behaviour may accrue relying on the nature of the polymer and polymer–surfactant interactions [154]. The first one, the surfactant micellization shows no influence by the polymer, which can keep the same CMC value as aqueous media. This behaviour maybe due to a repulsive polymer–

surfactant interaction. The second one, micellization shows an influence by the polymer which can decrease the value of the CMC. That behaviour could be due to an attractive polymer– surfactant interaction [155].

One of the key aspects of this project is to explore the effects of salts on critical micelle concentrations (CMC's) of representative amphiphiles and how this might influence such measurements in the gel phase. From previous work performed by Mr Kamal Albdeery [124] in this laboratory, it was demonstrated that the CMC of the anionic amphiphile SDS decreased significantly when moving from the non-salt containing aqueous phase to a silica hydrogel environment. Also, in Section 3.2.2 is shown that the change in CMC values in the presence of salts depends on the cationic ions in the salts. In this section, we examine the effects of additional salt content within the silica hydrogel phase on CMC values of the amphiphile SDS.

CMC were measured by the same way as that mentioned in the Section 3.2. The measurement of the absorbance level of different concentrations of SDS between 500 and 650 nm in the hydrogel media found the wavelength of maximum absorbance (λ_{max}) to be 609 nm which is in good agreement with the results reported by [110, 156].

For better comparison, the CMC of SDS itself at a range of different concentrations was obtained in silica hydrogel to see the effect of adding salts on the CMC values of SDS.

3.2.5.1 Measuring the Critical Micelle Concentration of SDS in 0.5 M Silica

The key point here is that measuring the CMC of SDS in SHG phase with no adding salts to compare it with silica hydrogel with salts, allows us to see any effect on the CMC. As it shown in Fig. 3-20. The CMC of SDS with 0.5 m SHG reveals a very big decrease in the CMC with 1.2 ± 0.3 mM with 95% confidence, comparing with aqueous phase, which is similar to the value obtained by another researcher in this group, 1.4 M for 0.5 M SHG. That is because of the presence of salts in the structure of the SHG as EDX analysis displays Section 2.3.2.2.

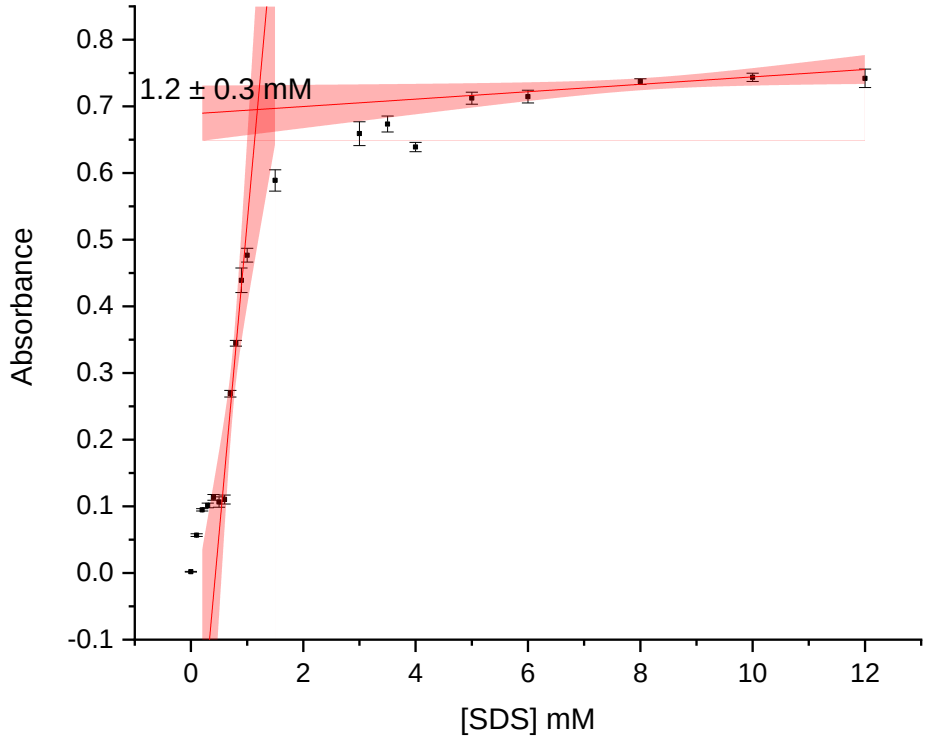

Figure 3-20: Estimation of the CMC values by plotting specific absorbance of SDS versus concentration at the wavelength of 609 nm in 0.5 mM SHG. The shaded line represents the fitting line with 95% confidence.

3.2.5.2 Measuring the Critical Micelle Concentration of SDS in 0.5 M Silica in the Presence of Salts

One of the key aspects of this study is to explore the effects of selected salts on the CMC of SDS in aqueous phase and how this might influence such measurements in the 0.5 M SHG phase.

3.2.5.2.1 In the Presence of Sodium Carbonate Salts

The CMC of SDS has been measured using the same method. Five different concentrations of sodium carbonate were used (0.015, 0.025, 0.04, 0.05, 0.1 M) to make a comparison between these different concentrations. Basically, Fig. 3-21 of sodium carbonate in the hydrogel phase show the similar value of the CMC (1.1 ± 0.4 mM), even though the concentration of carbonate increases.

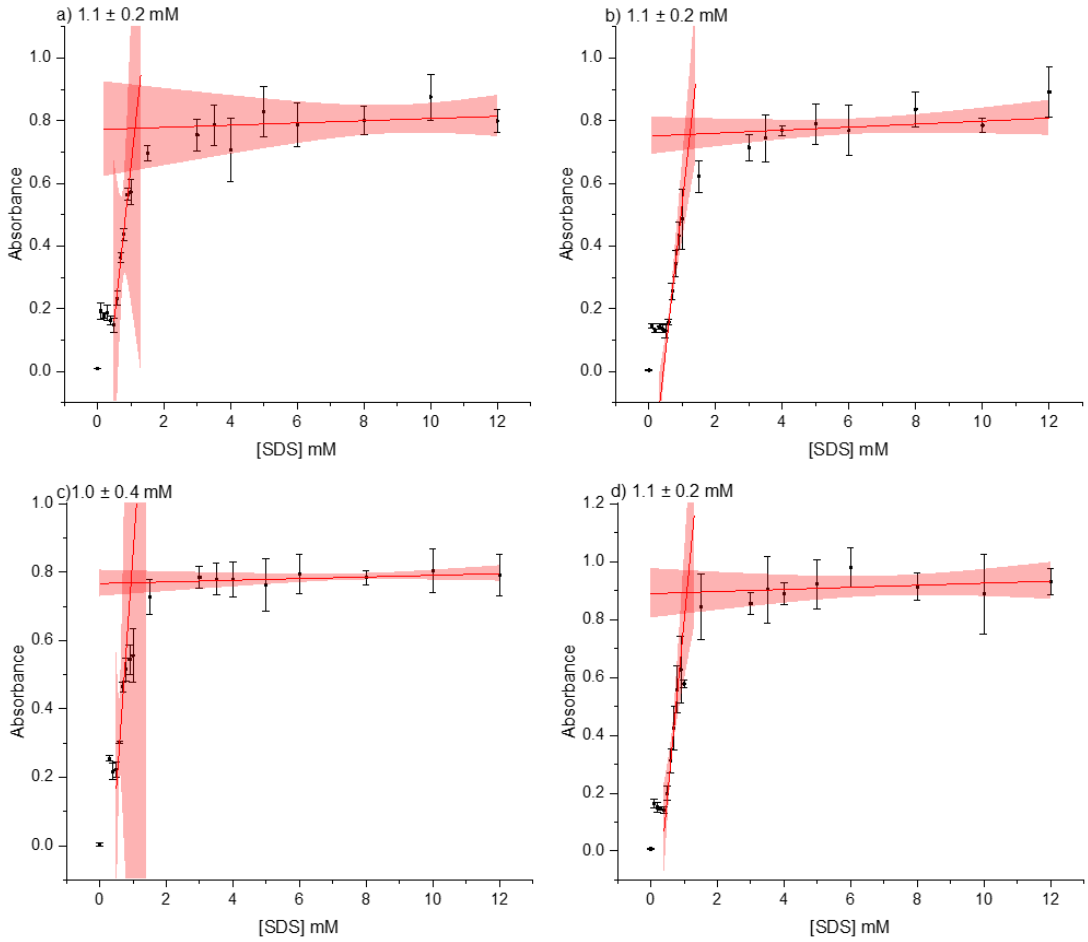

Figure 3-21: Estimation of the CMC values by plotting specific absorbance of SDS versus concentration at the wavelength of 609 nm in carbonate in SHG phase: a) 0.015 M , b) 0.025 M , c) 0.04 M , d) 0.05 M . The shaded line represents the fitting line with 95% confidence.

The precipitation can be explained by that electrostatic interactions on the head group by adding electrolyte reduces the CMC stimulates micellar growth and increases the adsorption in anionic surfactants. The latter is affected by varying concentrations of mono or divalent electrolytes. High concentration can cause a strong binding associated with positive ions which are responsible for precipitation [157] which can be seen in the 0.1 M carbonate.

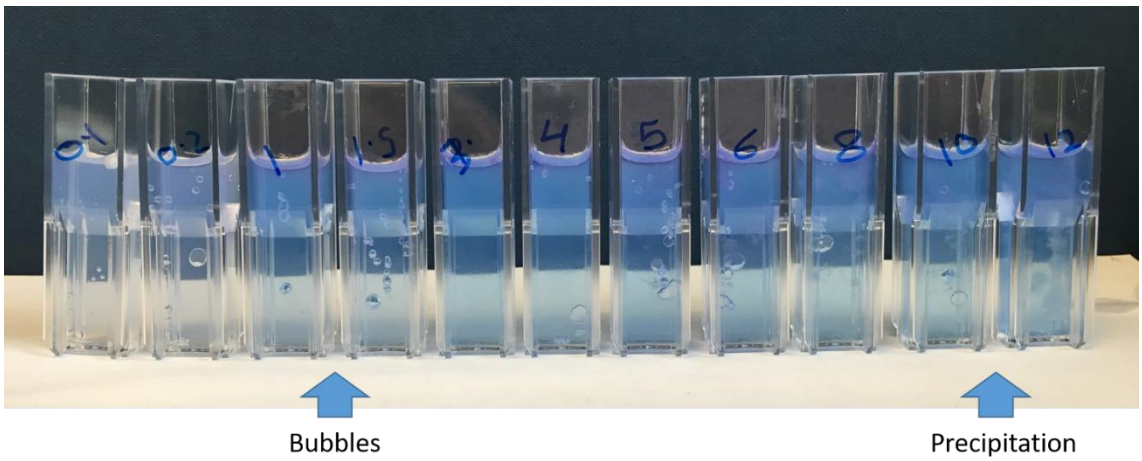

Figure 3-22: The appearance of precipitation and formation of bubbles in 0.1 M sodium carbonate with different concentrations of SDS.

The formation of bubbles could be because of the reaction between sodium carbonate and acetic acid which result in producing carbon dioxide [158].

$Na_2CO_3 + 2\ CH_3COOH \rightarrow 2\ CH_3COONa + H_2O + CO_2$

3.2.5.2.2 In the Presence of Sodium Sulphate Salts

The CMC of SDS has been measured in the hydrogel media with addition of two different concentration of sodium sulphate, 0.015, 0.025 M. The result with 0.015 M sodium sulphate showed similar CMC in the SHG,1.4 ± 0.5 mM (Fig. 3-23), but with other concentration of 0.025 M, the solution got cloudy because of precipitation as explained in Section 3.2.5.2.1.

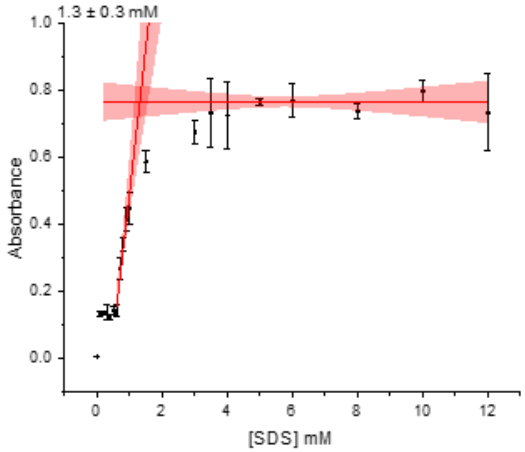

Figure 3-23: Estimation of the CMC values by plotting specific absorbance of SDS versus concentration at the wavelength of 609 nm in sulphate in SHG phase of 0.015 M. The shaded line represents the fitting line with 95% confidence.

The CMC of SDS has been measured in the hydrogel media with addition of two different concentration of sodium sulphate, 0.015, 0.025 M. The result With 0.015 M sodium sulfate shown similar CMC in the SHG,1.4 ± 0.5 mM (Fig. 3-24), but with other concentration of 0.025 M, the solution got cloudy because of precipitation as explained in Section 3.2.5.2.1..

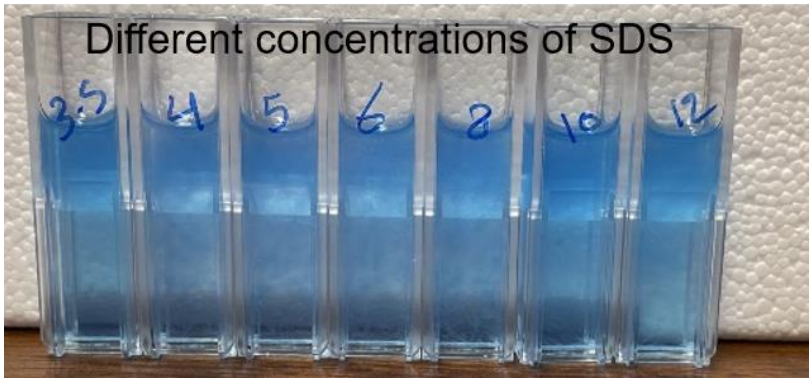

Figure 3-24: Precipitating sample with 0.025 M sodium sulphate.

3.2.5.2.3 In the Presence of Sodium Chloride Salts

The CMC of SDS has been measured for sodium chloride in the SHG phase using the same method. Six different concentrations of chloride were used including 0.015, 0.025, 0.04, 0.05, 0.1, 0.15, and 0.2 M . To make a comparison between these different concentrations, it is worth mentioning that the value of the CMC obtained for 0.5 M SHG is similar to the CMCs of sodium chloride at different concentrations.

Fig. 3-25 for sodium chloride in the hydrogel phase shows insignificant change in CMC value (1.2 ± 0.3 mM), even though the concentration of sodium chloride concentration increased.

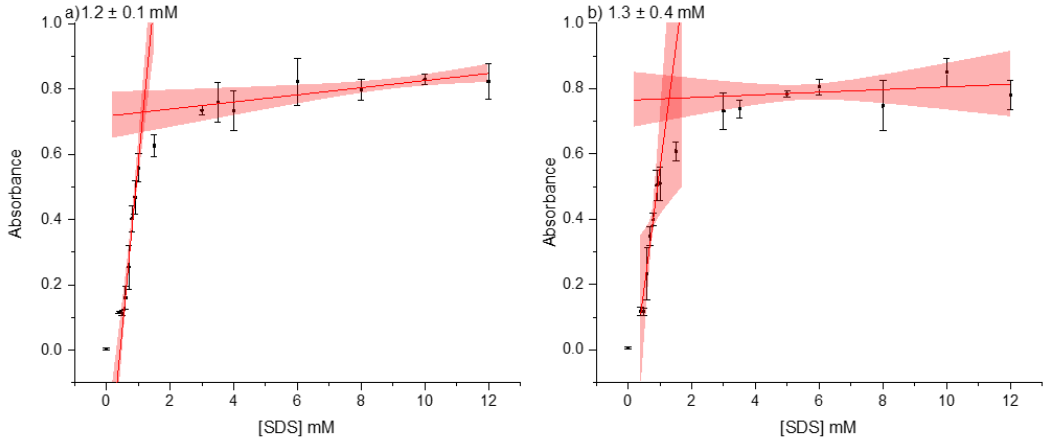

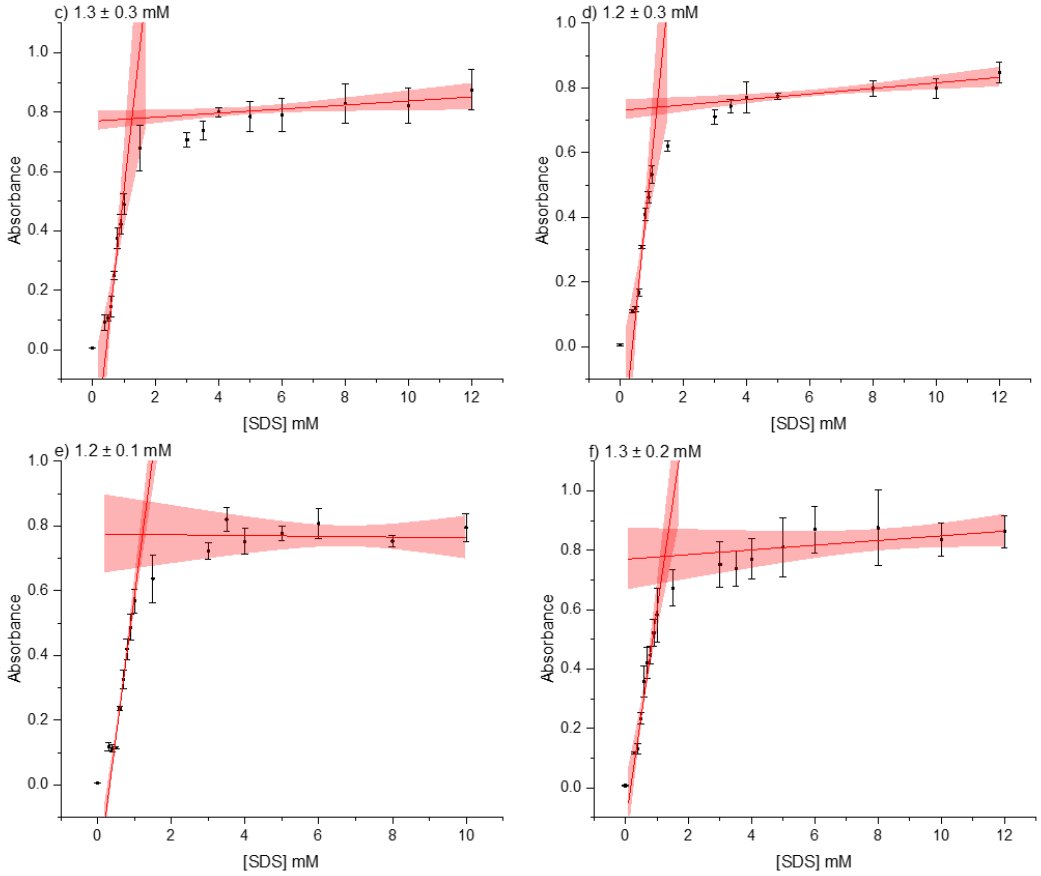

Figure 3-25: Estimation of the CMC values by plotting specific absorbance of SDS versus concentration at the wavelength of 609 nm in chloride in SHG phase : a) 0.015 M , b) 0.025 M , c) 0.04 M , d) 0.05, e) 0.1, f) 0.15, and g) 0.2 M. The shaded line represents the fitting line with 95% confidence.

At 0.2 M of sodium chloride, the solution became cloudy because of precipitation as explained in Section 3.2.5.2.1.

3.2.5.2.4 In the Presence of Disodium Phosphate Salts

The CMC of SDS has been measured in the hydrogel media with the addition of two different concentrations of disodium phosphate, 0.015, 0.025 M. The result with 0.015 M sodium phosphate showed similar CMC in the SHG,1.2 ± 0.3 mM (Fig. 3-26). However, it was too difficult to measure the CMC of SDS at 0.025 M due to cloudiness.

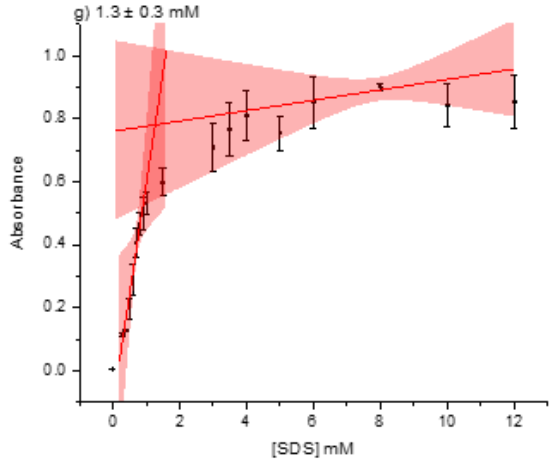

Figure 3-26: Estimation of the CMC values by plotting specific absorbance of SDS versus concentration at the wavelength of 609 nm in 0.015 M phosphate in SHG phase.

3.2.5.2.5 In the Presence of Magnesium Chloride

The CMC of SDS has been measured in the hydrogel media with the addition of 0.5 mM magnesium chloride. The result showed similar CMC in the SHG in the absence and the presence of salts,1.2 ± 0.3 mM (Fig. 3-16).

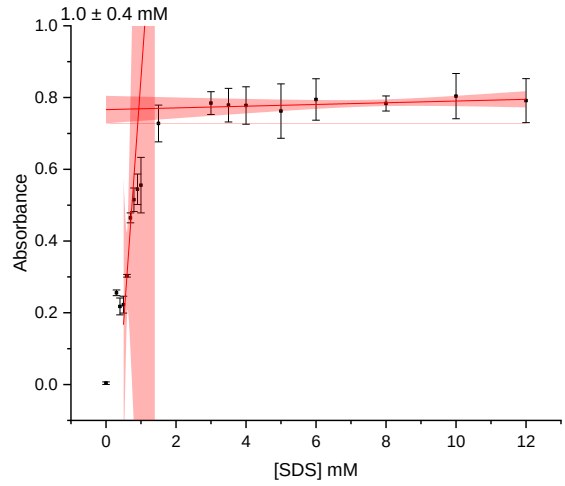

Figure 3-27: Estimation of the CMC values by plotting specific absorbance of SDS versus concentration at the wavelength of 609 nm in 0.5 mM magnesium chloride in SHG phase.

3.2.5.3 Measuring the Critical Micelle Concentration of SDS in 0.5 M Silica in the Presence of Seawater

This section aims to explore the effects of seawater on the CMC of SDS in the aqueous phase and how this might influence such measurements in the 0.5 M SHG phase. Seawater was used in two different ratios in SHG to keep the

percentage of seawater constant in every sample, and also keep the same volume ratios with aqueous phase, 1:5 and 1:10 with the total volume of 2000 µL, 400, 200 µL respectively.

The CMC of SDS has been measured in the hydrogel media with two mentioned volume ratios of seawater (Fig. 3-28), and the result showed similar CMC in the SHG with and without added salts.

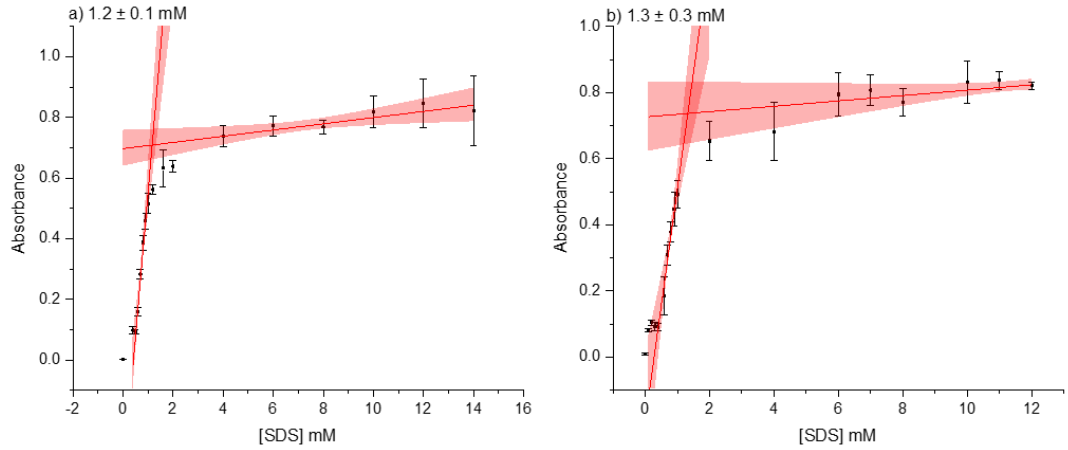

Figure 3-28: Estimation of the CMC values by plotting specific absorbance of SDS versus concentration at the wavelength of 609 nm in seawater : a) 1:10, b). 1:5 ratio of total 2000. The shaded line represents the fitting line with 95% confidence.

In general, the results of the CMC of SDS in the SHG phase in the absence and presence of salts seem almost the same.

3.2.6 Effect of the Concentration of Electrolytes on CMC Values in SHG Phase

Measurements of the CMC of self-assembly amphiphile behaviour of SDS in the presence of selected salts and simulated seawater in SHG (0.5) was conducted to see to what extent the change in CMC measurement reflects the absence and presence of salts and the type of salt present in the hydrogel phase. It was found that the CMCs of SDS showed a very significant change in their results in comparison with deionised water, and interestingly, the same results were maintained across the series of selected salts in 0.5 M SHG, which means that adding salts did not affect the CMC of SDS in the SHG phase.

Estimating the CMC of SDS in the absence and presence of salts showed almost the same results, which means almost the same decrease obtained in all

experiments in the SHG phase compared to deionised water. That can be explained by the reactions of surfactants with polymer, in this case, the structure of the polymer, SHG, with SDS surfactant. The micellization of SDS shows a significant influence by the SHG, which causes a decrease in the CMC value compared to aqueous media. This behaviour could be due to an attractive polymer–surfactant interaction [154]. In the SHG, as seen in the previous section, there is considerable salts content in the silica matrix shown by EDX analysis. We suggested that this decrease was caused by charge screening and reduced the dielectric constant because of the Na^+ presence (from sodium hydroxide and sodium silicate) in the structure of SHG [99], which causes a significant decrease in the CMC of SDS in the SHG phase.

By contrast, the repulsive polymer–surfactant interaction does not change the CMC value, as reported by Rangel and coworkers [159]. They indicated no effect of anionic polymers on the CMC of the SDS, which has the same charge due to repulsion reaction. Similarly, it has also been reported by Dhara et al. [160] that SDS does not interact with poly (acrylic acid), Na salt, and carboxymethyl cellulose because of the same charge in each.

Another aspect of this discussion is that, depending on the features of the silica hydrogels, the network of the SHG retains a high content of water and have a porous structure, which can keep the micellization of SDS with almost the same CMCs in the presence of salts. This feature was mentioned by another study [161] because the pores of hydrogels (partially dried gels) contain water, the protein molecules are solvated and retain their properties. In a similar situation, Ellerby and co-workers [162] used the sol-gel method that proved compatible with proteins that had recently been encapsulated in silica glass. This was the method that enabled the relatively easy entrapment of proteins.

In sol-gel, glasses and composite materials obtained from them have maintained their properties. Because they are porous, relatively small molecules can move through the pores and reach the relatively large molecules that are trapped inside. Those trapped compounds can keep their physical properties [161-163].

Adding various salts with different concentrations seems not to have any impact on the CMCs of SDS in the 0.5 M SHG phase since they are similar in their values. It is important to mention that these salts are consumed for attractive

reactions decreasing the gelation time [164] which will be discussed in Chapter 6.

Based on those studies and the results of the CMC of SDS after adding different concentrations of different electrolytes that produce similar values of CMC, it was concluded that silica hydrogel retains the physical properties (CMC value) of the trapped compounds (Fig. 3-29).

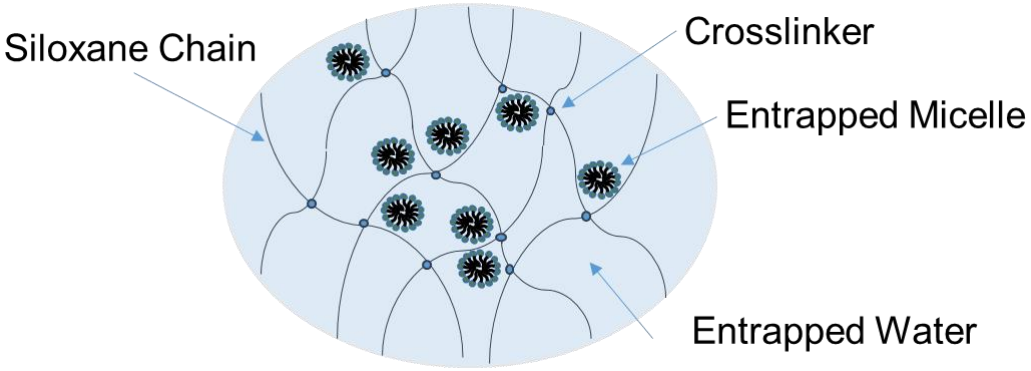

Figure 3-29: Schematic representation of trapped micelle structure in the SHG network.

3.3 Conclusion

Overall, the main conclusions from this Chapter can be summarised with the following points:

1. In the aqueous phase, the critical micelle concentrations (CMC) of the surfactant SDS in the presence of salts and seawater have been measured by using UV-VIS spectrophotometry with pinacyanol chloride as a probe, and the result reveals that the addition of salts reduces the CMC of SDS depending on the type and the concentration of the cation counterion
2. In the silica hydrogel phase, the CMC of SDS was decreased by the Na^+ presence of the SHG structure. However, CMC of SDS in the presence of salts did not show any significant change in the CMC o SDS in SHG.
3. Adding salts to the SHG can help reduce the gelation time.

Chapter 4 Measuring Critical Micelle Concentration of Sodium Dodecyl Sulfate in Aqueous and Hydrogel Phase in the Presence Normal 1-Alcohol (C_2, C_6 - C_{12})

4.1 Aim of this chapter

The aim of this chapter is to explore the effects of adding organic substances, particularly normal 1-alcohol (C_2, C_6 -C_{12}), by measuring the CMC's of representative amphiphiles, and how this might influence such measurements in the gel phase.

Self-assembly of amphiphiles is considered one of the important processes in the origin of life. Those amphiphilic molecules in aqueous solution can form different structures such as micelle, vesicle, bilayer, etc, which depends on many factors such as temperature, concentration, or additives. As mentioned previously, the selection of sodium dodecyl sulphate (SDS) was based on simplicity, and mono-chain amphiphiles similar in nature to those that may have been prevalent on the early earth. Adding 1-alkanols was able to form and stabilise vesicles formation at high pH [92, 165], which is very important for exploring their existence if any in alkaline SHG which will be discussed in Chapter 5.

Investigation studies in both chemistry and biology have the possibility to shed insight on how primitive cellular structures may be synthesis from inorganic materials, trying practically to understand paths for the emergence of life [127]. Life emerges from inorganic materials through the spontaneous and gradual accumulation of molecular complexity [166]. Therefore, the general thought is that protocells were greatly simpler than any form of contemporary biological membrane [127]. Protocells are supramolecular systems used for several systems chemistry and biological synthesis applications. Certain forms of protocells mimic possible prebiotic compartments, such as vesicles formed from amphiphiles. These hypotheses can be studied to help understand the emergence of life from a non-living organic molecule. They are helpful tools because they suggest the possibility to understand the formation, metabolism, replication, and evolution of the living cellular system. Protocells offer the investigation of the interactions of chemical compounds [167]. From the point of view of prebiotic chemistry, the first cell membranes compose of single chain amphiphiles (SCAs) are very attractive [28]. An enormous variety of organic compounds is essential for protocell formation, such as SCAs, phospholipids and

fatty acids that doubtlessly played an important role in the abiogenesis [90]. It is worth mentioning that compositional diversity can offer more stable membrane assemblies of protocellular life [39]. In this regard, the lipids formed from long-chain fatty acids and 1-alkanols, particularly C_6–C_{16} can offer a more stable membrane when mixed with fatty acids [168]. It is worth mentioning that linear fatty alcohols starting from C_6 to C_{23} is considered as surfactants that are of possibly prebiotic relevance [168].

The use of amphiphiles is encouraged by their possible availability on the origin of life and their ability to spontaneous self-assembly into vesicles structure [169]. One of the limitations of using pure fatty acid membranes as possible protocells in practical research is that they cannot keep a pH gradient through the bilayer [170]. For instance, when alkali metal ions are present in the solution, the pH gradient decays quickly. Also, in the stage of pre stabilise pH gradient, the vesicle structure of phospholipid will be destroyed because pH gradient decays immediately after adding fatty lipid. As mentioned previously, vesicle formation depends on several factors such as concentration, temperature, and pH. The latter can be stable in a wide range of pH by adding fatty alcohol into the fatty acid mixture [171]. In another study [90], they found that increasing the content of 1-alkanols causes a greater effect of stabilising. A mixtures of 1:1 of fatty acids and 1-alkanols produce stable vesicles at pH 12.

In this regard, it is worth noting that organic alcohols, as opposed to inorganic salts, can interact with the more hydrophobic parts of the micelle. SDS itself can form a micellar structure by hydrophobic effect reactions. Also, SDS molecules and long-chain alcohols might interact with each other via H-bonding. The reaction between alcohol and SDS aqueous structure can be formed by the H-bond of a hydrophilic group of alcohol and the aqueous solution of SDS by hydrophilic interaction, which disrupts the aqueous structure of the SDS. Also, the hydrophobic hydration, which promotes the aqueous structure of SDS molecules surrounding the alkyl group of alcohol [172]. SDS molecules and long-chain alcohols might interact with each other to produce double-tailed amphiphiles by hydrogen-bonding [83].

In this chapter, particularly, we wished to answer this question: *to what extent does the change in CMC measurement reflect the presence of normal 1-alcohol* (C_2, C_6 -C_{12}*) and is there any dependence on the tail length present in the SHG*

phase. Therefore, in order to address this issue, we have constructed two experimental sets:

1. To measure the CMC of SDS in the aqueous phase in the presence of different concentrations of normal 1-alcohol (C_2, C_6 -C_{12}).
2. To measure the CMC of SDS in SHG phase in the presence of different concentrations of normal 1-alcohol (C_2, C_6 -C_{12}).

4.2 Measuring the Critical Micelle Concentration of SDS with Normal 1-Alcohol (C_2, C_6 - C_{12}) in Aqueous Phase

CMC of SDS with normal-alcohol were measured using the same technique and the same probe as those stated in previous chapters to measure the absorbance level of different concentrations of SDS between 500 and 650 nm . It was found that the wavelength of maximum absorbance (λ_{max}) was 607nm. Each absorbance at λ_{max} of 607 nm was plotted against the concentration of the SDS surfactant and from the plots of absorbance vs the concentration of SDS, were observed discontinuities which represent the transition line from molecular amphiphiles to micelle formations, which is indicated by the intercalation of the pinacyanol cation into the self-assembled structure of the SDS. This results in a rather pronounced change to the self-assembly behaviour of pinacyanol chloride itself and hence to the colorimetric properties of the reporter dye from which CMC measurements can be obtained as mentioned in Chapter 3. All experiments with different alcohols were performed at least three or four times. The two lines drawn in every figure were determined by the correlation coefficient, and the equation of all fitted lines are as shown in the Appendix (9.2.3) for both phases.

4.2.1 Measuring the Critical Micelle Concentration of SDS in the Presence of Ethanol

The key thing here with ethanol experiments is to see if it could be having a positive effect upon amphiphile self-assembly. Ethanol in this study was used as a cosolvent for preparing other alcohol because of miscibility problems, especially with dodecanol and decanol [173]. Therefore, there is a need to mix all those additives with ethanol to offer the same condition firstly, and then see their influence on the CMC of SDS value in the aqueous solution. In addition to that, ethanol was used as an additive with different high concentrations compared to

other alcohols. The latter case was tested with six different concentrations, including 0.14, 0.4, 0.6, 0.9, 1.1, and 1.3 M. The value obtained in aqueous media with mentioned volumes are (6.7 ± 0.0, 6.3 ± 0.5, 6.0 ± 0.4, 6.0 ± 0.2, 5.8 ± 0.3 and 7.1 ± 0.2 mM respectively) as it is shown in Fig. 4-1.

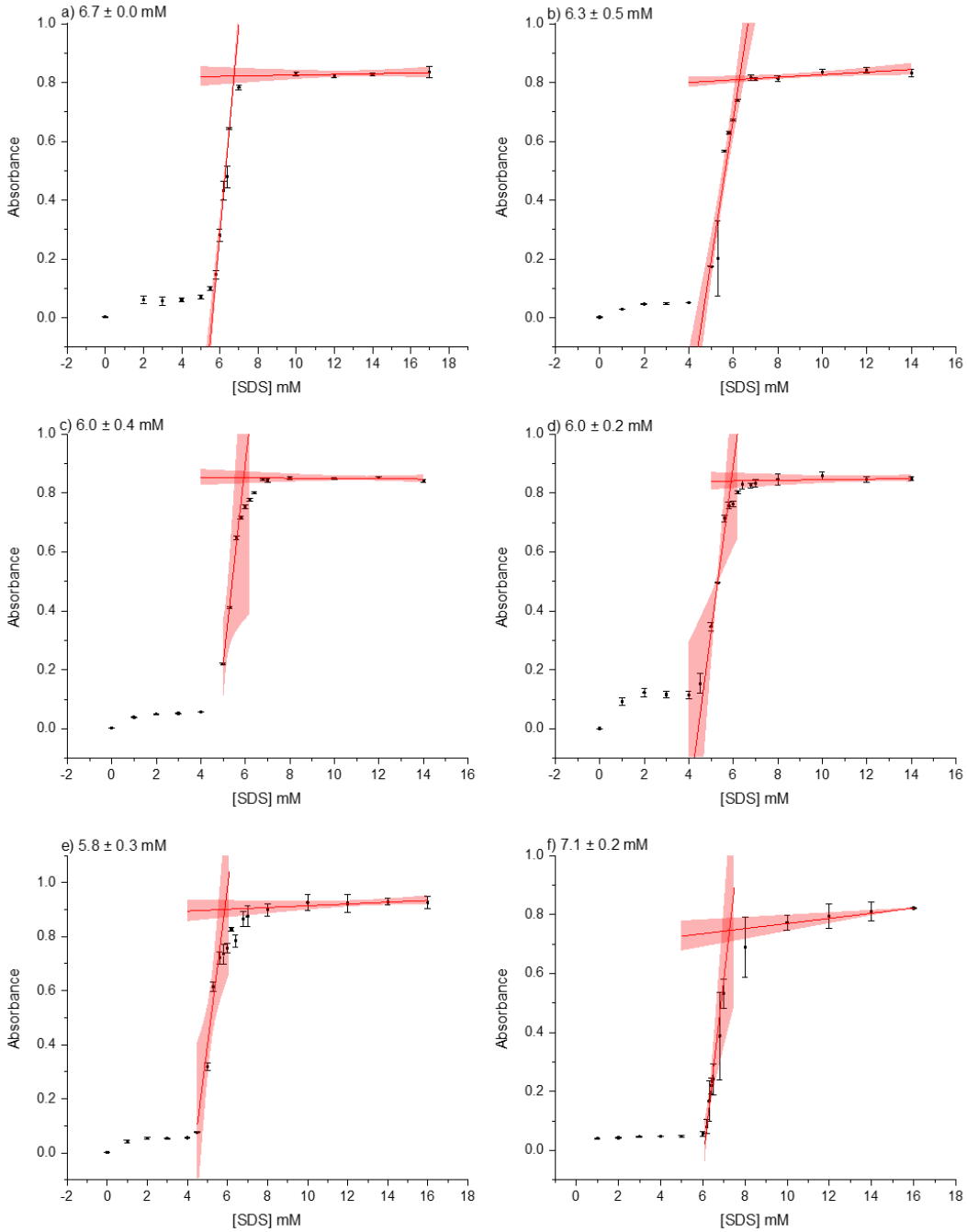

Figure 4-1: Estimation of the CMC value with different volumes of ethanol in aqueous solution: a) 0.14 M, b) 0.4 M, c) 0.6 M, d) 0.9 M, e) 1.1 and f) 1.3 M by plotting specific absorbance of SDS versus concentration at the wavelength of 607 nm. The shaded line represents the fitting line with 95% confidence.

The CMCs of SDS with 95% confidence indicate the gradual decrease of value of CMCs. However, the highest concentration with ethanol indicates high value of the CMC of SDS in the presence of high volume of ethanol compared to other concentrations. Relevant values of the CMC of SDS are recorded in Table 4-1 and Fig. 4-2.

Table 4-1 Summary of CMC values (to 95% confidence) of SDS with different concentrations of ethanol.

[Ethanol] M	[CMC of SDS] mM
0	6.7 ± 0.3
0.14	6.7 ± 0.0
0.4	6.3 ± 0.5
0.6	6.0 ± 0.4
0.9	6.0 ± 0.2
1.1	5.8 ± 0.3
1.3	7.1 ± 0.2

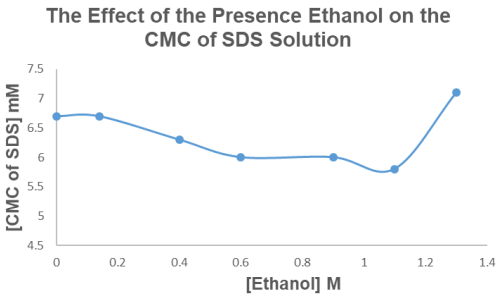

Figure 4-2: The CMCs value of SDS in the presence of ethanol.

4.2.2 Measuring the Critical Micelle Concentration of SDS in the Presence of Hexanol

The point of this experiment is to complete this project with organic additives starting with normal 1-hexanol to see how they can affect the CMC depending on the number of carbon atoms in the normal 1- alcohol chain and their concentrations. The solubility of 1-hexanol in water is low, and it increases in SDS micelle solution with the increase in surfactant concentration [174]. However, to make the condition of this study the same for all selected alcohol, hexanol was mixed with ethanol.

Hexanol was tested with five different concentrations including 0.0625, 0.125, 0.25, 0.5, and 1.0 mM. The results of the CMCs obtained in aqueous media with hexanol are similar to the CMC in aqueous media without adding additives, especially with low concentration of hexanol. However, With the highest concentration of hexanol (1.0 Mm), there is a small decrease in the CMC of SDS compared to other concentrations (Fig 4-3), and this results of hexanol shows the same trend in reported elsewhere [175].

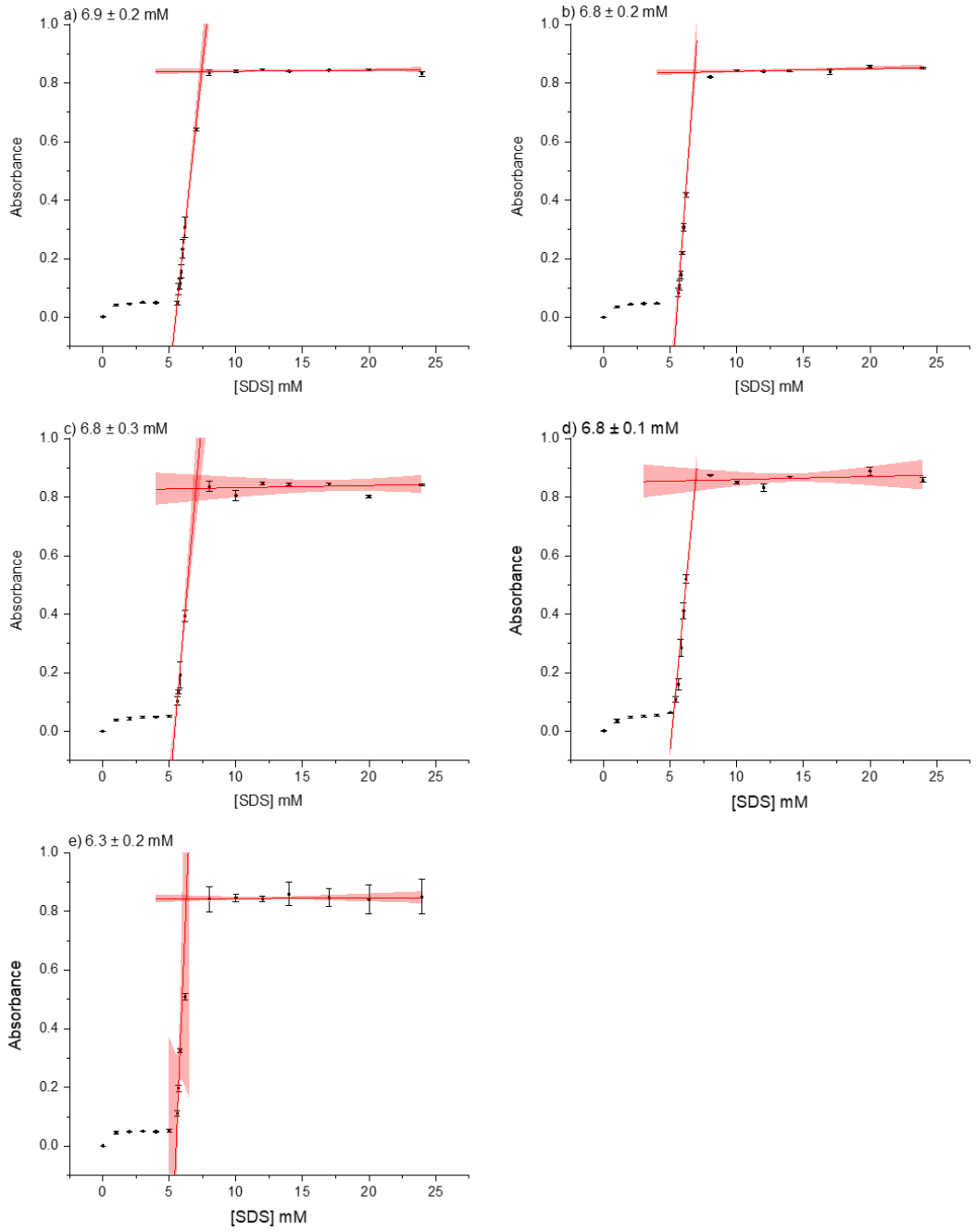

Figure 4-3: Estimation of the CMC value with different concentrations of hexanol in aqueous solution: a) 0.0625 M, b) 0.125 M, c) 0.25 M, d) 0.5 M, and e) 1.0 M by plotting specific absorbance of SDS versus concentration at the wavelength of 607 nm. The shaded line represents the fitting line with 95% confidence.

Relevant values of the CMC of SDS are recorded in Table 4-2 and Fig. 4-4.

Table 4-2 Summary of CMC values (to 95% confidence) of SDS with different concentrations of hexanol.

[Hexanol] Mm	[CMC of SDS] mM
0	6.7 ± 0.3
0.0625	6.9 ± 0.2
0.125	6.8 ± 0.2
0.25	6.8 ± 0.3
0.5	6.8 ± 0.1
1	6.3 ± 0.2

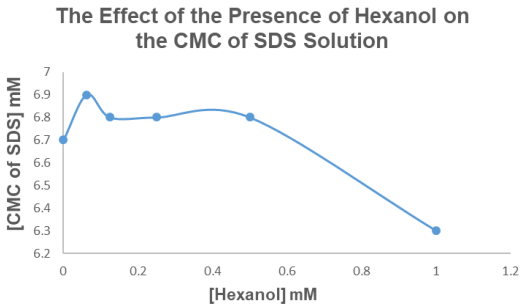

Figure 4-4: The CMCs value of SDS in the presence of hexanol.

4.2.3 Measuring the Critical Micelle Concentration of SDS in the Presence of Octanol

To complete estimating the CMC of SDS in the presence of alcohol, experiments were conducted at five concentrations of normal 1-octanol to see how those concentrations might affect the CMC of SDS. For the same solubility issue as 1-decanol in water, the samples were prepared in ethanol.

The results obtained with octanol revealed a gradual decrease in the CMCs of SDS value with increasing concentrations (Fig. 4-5), the same trend was observed in elsewhere [176].

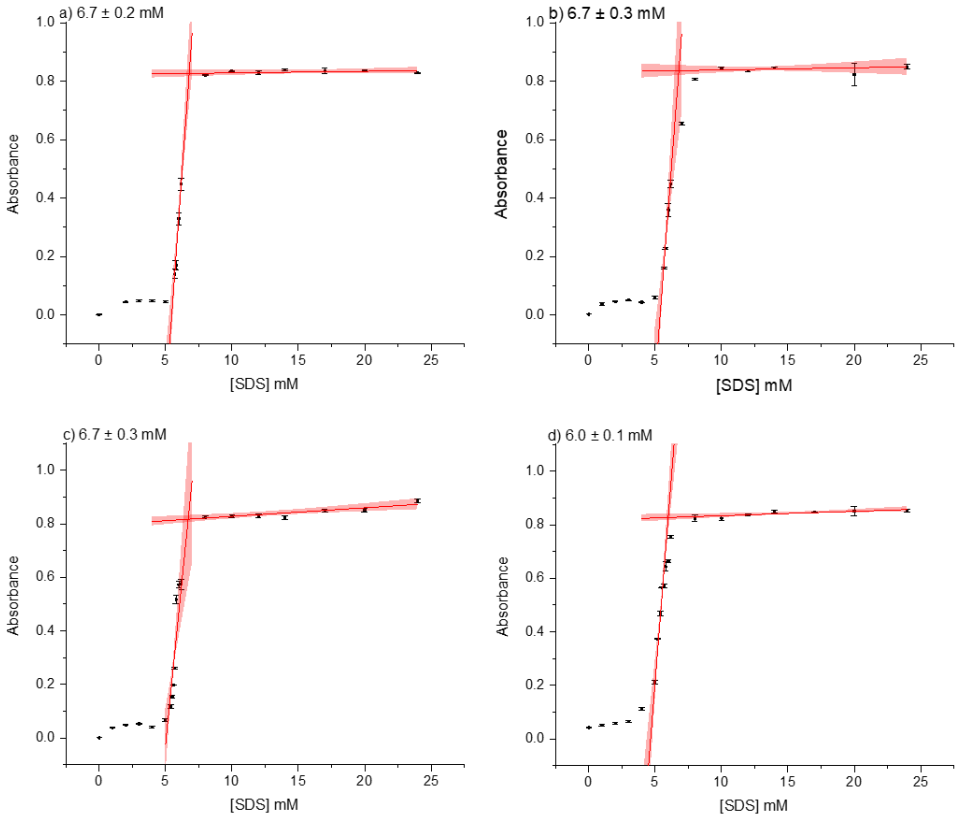

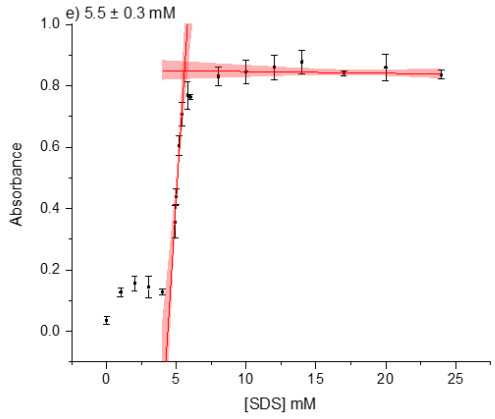

Figure 4-5: Estimation of the CMC value with different concentrations of octanol in aqueous solution: a) 0.0625 M, b) 0.125 M, c) 0.25 M, d) 0.5 M, and e) 1.0 M by plotting specific absorbance of SDS versus concentration at the wavelength of 607 nm. The shaded line represents the fitting line with 95% confidence.

Table 4-3 and Fig. 4-6 summarised the values of the CMC of SDS.

Table 4-3 Summary of CMC values (to 95% confidence) of SDS with different concentrations of octanol.

[Octanol] mM	[CMC of SDS] mM
0	6.7 ± 0.3
0.0625	6.7 ± 0.2
0.125	6.7 ± 0.3
0.25	6.7 ± 0.3
0.5	6.0 ± 0.1
1	5.5 ± 0.3

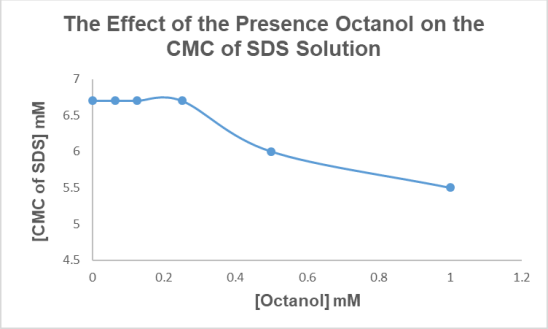

Figure 4-6: The CMCs value of SDS in the presence of octanol.

4.2.4 Measuring the Critical Micelle Concentration of SDS in the Presence of Decanol

For estimating the CMC of SDS in the presence of fatty alcohol, five concentrations of normal 1-decanol were tested to see how those concentrations can affect the CMC of SDS. The same problem with the solubility of 1-decanol in water, it was prepared in ethanol.

Unusually, the results obtained with decanol revealed a gradual increase in the CMCs of SDS value with increasing concentrations (Fig. 4-7) which is opposite of what was expected.

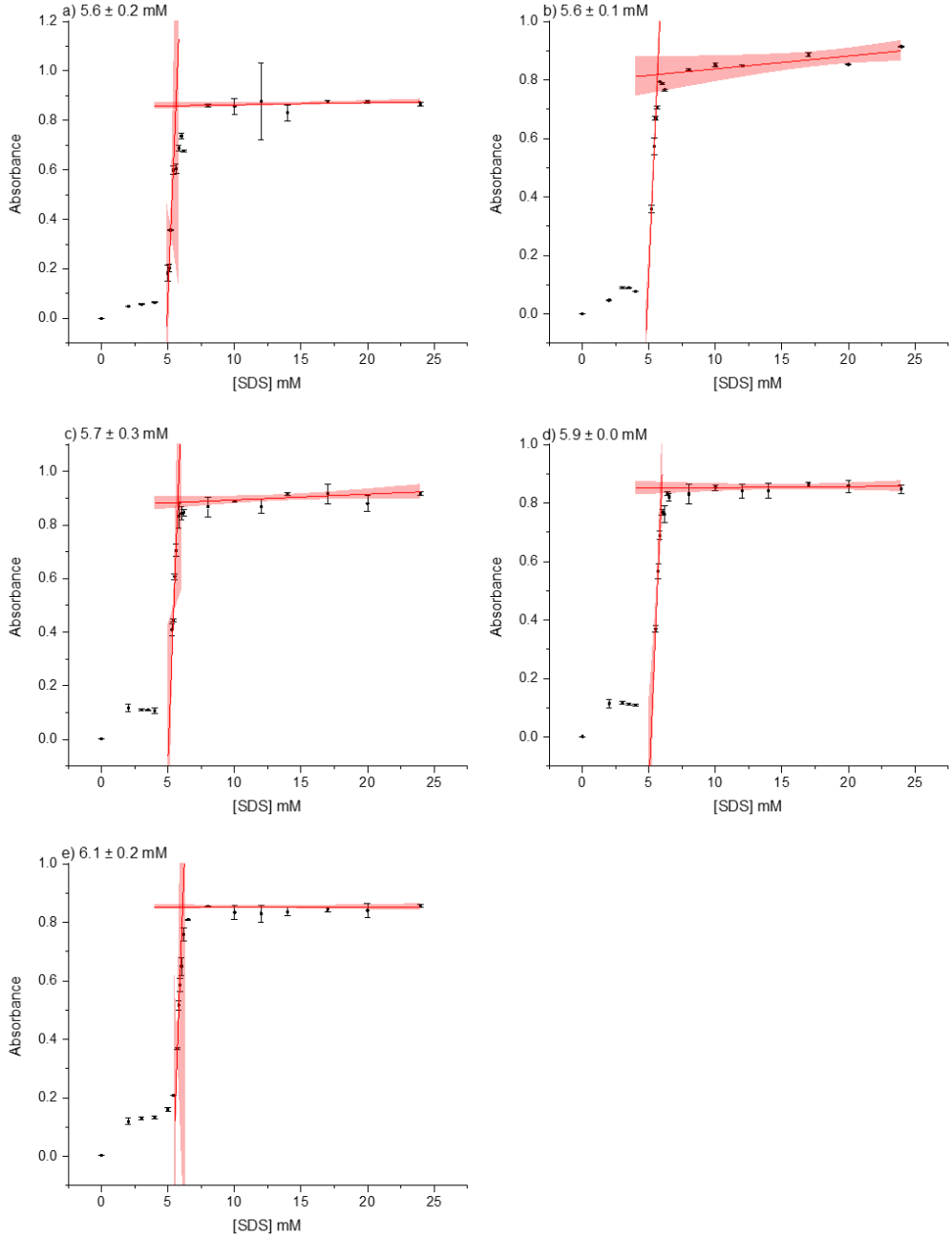

Figure 4-7: Estimation of the CMC value with different concentrations of decanol in aqueous solution: a) 0.0625 M, b) 0.125 M, c) 0.25 M, d) 0.5 M, and e) 1.0 M by plotting specific absorbance of SDS versus concentration at the wavelength of 607 nm. The shaded line represents the fitting line with 95% confidence.

Relevant results of the CMCs of SDS are shown in Table 4-4 and Fig. 4-8.

Table 4-4 Summary of CMC values (to 95% confidence) of SDS with different concentrations of decanol.

[Decanol] mM	[CMC of SDS] mM
0	6.7 ± 0.3
0.0625	5.6 ± 0.2
0.125	5.6 ± 0.1
0.25	5.7 ± 0.3
0.5	5.9 ± 0.0
1	6.1 ± 0.2

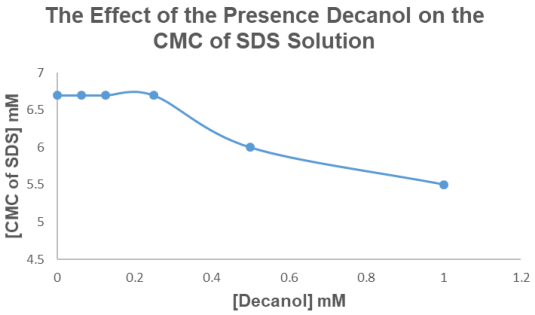

Figure 4-8: The CMCs value of SDS in the presence of decanol.

4.2.5 Measuring the Critical Micelle Concentration of SDS in the Presence of Dodecanol

Dodecanol stock solution was prepared with ethanol as solvent to avoid the problem with solubility. For estimating the CMC of SDS in the presence of dodecanol, five concentrations of normal 1-dodecanol were tested to see how those concentrations can affect the CMCs of SDS. Similarly with decanol, the results were obtained with dodecanol revealed a gradual increase in the CMCs of SDS value with increasing concentration (Fig. 4-9) which is opposite of what was expected.

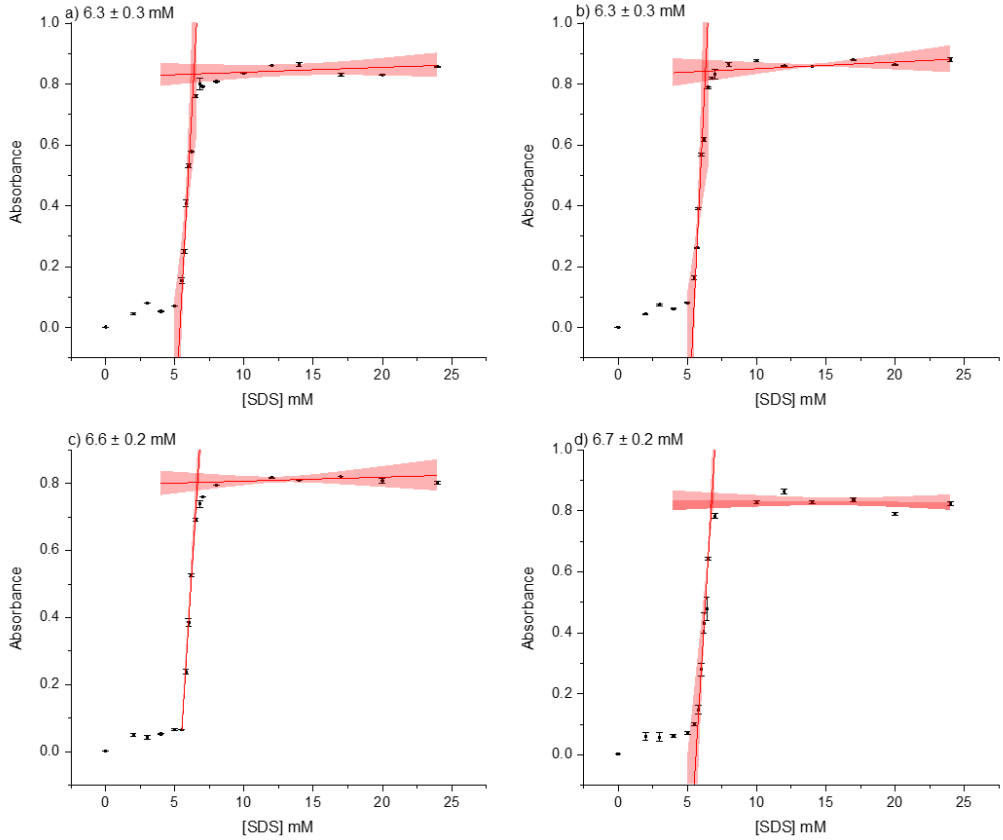

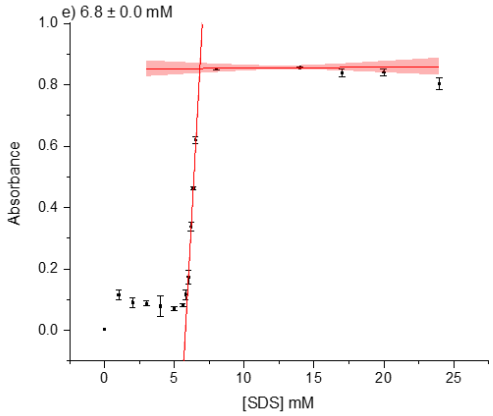

Figure 4-9: Estimation of the CMC value with different concentrations of dodecanol in aqueous solution: a) 0.0625 M, b) 0.125 M, c) 0.25 M, d) 0.5 M, and e) 1.0 M by plotting specific absorbance of SDS versus concentration at the wavelength of 607 nm. The shaded line represents the fitting line with 95% confidence.

Values of the CMC of SDS are recorded in Table 4-5 and Fig. 4-10.

Table 4-5 Summary of CMC values (to 95% confidence) of SDS with different concentrations of dodecanol.

[Dodecanol] mM	[CMC of SDS] mM
0	6.7 ± 0.3
0.0625	6.3 ± 0.3
0.125	6.3 ± 0.0
0.25	6.6 ± 0.2
0.5	6.7 ± 0.2
1	6.8 ± 0.0

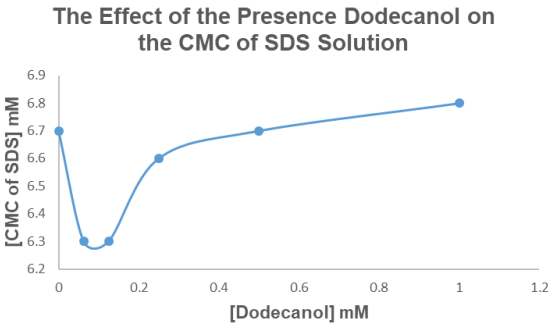

Figure 4-10: The CMCs value of SDS in the presence of dodecanol.

4.2.6 Effect of the Concentration of Normal 1-Alcohol (C_2, C_6 - C_{12}) on CMC Values in Aqueous Phase

The formation of micelles from ionic/non-ionic surfactants is the major aggregate morphologies that take in the solutions [177]. The variation in CMC of SDS with various additives both hydrophilic and hydrophobic has been studied widely by several researchers [97, 178] depending on the utilities of physicochemical properties of surfactant solutions such as spectrophotometric measurements [179], tensiometry and the conductivity [180]. The physicochemical properties of surfactant systems display dependence on the alkanol chains of alcohol with short [181], medium [182] and long chain [183].

In this part, self-assembly of SDS solution in the aqueous phase in the presence of alcohol with an even number starting from C_6 to C_{12} by using the UV-Vis technique was studied. The long chain of alcohol has a low level of solubility, so ethanol was used to help dissolve the fatty alcohol, and also their solubility is lower than their CMC that would show [184]. Therefore, it is worth trying determining the best concentration of ethanol that will not affect the CMC of selected alcohol. The CMCs of SDS with ethanol have been measured by using the same method as described in Section 3-2 with six different concentrations of ethanol to see their effect on the CMC including 0.14, 0.4, 0.6, 0.9, 1.1, and 1.3 M. The results reveal gradual decreases in the CMC of SDS with all selected concentrations excep the highest one which is shown increasing in the CMC.

Many studies suggest that short alcohol soluble in water starting from methanol to butanol are largely dissolved in the water phase, and the CMC may be increased or decreased depending on alcohol concentration [185-187].

Starting with the lowest concentration of ethanol, 0.14 M, the CMC value of SDS did not show any significant change compared to the aqueous phase, and they almost have the same CMC, which is 6.7 mM. This result is in a good agreement with literature [188] reporting that "*a decrease of CMC of surfactant is observed when ethanol is added to water up to 8%"*. That also provides a good agreement when adding more ethanol content in this study with other concentrations. It can be seen that the CMC value started decreasing to 6.3 ± 0.5, 6.0 ± 0.4, 6.0 ± 0.2, and 5.8 ± 0.3 mM of 0.4, 0.6, 0.9, and 1.1 M respectively compared with the CMC of SDS in water at 6.7 mM. That means that the quantity of ethanol is not sufficient to dissolve SDS monomers, so they aggregate into micelle which is much easier to decrease the entropy of the system. This result agreed with the same trend reported by other studies using different techniques namely potentiometry [186], and conductivity [189].

With the highest concentration of ethanol, 1.3 M, the CMC of SDS revealed an increase at 7.2 mM. This increase in the CMC may be explained by that SDS dissolves in ethanol easier than in water because of higher solubility in ethanol than in water. Therefore, association of SDS molecules into micelle in the presence of ethanol will be more difficult, and also, the formation of micelle is due to the alkyl chain driven by the hydrophobic effect which is not favoured by the presence of high content ethanol solution [190]. In other word, high

concentrations of ethanol favours decay of micelles as a result of the increase in solubility of monomers which increases the entropy of the system by breaking the hydrogen bonds between water molecules, and this effect also contribute to an increase in CMC. This result shows the same trend of CMC of SDS by using surface tension method [191]

In general, alcohols with short chain may have no effect on the CMC; they act as cosolvents, particularly, at high concentration; they are localised in the continuous phase and affect the solvent structure around the head group [185].

In addition to ethanol, hexanol, octanol, decanol, and dodecanol were examined with five different concentrations of each with SDS solution including 0.0625, 0.125, 0.25, 0.5 and 1 mM. For preparing these solutions, based on the following method mentioned elsewhere [192], ethanol is added, and heating are needed to increase solubility (40°C). The temperature plays a significant role in the micellization process. Increasing the temperature can raise the kinetic energy of the amphiphile molecules which can break the weak bond of the micelle and increase the CMC value [193]. All the following alcohols have the same preparation method by heating the samples, which slightly increases the CMC of SDS in the presence of alcohols.

In the case of hexanol, at first, the increase in CMC after adding the low concentration of hexanol is not significant with 6.9 ± 0.2, 6.8 ± 0.2, 6.8 ± 0.3, and 6.8 ± 0.1 of 0.0625, 0.125, 0.25, and 0.5 mM respectively, because the SDS solubility in water is increased by heating which helps to dissolve the SDS monomers which is with a good agreement with literature [97, 194]. At the highest concentration, 1.0 mM, the experiment points toward a decrease in the CMC of the mixture with 6.3 mM. The results obtained are similar to those reported in some literatures [97, 194]. The result of the CMC at high concentration indicated that CMC decreases as hexanol is present in solution, in a micellar medium. The entropic decrease originating from the hexanol molecules in water may be counteracted by the transfer of alcohol and surfactant molecules from the aqueous to the micellar phase, explaining thus the decrease in the CMC. A second factor that may explain CMC decrease by hexanol is that hexanol molecules in the micellar phase are positioned with their alkyl chain toward the micellar core, while their hydroxyl groups are located between the ionic heads of SDS molecules, thus increasing the length between them which decreases

repulsions. This factor contributes to the micelle stability, therefore decreasing the CMC of SDS, which is in good agreement with [195].

The second alcohol that was examined using the procedure with heating and adding ethanol was octanol solution with the same mentioned concentrations of hexanol solutions. These examined concentrations did not show any significant changes in the CMC of SDS compared with deionized water with 6.7 mM, they are almost the same results. That can be explained by the fact that the SDS solubility in water is increased by the presence of octanol. However, with 0.5 and 1.0 mM which are considered a high concentration compared with other octanol concentrations, the CMC of SDS decreased to 6.0 ± 0.1 and 5.5 ± 0.3 mM respectively. As was mentioned previously for possible explanation, the CMC value decreased due to octanol chain tail. Octanol molecules in the micellar phase are located with their alkyl chain toward the micellar core, whereas their hydroxyl groups are positioned between the ionic heads of SDS molecules, hence increasing the length between them which decreased repulsions [196]. This factor contributes to the micelle stability, so decreasing the CMC. The CMCs values obtained of the mixture SDS/Octanol were in good trend agreement with [195].

The following alcohol examined was decanol, which revealed a decrease in the CMC value, especially with low selected concentrations of 0.0625, and 0.125 with 5.6 ± 0.2 and 5.6 ± 0.1, respectively, which seems to have been affected by the length of the decanol chain tail, which helped to increase length between the head group of SDS, thus stabilising the micellar formation. However, what was not expected was that at higher concentrations, namely 0.25, 0.5, and 1.0 mM, the CMCs of SDS started to increase gradually with 5.7 ± 0.3, 5.9 ± 0.0, and 6.1 ± 0.2 mM, respectively. To explain that, it is worth mentioning that the main problem of selected alcohol is the solubility [197], and the chosen method to help dissolve alcohols was heating and adding the minimum volume of ethanol to make the low concentrations of decanol and dodecanol soluble in low concentrations of SDS during the preparation process.

Therefore, the higher decanol concentration may not be soluble in water completely (although not noticed by the naked eye). That means the presence of decanol in water solution more than in the micelles phase compared with low

concentrations, which can easily be soluble in the mixture. The next chapter with visualisation result can help provide evidence of oil droplets in a low concentration of decanol and SDS solution.

With the final examined alcohol, namely dodecanol, the CMC started with a low value with 6.3 ± 0.3 and 6.3 ± 0.3 mM of 0.0625 and 0.125 mM in the same order, then a gradual increase was noticed as the concentration increased, especially with 1.0 mM, which shows a higher value of the CMC compared with deionised water, which is in good agreement with other study [198]. That can also be explained in the same way as decanol, considering the solubility difficulties compared with decanol because the chain length in decanol is shorter than dodecanol, which has less solubility than decanol solution. Dodecanol with 1.0 mM concentration in another study was not used because of the problem of solubility [198]. Also, the next chapter will offer evidence of the presence of a droplets of oil in the images obtained by fluorescent microscopy.

In general, the CMC of SDS in the presence of alcohols depends on the length of the hydrophobic tail. Their CMCs decreased as the concentration and the length chain increased. That is because the hydroxyl group in alcohol reduces the repulsion with the head group of SDS by increasing the length in the head group. In this study, upon comparing the results, the effect of the chain length of the selected alcohols on the CMC of SDS can be easily seen with hexanol and octanol, which is with the same trend in the literature. Even though decanol and dodecanol decreased the CMC values, they did not follow the rules due to solubility problems. This decrease in the CMCs of SDS in the presence of hexanol and octanol was not observed for decanol and dodecanol (Fig. 4-11)

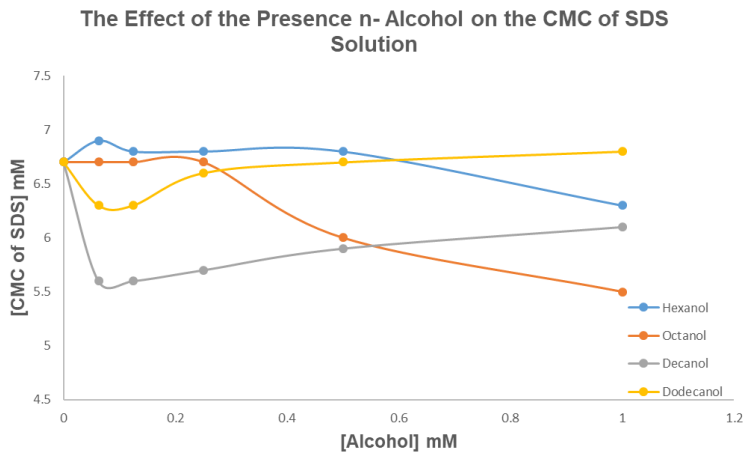

Figure 4-11: The effect of the presence of n-alcohol on the CMC of SDS

It is interesting to note that the CMCs of fatty alcohol such as decanol and dodecanol in the aqueous phase display the incredible value of CMCs, especially with a high concentration of alcohol due to solubility issues. These problems are because of the presence of insufficient concentrations of SDS solution in a set (contains gradual concentrations of SDS) that can help increase the solubility of decanol and dodecanol with high concertation of SDS. The melting point of dodecanol at room temperature is approximately 24 °C, so it shows a very low aqueous solubility [199].

4.3 Measuring the Critical Micelle Concentration of SDS with Normal 1-Alcohol (C_2, C_6 - C_{12}) in SHG Phase

Similarly with aqueous solution with normal- alcohols, CMC of SDS in the SHG phase were measured by using the same technique and the same probe (PIC) as previous experiment to measure the absorbance level of different concentrations of SDS between 500 and 650 nm. It was found that the wavelength of maximum absorbance (λ_{max}) was 608 nm. Each absorbance at λ_{max} of 608 nm was plotted against the concentration of the SDS surfactant and from the plots of absorbance vs. the concentration of SDS, there are discontinuities which represent the transition line from molecular amphiphiles to micelle formations, which is due to the intercalation of the pinacyanol cation into the self-assembled structure of the SDS. All experiments in the SHG phase with different alcohols were performed four times. It is worth mentioning that the CMCs of all the previous alcohols were measured with the condition of the clear SHG phase. Otherwise, cloudy SHG can be a big issue for the UV/Vis method.

4.3.1 Measuring the Critical Micelle Concentration of SDS in the Presence of Ethanol

The key thing here with ethanol experiments is to see if it could positively affect amphiphile self-assembly in the SHG phase. Ethanol in SHG was measured with only two concentrations, the lowest and the highest used concentration. As mentioned, ethanol was used as a cosolvent, therefore, there is a need to see at what expand the limit of using ethanol that cannot affect the CMC of SDS in SHG

phase because the addition of ethanol was at high concentration compared to other alcohols.

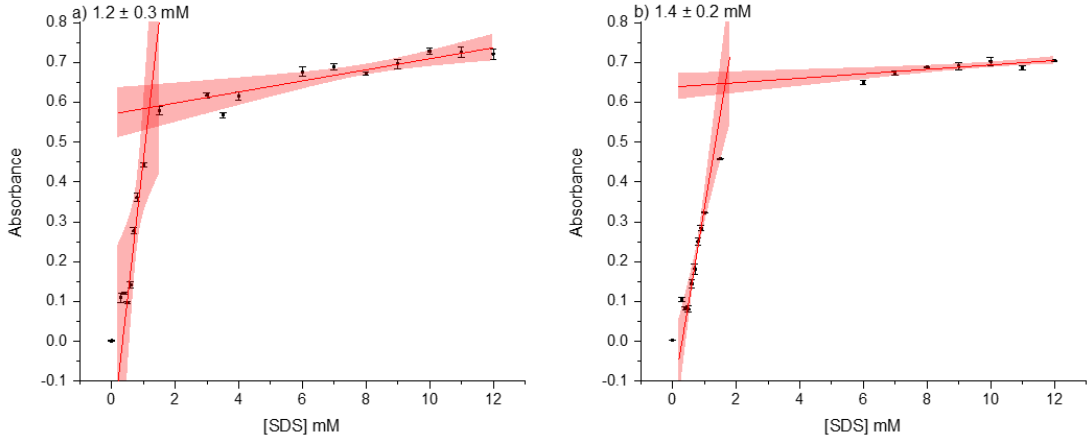

Figure 4-12: Estimation of the CMC value with different concentrations of ethanol in SHG: a) 0.14 M, b) 0.1.1 M by plotting specific absorbance of SDS versus concentration at the wavelength of 608 nm. The shaded line represents the fitting line with 95% confidence.

The obtained result indicates no significant changes due to the presence of ethanol, in CMCs of SDS in the SHG phase, including 0.14, and 1.1 M . The values acquired in SHG media with mentioned volumes were 1.2 ± 0.3, and 1.4 ± 0.2 mM, respectively (Fig. 4-12), compared to the CMC of SDS in the SHG phase without adding other additives.

4.3.2 Measuring the Critical Micelle Concentration of SDS in the Presence of Hexanol

The aim of this experiment is to see how the CMC of SDS can be affected by the SHG phase and chain length of selected alcohols in the aqueous phase.

The exact concentrations used in the aqueous solution of hexanol used in the SHG phase were 0.0625, 0.125, 0.25, 0.5, and 1.0 M. In the SHG phase, the values of the CMCs of SDS indicated no significant change (Fig. 4-13)

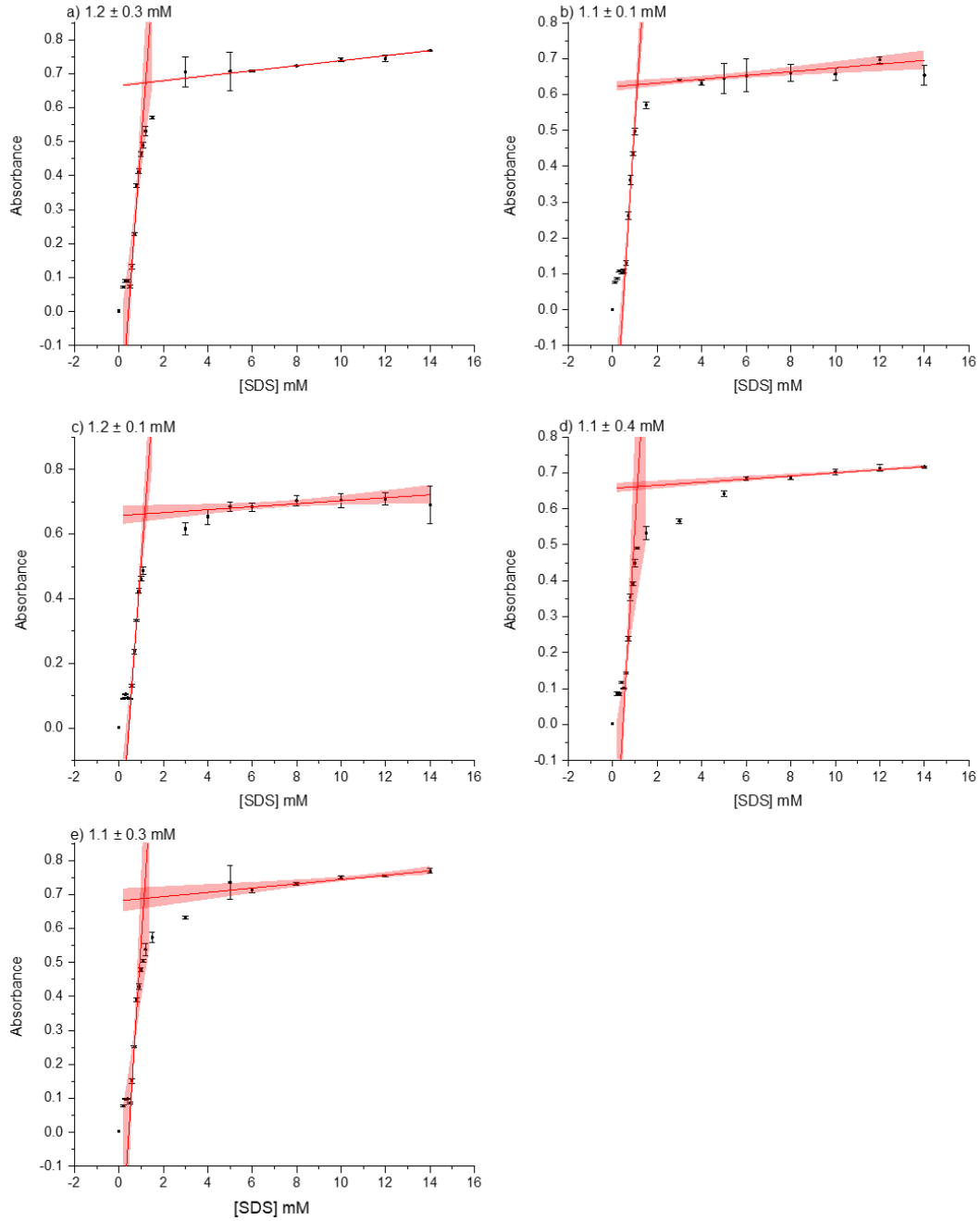

Figure 4-13: Estimation of the CMC value with different concentrations of hexanol in SHG phase: a) 0.0625 M, b) 0.125 M, c) 0.25 M, d) 0.5 M, and e) 1.0 M by plotting specific absorbance of SDS versus concentration at the wavelength of 608 nm. The shaded line represents the fitting line with 95% confidence.

4.3.3 Measuring the Critical Micelle Concentration of SDS in the Presence of Octanol

Following the same aim as for hexanol, the same concentrations used for experiments with hexanol were used in the presence of octanol in the SHG phase.

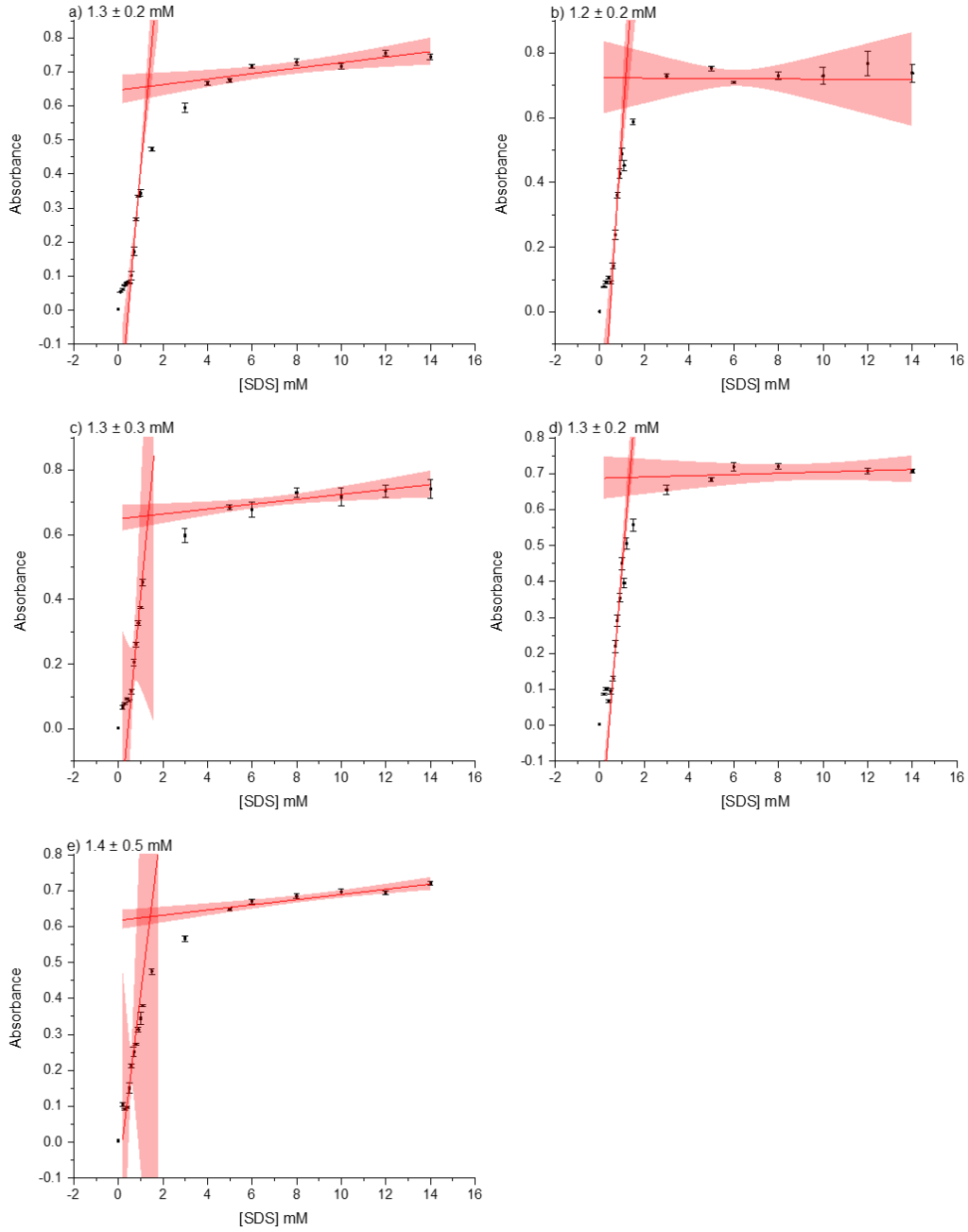

Figure 4-14: Estimation of the CMC value with different concentrations of octanol in SHG phase: a) 0.0625 M, b) 0.125 M, c) 0.25 M, d) 0.5 M, and e) 1.0 M by plotting specific absorbance of SDS versus concentration at the wavelength of 608 nm. The shaded line represents the fitting line with 95% confidence.

Similar to those for hexanol, the obtained results indicated no noteworthy changes in the presence of octanol (Fig. 4-14) in CMCs of SDS in the SHG phase, including 1.3 ± 0.2, 1.2 ± 0.2, .1.3 ± 0.3, 1.3 ± 0.2 and 1.4 ± 0.5 mM of 0.0625, 0.125, 0.25, 0.5 M, and 1.0 M respectively.

4.3.4 Measuring the Critical Micelle Concentration of SDS in the Presence of Decanol

Following the same aim as for the previous alcohols, these experiments were conducted to see how the CMC of SDS can be affected by the SHG phase and chain length of selected alcohols compared to the aqueous phase by using the same concentrations used in the aqueous solution.

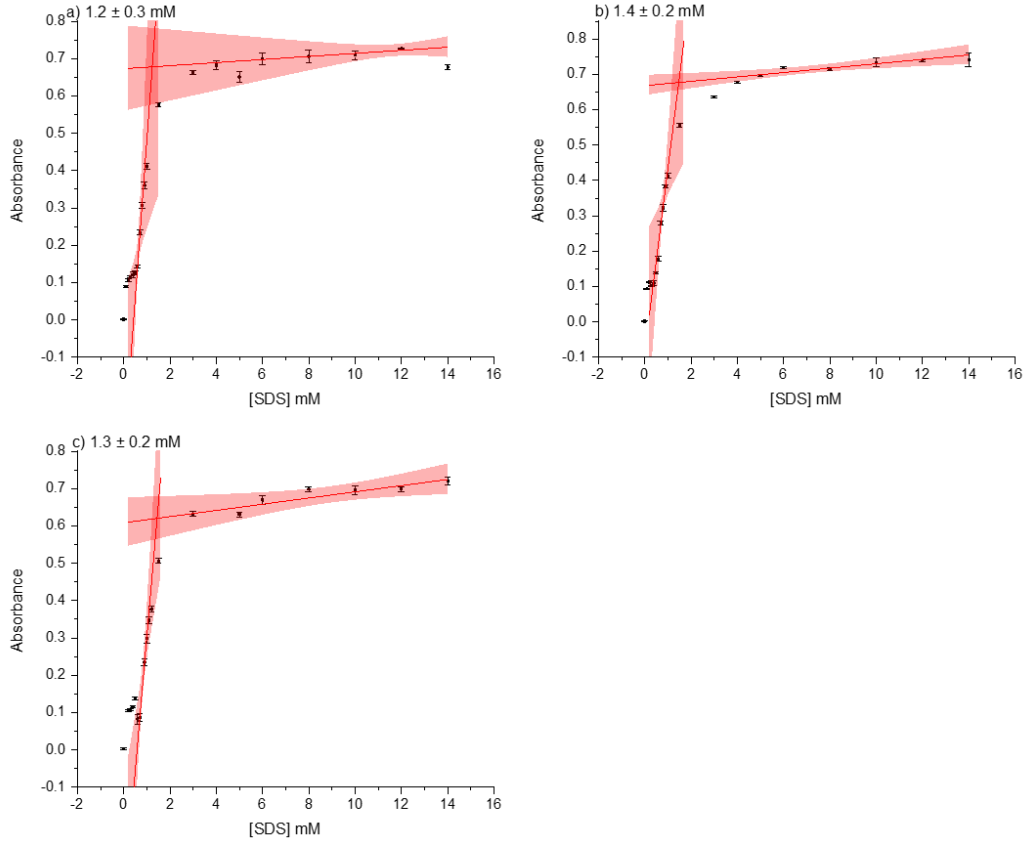

Figure 4-15: Estimation of the CMC value with different concentrations of decanol in SHG phase: a) 0.0625 M, b) 0.125 M, and c) 0.25 M by plotting specific absorbance of SDS versus concentration at the wavelength of 608 nm. The shaded line represents the fitting line with 95% confidence.

The results also did not show any significant changes in the CMC of SDS in the presence of decanol in the SHG phase with1.2 ± 0.3, 1.4 ± 0.2, and 1.3 ± 0.2 mM of 0.0625, 0.125, and 0.25 M in the same order.

At the concentrations of 0.5 and 1M decanol, turbid SHG appeared, which caused a problem in the absorbance measurements, which was possibly due to the undissolved molecules.

4.3.5 Measuring the Critical Micelle Concentration of SDS in the Presence of Dodecanol

Previous aim of other alcohol was followed in this section, with the same concentrations.

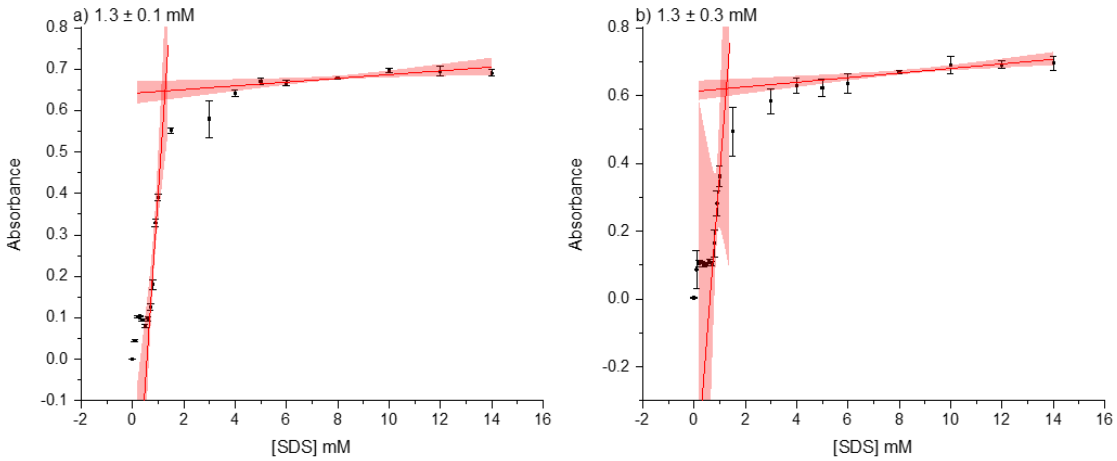

Figure 4-16: Estimation of the CMC value with different concentrations of decanol in SHG phase: a) 0.0625 M, b) 0.125 M by plotting specific absorbance of SDS versus concentration at the wavelength of 608 nm. The shaded line represents the fitting line with 95% confidence.

The CMCs of SDS in the presence of dodecanol were 1.3 ± 0.1, and 1.3 ± 0.3 mM of 0.0625, and 0.125 M respectively. These results indicate there are no significant changes, as shown in Fig. 4-16. In the presence of a high concentration of dodecanol in the SHG phase, the same problem of turbid phase appearing was faced in the SHG phase, including 0.25, 0.5, and 1M.

In general, by using the SHG as a medium for the self-assembly of SDS amphiphile in the presence of normal alcohol, the CMCs of SDS decreased by the presence of the cationic charge of silica hydrogel structure. Using various concentrations of alcohols did not show a significant change in the CMC of SDS.

4.3.6 The Effect of the Concentration of Normal 1-Alcohol (C_2, C_6 - C_{12}) on CMC Values in SHG Phase

CMC measurement property using UV/vis with PIC dye as a probe was chosen as an optimal method to measure the absorbance in the SHG phase. Interestingly, the measurements of CMC of SDS in the presence of organic substances, particularly normal 1-alcohol (C_2, C_6 -C_{12}) with an even number, in 0.5 M SHG, revealed significant changes in their CMCs, with almost the same

value of the CMCs in the presence of salts (Section 3.2.6). Even though there are different alcohols with various concentrations, the CMCs of SDS in the presence of selected alcohol were almost the same in the 0.5 M SHG, which provides another evidence of the reason for decrease in the CMC, which is the structure of SHG.

First of all, the decrease in the CMC of SDS in 0.5 M SHG compared with deionised water can be explained by that there is considerable salts content in the silica matrix shown by EDX analysis as seen in Section 2.3.2.2. It is suggested that there is a decrease through charge screening and reducing the dielectric constant of the SHG phase by the presence of Na^+ in the structure of SHG [99], which results in neutralising the repulsion in the SDS head group and decreasing the CMC significantly in the 0.5 M SHG phase compared with deionised water. Interestingly, adding alcohol, like salts (previous chapter), did not show any significant changes in the CMCs of SDS at the 0.5 M SHG compared with CMC of SDS only at 0.5 M SHG.

The results of having almost the same CMCs of SDS in 0.5 M SHG in a different concentration of normal 1-alcohol (C_2, C_6 -C_{12}) can be explained by several points. The first suggestion that can be behind the similar obtained CMCs and maintain the micellar structure is the SHG's structure and the SDS amphiphile. The structure of the silica hydrogel has a negative charge [200]. It has silanolate (Si–O-) and silanol (Si-OH) groups that are likely to interact strongly with positive charge species and reasonably with neutral chains, but not with negative charge species [201]. The maximum used concentration of SDS was 24 mM to form micellar structure in Å scale.

Depending on that, the reaction between the SHG (negative charge) and SDS (anionic surfactant) is not preferred. This agreed with another study conducted by [160]. They studied the impact of cationic [poly(ethyleneimine), PEI] and anionic water-soluble polymers [Poly (acrylic acid), PAA Na, Na salt] and (Carboxymethyl cellulose, CMC Na, Na salt) on the stability of SDS micelles by conductivity detection. The stability was explained by forming aggregates of 200 mM SDS, at which formed a stable micelle structure in the absence of the polymer. In the presence of the mentioned polymers, it was found that the anionic polymer facilitated the formation of SDS micelle because the interaction between 200 mM SDS and the anionic polymer is not possible due to repulsion force. On

the other hand, the cationic polymer reduced the stability of the micelle. The results indicated that the cationic polymers interacted strongly with 200 mM SDS and decreased the micellar structure stability because of the very strong electrostatic forces of attraction reaction. Study, by Zana et.al [202] reported similar result, SDS did not interact with PAA Na and CMC Na for the same reason. Also, a study by Vinot and co-worker [203] indicated that there is no effect of anionic polymers on the CMC of the SDS which has the same charge due to repulsion. These investigations about polymer-surfactant reaction are compatible with SHG with negative charged structure and SDS with maximum concentration of 24 mM that was examined in this study.

This study revealed the same trend as another study obtained by Barron and co-worker [204], but in the opposite way. They prepared liquid phase deposition, LPD, of silica with low pH (2), using the sol-gel method, and they tested their morphology in the presence of different charged surfactants. In the case of the existence of cationic surfactant (dodecyl trimethyl ammonium bromide, DTAB), they reported that the individual sphere present in the reaction solution is consistent with maintaining a separate micelle. The growth of silica spheres is greater than the growth of the sphere in the presence of cationic surfactant, which is compatible with a defined number of micelles. And also, they noticed that the growth of the micelle depends on the cationic surfactant concentration in the case of constant conditions (acidity and temperature) of the preparation method. The size of the silica sphere is inversely proportional to the micelles number of a given size. The following SEM images show the growth of LPD silica in the presence of DTAB with two different concentrations. The images of low concentration (Fig.4-17 a and b) show uniform spheres, while the images of high concentrations show more smaller spheres (Fig. 4-17 c and d). All images of silica in the presence of DTAB revealed a narrow size distribution.

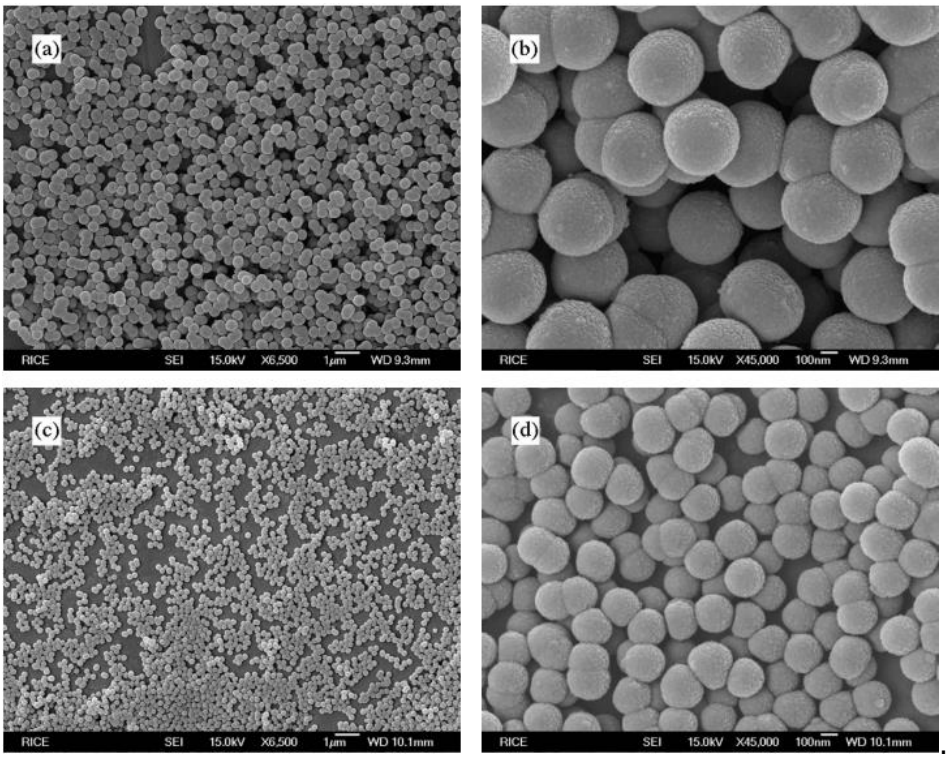

Figure 4-17: SEM analysis of the growth of LPD silica in the presence of DTAB with16 mM (a, b), and 64 mM (c, d), [204].

The other case of Barron's study is the presence of the anionic surfactant (sodium dodecyl sulfate, SDS).

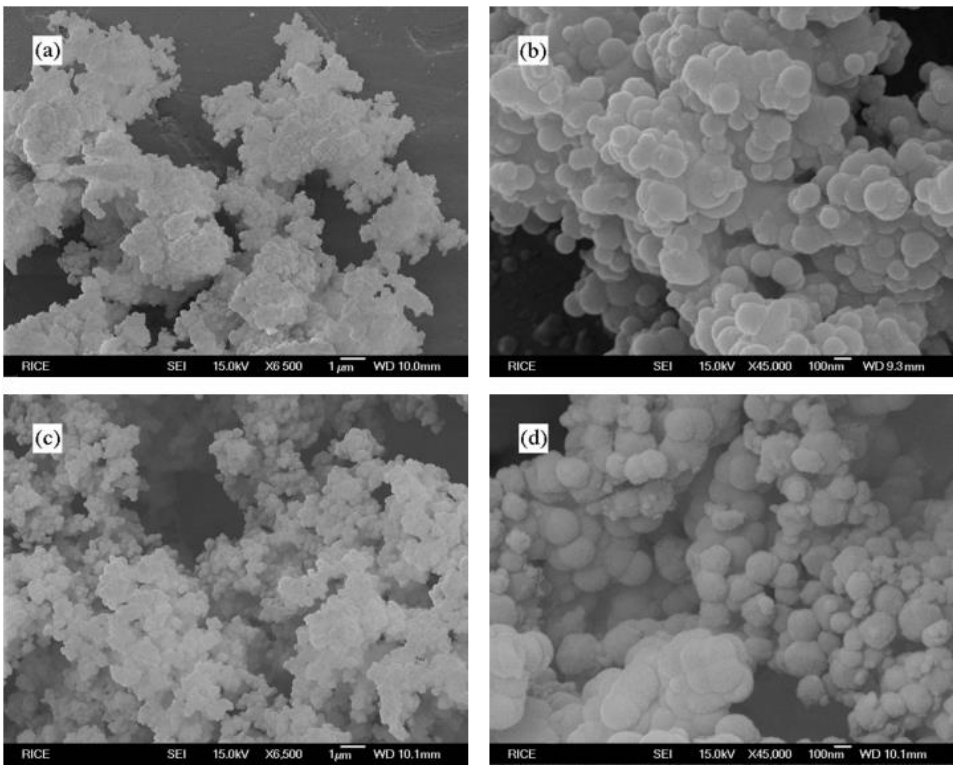

Figure 4-18: SEM analysis of the growth of LPD silica in the presence of SDS with 8 mM (a, b), and 32 mM (c, d), [204].

They observed the partially or completely collapse of anionic surfactant micelles with the same conditions, the silica results in extremely fused structures. Adding low concentration of SDS resulted in branched tree-like morphologies Fig. 4-18 (a, b), whereas adding high concentration resulted in greater intra-agglomerate porosity of the silica Fig. 4-18 (c and d). As a final result of this study in the acidic solution, they found that the stability of cationic micelles in low pH was greater than the stability of anionic surfactant.

The other suggestion of this discussion depends on the features of the silica hydrogels network since they retain a high content of water and have a porous structure, which can possibly facilitate the exchange of gas, nutrients, and bio-molecules [205].

With the same feature, Yamanaka and co-workers [206] used the sol-gel method that proved compatible with proteins recently encapsulated in silica glass. They stated that the protein molecules were solvated, and they retained their properties in the hydrogel media. This method enabled the relatively easy, non-invasive entrapment of proteins because the pores of hydrogels (partially dried gels) contain water.

Based on those studies and the results of the CMC of SDS after adding different concentrations of different selected alcohol that produce similar values of CMC, this is evidence of the efficiency of silica hydrogel retaining the micelle formation that presents one of the physical properties (CMC value of SDS/Alcohol). The preparation of 0.5 M SHG by sol-gel in this study has two main properties. Firstly, they are porous, so relatively small molecules can move through the pores and reach the relatively large molecules trapped inside. Secondly, these glasses are transparent in the UV-Visible range, and their reactions can be studied by optical spectroscopic methods [161], which helps the measurement of the CMC of SDS/Alcohol.

In general, previous studies indicate that the trapped compounds keep their physical properties in the hydrogel phase [162, 206]. The loading of SDS/Alcohol amphiphile in 0.5 M SHG based on self-assembly is being studied in this chapter to help understand the origin of life.

4.4 Conclusion

Overall, the main conclusions from this section can be summarised with the following points:

1. In the aqueous phase, the critical micelle concentrations (CMC) of the surfactant SDS in the presence of alcohol have been measured using UV-Vis spectrophotometry with pinacyanol chloride as a probe. The result shows:
   a. Ethanol behaves as a co-surfactant with low concentrations, including 0.14, 0.4, 0.6, 0.9, and1.1 M, but it behaves as a cosolvent with a higher concentration (1.3 M).
   b. Hexanol and octanol follow the role of addition additives depending on the chain length. The CMCs value of SDS decreases as the length of the chain increases.
   c. Decanol and dodecanol have a problem with solubility, which prevents them from following the role, especially with high concentrations.
2. In the silica hydrogel phase with using the same procedure, the CMC of SDS was decreased by the Na^+ presence of the SHG structure. However, CMC of SDS in the presence of alcohol did not show any significant change.

Chapter 5 Examining Vesicle Formation of SDS-Alcoholic Composites in Aqueous and Silica Hydrogels by Fluorescent Microscopy Techniques

5.1 Aim of This Chapter

In this section, we have attempted to visualise the self-assembly between fatty alcohols, namely decanol and dodecanol, with a low concentration of amphiphile SDS in both the aqueous and silica hydrogel (SHG) phases. In both cases, Nile red (NR) dye was used as a probe with two types of fluorescent microscopy, epifluorescent microscopy, and confocal fluorescent microscopy. The latter was used because it can potentially create images in the silica hydrogel phase, which is not possible using the widefield technique in this phase.

While previous chapters in this work have focused on the formation of micelle structures within a silica hydrogel (SHG) environment, this chapter attempts to see if it is possible to visualise larger, vesicular, structures in SHG media from mixtures of SDS and long chain alcohols.

The previous chapter described the self-assembly of the SDS/alcohol mixture, which occurred with micellar formation. By altering some conditions of the procedure used, in particular the ratio of SDS to alcohol, this chapter shifts to examining the self-assembly of vesicle formation.

Self-assembly of amphiphilic materials is thought to be one of the more important driving forces behind the origin of life [207-209], which is influenced by environmental circumstances [210]. The formation of the bilayer is considered a critical stage in this procedure [82]. If early membranes assembled from typical amphiphiles derived from hydrocarbon chains, a source of relatively long chains must have been available [83]. The morphology structure of the amphiphile depends on the medium circumstances such as temperature, solvent, and additives that can provide nanostructures such as micelles, vesicles, or nanotubes [211].

The surfactant of SDS is widely used as a bio-surfactants mimicking primitive membranes because it has a 12-carbon alkyl chain bonded to a small negatively charged sulfonate head [212]. This structure is close to the membrane’s phospholipid molecules that have great biocompatibility because of their similar composition to the contemporary biological cell. Phospholipid molecules can

assemble to form giant vesicles because they possess a hydrophilic head group and two hydrophobic hydrocarbon chains [213]. SDS molecules and long-chain alcohols might interact to produce double-tailed amphiphiles, such as a phospholipid membrane, to produce a membrane structure through vesicle formation by a hydrogen bond Fig. 5-1 [83].

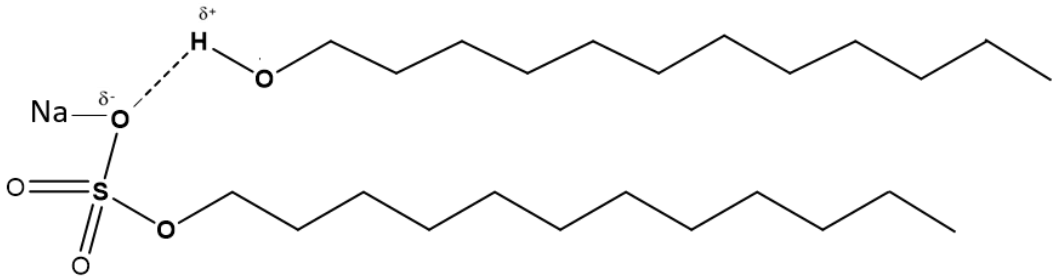

Figure 5-1: Possible reaction of SDS surfactant and dodecanol by forming a hydrogen bond to produce double-tailed amphiphiles.

Fatty alcohols from C_{10} to C_{18} have been given significant attention regarding their use as non-ionic surfactants [92]. Even though they have issues with solubility in water [214], they are commonly used in water as co-surfactants that possibly help to form stable vesicles in the aqueous phase [215]. It is worth mentioning that the presence of ethanol does not affect vesicle formation and stability in the solution [215, 216]. On this basis, the same stock solution of decanol and dodecanol was used in this study.

The microstructures and properties of spontaneous vesicles have been studied extensively [217-219]. For instance, anionic surfactant assembles in an aqueous solution by varying the mixing ratio between the ionic amphiphilic surfactants and the charge of the aggregates. This gives rise to a wide range of self-assembly forms, which are influenced by many factors such as molecular structure, temperature, surfactant concentration, and added salt [220]. Changing the conditions can result in formation of micelles, and unilamellar or multilamellar vesicles can be formed [221].

In Chapter 3, it is seen that the micelle structure can be formed with high pH (carbonate and silicate). Presumably, the formation of a micellar structure at high pH is needed as the precursor to vesicle formation [222]. Additionally, the presence of salts is very important to offer stable vesicles [82].

Based on these points, sodium carbonate was used to provide high pH to see how it can help in vesicle formation. Besides that, the presence of salt is essential to vesicle stability, possibly because of the screening charge in the head group, as in the case of fatty acids [87].

In every experiment, the concentrations of the components used in each sample were lower than the CMC of SDS/alcohol in both aqueous and SHG phases, which were used to prepare the sample SDS/alcohol sets. It should be mentioned here that our selection of tested concentrations of SDS/alcohol sets in the following experiments was based on other researchers' concentrations or by testing the lower concentrations used in the previous chapter in the presence of sodium carbonate [82].

Nile Red is a hydrophobic dye and poorly soluble in water, with an environmental polarity that identifies spectral properties [223]. Indeed, it is stable photochemically, provides strong fluorescence naturally [224], and is not sensitive to changing pH, which enables a wide range of practical work [115]. The significant advantage is that it can contact lipids and emit fluorescence when dissolved in a nonpolar organic solvent. However, this fluorescence is quenched in the aqueous solution. This behaviour of NR in hydrophilic and hydrophobic mediums makes it a good candidate for staining lipid molecules [225]. Thus, due to these advantages, NR was used as a probe in this study (Fig. 1-27).

In the following images of visualisation experiments with both epifluorescence microscopy and confocal microscopy, various morphology structures were obtained, including vesicles, oil droplets, or crystals, indicating contact of NR with the lipophilic layer of the SDS/alcohol mixtures. It is worth mentioning that the colour emission of NR varies from red to strong gold in lipophilic environments [226], which makes it easy to observe structures during the monitoring by both devices but not in the obtained images, which suffer from low quality.

5.2 Visualisation of the SDS/Alcohol Composite Using Epifluorescence Microscopy in the Aqueous Phase

Epifluorescence microscopy was used to visualise samples in the aqueous phase, including SDS/decanol and SDS/dodecanol, to determine their capacity to self-assemble into vesicles. The preparation consisted of several systems for

each of them. The aim was to find the optimal concentration needed to form vesicles with NR staining.

5.2.1 Visualisation of the Composite SDS/Decanol

Epifluorescence microscopy was applied to visualise the samples of SDS/decanol and determine whether they could self-assemble into vesicles. Several different preparation systems were used:

(i) 1.5 mM of SDS and 1.0 mM of decanol with different concentrations of sodium carbonate.

(ii) 4% decanol: 1.0 mM of SDS and 0.04 mM of decanol with varying carbonate concentrations.

The aim was to find the optimal concentration needed to form vesicles.

5.2.1.1 Mixtures of 1.5 mM of SDS and 1.0 mM of Decanol with Different Concentrations of Sodium Carbonate

Epifluorescent microscopy was used to visualise samples with a 1.5:1 SDS/decanol ratio with and without sodium carbonate. In the absence of sodium carbonate, the image looked like little oil droplets, as shown with blue arrows (Fig. 5-2 a), and they moved in the solution. In the rest of the images, after adding low concentrations of salt (0.015 with Fig. 2-5 b, and 0.025 M with Fig. 2-5c and d), the appearance of solid precipitates was revealed, as shown with red arrows. With higher concentrations of salt (0.04 and 0.05 M), further growth of oil droplets appeared (Fig. 5-2 e and f for 0.04 M, and Fig. 5-2 g for 0.05 M, respectively) which means the alcohol did not fully insert into the vesicle [178], particularly with 0.05 M of sodium carbonate. However, the image with the highest concentration (0.1 M of salt) indicates the appearance of what may appear to be crystals (Fig. 5-2 h). It seemed that the NR may have been quenched in the last case of the highest carbonate concentration. Low NR fluorescence can be explained by this because the salted media, which strongly affected the solubility of the solvent, resulted in a change in the miscibility of NR [115, 227].

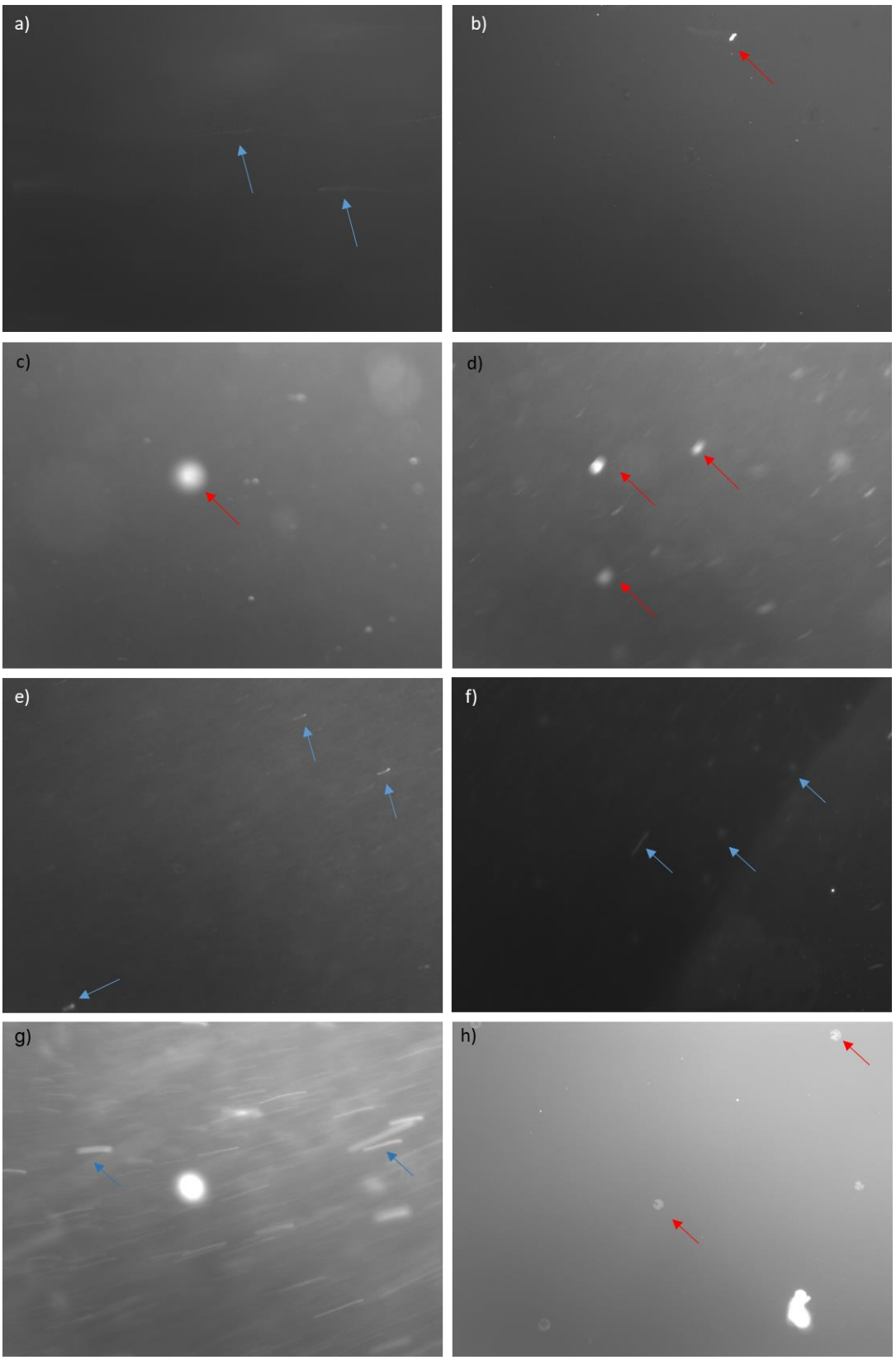

Figure 5-2: Epifluorescence microscopy images with NR stained of 1.5 mM SDS, 1.0 mM decanol with different concentrations of sodium carbonate: a) 0.0, b) 0.015, c and d for 0.025, e and f for 0.04, g) 0.05, and h) 0.1 M.

5.2.1.2 Mixtures of 1.0 mM of SDS and 0.04 mM of Decanol with Different Concentrations of Sodium Carbonate

These low concentrations were selected because the results in previous preparations revealed the appearance of what appeared to be oil droplets. The latter appeared because of a high concentration of decanol that is not completely soluble in the solution. Monnard and co-workers [178] found that more vesicles can be formed with different pH ranges with decylphosphate mixed with 4% decanol rather than 2% decanol. Therefore, the following concentrations represent the mixture of SDS with 4% decanol and different concentrations of sodium carbonate.

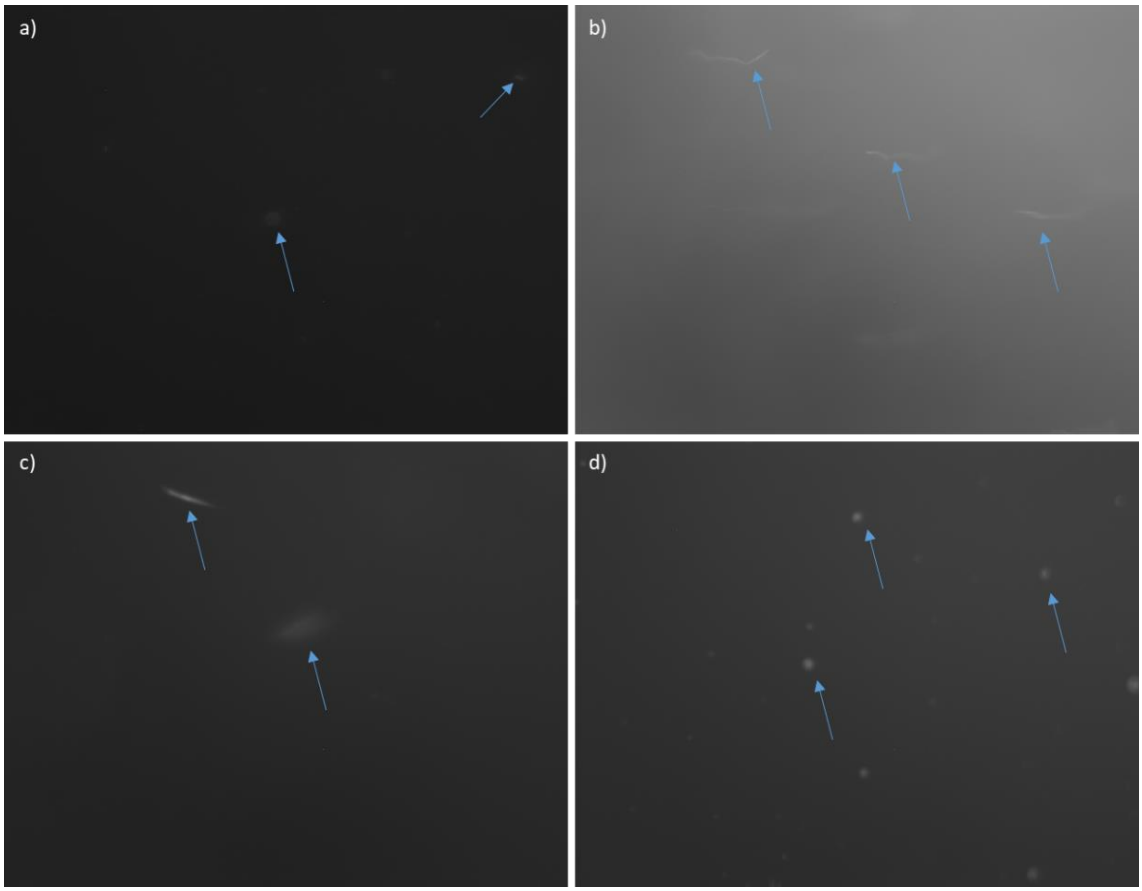

Figure 5-3: Epifluorescence microscopy images with NR stained of 1.0 mM SDS, 0.04 mM decanol with different concentration of sodium carbonate: a) 0.0, b) 0.04 M, c) 0.05, and d) 0.06 M.

Epifluorescence microscopy was used to visualise samples with a 1:0.04 SDS/decanol ratio in the presence and absence of sodium carbonate. In general, the images of SDS/decanol obtained using epifluorescence microscopy revealed the movement of structures in most of these systems. They could be oil droplets

because of high concentrations of materials used [178], or they could be vesicle structures, but they are unclear because of the low visualisation quality.

5.2.2 Visualisation of the SDS/Dodecanol Composite

Similar to the SDS/decanol mixture, SDS/dodecanol was visualised by epifluorescence microscopy to determine its ability to self-assemble into vesicles. Three systems were prepared with dodecanol:

i. 0.25 mM of dodecanol and 0.04 M of sodium carbonate with different concentrations of SDS.
ii. 0.125 mM of SDS and 0.0625 mM dodecanol with different concentrations of sodium carbonate.
iii. Mixtures of 0.25 mM of SDS and 0.125 mM of Dodecanol with Different Concentrations of Sodium Carbonate
iv. 1.0 mM of SDS and 0.04 mM of dodecanol with different concentrations of sodium carbonate.

5.2.2.1 Mixtures of Different Concentrations of SDS and 0.25 mM of Dodecanol with 0.04 M of Sodium Carbonate

With the same aim mentioned previously, epifluorescence microscopy was used to visualise the SDS/dodecanol mixture and explore the self-assembly structure. A series of different SDS concentrations were prepared with 0.25 mM of dodecanol in the presence of 0.04 M of sodium carbonate.

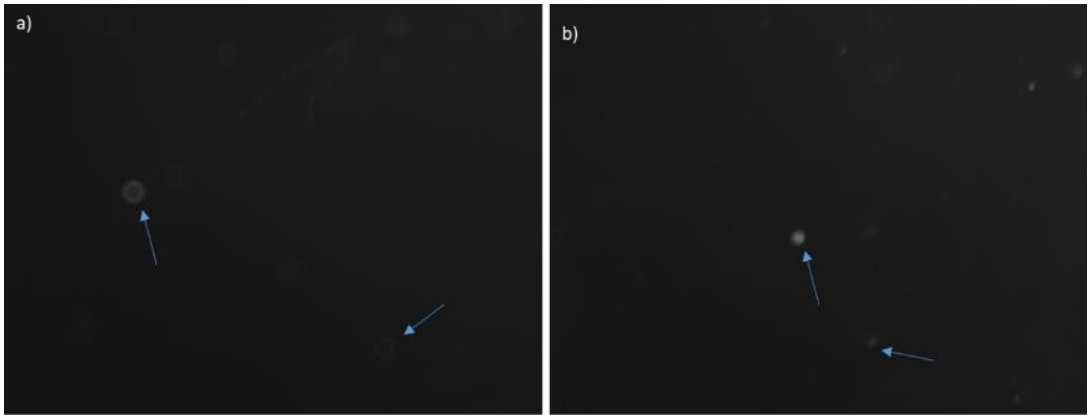

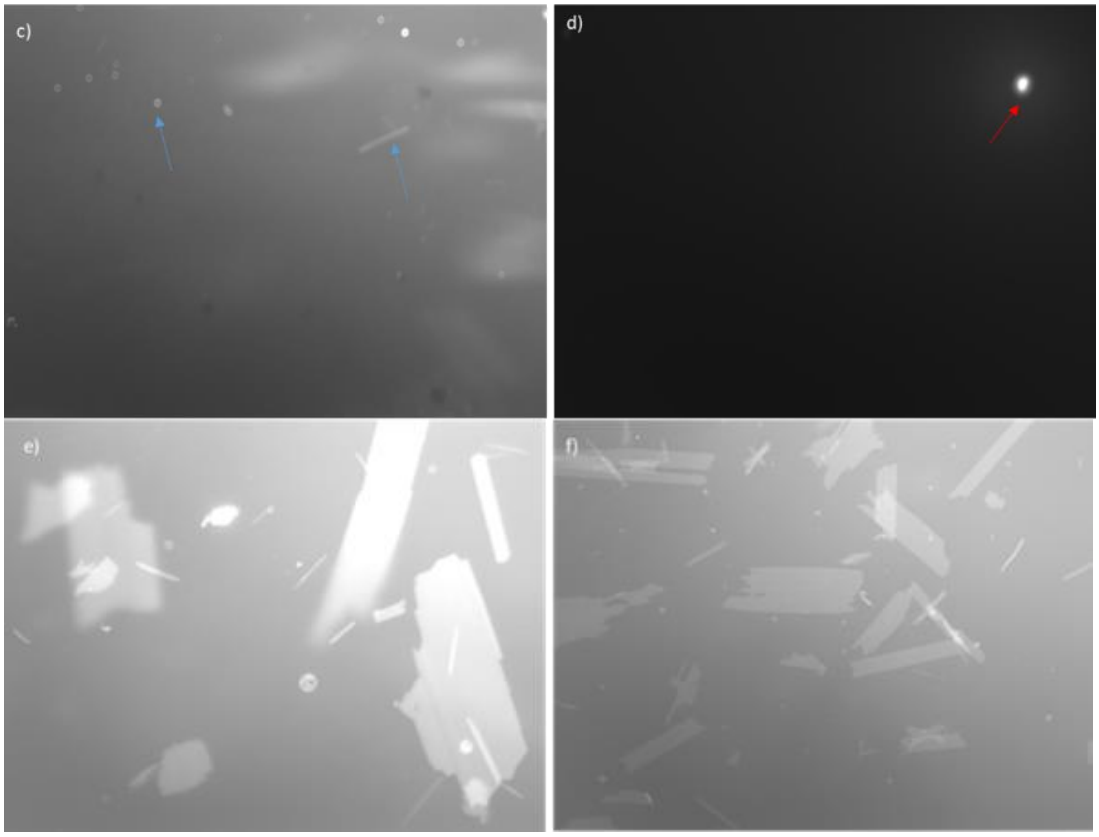

Figure 5-4: Epifluorescence microscopy images with NR stained of 0.25 mM dodecanol and 0.04 M sodium carbonate with different concentrations of SDS: a, b and c of 0.5 mM, d) 1.0 M, e) 1.5, and f) 2.0 mM.

The images of dodecanol with different concentrations of SDS show oil droplets (blue arrows) and possible vesicle structures with the lowest used SDS concentration of 0.5 mM, as shown in Fig. 5-4 a, b and c. However, with the other concentrations of SDS, the appearance of solid precipitates was revealed, as shown in Fig. 5-4 e and f.

5.2.2.2 Mixtures of 0.125 mM of SDS and 0.0625 mM of Dodecanol with Different Concentrations of Sodium Carbonate

In these cases, the millimolar ratios of SDS/dodecanol 2 :1 were conducted with two different concentrations of carbonate. With the lower salt concentration, the image indicates the formation of oil droplets (Fig. 5-5 a). However, with the higher concentration of salts, the image revealed possible vesicle formation (Fig. 5-5 b). With this ratio, vesicles formed in certain areas [178]. Indeed, a higher concentration of alcohol resulted in the formation of oil droplets, which agrees with previous studies [92].

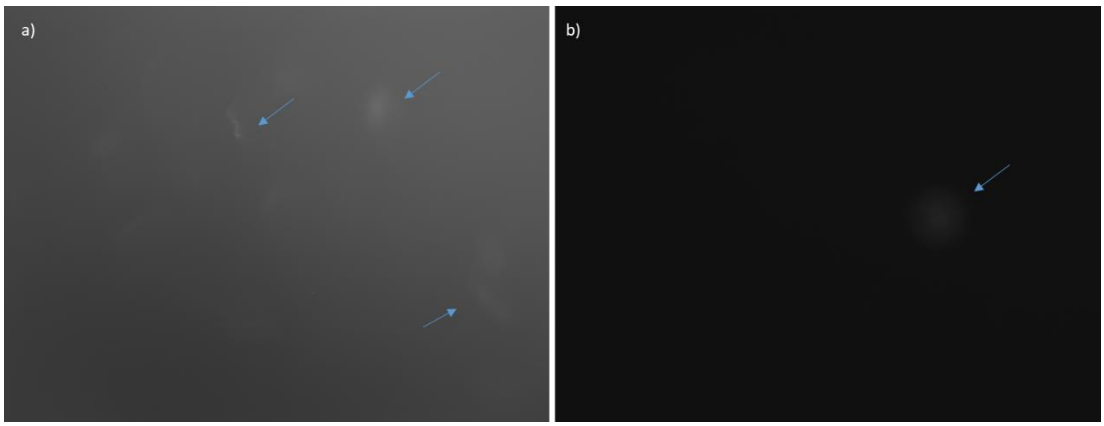

Figure 5-5: Epifluorescence microscopy images with NR stained of 0.125 mM SDS,0.0625 mM dodecanol with two concentrations of sodium carbonate: a) 0.02, and b) 0.04 M.

5.2.2.3 Mixtures of 0.25 mM of SDS and 0.125 mM of Dodecanol with Different Concentrations of Sodium Carbonate

The same situation as the previous one was tested with the same millimolar ratio of SDS/dodecanol (2:1), but with double concentrations of each of them.

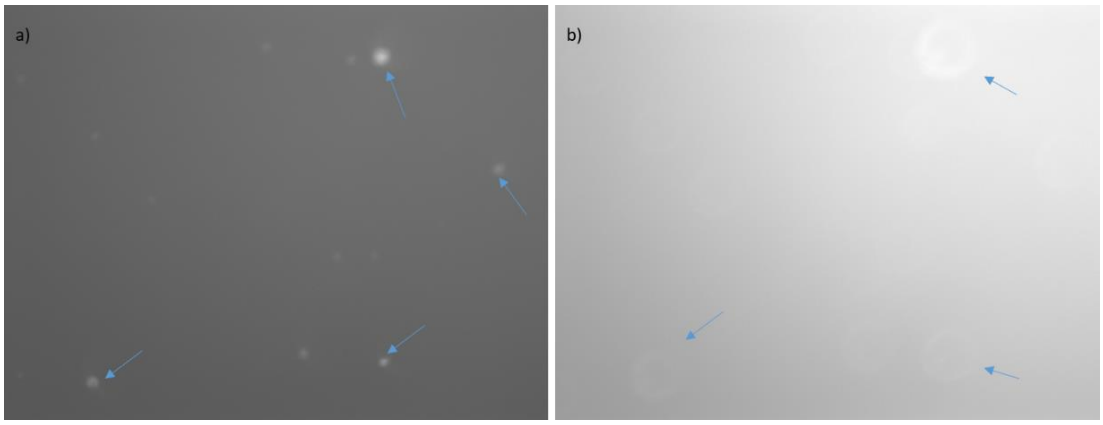

Figure 5-6: Epifluorescence microscopy images with NR stained of 0.25 mM SDS, 0.125 mM dodecanol with two concentrations of sodium carbonate: a) 0.02, and b) 0.04 M.

The appearance of oil droplets in both cases with different concentrations of salt was observed, as shown with blue arrows, which did not agree with the study by Monnard and co-workers [178], who found that this ratio can results in vesicle formation. A 2:1 ratio of SDS to alcohol is quite a large proportion of alcohol, this might be contributed to the oil droplet formation.

5.2.2.4 Mixtures of 1.0 mM of SDS and 0.04 mM of Dodecanol with Different Concentrations of Sodium Carbonate

The 1:0.04 SDS/dodecanol ratio was used with various concentrations of sodium carbonate to see if there was any vesicle formation. In each case of adding salt, the oil droplet formation (blue arrows) was indicated, as the image shows (Fig. 5-7 a). However, with 0.04 M and 0.05 M of salt, the image displayed possible vesicle formation, as indicated by the green arrows (Fig. 5-7 b for 0.04 M and Fig. 5-7 c for 0.05 M).

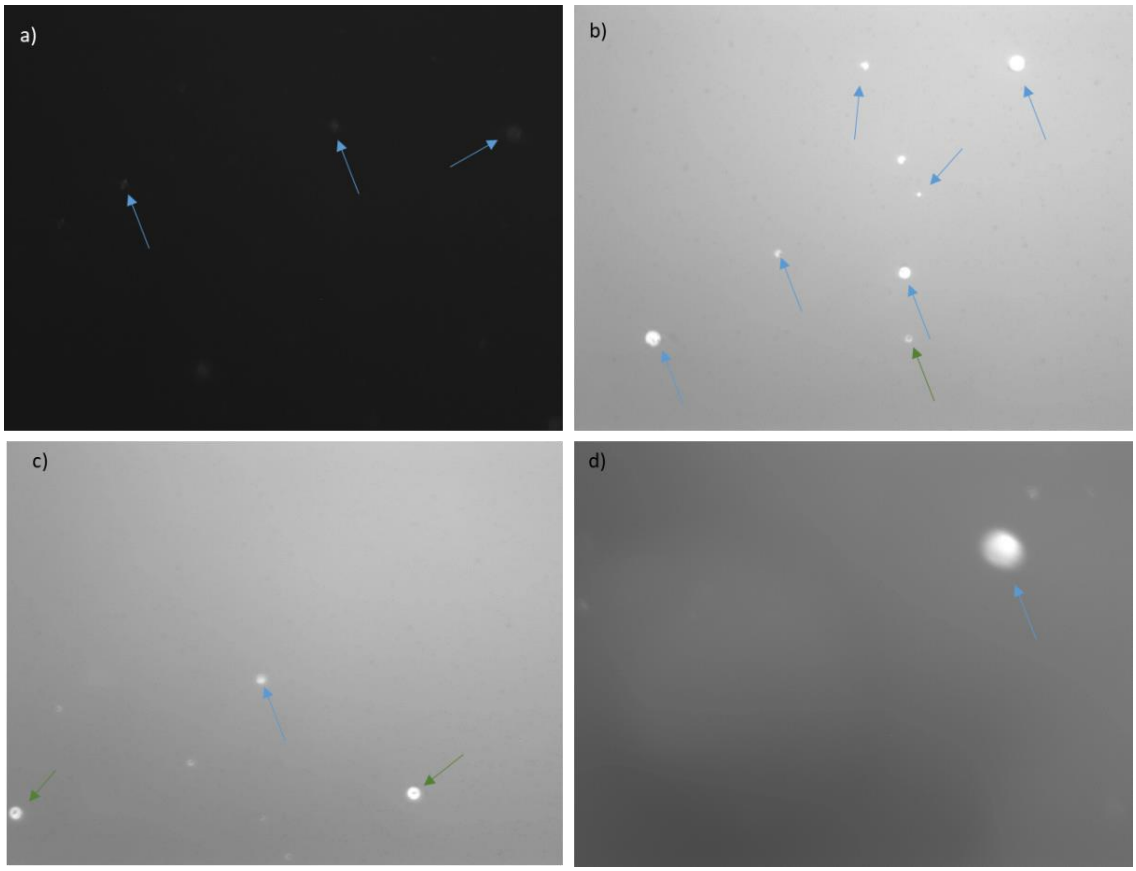

Figure 5-7: Epifluorescence microscopy images with NR stained of 1.0 mM SDS, 0.125 mM dodecanol with different concentrations of sodium carbonate: a) 0.0, b) 0.04, c) 0.05, and d) 0.06 M.

Three systems were visualised of the admixture of SDS/alcohol in the absence or presence of different concentrations of salt. All images showed the formation of droplets or vesicle. That means that all used concentrations of the sodium carbonate did not resulted in any crystal appearance that affect the formation of any structures.

It is possible for vesicles and oil droplets to form in the same solution, as demonstrated in the image obtained by [178]. In this research, the reaction of decyl phosphate and decanol formed vesicles (pointed out by arrows) and oil droplets (indicated by arrowheads), as shown in the Fig. 5-8, using NR as a probe to visualise the sample with a confocal microscope.

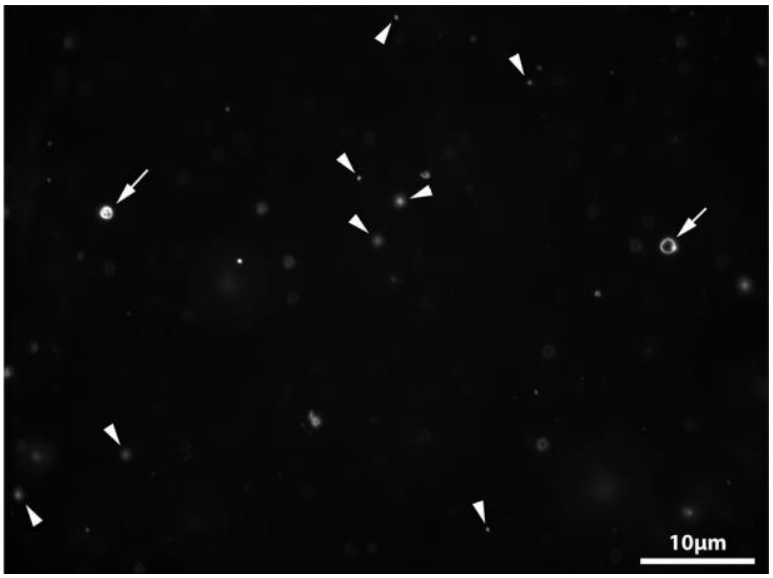

Figure 5-8: The formation of vesicle (arrows) and oil droplets (arrowhead) in the same solution (reaction of decyl phosphate and decanol), [178].

In general, using epifluorescence microscopy in both mixtures of decanol and dodecanol with SDS surfactant showed different structure formation in the aqueous phase. The formation of vesicles, oil droplets, or crystals occurred because of the various concentrations of materials used. It is difficult to determine the structure formed because of the low visualisation quality. Consequently, we moved to explore fluorescent microscopy.

5.3 Visualisation of the SDS/Decanol Composite by Epifluorescence Microscopy in the SHG Phase

Epifluorescence microscopy was used to visualise samples in the SHG phase after four hours with SDS/decanol only to see if they could self-assemble into vesicles. The SDS/decanol mixture was prepared in four systems depending on the sodium carbonate concentration.

5.3.1 Mixtures of 1.0 mM of SDS and 0.04 mM of decanol with Different Concentrations of Sodium Carbonate after Four Hours

Epifluorescence microscopy was used to visualise two systems after four hours, which were still in their liquid phase at room temperature, so it was easy to transfer them onto the slide. The first system included no added sodium carbonate, and the other 0.06 M, to determine the capacity of SDS/decanol to self-assemble into vesicles in this phase. With both concentrations, the images revealed crystal formation, and their growth was evident with a high salt concentrations.

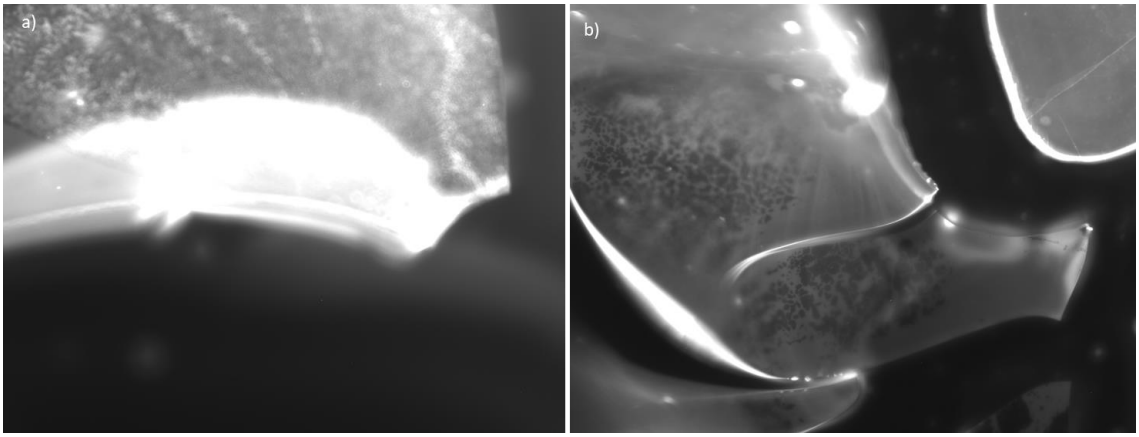

Figure 5-9: Epifluorescence microscopy images with NR stained of 1.0 mM SDS, 0.04 mM decanol with different concentrations of sodium carbonate: a) 0.0, and b) 0.06 M after 4 h in SHG phase.

5.3.2 Mixtures of 1.0 mM of SDS and 0.04 mM of Decanol with Different Concentrations of Sodium Carbonate after 24 Hours

The same samples were visualised after 24 hrs in the SHG phase. In both samples, the images revealed crystal formation [215, 228].

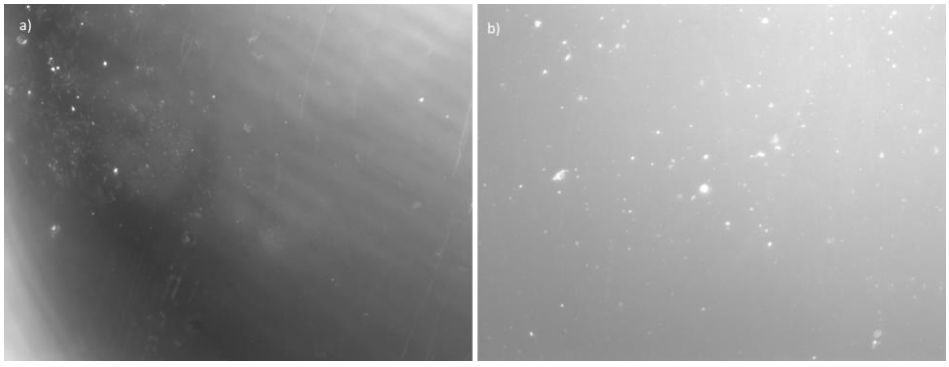

Figure 5-10: Epifluorescence microscopy images with NR stained of 1.0 mM SDS, 0.04 mM dodecanol with different concentrations of sodium carbonate: a) 0.0, and b) 0.06 M after 24 h in SHG phase.

Unfortunately, the images obtained by epifluorescence microscopy in the SHG phase indicated no vesicle formation.

In general, using epifluorescence microscopy in both mixtures of decanol and dodecanol with SDS surfactant showed different structure formation in the aqueous phase. The formation of vesicles, oil droplets, or crystals appeared because of the various concentrations of materials used and the effect of carbonate concentration. In most prepared systems, it was difficult to determine the structure formed because of the low visualisation quality. The imaging resolution obtained by conventional fluorescence did not offer a clear vision of the structure formed. Blurred images were obtained in most prepared systems. Therefore, confocal microscopy was used in the following section to obtain a better imaging resolution. Confocal microscopy can offer clear optical sections; image processing can be used to enhance confocal images to 3D images, and the images obtained can be analysed using computer software.

5.4 Visualisation of the SDS/Decanol Composite Using Confocal Florescent Microscopy

Confocal fluorescent microscopy was used to visualise samples with better resolution in both phases, particularly in the SHG phase, which is difficult to visualise with the epifluorescent microscope, to investigate whether the structure formed with SDS/decanol by self-assembly included vesicles. To achieve this, the samples were prepared with the same concentration of SDS/decanol in the presence and absence of sodium carbonate in the aqueous solution and then compared with the SHG phase. The experiments aimed to determine the ability of SHG to maintain the self-assembly of vesicle formation, if any such formation occurred.

Confocal florescent microscopy can produce 3D images because of its ability to scan the z-axis, from the top of the sample to the bottom [229], image processing can be used to enhance confocal images for 3D images allowing real-time observation [230], and it can analyse the images obtained through specific computer software such as ImageJ.

To achieve that, the same concentration of SDS/Decanol was prepared in the presence and absence of sodium carbonate as described above for aqueous

solution then compare them to the SHG phase. The experiments aim to see the ability of SHG to maintain the self-assembly of vesicle formation if any.

The confocal florescent microscopy was used, which can produce 3D images because of its ability to scan z-axis [231]. The aqueous phase was examined first; the preparation consisted of four different concentrations of sodium carbonate (0.0, 0.04, 0.05, and 0.06 M) with 1.0 mM of SDS and 0.04 mM of decanol. For image analysis, ImageJ software was used [232].

5.4.1 Mixtures of 1.0 mM of SDS and 0.04 mM of Decanol with and without Sodium Carbonate in the Aqueous Phase

This experiment was conducted using confocal microscopy, and the images indicate unclear structural movement (Section 5.2.1). For better images and comparison, the experiment was repeated to be visualised by confocal fluorescent microscopy. In addition, using the SHG phase as the medium to visualise this system involved four different concentrations (0.0, 0.04, 0.05, and 0.06 M) of sodium carbonate in 1.0 mM of SDS and 0.04 mM of decanol.

The results can be broken down into three main points. Firstly, the images of the presence of both 0.04 and 0.05 M of sodium carbonate revealed no formation of vesicles by the SDS/decanol mixture (Fig. 5-12a and b for 0.04 and 0.05, respectively).

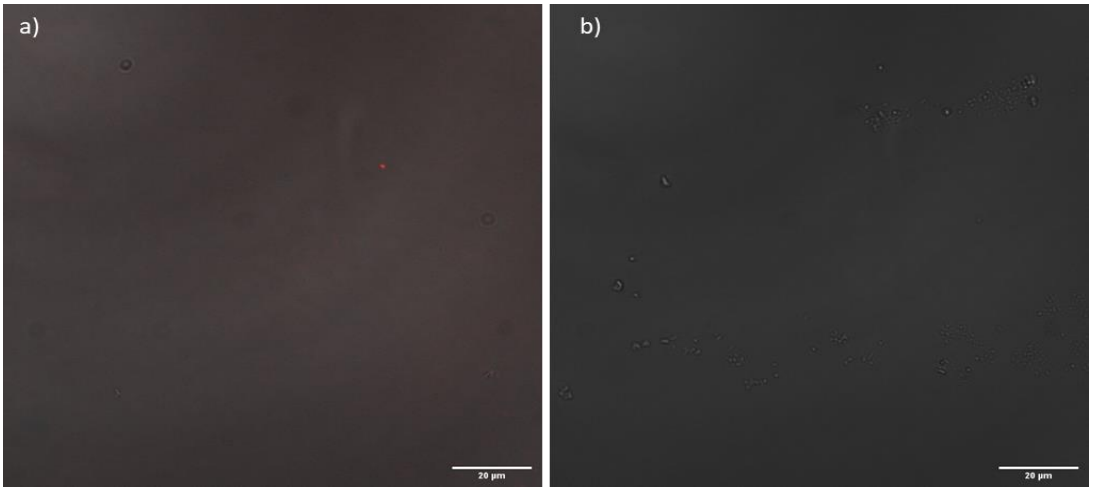

Figure 5-11: Confocal microscopy images with NR stained of 1.0 mM SDS, 0.0.04 mM decanol with different concentrations of sodium carbonate: a) 0.04, b) 0.05 M, (scale 20 µm).

The second point is that in the absence of sodium carbonate with the SDS/decanol mixture, the confocal microscopy images revealed the formation of oil droplets (blue arrows), and what we envisage to be large unilamellar vesicles (LUV) with ca size 2 µm and multi-vesicular vesicles (MVV) with ca size 2 µm as indicated by green arrows.

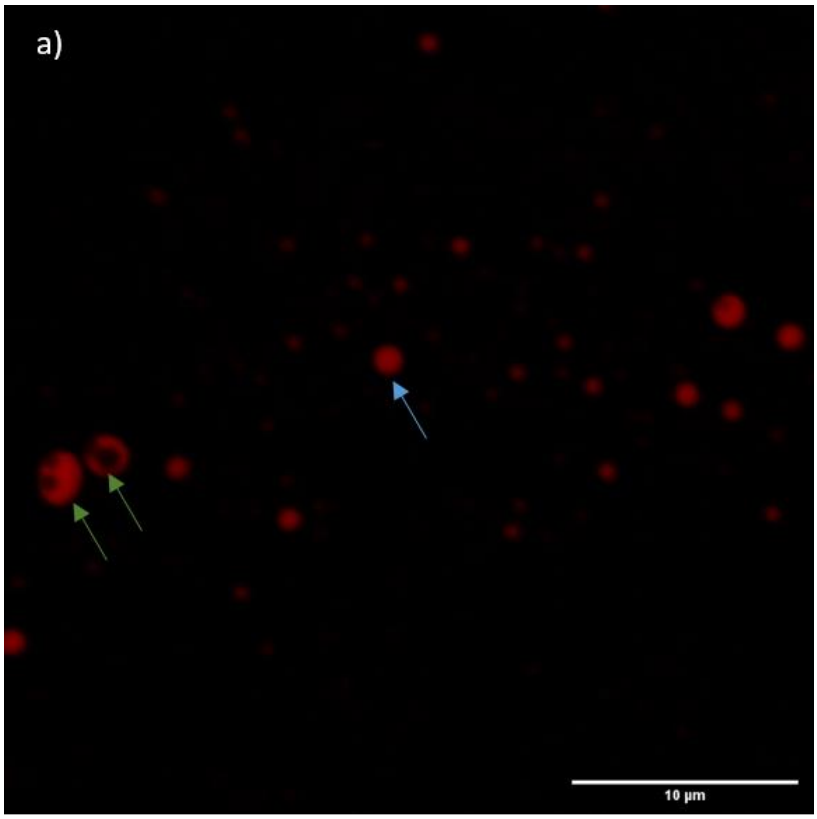

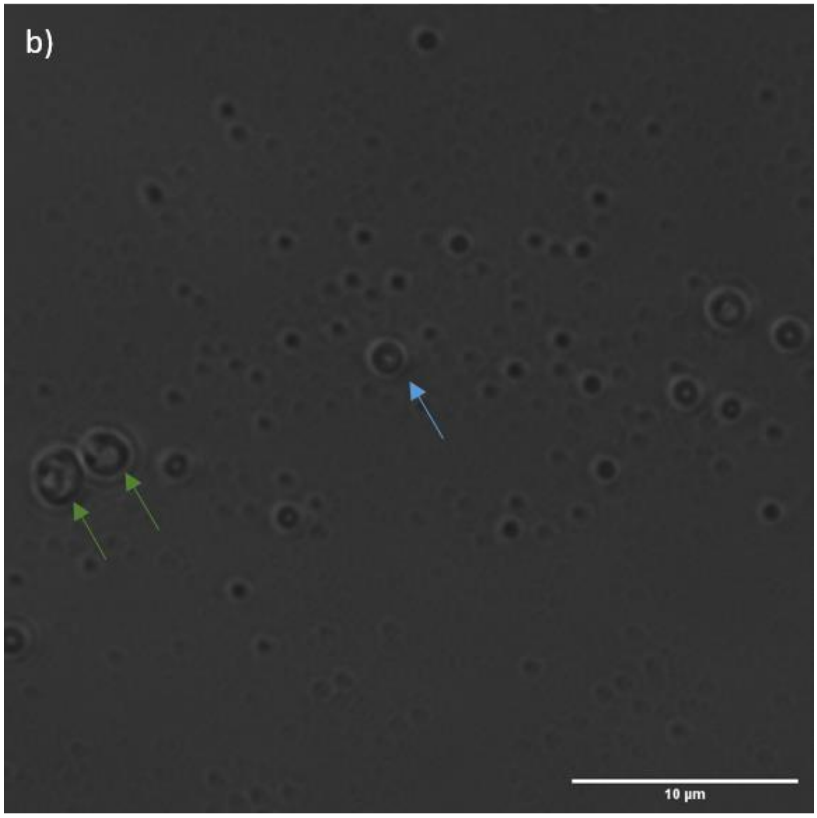

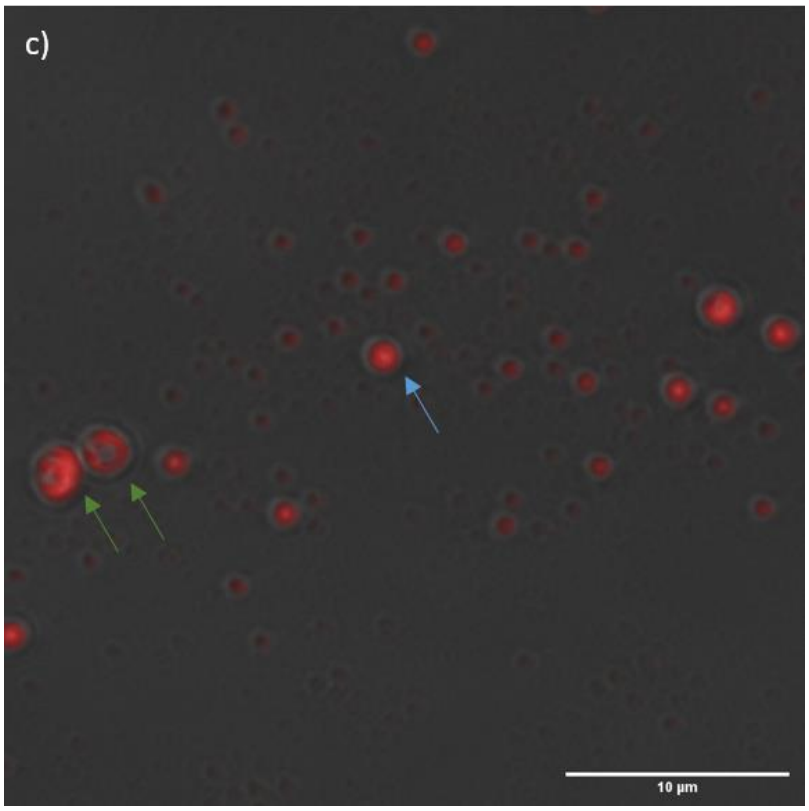

Figure 5-12: Confocal microscopy images with NR stained of 1.0 mM SDS, 0.04 mM decanol, vesicle with green arrows, oil droplets with blue arrows, (scale 10 µm).

The images show the location of the NR (Fig. 5-13 a) and bright-field (b), and the last image merges the first and second images (c).

It is worth mentioning that the bright-field microscope is considered the simplest technique of optical microscopes since they use visible light and several lenses for image magnification of the specimen for more details. This technique uses light rays to produce a dark image with a bright background [233].

An interesting result of this preparation here is that the SDS/decanol mixture is able to form vesicles directly without any addition of salt and unbuffered water [208, 234, 235], which is required in many researches. This makes decyl sulphate a stimulating candidate presenting a bilayer component in primitive cell systems in an easy way.

The last point is that in the presence of 0.06 M of sodium carbonate with the SDS/decanol mixture, the images revealed the formation of oil droplets without any vesicle formation. The images show the location of the NR (Fig. 5-14 a) and

bright-field (Fig. 5-14 b), and the last image merges the first and second images (Fig. 5-14 c).

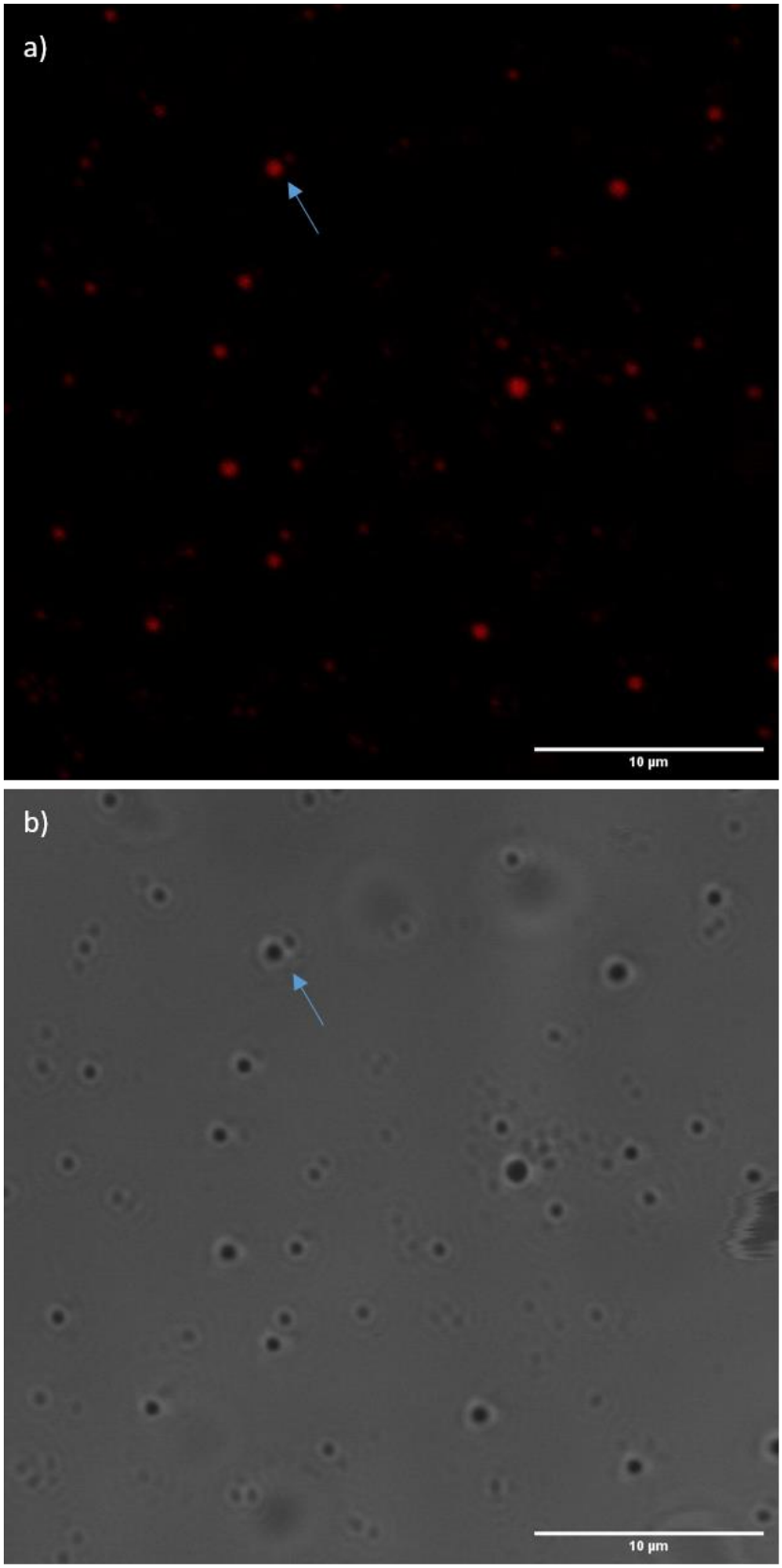

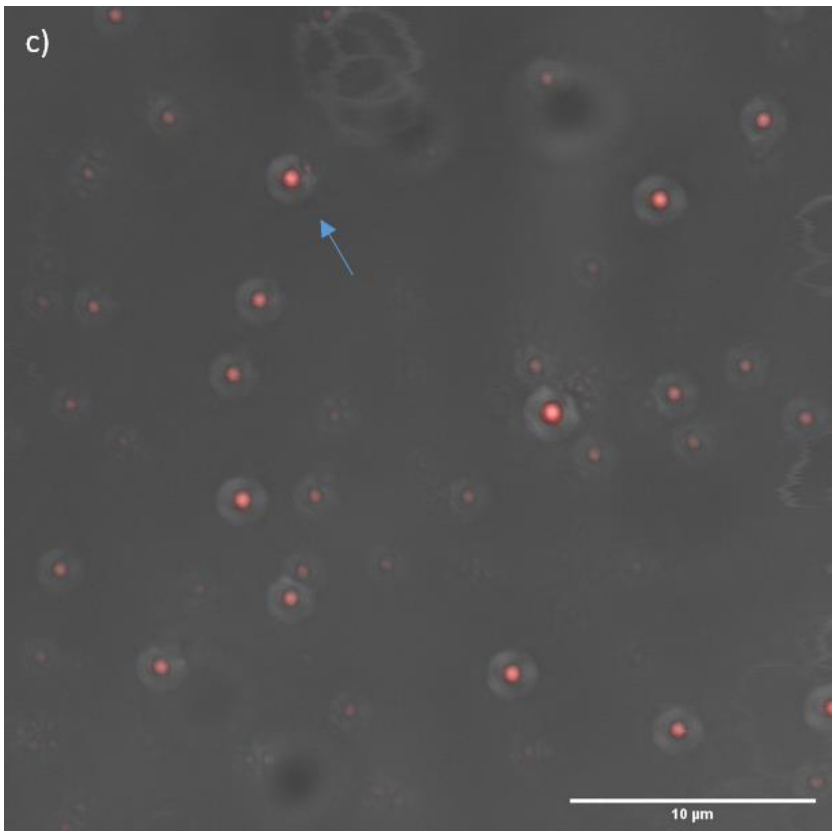

Figure 5-13: Confocal microscopy images with NR stained of 1.0 mM SDS, 0.04 mM decanol 0.06 M sodium carbonate, oil droplets with blue arrows, (scale 10 µm).

Candidate mixtures that resulted in vesicle and oil droplets with 1.0 mM of SDS and 0.04 mM of decanol in the presence and absence of 0.06 M of sodium carbonate were chosen for confocal fluorescent microscopy visualization in the SHG phase.

5.4.2 Mixtures of 1.0 mM of SDS and 0.04 mM of Decanol with and without Sodium Carbonate in the SHG Phase

Confocal fluorescent microscopy was used to visualise SDS/decanol in the SHG phase, which is difficult to visualise with an epifluorescent microscope because of the appearance of bright crystals of salts (Section 5.3). To investigate the structures formed with SDS/decanol self-assembly, the same concentrations of SDS/decanol were prepared with 0.0 and 0.06 M of sodium carbonate, which resulted in vesicle formation and oil droplets in the aqueous phase, to see if SHG could maintain them.

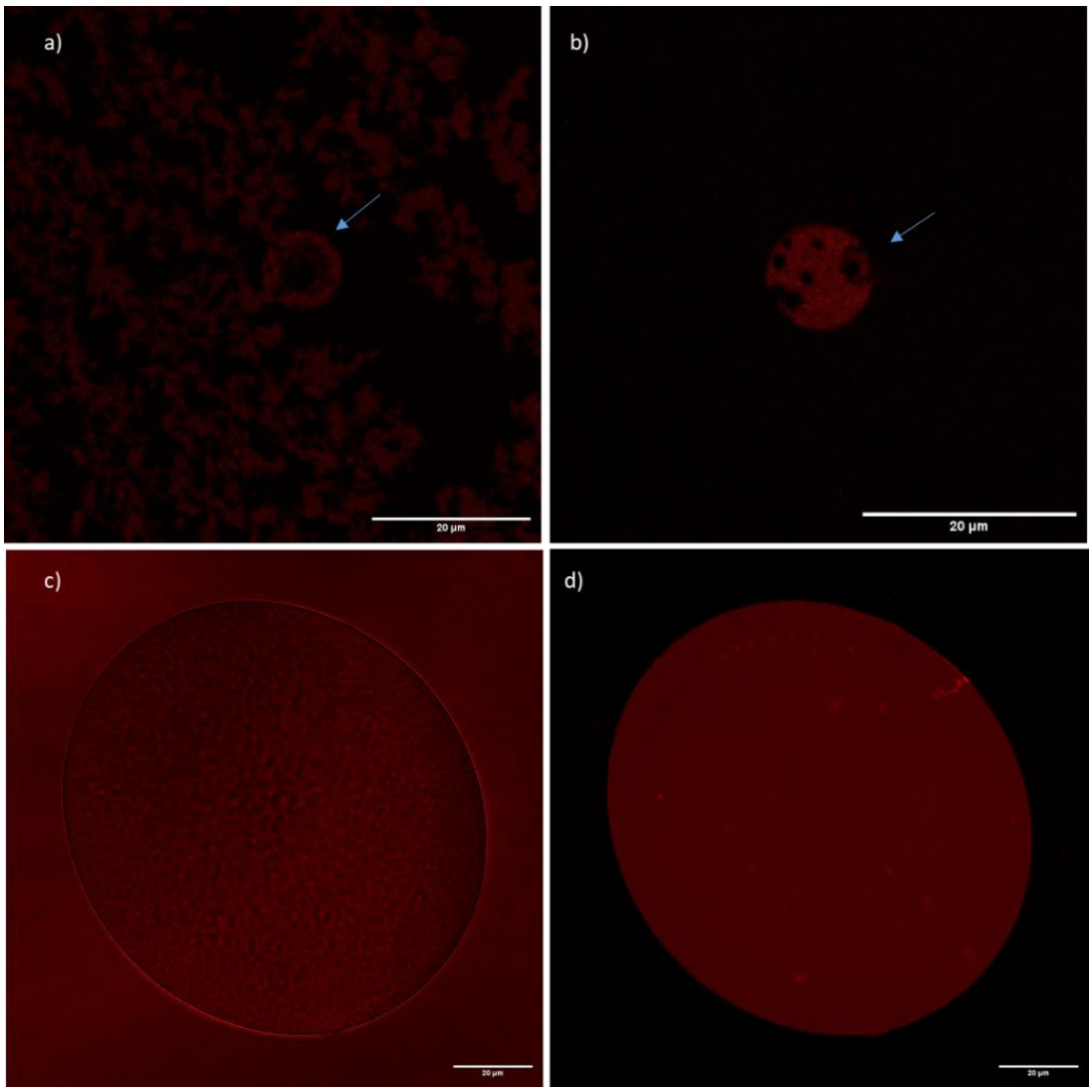

Figure 5-14: Confocal microscopy images with NR stained of 1.0 mM SDS, 0.04 mM decanol, vesicle with blue arrows, (scale 20 µm).

In the absence of sodium carbonate, Fig. 5- 14 a shows the formation of giant unilamellar vesicle (GUV) with ca size 10 µm, and Fig. 5-14 b shows multi-vesicular vesicle (MVV) with ca size 5 µm, indicated by blue arrows. Fig. 5-14 c, located with NR, shows the oil droplets or possibly GUV with ca size 100 µm, and in Fig. 5-14 d, the same image shows the NR in the droplet or the vesicle.

This possible investigation of the size of vesicles depends on the other such structures been reported to have in other literature studies [236] which be collected in the following Fig. 5-15. This figure represents phospholipid molecules that have a polar head group contacting the aqueous core, the exterior medium, and a nonpolar hydrocarbon chain orientated in the centre of the lipid bilayer.

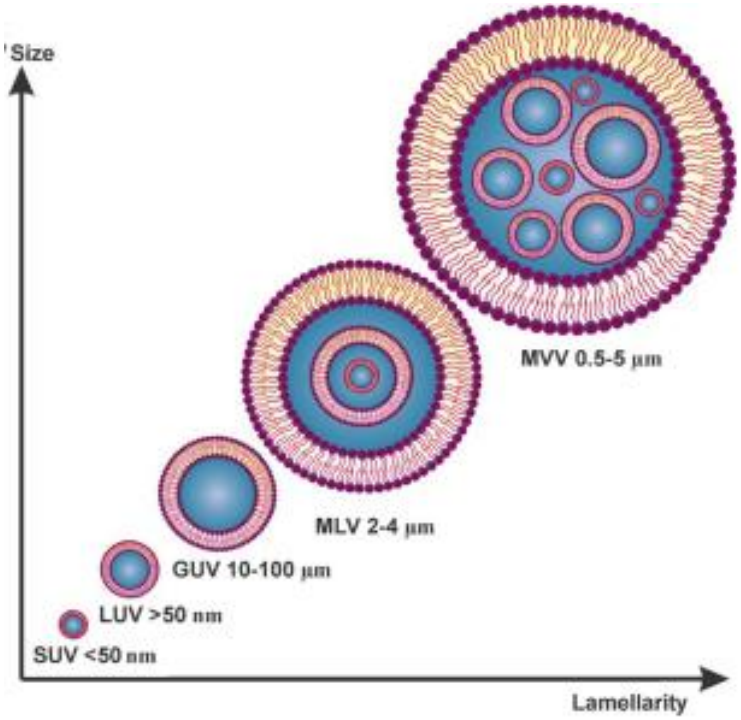

Figure 5-15: Classification of vesicle size. Abbreviations: MLV, multilamellar vesicle; MVV, multi-vesicular vesicle; GUV, giant unilamellar vesicle; LUV, large unilamellar vesicles; SUV, small unilamellar vesicles [236].

In the presence of sodium carbonate, Fig. 5-15 a and b for the same images with located dye show the formation of oil droplets or LUV with ca size 50 nm, indicated by blue arrows.

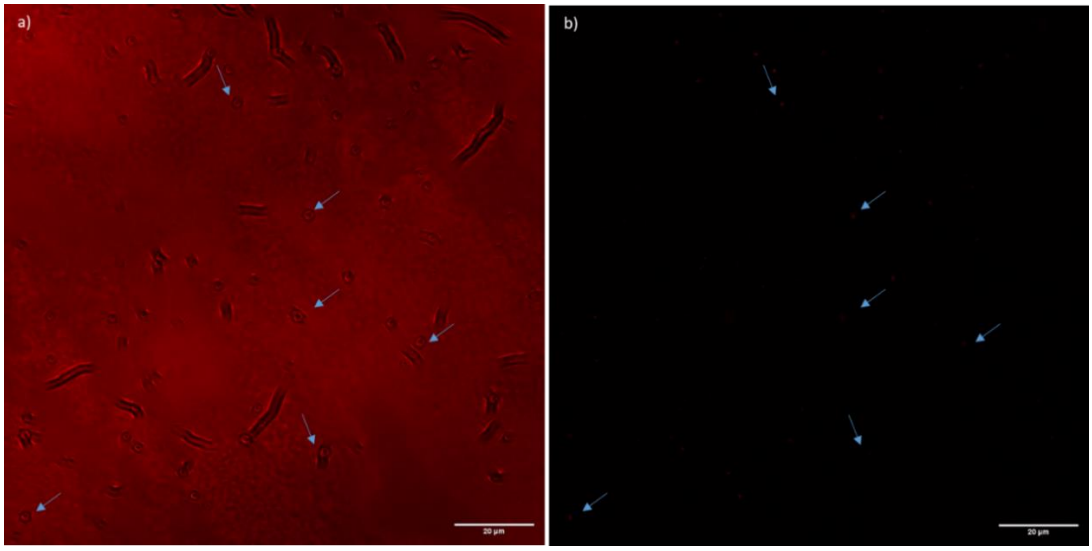

Figure 5-16: Confocal microscopy images with NR stained of 1.0 mM SDS, 0.04 mM decanol, 0.06 M sodium carbonate, oil droplets with blue arrows, (scale 20 µm).

It is worth mentioning that the classification of vesicle size by estimating; that means no tools was used to measure the size of vesicle.

In general, the visualisation of the self-assembly of fatty alcohols, namely decanol and dodecanol, with a low concentration in the presence and absence of salt (sodium carbonate) in aqueous and SHG phases using confocal fluorescent microscopy with NR as a probe shows the possibility of SHG's ability to maintain the formation of vesicles or oil droplets. That means that SHG is considered a suitable environment for the growth of SDS mixed with fatty alcohol to form vesicles in the presence or absence of salt. SHG combined with surfactants is a promising medium to help understand how the primitive cell began, such as cytoplasm in the biological cell.

5.5 Conclusion

To summarise, we have performed a preliminary examination of the self-assembly of SDS-long chain alcohols in both the aqueous salt phase and silica hydrogel phase, also salt-rich. Our initial studies using epifluorescence microscopy led to only limited success as the technique does not allow much depth control nor structural resolution. However, confocal microscopy has provided us some more informative images. In terms of summarising the key points from this chapter, we can make the following points concerning structures visualised from mixtures of SDS-decanol in the presence of Na_2CO_3 salts in both aqueous and silica hydrogel media:

i. The images obtained using epifluorescence are not clear enough to see the structures that were formed.
ii. Confocal microscopy images revealed what appear to be the formation of oil droplets and vesicles with different concentrations that are much smaller than the CMCs of SDS/alcohol mixtures in the previous chapter.
iii. SDS-decanol mixtures of 1.0 mM SDS, 0.04 mM decanol in aqueous phase, in the absence of salt appeared to show LUV (ca 2 µm), MVV (ca 2 µm), and oil droplet Fig. 5-12, and in the presence of salt (0.06 M Na_2CO_3) appeared to show oil droplet, Fig. 5-13 a to c.
iv. SDS-decanol mixtures of 1.0 mM SDS, 0.04 mM decanol in SHG phase in the absence of salt appeared to show GUV (ca 10 µm), MVV (ca 5 µm)

and oil droplet (Fig. 5-14 a to c), and in the presence of salt (0.06 M Na_2CO_3) appeared to show oil droplet (Fig. 5-16).

Chapter 6 Determination of the Gelation time of Silica Hydrogel in the Presence of SDS and Salts

6.1 The Aim of Chapter

In the studies related to the origin of life, it is considered that protocellular environments were most likely saline environments [82], and that the cytoplasm in a primitive cell is better described as a hydrogel instead than water suspension, in the same way as a contemporary biological cell [24]. The porous structure that was investigated in Chapter 2 and high water content and biocompatibility [205], mean that hydrogel can retain materials properties, for example, enzymes preserved their activities when they are immobilised in an inorganic matrix [206]. In the third chapter, UV spectrophotometry was used to estimate the CMCs of SDS, which has a polar head and apolar tail and can self-assemble under the influence of hydrophobic and hydrophilic interactions to form micellar structures in both aqueous and silica hydrogel phase in the presence of salts. The results obtained from Chapter 3 indicated that the CMCs of the SDS amphiphile in the presence of different concentrations of different salts were very similar to each other in the silica hydrogel (SHG) phase. Adding salts can affect gelation rate, which increases with adding salt because the latter is effective at screening electrostatic interactions [164].

As mentioned previously, Section 2.1, the sol−gel method was used for the SHG preparation process consisted of the hydrolysis of the sodium silicate as a precursor, and the condensation into colloidal particles, then the polymerisation to convert the sol into a gel [237]. This reaction depends on the sodium silicate concentration and pH condition [238-240], and it can be broken into three steps: the first one is the oligomerisation, in this step, silicic acid reacts together to form oligomers, dimers, and trimers and then produces linear clusters. The next step is the polymerisation in which clusters can bind into greater colloids called a sol. The final step is the gelation that can form a 3D network by linking the sol particles (Fig. 6-1) [111].

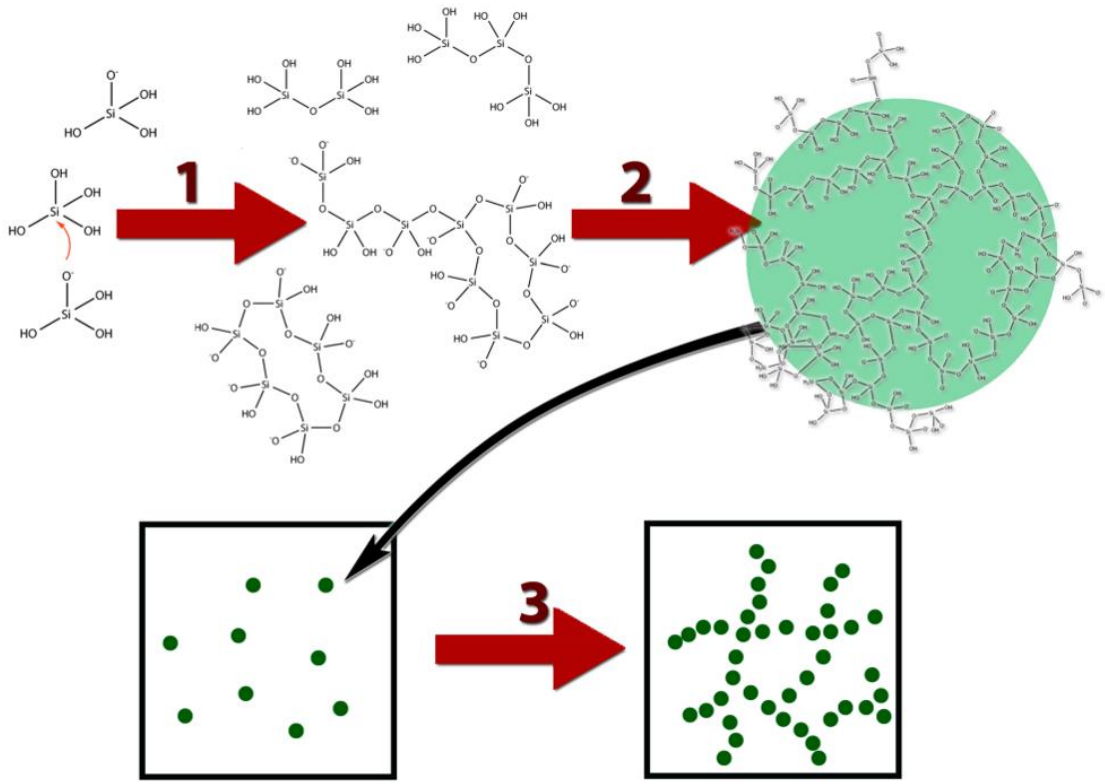

Figure 6-1: The steps of the schematic sol-gel reaction of the silicates in the acid medium (1) oligomerization, (2) polymerization, and (3) gelation of the sol [111].

Through the gelation process, the polymeric network grows until the system is solid. The consumed time is called gelation time [241]. To determine the gelation time, the structure change during the sol−gel process at which the number and the size of particles increase during oligomerisation and polymerisation was monitored [111]. This results in increasing the scattered intensity over the process, which provides an effective way for determining gelation times by the scattering profiles. To express how light scattering from particulates in a hydrogel, albeit indirectly, might give us some indication as to a hydrogel gelation time.

In this chapter, light scattering has been used to explore the changes in particular scattering from gelling silica samples as a function of time. The idea being to try to determine approximate gelation times, any aging phenomena, and the effects of additives such as salts upon these processes. To achieve that, the gelation time of three different concentrations of SHG (0.5, 0.7, and 0.9 M) has been explored in the presence of three (3) different concentrations of SDS (3.0,10.0, and 18.0 mM). Also, the gelation time of 0.5 M SHG in the presence of sodium chloride and sodium carbonate by using UV-Vis and turbidity meter was estimated.

6.2 By using UV/Vis

UV-Vis spectrophotometry, which can offer a simple way of optical measurements and a more precise method because of the use of digital processing [111], was used to determine the attenuation of light intensity by silica hydrogel. The detector in this device recorded the light transmitted through the sample, T, relative to a reference sample (a blank cuvette) [111]. Transmitted light, therefore, takes account of light that is both absorbed and scattered. The silica hydrogels were selected as they did not have any noticeable colour absorption across the visible region of the spectrum. Thus transmitted light is related directly to isotropic scattering effects. To monitor light scattering changes along the gelation process, the process was supervised by recording scans of the entire spectra (the baseline shifted in the kinetics scan from 400 to 800 nm at room temperature), and analysed by Origin. It is worth mentioning that it is essential to check the wavelength of the used disposal cuvettes because of their limitations. One of the disadvantages of using polystyrene cuvette is that it has a limited wavelength range (there is the absorbance of polystyrene at 330 nm). Also, it has lower optical performance than quartz. In addition, the cell path length is not accurate, which results in low level quantitative accuracy implications when taking into the consideration of the Beer-Lambert law [149]. The 400, 500, and 600 nm (at which no silica absorbs) wavelengths were chosen to follow the kinetics studies after baseline correction because of minus value and noise, and to ensure that they all had the same pattern. Then, the first derivative was applied using Origin software, which is a valuable tool for better results as an equilibrium or stasis point or reached when the first derivative of intensity vs. time reaches zero. This method plots the rate of change of the absorbance spectrum versus time. The graph passes through zero on the time ordinate [149], which indicates a stasis point (this being a point at which no further change is observed via this method).

6.2.1 Determination of the Gelation Time of Silica Hydrogel in the Presence of SDS

Silica hydrogel with three different concentrations, including 0.5, 0.7, 0.9 M, and with varying concentrations of SDS including 0.0, 3.0, 10.0, and 18.0 mM, were examined. For better comparison, firstly, SHG without SDS was examined to provide a benchmark against which concentrations of SDS can be assessed to

affect the gelation time. For all following experiments, depending on scattering theory, the shorter the wavelength, the more the scattering and the greater the absorbance value [242]. Also, the increase in absorbance corresponds to the growth in aggregate size, and when the formation of the network is completed, a plateau is reached [243].

6.2.1.1 Light scattering of 0.5 M SHG in the Presence of Different Concentrations of SDS

The 0.5 M SHG was examined at four different concentrations of SDS. Fig. 9-26 (appendix) shows the raw data of the UV/Vis-spectra recorded simultaneously with the 0.5 M SHG. Also, the error bar of the UV-Vis spectra at 400, 500, and 600 nm for determining gelation time of 0.5 M SHG in the presence of 0.0, 3.0,10.0,18.0 mM SDS was shown in Fig. 9-27 (Appendix). The spectra are featureless in terms of specific absorption patterns, as expected, showing only a general rise in apparent absorbance rise during data acquisition due to light scattering for suspended particulates as the gel formed. A slow rise in absorption was observed at the early stage, then, the absorption at the final stage became almost steady which means there is no significant change in spectra. It was observed by the naked eye that the liquid phase, after mixing silicate and the acid to form the gel phase, was still clear around 100 min. After this time, the solution started to become more turbid, which we take to mean that gelation was occurring.

Fig. 6-2 (a, c, and e of 400, 500. And 600 nm, respectively) shows the relationship between the time and the absorbance at mentioned wavelength, through which can be displayed the transition behaviour from sol to gel phase as a function of time. After this time, the formation of the SHG began gradually. After 447 min, the change in absorbance due to light scattering appeared to reach a stable state. The light scattering has a strong influence on the shorter wavelength (400 nm) compared to the longer wavelength (600 nm). That can be explained by that when a specific particle with a specific radius of SHG passes the range of wavelength from 400 to 800 nm. There are two cases. In the first case of a longer wavelength, this particle is much smaller than the longer wavelength of the incident light. Therefore, the scattering process is lost, or it absorbs energy. However, in the second case of the shorter wavelength, the same particle scattered light more strongly than in the longer wavelength [244]. It is worth mentioning that the

presence of different concentrations of SDS did not make a significant change in the time required to complete the gelation process.

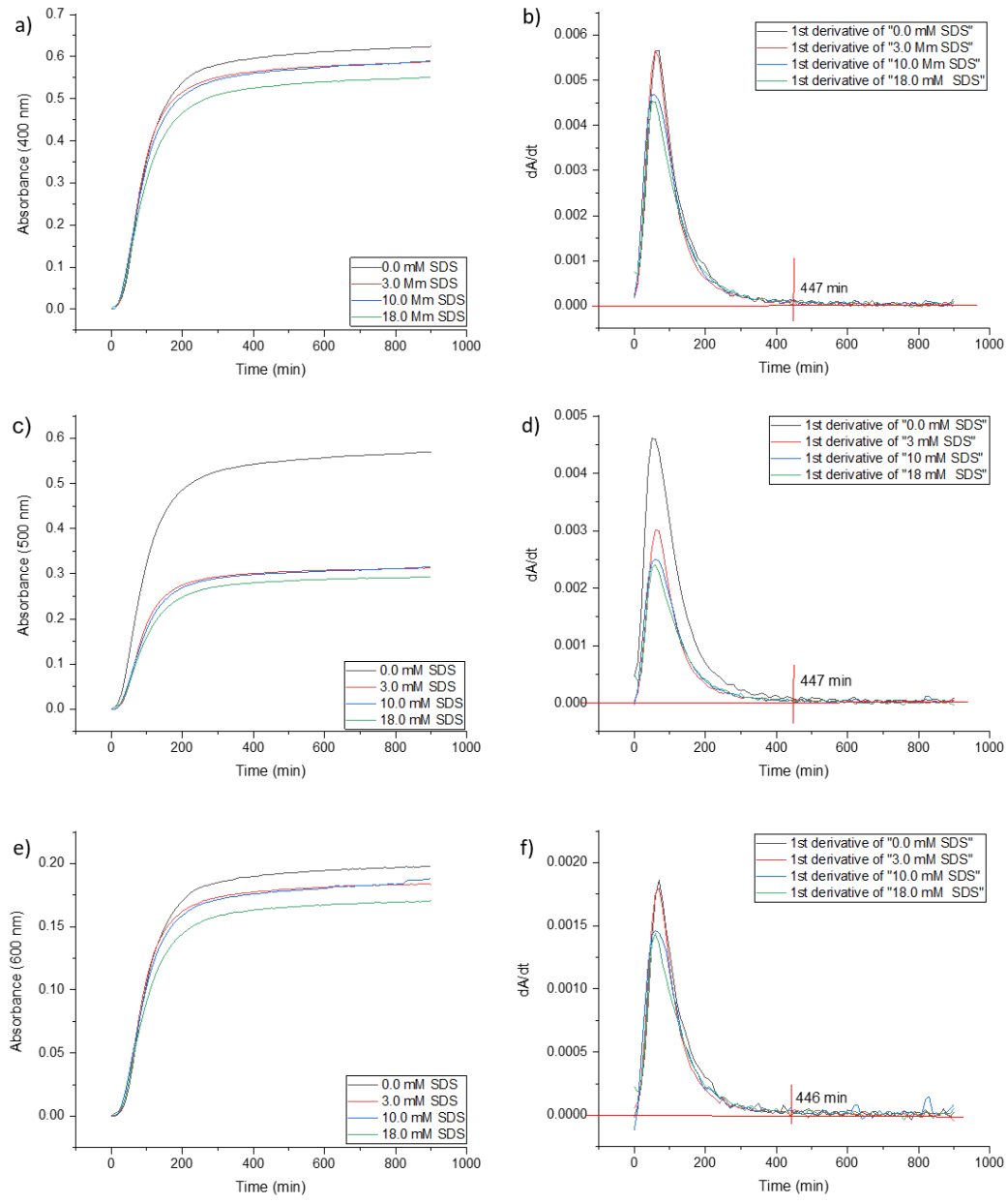

Figure 6-2: 0.5 M SHG within 900 min: The variation of light scattering after background correction with different concentrations of SDS at fixed wavelengths a) 400 nm, c) 500 nm, and e) 600 nm. Estimation of the gelation time by using first derivatives with different concentrations of SDS at fixed wavelengths: b) 400 nm, d) 500 nm, and f) 600 nm.

However, it is difficult to estimate the gelation time by using these figures. Therefore, the light scattering was plotted as a function of time at a selected fixed wavelength to help determine the gelation time more clearly by using the first derivatives (Fig. 6-3 b, d, and f of 400, 500, and 600 nm, respectively). The first

differential plot reveals the point at which dA/dt reached zero which indicates the point at which light scattering appears to have reached some equilibrium point for 0.5 M SHG, presumably associated with gelation being completed.

6.2.1.2 Light scattering of 0.7 M SHG in the Presence of Different Concentration of SDS

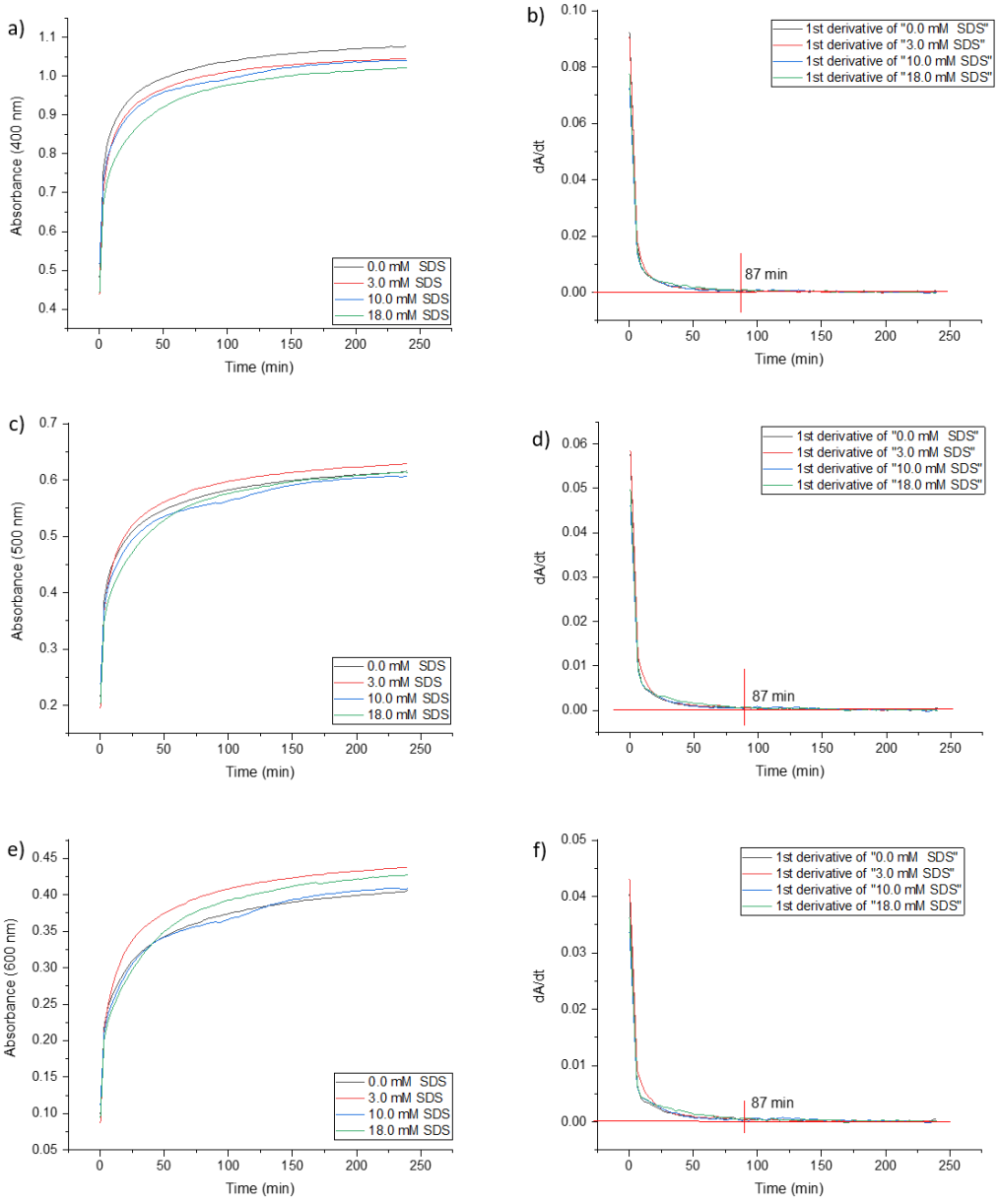

Figure 6-3: 0.7 M SHG within 240 min: The variation of light scattering after background correction with different concentrations of SDS at fixed wavelengths a) 400 nm, c) 500 nm, and e) 600 nm. Estimation of the gelation time by using first derivatives with different concentrations of SDS at fixed wavelengths: b) 400 nm, d) 500 nm, and f) 600 nm.

Similar to 0.5 M SHG, 0.7 M SHG was examined at four different concentrations of SDS. It was observed by the naked eye that the liquid started becoming turbid after mixing the solutions of sodium silicate and the acid immediately, which means the gelation process began.

In Fig. 9-28 (Appendix) the raw data of the UV/Vis-spectra recorded simultaneously with the 0.7 M SHG are displayed. Also, the error bar of the UV-Vis spectra at 400, 500, and 600 nm for determining gelation time of 0.7 M SHG in the presence of 0.0, 3.0,10.0,18.0 mM SDS was shown in Fig. 9-29 (Appendix). The spectra are also featureless, showing only a general absorbance rise during data acquisition. A quick rise in absorption is observed at the early stage, compared to 0.5 M SHG. Then, the absorption at the final stage became almost steady, which means that there is no significant change in absorption, presumably as with the 0.5 M SHG samples, light scattering due to gelation having reached an equilibrium stage (Fig. 6-3 a, c, and e of 400, 500. And 600 nm, respectively).

Every figure displays the transition behaviour from sol to gel phase as reflected in light scattering as a function of time. The formation of the 0.7 M SHG began at an earlier time compared to 0.5 M (Fig. 6-3 b, d, and f of 400, 500. And 600 nm, respectively), and the curve showed the absorbance increased with the time until it reached a stable state. Also, it is noticed that light scattering has a strong influence on the shorter wavelength (400 nm) compared to the longer wavelength (600 nm). In a similar way to 0.5 M SHG, the presence of different concentrations of SDS up to 18 mM, which is above the CMC of this amphiphile in the SHG phase, did not appear to make any significant change in the time to complete the gelation process.

6.2.1.3 Light scattering of 0.9 M SHG in the Presence of Different Concentrations of SDS

Light scattering data and the error bar at 400, 500, and 600 nm for 0.9 M SHG are presented in Fig. 9-30 (Appendix), and Fig. 9-31 (Appendix), respectively, examined at four different concentrations of SDS in an analogous manner to hose data collected for 0.5 M and 0.7 M SHG. It was observed by the naked eye that the liquid started becoming turbid immediately after mixing the solutions of sodium silicate and the acid, and because it was faster in forming the gel than

0.7 M SHG, it was difficult to shake it gently to help make a homogenous phase, which caused the formation of bubbles in some samples.

Figure 9.3.5 (Appendix) shows the raw data of the UV/Vis-spectra recorded simultaneously with the 0.9 M SHG. The spectra are also featureless, showing only a general absorbance rise during data acquirement. A rapid rise in absorption is observed in the early stage, compared to 0.7 M SHG, then, the absorption at final stage became almost steady, which means that there is no significant change in absorption.

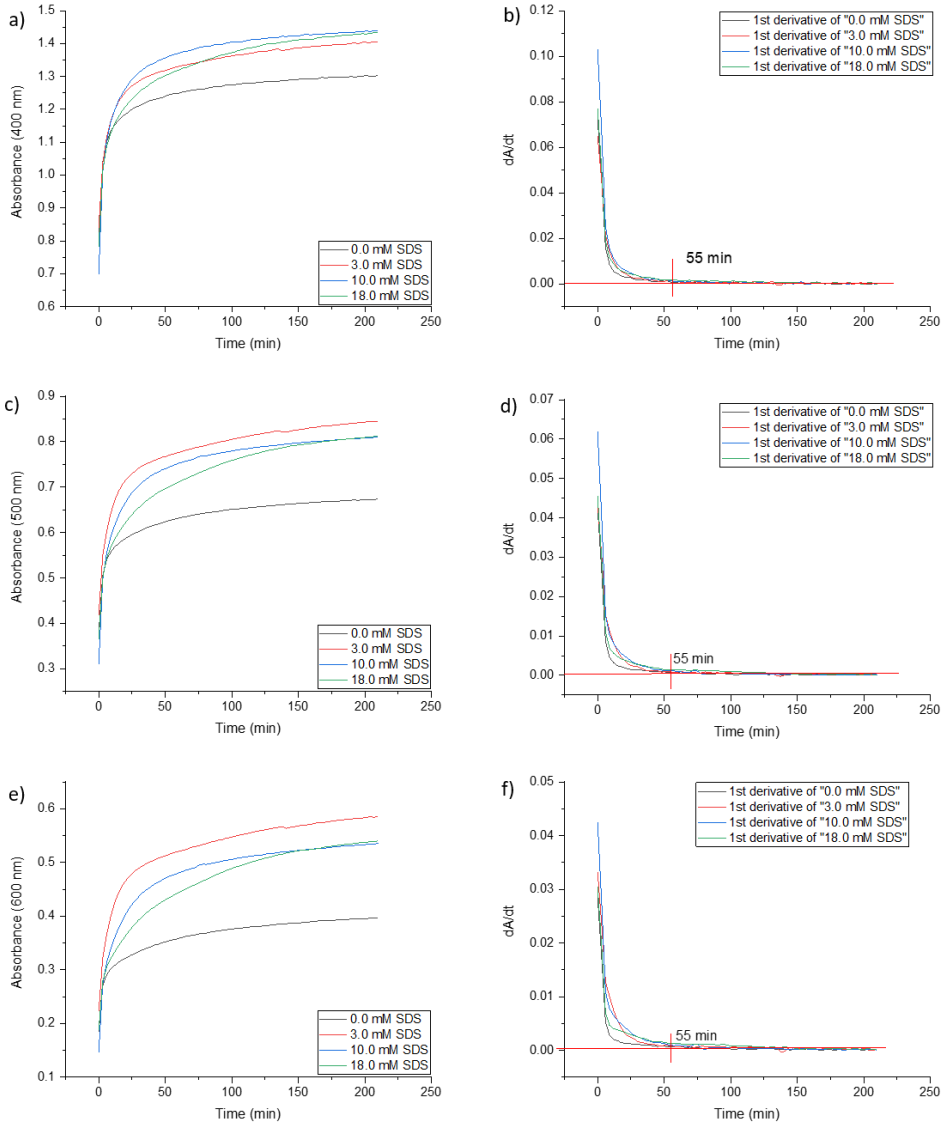

Figure 6-4: 0.9 M SHG within 240 min: The variation of light scattering after background correction with different concentrations of SDS at fixed wavelengths a) 400 nm, c) 500 nm, and e) 600 nm. Estimation of the gelation time by using first derivatives with different concentrations of SDS at fixed wavelengths: b) 400 nm, d) 500 nm, and f) 600 nm.

The curves showed (Fig. 6-4 a, c, and e of 400, 500, and 600 nm, respectively) that the absorbance increased over time until it reached a stable state. Also, it is noticed that light scattering has a strong influence on the shorter wavelength (400 nm) compared to the longer wavelength (600 nm). In a similar way to 0.5 M and 0.7 M SHG, the presence of different concentrations of SDS did not make any significant change in the time to complete the gelation process. Then, the gelation time was estimated by plotting the absorbance as a function of time at a fixed wavelength using the first derivatives (Fig. 6-4 b, d, and f of 400, 500. and 600 nm, respectively).

In general, the determination of gelation time using UV/Vis scanning kinetics relied on the variation in scattering intensity at a specific time; during the gelation process, the intensity of the scattered light increases as the growth in particle size increases [245].

Table 6-1 shows the recording of the gelation time of the selected concentrations of SHG in the presence of different concentrations of SDS.

Table 6-1 The summary values of gelation time with different concentrations of silica hydrogel in the presence of different concentrations of SDS.

	Time (min)		
Wavelength	**0.5 M SHG/SDS**	**0.7 M SHG/SDS**	**0.9 M SHG/SDS**
400 nm	447	87	55
500 nm	447	87	55
600 nm	447	87	55

As seen, 0.5 M SHG took the longest time to complete gelation with around 447 min compared with other concentrations of 0.7 and 0.9 M SHG (87 and 55 min, respectively). That means that increasing the sodium silicate concentration significantly decreased the time needed to obtain silica hydrogels. For all selected concentrations of SHG, the light scattering had a strong influence on the shorter wavelength (400 nm) and increased as the concentration of silicate increased. It was observed that the highest light scattering intensities were found for 0.9 M SHG (Fig. 6-4 a) because of their opacity; in addition, the gelation process of these concentrations happened immediately, making it easy to visualise them. However, the shorter light scattering was observed for 0.5 M SHG because it is more transparent than others [245], and presumably is composed of particulates whose size is less conducive to light scattering.

According to the results, it can be concluded that with different concentrations of the silica hydrogel, the gelation time changed significantly, especially when a comparison was made between 0.5 M and 0.7 and 0.9 M (447, 87, and 58 min, respectively). These experiments demonstrated a relationship between gelation time and sodium silicate concentration (Fig. 6-5), namely that gelation time decreases with the increase of silica concentration. This is reported by another study which found that when the silicate concentration increased, gelation time decreased because the increasing particle concentration accelerates aggregation [243].

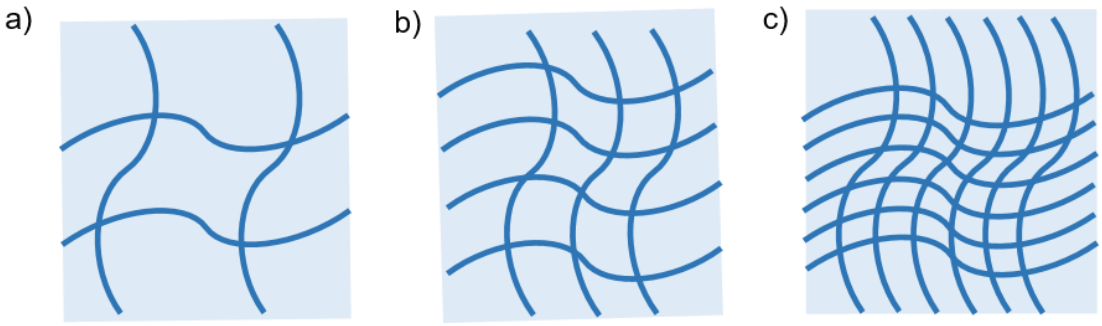

Figure 6-5: Schematic representation of network structure in the different concentrations of SHG: a) 0.5 M, b) 0.7 M, and c) 0.9 M.

Silica hydrogel in this project was prepared by the sol−gel process, which consists of preliminary hydrolysis of silicate, condensation into colloidal particles, and polymerisation of the sol into silica hydrogel [246]. The gelation time in these experiments depends on only the silicate concentration being changed. To explain that finding, the same concentration of GAA, a specific value of pH, was used in these experiments. That means the condensation rate of silicic acid is increased with silicate content [245], so the gelation time of the selected concentration was 0.9 M < 0.7 M < 0.5 M, the same trend of gelation time was found in other research [247]. Indeed, increasing silicate content can help form uniform particles in the sol phase, which produce large pore volume, and the kinetics of condensation is faster than hydrolysis [248, 249].

It is worth mentioning that adding acid to the SHG can make a long polysiloxane chain that contains cross-linking, whereas adding more silicate allows the formation of a branched network (Fig. 6-6), so the light scattered intensity is useful to detect the gelation time [250].

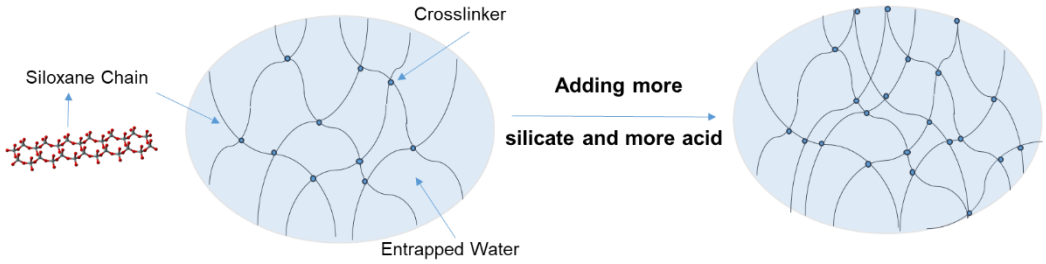

Figure 6-6: Schematic representation of network structure in the case of increasing the content of silicate and the acid, (siloxane chain: Red and gray balls represents oxygen, and silicon atoms respectively, https://www.coursehero.com/study-guides/trident-boundless-chemistry/silicates/)

However, in the presence of different concentrations of SDS at a specific concentration of silica hydrogel, the gelation time did not vary significantly, which means that the gelation time does not seem to depend on the SDS concentration, which could be because of the small size of micelle or the low concentration used. Regarding the size, Matsui and co-worker [251] stated that the pores of SHG are naturally large, so that SDS micelles (the average radius of the SDS micelles is around 18.4 Å) can incorporate into the SHG cage.

To sum up, the differences in scattered intensity of various concentrations of sodium silicate used are reasonably reliable for estimating gelation time. In contrast, the presence of different concentrations of SDS at a specific concentration of silica hydrogel did not show a significant change in the gelation time.

6.2.2 Determination of the Gelation Time of 0.5 M Silica Hydrogel in the Presence of Salts

Silica hydrogels (0.5 M SHG) with different concentrations of salts, including sodium chloride and sodium carbonate, were used to examine their effects on the silica gelation time. As a starting sample, 0.5 M SHG was selected because of the relatively longer gelation time (Section 6.2.1.1) compared to the 0.7 and 0.9 M samples discussed above. Thus, a sample of 0.5 M SHG was examined using UV-Vis light scattering in the presence of (i) 0.1 M NaCl, (ii) 0.2 M NaCl, and (iii) 0.1 M Na_2CO_3.

To determine the gelation time of the silica hydrogel in the presence of the above mentioned solutions of salts, the same procedure used in the presence of SDS was also followed here. The process was supervised by recording scans of the

entire spectra. Fig. 9-32 of the baseline shifted in the kinetics scan from 400 to 800 nm and Fig. 9-33 of the error bar (a, b and c of 0.1 M NaCl, 0.2 M NaCl, and 0.1 M Na_2CO_3 respectively for both figures) are shown in the appendixes, in the presence of mentioned salts. The 400, 500, and 600 nm wavelengths were chosen to follow the kinetics studies also; again not for any reason as to whether those frequencies were special, but they covered a consistent and middle-range.

The following figures indicate data of the system treated with 0.1 and 0.2 M NaCl and 0.1 M Na_2CO_3. Fig. 6-7 (a, c, and e of 0.1 M NaCl, 0.2 M NaCl, and 0.1 M Na_2CO_3 respectively) shows the relationship between time and measured absorbance (which is perhaps more accurately referred to as light scattering), which can display the transition behaviour from sol to gel phase with increasing absorbance. It was observed that the highest light scattering intensities was found for 0.1 M Na_2CO_3.

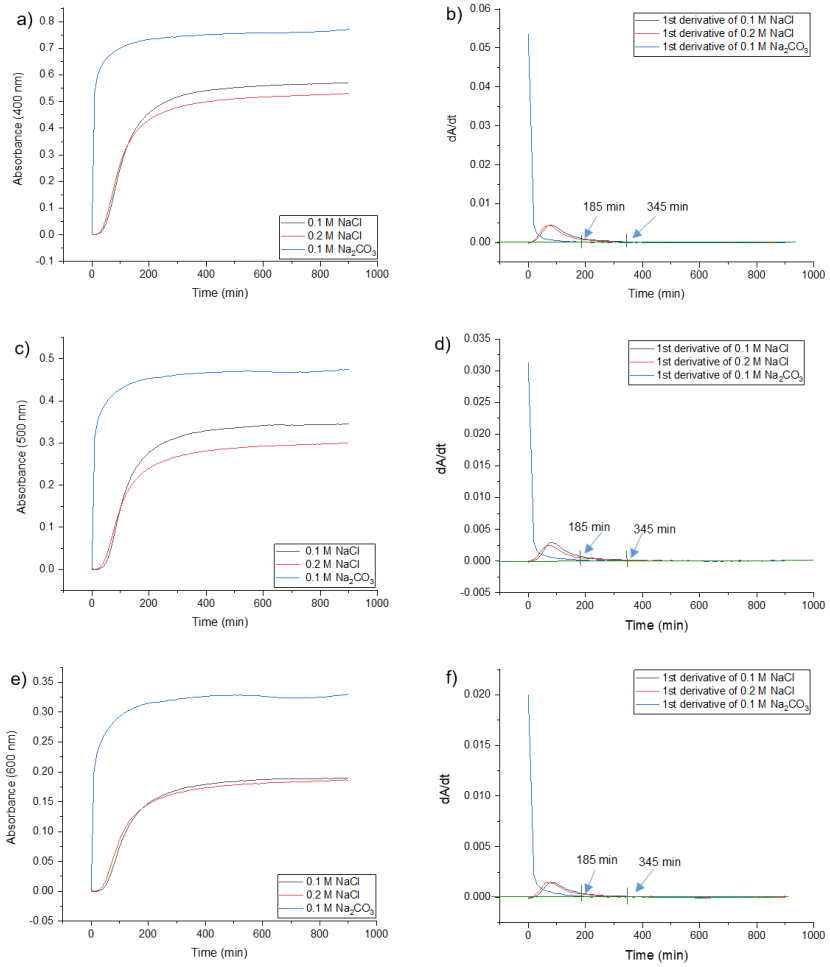

Figure 6-7: The variation of light scattering after background correction in the presence of 0.1, and 0.2 M NaCl, and 0.1 Na_2CO_3 in 0.5 M SHG at fixed wavelength a) 400, b) 500, and c) 600 nm within 900 min. Estimation of the gelation time of 0.5 M SHG of 0.1, and 0.2 M NaCl, and 0.1 Na_2CO_3, in 0.5 M SHG at fixed wavelength: b) 400, d) 500, and f) 600 nm by using first derivatives within 900 min.

For all concentrations of salts in 0.5 M SHG, the light scattering has a strong influence on the shorter wavelength (400 nm light scattering). The spectra are also featureless, showing only a general light scattering rise during data acquirement which confirms that no specific molecular light absorption is present as an additional feature. A quick rise in absorption is observed at the early stage in the presence of sodium carbonate, compared to sodium chloride with both concentrations. Subsequently, the absorption at the final stage became almost steady which means that there is no significant further change in spectra which we interpret as indicating no further dynamic change in particulate size and hence light scattering.

Yet, it is difficult to estimate the gelation time by using these figures. Therefore, if one makes the observation that the rate of change of absorbance (light scattering) with time is gradually decreasing until a plateau point is reached, then that plateau point must represent the point at which no further particulate light scattering is taking place as a result of a stable distribution in scattering particle size. Thus, if we then elect to plot the gradient of the scatter vs. time plots, one should be able to see where dA/dt approaches zero [153]. The absorbance as a function of time at a fixed wavelength of 400, 500, and 600 nm (different ranges) was plotted to allow determine the gelation time clearly.

To overcome that, first derivatives was applied on the data obtained for all the concentrations of salts in 0.5 M SHG. The first differential plot reveals the point at which dA/dt reached zero, indicating the equilibrium point (gelation time point). It is worth mentioning that the gelation process of 0.1 M Na_2CO_3 happened faster than both concentrations of NaCl (Fig. 6-7 b, d, and f of 400, 500, and 600 nm, respectively).

6.2.3 The Effect of Salts on the Gelation Time on the 0.5 M SHG

According to the results using UV/Vis, with different concentrations of NaCl and Na_2CO_3, the gelation time was found to be ca 345 min for both concentrations (0.1, and 0.2 M) of sodium chloride and ca 185 min for sodium carbonate, which is considered a significant change, especially when a comparison was made between them and 0.5 M SHG without adding salt (in the previous section: ca 447min). These experiments demonstrate a relationship between gelation time

and the salts concentration, namely that gelation time decreases with the increase of salt concentration, certainly those salts that we have examined. This has also been reported by another study which found that when the NaCl concentration increases, gelation time of silica nano particles decreases [243]. That is because adding salt into the alkaline solution causes charge screening on the surface silanol group, which can decrease the gelation time of SHG [243, 245]. Even though the monovalent salt is less effective in screening the negative charge in the silica particles, they accelerate the gelation time, but not like divalent [252].

As sodium chloride and sodium carbonate were added to the sodium silicate solution and GAA, the ionic strength of the solution increased. Also, ionic strength should affect the gelation time due to decreased repulsion between charged particles by screening the ionic double layer in aqueous solutions [253].

However, the difference in the gelation time between sodium carbonate and sodium chloride is presumably because of the presence of two Na^+ cations which can make more screening charge because of the increasing ionic strength of the solution, which causes decrease in the gelation time. It was found that sodium sulfate can reduce the gelation time more than sodium chloride under the same concentrations because of rising ionic strength [253], sodium sulfate should be similar then in this regard to sodium carbonate.

To sum up, the results obtained by the UV/Vis method in this study revealed different gelation times of 0.5 M SHG in the presence of various salts, with varying concentrations (Table 6-2) because of screening negative charge of the SHG structure by monovalent (Na^+) depending on ionic strength.

Table 6-2 The summary values of gelation time with different concentrations of silica hydrogel in the presence of different concentrations of salts.

	Time (min)		
Wavelength	**0.5 M SHG**	**0.1, 0.2 M NaCl/0.5 M SHG**	**0.1 M Na_2CO_3/0.5 M SHG**
400 nm	447	345	185
500 nm	447	345	185
600 nm	447	345	185

6.3 Turbidimery Measurements

The TN-100 Eutech turbidity meter was used to monitor the turbidity of 0.5 M SHG in the presence of salts during the gelation process with a view to comparing the overall light-scattering measurements in both media. The same procedure to form 0.5 M SHG was used with 16 mL salt-containing solutions. The measurement of gelation time started after mixing the silicate solution with GAA solution immediately, then the first reading with the time of zero was recorded, and finally data at every 10 min for 900 min were collected. Subsequently, the first derivative was applied by using Origin software, which is a valuable tool for better locating the point at which the rate of change of light scattering with time reaches zero and hence the process of building light scattering particles has presumably reached some steady state. This method plots the rate of change of the light scattering versus time. The measurement for every sample was repeated three times to afford an average and standard deviation for each concentration.

6.3.1 Determination of the Gelation Time of Silica Hydrogel in the Presence of Salts

0.5 M SHG in the absence and presence of salts, including 0.5 M SHG, 0.5 M SHG/0.1 M NaCl, 0.5 M SHG/0.2 M NaCl, 0.5 M SHG/0.1M Na_2CO_3 were examined. Firstly, a sample of SHG without salts was examined to see how other concentrations of salts can affect the gelation time. As mentioned, turbidity is a wavelength-independent that decreases in transmittance due to scattering by particle growth [254].

In general, changes in the turbidity were observed as gelation continued, and salts were observed to influence these changes in turbidity particularly sodium carbonate, which rapidly changed the turbidity. The problem with this method was that the reading kept changing with the silica hydrogel with/without NaCl; even though they were slight changes, it seemed not to reach the equilibrium point ultimately.

The measurement of gelation time for 0.5 M SHG and with 0.5 M SHG with adding both different concentrations of NaCl was shown in Fig. 6-8. Generally, the turbidity curve increased gradually over time. Obviously, a gradual increase in turbidity was observed with all samples; sodium silicate with 0.2 M NaCl changed the turbidity curve slightly differently from 0.5 M SHG and 0.1M NaCl/0.5 M SHG.

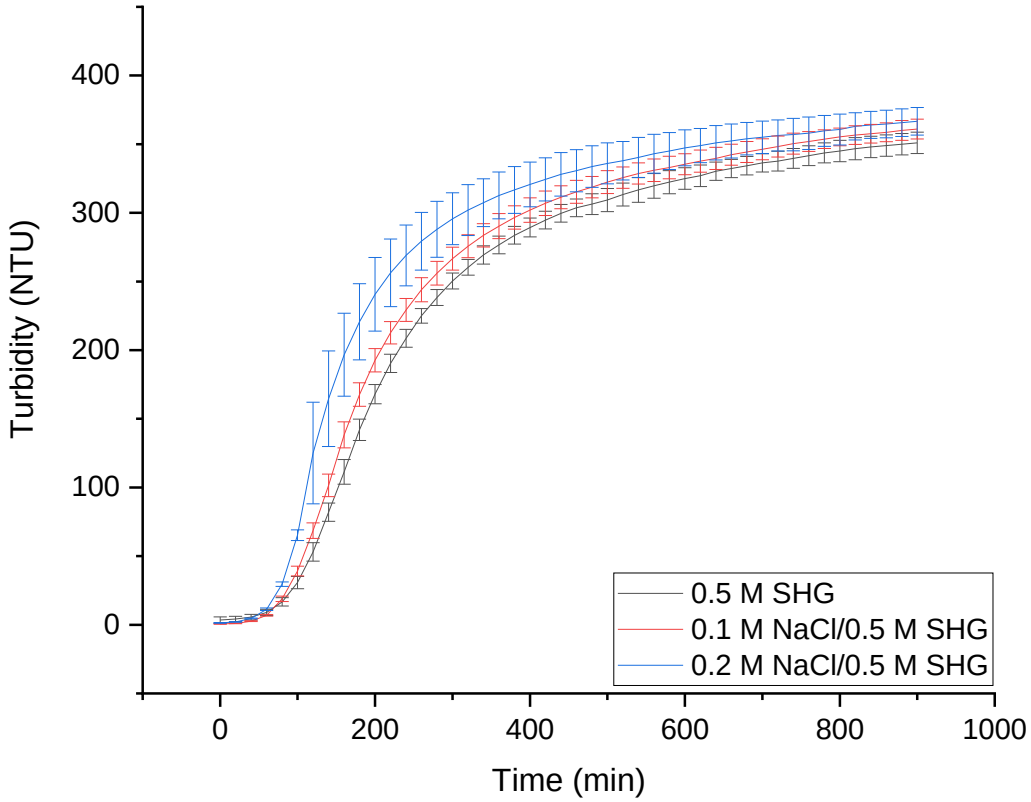

Figure 6-8: Turbidity meter results of 0.5 M SHG, 0.1 M NaCl/0.5 M SHG, and 0.2 M NaCl/0.5 M SHG with S.D.

In all samples, the change in the turbidity consumed a long time. The first derivatives curve revealed no equilibrium point within 900 min yet. Therefore, the green line (Fig. 6-9) did not reach the zero point.

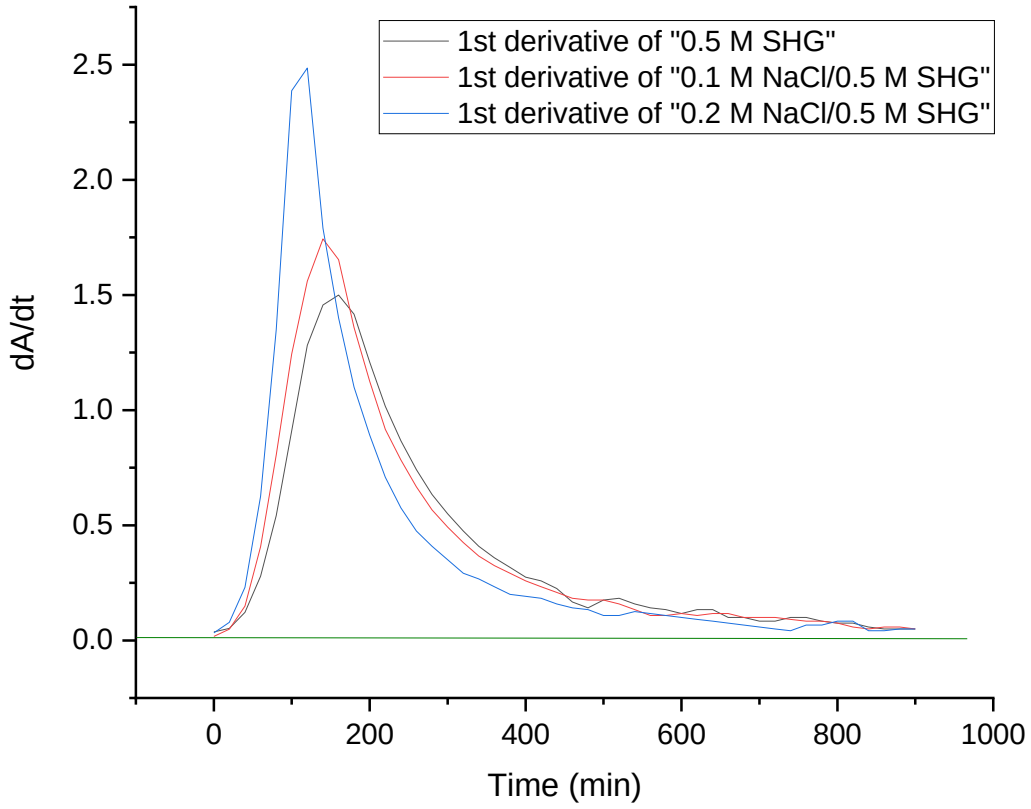

Figure 6-9: Estimation of the gelation time by using first derivatives within 900 min of 0.5 M SHG, 0.1 M NaCl/0.5 M SHG, and 0.2 M NaCl/0.5 M SHG by using turbidity meter.

The turbidity meter was calibrated with four solutions for an accurate result (described in the experimental section), and it is very sensitive. Its sensitivity may be the reason behind the changing readings each time the turbidity measured which did not show the zero point, or the reason can be due to using the device for a long time (900 min).

In the case of adding 0.1 M sodium carbonate into 0.5 M SHG, it showed a rapidly increasing trend over other samples in the first 25 minutes (Fig. 6-10 a); the turbidity reading jumped to around 350 nephelometric turbidity units (NTU), which seemed to complete the most of the gelation process, then the turbidity curve started to level and reached the zero point as shown in Fig. 6-10 b with the first derivative around 84 min for gelation time.

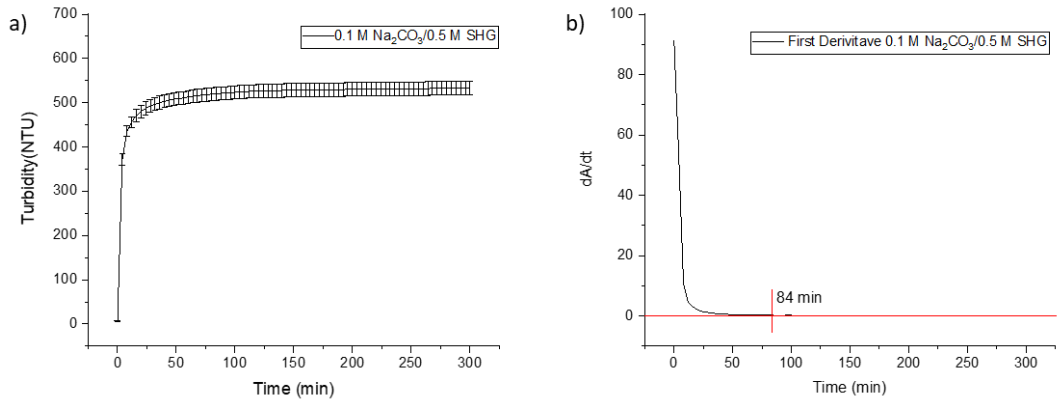

Figure 6-10: Turbidity meter results of 0.1 M $Na2CO_3$/0.5 M SHG. b) Estimation of the gelation time of it by using first derivatives within 300 min.

6.3.2 The Effect of Adding Salt on the Gelation Time of 0.5 M SHG

According to the results obtained using a turbidity meter, there were slight differences (Fig. 6-7) in the gelation time of 0.5 M SHG and the presence of sodium chloride at both concentrations. A very slight change with 0.2 M NaCl/ 0.5 M SHG can be observed because of the high ionic strength compared to 0.1 M NaCl/0.5 M SHG. That is because the monovalent is less effective in charge screening compared to divalent [252], similar trend was found in [255]. In the case of sodium carbonate, a rapid decrease in the gelation time was observed even though it was also a monovalent salt. The suggestion behind that could be because of higher ionic strength, or could be by the high pH of sodium carbonate (see Appendix 9.1.4.2). It is worth mentioning that gelation time depends on the pH [245]. That is because adding base solution can accelerate gelling kinetics by condensing the silanol groups to the siloxane group [249].

To summarise, regarding 0.5 M SHG and NaCl, the main conclusion is that turbidimetry identifies relatively little difference in gelation dynamics of SHG between the presence of 0.1 M NaCl and 0.2 M NaCl. However, the presence of salt itself is demonstrated to have a significant influence over gelation kinetics as illustrated in the derivative plot Fig. 6-9.

One can see from Fig. 6-9 clearly that the rate of change of light scattering increases from zero to a maximum which is reached between 100-200 min. Following this, the rate of change of turbidity decreases and does so differentially between salt-free and salt-containing samples. One can also see from Fig. 6-9,

that the derivative maximum is largest for the salt-free gel samples, and it is also clear from the image that the derivative maximum is achieved at different times across the salt-free and salt-present samples. This may hint at differences in the rate of light scattering particle formation, which in turn should conceivably be linked to gelation rates. The data might suggest then that the rate of change of light scattering takes slightly longer to move from a positive value to a negative one. What is less straightforward to assign is whether or not this change is linked to the size distribution of light scattering particles. Perhaps dynamic light scattering might shed more light on this.

On the other hand, addition of sodium carbonate showed a significant decrease in the gelation time which could duet to high pH or high ionic strength.

6.4 Conclusion

Overall, the main conclusions from this chapter can be summarised with the following points:

1. UV/Vis spectrophotometry in kinetic mode can be used to examine the light scattering behaviour of silica hydrogels during the process of gelation
2. This light scattering effect appears not to be influenced significantly by the wavelength at which light scattering is observed. This seems to be supported by the observations that the rate of change of light scattering with time, the derivative plots, of silica hydrogels, is un-changed at 400 nm, 500 nm and 600 nm.
3. Light scattering of silica hydrogels during the process of gelation indicates that silicate concentration has a clear influence over gelation times.
4. Our experiments suggest also that addition of sodium dodecyl sulfate (SDS) does not significantly alter the light scattering behaviour and presumably neither the gelation times.
5. The presence of additional salts and the ionic strength of those salts also have a significant effect on the gelation process as indicated by the light scattering effects.
6. Turbidimetry experiments also show that light scattering can be influenced by this salt presence.
7. We can see a difference in gelation behaviour between sodium chloride and sodium carbonate which may indicate either ionic effects, counter

anion effects or pH influences also being in operation. These have not been examined in this study.

Chapter 7 Experimental Section

7.1 Materials

All chemicals used and materials are listed in the following table without further purification.

Table 7-1 Chemicals and materials.

Materials	Supplier	Purity	Usage
Sodium silicate solution	Merck KGaA	(≥ 27% of silicate; ≥10 sodium hydroxide	Preparing silica hydrogel. Preparing a stock solution of silicate solution
Glacial acetic acid	Sigma-Aldrich	≥ 99.85%	Catalyst for Preparing silica hydrogel
Sodium Dodecyl Sulfate	Aldrich	≥ 99.0 %	Forming Micelle
Pinacyanol chloride	Aldrich		Staining for visual observation
Ethanol	Sigma-Aldrich	99.5%	Preparing pinacyanol chloride, Nile red,
Sodium carbonate anhydrous	Fisher Scientific	≥ 99.9%	Preparing a stock solution of carbonate solution and seawater.
Sodium sulfate anhydrous	Fisher Scientific	≥ 99%	Preparing a stock solution of sulfate solution and seawater.
Sodium chloride	Fisher Scientific	≥ 99.5%	Preparing a stock solution of chloride solution and seawater.
Sodium phosphate dibasic	Fluka	≥ 98%	Preparing a stock solution of phosphate solution and seawater.
NaF	Sigma-Aldrich	99 %	Preparing seawater.

KBr	Sigma-Aldrich	98 %	Preparing seawater
KCl	Thermo Fisher Scientific	99 %	Preparing seawater
$CaCl_2.2H_2O$	Sigma-Aldrich	≥ 99%	Preparing seawater
$MgCl_2.\ 6H_2O$	VWR	98 %	Preparing seawater
H_3BO_3	Sigma-Aldrich	98 %	Preparing seawater
Water	Water purifying system of our lab; Purite Select Analyst Deionisation system		All uses
1-Hexanol	Sigma-Aldrich	98 %	Preparing a stock solution of 1-hexanol solution.
1-octanol	Aldrich	99 %	Preparing a stock solution of 1-octanol solution.
1-decanol	Alfa Aesar	98 %	Preparing a stock solution of 1-decanol solution.
1-dodecanol	Alfa Aesar	98 %	Preparing a stock solution of 1-dodecanol solution.
Nile Red	Sigma-Aldrich	97 %	Fluorescent microscopy visualization
Bovine Serum Albumin	Sigma-Aldrich	≥ 98%	passivate the surface of glass slides

7.2 Preparation of Silica Hydrogels

Table 7-2 Preparing of silica hydrogel by Barge method with three different concentration of 0.5, 0.75, and 1M.

	Solution A		**Solution B**	
[silicate] M	**$V_{(silicate)}$ µL**	**$V_{(water)}$ µL**	**$V_{(acetic\ acid)}$ µL**	**$V_{(water)}$ µL**

0.5	1283	6757	360	7600
0.75	1924	6116	360	7600
1	2565	5475	360	7600

To prepare the following concentration of silica hydrogels 0.5, 0.75 and 1.0 M, two solutions were prepared separately as shown in the Table 4-1, Solution A was composed of sodium silicate solution which contains (≥ 27% of silicate) and (≥10 sodium hydroxide) in (w/v %) mixed with deionised water, and Solution B which comprised of glacial acetic acid in deionised water. Upon the addition of Solution A to Solution B in a test tube, the combined mixture was inverted 2-3 times very slowly and with care to make sure that the components are mixed effectively, and also to prevent air bubble formation which may be caused by shaking the test tube. Subsequently, the mixture was left to up to stand 24 hours without disturbance for the gelation process to be complete. Formation of silica hydrogel can be easily noticed by the naked eye, by becoming solid and homogenous and cloudy matrix. Also, hydrogel formation is confirmed by inversion of the tube whereupon the contents are seen to be fixed in place.

7.2.1 Preparation of Silica Hydrogel 0.75 M for SEM /EDX Surface Analysis

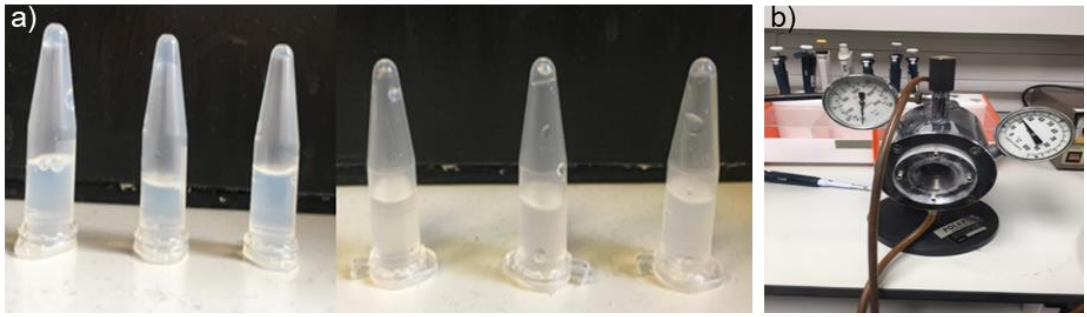

Figure 7-1: a) Preparing six samples of 0.75 M silica hydrogel for CPD process, b) Critical point drying device, faculty of biological science.

Samples (six in total, Fig 7-1 a) of silica hydrogel (0.75 M formulation) was prepared separately by mixing 857.3 µL deionised water, then 120.2 µL sodium silicate and finally 22.5 µL glacial acetic acid by using micropipette, in micro centrifuge tube (1.5 mL) with cap, within the top of each had been perforated with a needle to allow gas and fluids to enter and exit the cuvettes. Samples were left to gel for a period of 24 h prior to being handed to Mr Martin Fuller (UoL, FBS) for CPD dehydration using a Polaron E3000 system (Figure. 7-1 b)**.**

Following sample dehydration *via* CPD, the samples were analysed by SEM-EDX by Dr Alexander Kulak (School of Chemistry). The SEM-EDX analysis was performed using SEM (FEI Nova Nano SEM 450) equipped with an energy dispersive X-ray system (AMTEK). The sample was coated with iridium, utilising the sputter coater Cressington, in order to provide an electrical conductive surface. The conditions of this process were set at an accelerating voltage of 3 kV for SEM and 18 kV for EDX. The SEM was carried out to collect images on different scales of images, focusing on the size and shape of the pores present on the hydrogel by using secondary electron mode. The EDX analysis carried out to show the percentage of each element present in the sample with both qualitative and quantitative measurements. EDX analysis identified the presence of sodium salts, most probably sodium hydroxide present in the silicate solution. In order to remove such salts, the silica matrix was dialysed sequentially for 48 hr and then 96 hrs prior to freeze-drying and re-analysis with EDX.

7.2.1.1 Dialysis Process

The appropriate length of a semi-permeable membrane (Fig.7-2) was chosen (20 cm) to load hydrogel powder. The tubing was sealed and placed in deionised water as dialysate for a period of 48 hours. During this time, at ambient temperature, the dialysate was changed twice each day. Following dialysis, the sample was subjected to freeze-drying prior to SEM-EDX analysis. Following the first round of microscopy, the sample was subjected to a further 48 h period of dialysis followed by the further microscopic investigation at the room temperature.

Figure 7-2: Semi-permeable membrane for dialysis Process of 0.5 M SHG.

7.2.1.2 Freeze-Drying

The silica hydrogel was frozen and lyophilised in order to prepare them for SEM/EDX again after each dialysis process. The post-dialysis sample was first transferred to a 20 mL tube with perforated cap, which was frozen by immersing the tube in liquid nitrogen by using different size of beakers inside each other with cotton isolation between them. This process took 15 min. Finally, the sample was placed in a Virtis BenchTop Pro freeze-dryer with a condenser temperature of -105.2°C. Lyophilisation (Fig. 7-3 a) was performed at a pressure of 0.12 mbar for both 48 hours and then for 96 hours (Fig. 7-3 b).

Figure 7-3: The process of a. The freezing, and b. Drying of the 0.75 M silica hydrogel.

7.2.2 Preparation of Silica Hydrogel 0. 5 M for cryo-SEM Surface Analysis

To prepare silica hydrogels with 0.5 M, the same procedure was followed that was mentioned to prepare 0.75 M SHG in Section 7-2, by using the same quantity of preparing 0.5 M in sample vail as shown in Table 7-2. After 24 hours without disturbance for the gelation process to be complete, the sample was ready for cryo-SEM analysis.

For magnification, Cryo-SEM imaging was conducted at Leeds Electron Microscopy and Spectroscopy Centre (LEMAS) by using a Hitachi SU8230 high performance cold field emission (CFE) SEM, Ultra high resolution, low kV, with nanoscale resolution**.** In this method**,** small fragments of the prepared silica hydrogel (0.5 M) are mechanically fixed onto the specimen holder of a cryo

transfer system and immersed into subcooled liquid nitrogen which is essential to making rapid freezing to prevent ice formation. Also, to lowering the pressure of liquid nitrogen to allow the formation of nitrogen slush which can absorb heat. Then, the prepared silica hydrogel was transferred onto the cold stage of the scanning electron microscope chamber. Also, freeze-drying and dialysis have been done two times for 0.5 M SHG for EDX analysis and BET measurement.

7.3 Instrumentation for Measuring the Critical Micelle Concentration of SDS

The technique of UV/vis spectrophotometry was used to measure CMC values in different media, aqueous deionized water, deionized water containing sodium silicate, sodium carbonate, sodium sulfate, sodium chloride, disodium phosphate solutions separately at various concentrations and magnesium chloride solution with one concentration. Measurements were recorded on a Cary 100 (Australia) instrument from Agilent Technology (University of Leeds) as it shown in Fig. 7-4 with the 4.20 version software, by using disposal polystyrene cuvettes.

Figure 7-4: UV/Vis spectrophotometry (University of Leeds).

The control in each case was deionised water. Scan rates of 600 nm/min with 1 nm intervals were employed. The procedure consisted of measuring the absorbance of the reporter dye molecule, pinacyanol chloride between 500-650 nm, in the presence of different concentrations of SDS. Then, the wavelength of

maximum absorbance (λ_{max}) was identified (608 nm). Each absorbance at λ_{max} was plotted against the concentration of the SDS surfactant. This procedure was carried out for all samples including a blank (just deionised water) and each particular concentration of selected salts solution. For silicate solution, the concentration used include 0.015, 0.025, .04, 0.05, 0.1, 0.15, 0.2, 0.25, 0.35, 0.5, 0.7, 0.9, 1.2, and 1.4 M. Similarly, the concentration of carbonate solution include 0.015, 0.025, .04, 0.05, 0.1, 0.15, 0.2, 0.25, 0.35, 0.5, 0.7, 0.9, and 1.2 M. With other selected salts, including sulfate, chloride, and phosphate, it was used the same concentration including 0.015, 0.025, .04, 0.05, 0.1, 0.15, 0.2, 0.25, 0.35, and 0.5 M. Finally, only one experiment was done for magnesium chloride with 0.5 mM. The total volume of the prepared deionised water (the control) and prepared solutions for every concentration of selected measured salts (the sample) was 8.0 mL. For each concentration of water and selected salts, the experiments were repeated four times, so the result is given as a mean with an error bar of standard deviation fitted line with 95% confidence by using Origin lab software to treat the data.

7.3.1 Measuring the CMC of SDS in the Presence of Selected Salts in the Aqueous Phase

For preparing pinacyanol chloride (PIC), 0.0097 g was dissolved in 25 mL of ethanol to afford a stock solution at a concentration of (1×10^{-3} M). Within experiments, pinacyanol chloride was used at a far lower concentration of 5×10^{-6} M. Solutions of SDS were prepared at 25 mM by dissolving 0.7209 g in 100 mL deionised water then sonicated for 25 min. This solution has to be fresh to prepare different concentrations of SDS as a set with every specific concertation of selected salts. The main problem of preparing SDS solution was that bubbles appeared when water was added to the SDS. To overcome this issue, the final addition of water was postponed until the bubbles had disappeared (it takes a few hours or more).

Sample solutions were prepared with various concentrations of SDS at a specific concentration of selected salts prior to the volume being made up to final mark with deionised water of 8000 µL as total volume in sample vials (Fig. 7-5). This process was follow to estimate the CMC of SDS of deionised water and selected salts.

Figure 7-5: Example of sample preparation in aqueous phase.

7.3.1.1 In Aqueous Media

In aqueous solution, the order of adding material for preparing the samples was first SDS solution, then water, and finally pinacyanol chloride. The quantity of the volumes used in preparing each sample vial is outlined in Table 7.3. Excel software was used to calculate the volume of each component.

Table 7-3 The quantity of volume of each solution in each sample vail in aqueous media.

[SDS] mM	SDS µL	Water µL
2	640	7320
3	960	7000
4	1280	6680
5	1600	6360
5.5	1760	6200
5.8	1856	6104
6	1920	6040
6.2	1984	5976
6.4	2048	5912
6.6	2112	5848
6.8	2176	5784
7	2240	5720
7.2	2304	5656
7.4	2368	5592
10	3200	4760
12	3840	4120
14	4480	3480
16	5120	2840

In the final stage of this procedure, the quantity of prepared solution is distributed to four cuvette to start the process of the measurement.

7.3.1.2 In the Presence of Selected Salts

Critical micelle concentrations of SDS were measured in the presence of selected salts, using pinacyanol. Stock solutions of specific salt was prepared at specific concentrations as will be mentioned in the following parts. The order of addition was the match volume of specific concentration of SDS solution, particular concentration of selected salt solution, then made up to the final mark with deionised water of 8000 µL as total volume in each sample vial. Finally, 40 µL pinacyanol chloride was added and left for equilibrium for 30 min before starting the measurement.

7.3.1.2.1 In the Presence of Sodium Silicate Salts

To prepare 2.0 M of sodium silicate, an aliquot of 32.05 mL of sodium silicate solution; containing (≥ 27% of silicate; ≥10 sodium hydroxide, density = 1.39 g cm^{-3}), was mixed with deionised water up to a volume of 100 mL in a volumetric flask. In order to prepare the 3 M silicate solution, 48.05 mL of sodium silicate was diluted with deionised water made up to 100 mL in a volumetric flask.

7.3.1.2.1.1 Preparing 0.015 M Silicate

For preparing the samples of SDS to estimate the CMC in the presence of 0.015 M sodium silicate from 2 M stock solution, the following concentrations 1, 2, 3, 3.4, 3.6, 3.8, 4, 4.2, 4.4, 4.6, 4.8, 5, 6, 8, 10, and 12 mM were used with volume 320, 640, 960,1088, 1152, 1216, 1280, 1344, 1408, 1472, 1536, 1600, 1920, 2560, 3200, and 3840 µL respectively. Then, 60 µL (0.0015M) sodium silicate was added.

7.3.1.2.1.2 Preparing 0.025 M Silicate

For preparing the samples of SDS to estimate the CMC in the presence of 0.025 M sodium silicate from 2 M stock solution, the following concentrations 1, 2, 3, 3.4, 3.6, 3.8, 4, 4.2, 4.4, 4.6, 4.8, 5, 6, 8,10 and 12 mM were used with volume 320, 640, 960, 1088, 1152, 1216, 1280, 1344, 1408, 1472, 1536, 1600, 1920, 2560, 3200, and 3840 µL. Then, 100 µL (0.025M) sodium silicate was added.

7.3.1.2.1.3 Preparing 0.04 M Silicate

For preparing the samples of SDS to estimate the CMC in the presence of 0.04 M sodium silicate from 2 M stock solution, the following concentrations 1, 2, 2.3, 2.6, 2.8, 3, 3.2, 3.4, 3.6, 3.8, 4, 6, 8, 10, and 12 mM were used with volume 320, 640, 736, 832, 896, 960, 1024, 1088, 1152, 1216, 1280, 1920, 2560, 3200, and 3840 µL. Then, 160 µL (0.004 M) sodium silicate was added.

7.3.1.2.1.4 Preparing 0.05 M Silicate

For preparing the samples of SDS to estimate the CMC in the presence of 0.05 M sodium silicate from 2 M stock solution, the following concentrations 1, 2, 2.3, 2.4, 2.5, 2.6, 2.8, 3, 3.2, 3.4, 3.6, 3.8, 4, 6, 8, and 10 mM were used with volume 320, 640, 736, 768, 800, 832, 896, 960, 1024, 1088, 1152, 1216, 1280, 1920, and 2560 µL. Then, 200 µL (0.05 M) sodium silicate was added.

7.3.1.2.1.5 Preparing 0.1 M Sodium Silicate

For preparing the samples of SDS to estimate the CMC in the presence of 0.1 M sodium silicate from 2 M stock solution, it was used the following concentrations 0.1, 0.2, 0.4, 0.6, 0.7, 0.9, 1.1, 1.4, 1.7, 2, 3, 5, 7, 9, and 13 mM were used with volume 32, 64, 128, 192, 224, 288, 352, 448, 544, 640, 960, 1600, 2240, 2880, and 4160 µL. Then, 400 µL (0.1 M) sodium silicate was added.

7.3.1.2.1.6 Preparing 0.15 M Sodium Silicate

For preparing the samples of SDS to estimate the CMC in the presence of 0.15 M sodium silicate from 2 M stock solution, the following concentrations 0.8, 1, 1.2, 1.3, 1.4, 1.5, 1.6, 1.7, 1.8, 1.9, 2, 2.2, 2.4, 4, 6, and 8 mM were used with volume 256, 320, 384, 416, 448, 480, 512, 544, 576, 608, 640, 704, 768, 1280, 1920,and 2560 µL. Then, 600 µL (0.15 M) sodium silicate was added.

7.3.1.2.1.7 Preparing 0.2 M Sodium Silicate

For preparing the samples of SDS to estimate the CMC in the presence of 0.2 M sodium silicate from 2 M stock solution, the following concentrations 0.2, 0.4, 0.6, 0.7, 0.9, 1.1, 1.2, 1.6, 2, 3, 5, 7, and 9 mM were used with volume 64, 128, 192, 224, 288, 352, 384, 512, 640, 960, 1600, 2240, and 2880 µL. Then, 800 µL (0.2 M) sodium silicate was added.

7.3.1.2.1.8 Preparing 0.25 M Sodium Silicate

For preparing the samples of SDS to estimate the CMC in the presence of 0.25 M sodium silicate from 2 M stock solution, the following concentrations 0.5, 0.6, 0.8, 1, 1.1, 1.2, 1.3, 1.4, 1.5, 1.6, 1.7, 1.9, 2, 2.2, 2.4, 4, 6, and 8 mM were used with volume 160, 192, 256, 320, 352, 384, 416, 448, 480, 512, 544, 608, 640, 704, 768, 1280, 1920, and 2560 µL. Then, 1000 µL (0.25 M) sodium silicate was added.

7.3.1.2.1.9 Preparing 0.35 M Sodium Silicate

For preparing the samples of SDS to estimate the CMC in the presence of 0.35 M sodium silicate from 2 M stock solution, the following concentrations 0.2, 0.5, 0.8, 0.9, 1, 1.2, 1.3, 1.4, 1.5, 1.6, 1.8, 2, 3.5, 5, 7, 9, and 12 mM were used with volume 48, 120, 192, 216, 240, 288, 312, 336, 360, 384 432, 480, 840, 1200, 1680, 2160, and 2880 µL. Then, 1400 µL (0.35 M) sodium silicate was added.

7.3.1.2.1.10 Preparing 0.5 M Sodium Silicate

For preparing the samples of SDS to estimate the CMC in the presence of 0.5 M sodium silicate from 2 M stock solution, the following concentrations 0.2, 0.3, 0.4, 0.5, 0.6, 0.7, 0.8, 0.9, 1, 1.5, 2, 3, 4, 5, and 6 mM were used with volume 64, 96, 128, 160, 192, 224, 256, 288, 320, 480, 640, 960, 1280, 1600, and 1920 µL. Then , 2000 µL (0.5 M) sodium silicate was added.

7.3.1.2.1.11 Preparing 0.7 M Sodium Silicate

For preparing the samples of SDS to estimate the CMC in the presence of 0.7 M sodium silicate from 2 M stock solution, the following concentrations 0.1, 0.2, 0.3, 0.4, 0.5, 0.6, 0.7, 0.8, 0.9, 1, 2, 3, 4, and 5 mM were used with volume 24, 48, 72, 96, 120, 144, 168, 192, 216, 240, 480, 720, 960, and 1200 µL. Then 2800 µL (0.7 M) sodium silicate was added.

7.3.1.2.1.12 Preparing 0.9 M Sodium Silicate

For preparing the samples of SDS to estimate the CMC in the presence of 0.9 M sodium silicate from 3 M stock solution, the following concentrations 0.1, 0.2, 0.3, 0.4, 0.5, 0.6, 0.7, 0.9, 1.1, 1.3, 1.5, 1.9, 2.4, 3, and 5 mM were used with

volume 32, 64, 96, 128, 160, 192, 224, 288, 352, 416, 480, 608, 768, 960, 1600, and 1920 µL. Then, 2400 µL (0.9 M) sodium silicate was added.

7.3.1.2.1.13 Preparing 1.2 M Sodium Silicate

For preparing the samples of SDS to estimate the CMC in the presence of 1.2 M sodium silicate from 3 M stock solution, it was used the following concentrations 0.1, 0.5, 0.7, 0.9, 1.1, 1.3, 1.5, 1.8, 2, 2.5, 3, 3.5, 4, and 6 mM were used with volume 32, 160, 224, 288, 352, 416, 480, 576, 640, 800, 960, 1120, 1280, 1600, and 1920 µL. Then, 2400 µL (1.2 M) sodium silicate was added.

7.3.1.2.1.14 Preparing 1.4 M Sodium Silicate

For preparing the samples of SDS to estimate the CMC in the presence of 1.2 M sodium silicate from 3 M stock solution, following concentrations 0.1, 0.2, 0.3, 0.4, 0.5, 0.7, 0.8, 0.9, 1, 1.3, 1.5, 2, 3, 5, 6 and 7 mM were used with volume 32, 64, 96, 128, 160, 224, 256, 288, 320, 416, 480, 640, 960, 1600,1920, and 2240 µL. Then, it was added 2400 µL (1.2 M) sodium silicate was added.

7.3.1.2.2 In the Presence of Sodium Carbonate Salts

The stock solution of sodium carbonate was prepared with three different concentrations of 1.0, 1.5, 2.0 M. All of them were prepared separately with deionized water in a 200 mL volumetric flask. For preparing 1 M of carbonate, 21.20 g of sodium carbonate was dissolved with deionised water in a 200 mL volumetric flask. For preparing 1.5 M of carbonate, 31.794 g of sodium carbonate was dissolved with deionised water in a 200 mL volumetric flask. With saturated solution; 2.0 M sodium carbonate, by using a 200 mL volumetric flask, 42.392 g of sodium carbonate was dissolved with deionised water, then stirred and heated gently for 20 min.

7.3.1.2.2.1 Preparing 0.015 M Sodium Carbonate

For preparing the samples of SDS to estimate the CMC in the presence of 0.015 M sodium carbonate from 1.0 M stock solution, the following concentrations 1, 1.5, 1.8, 2, 2.2, 2.4, 2.6, 2.8, 3, 3.5, 5, 7, 9 and 11 mM were used with volume 320, 480, 576, 640, 704, 768, 832, 896, 960, 1120, 1600, 2240, 2880, and 3520 µL. Then, 120 µL (0.015 M) sodium carbonate was added.

7.3.1.2.2.2 Preparing 0.025 M Sodium Carbonate

For preparing the samples of SDS to estimate the CMC in the presence of 0.025 M sodium carbonate from 1.0 M stock solution, following concentrations 0.5, 1, 1.5, 1.8, 1.9, 2, 2.1, 2.3, 2.5, 3, 3.4, 5, 8, 10 and 12 mM were used with volume 160, 320, 480, 576, 608, 640, 672, 736, 800, 960, 1088, 1600, 2560, 3200, and 3840 µL. Then, 200 µL (0.025 M) sodium carbonate was added.

7.3.1.2.2.3 Preparing 0.04 M Sodium Carbonate

For preparing the samples of SDS to estimate the CMC in the presence of 0.04 M sodium carbonate from 1 M stock solution, the following concentrations 0 0.7, 1, 1.2, 1.3, 1.4, 1.5, 1.7, 2.5, 3, 5, 8, 10, and 12 mM were used with volume 224, 320, 384, 416, 448, 480, 544, 800, 960, 1600, 2560, 3200 and 3840 µL. Then, 320 µL (0.04 M) sodium carbonate was added.

7.3.1.2.2.4 Preparing 0.05 M Sodium Carbonate

For preparing the samples of SDS to estimate the CMC in the presence of 0.05 M sodium carbonate from 1 M stock solution, the following concentrations 0.2, 0.3, 0.4, 0.5, 0.6, 0.7, 0.8, 0.9 1, 1.2, 1.6, 2, 4, 6, 8, 10, and 12 mM were used with volume 64, 96, 128, 160, 192, 224, 256, 288, 320, 384, 512, 640, 1280, 1920, 2560, 3200, and 3840 µL. Then, 400 µL (0.05 M) sodium carbonate was added.

7.3.1.2.2.5 Preparing 0.1 M Sodium Carbonate

For preparing the samples of SDS to estimate the CMC in the presence of 0.1 M sodium carbonate from 2 M stock solution, the following concentrations 0.2, 0.3, 0.4, 0.5, 0.7, 0.8, 0.9, 1, 1.2, 1.6, 2, 4, 6,and 8 mM were used with volume 64, 96, 128, 160, 224, 256, 288, 320, 384, 512, 640, 1280, 1920, and 2560 µL. Then, 400 µL (0.1 M) sodium carbonate was added.

7.3.1.2.2.6 Preparing 0.15 M Sodium Carbonate

For preparing the samples of SDS to estimate the CMC in the presence of 0.15 M sodium carbonate from 1 M stock solution, the following concentrations 0.2, 0.3, 0.4, 0.5, 0.6, 0.7, 0.8, 0.9, 1, 1.2, 1.6, 2, 3, 4, 5, 6, 8, 10, and 12 mM were used with volume 64, 96, 128, 160, 192, 224, 256, 288, 320, 384, 512, 640, 960,

1280, 1600, 1920, 2560, 3200, 3840, and 4480 µL. Then, 1200 µL (0.15 M) sodium carbonate was added.

7.3.1.2.2.7 Preparing 0.2 M Sodium Carbonate

For preparing the samples of SDS to estimate the CMC in the presence of 0.2 M sodium carbonate from 2 M stock solution, the following concentrations 0.1, 0.2, 0.3, 0.4, 0.5, 0.7, 0.8, 0.9, 1, 1.2, 1.6, 2, 4, 6, 8, 10, and 14 mM were used with volume 32, 64, 96, 128, 160, 224, 256, 288, 320, 384, 512, 640, 1280, 1920, 2560, 3200, 3840, and 4480 µL. Then, 800 µL (0.2 M) sodium carbonate was added.

7.3.1.2.2.8 Preparing 0.25 M Sodium Carbonate

For preparing the samples of SDS to estimate the CMC in the presence 0.25 M sodium carbonate from 2 M stock solution, the following concentrations 0.1, 0.2, 0.3, 0.4, 0.5, 0.7, 0.8, 0.9, 1, 1.2, 1.6, 2, 4, 6, 8, 10, 12, and 14 mM were used with volume 32, 64, 96, 128, 160, 224, 256, 288, 320, 384, 512, 640, 1280, 1920, 2560, 3200, 3840 and 4480 µL. Then, 2000 µL (0.25 M) sodium carbonate was added.

7.3.1.2.2.9 Preparing 0.35 M Sodium Carbonate

For preparing the samples of SDS to estimate the CMC in the presence 0.35 M sodium carbonate from 1 M stock solution, the following concentrations 0.05, 0.075, 0.1, 0.15, 0.2, 0.3, 0.4, 0.5,0.6, 0.7, 0.8, 0.9, 1, 1.2, 2, 3, 4, and 6 mM were used with volume 16, 24, 32, 48, 64, 96, 128, 160, 192, 224, 256, 288, 320, 384, 640, 960, 1280, and 1920 µL. Then, 2800 µL (0.35 M) sodium carbonate was added.

7.3.1.2.2.10 Preparing 0.5 M Sodium Carbonate

For preparing the samples of SDS to estimate the CMC in the presence 0.5 M sodium carbonate from 1 M stock solution, the following concentrations 0.1, 0.15, 0.2, 0.3, 0.4, 0.5, 0.6, 0.8, 0.9, 1.2, 2, 3, and 4 mM were used with volume 32, 48, 64, 96, 128, 160, 192, 256, 288, 384, 640, 960, and 1280 µL. Then, 4000 µL (0.5 M) sodium carbonate was added.

7.3.1.2.2.11 Preparing 0.7 M Sodium Carbonate

For preparing the samples of SDS to estimate the CMC in the presence 0.7 M sodium carbonate from 1 M stock solution, the following concentrations 0.1, 0.15, 0.2, 0.25, 0.3, 0.35, 0.4, 0.45,0.5, 0.6, 0.8, 1.2, 2, 3, and 4 mM were used with volume 32, 48, 64, 80, 96, 112, 128, 144, 160, 192, 256, 384, 640, 960, and 1280 µL. Then, 5600 µL (0.7 M) sodium carbonate was added.

7.3.1.2.2.12 Preparing 0.9 M Sodium Carbonate

For preparing the samples of SDS to estimate the CMC in the presence 0.9 M sodium carbonate from 1.5 M stock solution, the following concentrations 0.05, 0.1, 0.15, 0.2, 0.25, 0.3, 0.35, 0.45, 0.5, 0.6, 0.8, 1.2, 2, 3, 4, and 6 mM were used with volume 16, 32, 48, 64, 80, 96, 112, 144, 160, 192, 256, 384, 640, 960, 1280, and 1920 µL. Then, 4800 µL (0.9 M) sodium carbonate was added.

7.3.1.2.2.13 Preparing 1.2 M Sodium Carbonate

For preparing the samples of SDS to estimate the CMC in the presence 1.2 M sodium carbonate from 1.5 M stock solution, the following concentrations 0.05, 0.1, 0.15, 0.2, 0.25, 0.3, 0.35, 0.45, 0.6, 1, 1.2, 2, 3, and 4 mM were used with volume 16, 32, 48, 64, 80, 96, 112, 144, 192, 320, 384, 640, 960, and 1280 µL. Then, 6400 µL (1.2 M) sodium carbonate was added.

7.3.1.2.3 In the Presence of Sodium Sulphate Salts

Stock solution of sodium sulphate was prepared by dissolving 35.51 g of sodium sulfate with deionised water in a 250 mL volumetric flask. For preparing the samples, the same stock solution (1.0 M) was used.

7.3.1.2.3.1 Preparing 0.015 M Sodium Sulphate

For preparing the samples of SDS to estimate the CMC in the presence 0.015 M sodium sulphate, the following concentrations 1, 1.5, 2, 2.5, 3, 3.3, 3.6, 3.9, 4, 4.2, 4.5, 5, 6, 8, 10, and 12 mM were used with volume 320, 480, 640, 800, 960, 1056, 1152, 1248, 1280, 1344, 1440, 1600, 1920, 2560, 3200, and 3840 µL. Then, 120 µL (0.015M) sodium sulphate was added .

7.3.1.2.3.2 Preparing 0.025 M Sodium Sulphate

For preparing the samples of SDS to estimate the CMC in the presence 0.025 M sodium sulphate, the following concentrations 0.8, 1, 1.2, 1.4, 1.7, 2, 2.2, 2.4, 2.6,

2.8, 3, 4, 5, and 8 mM were used with volume 256, 320, 384, 448, 544, 640, 704, 768, 832, 896, 960, 1280, 1600, and 2560 µL. Then, 200 µL (0.025 M) sodium sulphate was added.

7.3.1.2.3.3 Preparing 0.04 M Sodium Sulphate

For preparing the samples of SDS to estimate the CMC in the presence 0.04 M sodium sulphate, the following concentrations 0.8, 0.9, 1, 1.1, 1.2, 1.4, 1.5, 1.7, 2, 2.2, 2.4, 3, 4, 8, and 10 mM were used with volume 256, 288, 320, 352, 384, 448, 480, 544, 640, 704, 768, 960, 1280, 2560, and 3200 µL. Then, 320 µL (0.04 M) sodium sulphate was added.

7.3.1.2.3.4 Preparing 0.05 M Sodium Sulphate

For preparing the samples of SDS to estimate the CMC in the presence 0.05 M sodium sulphate, the following concentrations 0.8, 0.9, 1, 1.1, 1.2, 1.3, 1.4, 1.5, 1.7, 2, 2.2, 3, 4, 5, 8, and 10 mM were used with volume 256, 288, 320, 352, 384, 416, 448, 480, 544, 640, 704, 960, 1280, 1600, 2560, and 3200 µL. Then, 400 µL (0.05 M) sodium sulphate was added.

7.3.1.2.3.5 Preparing 0.1 M Sodium Sulphate

For preparing the samples of SDS to estimate the CMC in the presence 0.05 M sodium sulphate, the following concentrations 0.4, 0.5, 0.6, 0.7, 0.8, 0.9, 1, 1.1, 1.2, 1.3, 1.4, 2, 4, 5, 8, and 10 mM were used with volume 128,160, 192, 224, 256, 288, 320, 352, 384, 416, 448, 640, 1280, 1600, 2560, and 3200 µL. Then, 800 µL (0.05 M) sodium sulphate was added.

7.3.1.2.3.6 Preparing 0.15 M Sodium Sulphate

For preparing the samples of SDS to estimate the CMC in the presence 0.15 M sodium sulphate, the following concentrations 0.3, 0.4, 0.5, 0.6, 0.7, 0.8, 0.9, 1, 1.1, 1.2, 1.3, 1.4, 2, 4, 5, 8, and 10 mM were used with volume 96, 128, 160, 192, 224, 256, 288, 320, 352, 384, 416, 448, 640, 1280, 1600, 2560, and 3200 µL. Then, 1200 µL (0.15 M) sodium sulphate was added.

7.3.1.2.3.7 Preparing 0.2 M Sodium Sulphate

For preparing the samples of SDS to estimate the CMC in the presence 0.2 M sodium sulphate, following concentrations 0.3, 0.4, 0.5, 0.6, 0.7, 0.8, 0.9, 1, 1.1,

1.2, 1.3, 2, 4, 5, 8, and 10 mM were used with volume 96, 128, 160,192, 224, 256, 288, 320, 352, 384, 416, 640, 1280, 1600, 2560, and 3200 µL. Then, 1600µL (0.2 M) sodium sulphate was added.

7.3.1.2.3.8 Preparing 0.25 M Sodium Sulphate

For preparing the samples of SDS to estimate the CMC in the presence 0.25 M sodium sulphate, following concentrations 0.1, 0.2, 0.3, 0.4, 0.5, 0.6, 0.7, 0.8, 0.9, 1, 1.1, 1.2, 1.3, 2, 4, 5, and 7 mM were used with volume 32, 64, 96, 128, 160, 192, 224, 256, 288, 320, 352, 384, 416, 640,1280, 1600, and 2240 µL. Then, 2000 µL (0.25 M) sodium sulphate was added.

7.3.1.2.3.9 Preparing 0.35 M Sodium Sulphate

For preparing the samples of SDS to estimate the CMC in the presence 0.35 M sodium sulphate, the following concentrations 0.1, 0.2, 0.3, 0.4, 0.5, 0.6, 0.7, 0.8, 0.9, 1, 1.1, 1.2, 1.3, 2, 4, 5,and 7 mM were used with volume 32, 64, 96, 128, 160, 192, 224, 256, 288, 320, 352, 384, 416, 640, 1280, 1600, and 2240 µL. Then, 2800 µL (0.35 M) sodium sulphate was added.

7.3.1.2.3.10 Preparing 0.5 M Sodium Sulphate

For preparing the samples of SDS to estimate the CMC in the presence 0.5 M sodium sulphate, the following concentrations 0.1, 0.2, 0.3, 0.4, 0.5, 0.6, 0.7, 0.8, 0.9, 1, 1.1, 1.2, 1.3, 2, 4, 5, and 7 mM were used with volume 32, 64, 96, 128, 160, 192, 224, 256, 288, 320, 352, 384, 416, 640, 1280, 1600, and 2240 µL. Then, 4000 µL (0.5 M) sodium sulphate was added.

7.3.1.2.4 In the Presence of Sodium Chloride Salts

Stock solution of sodium chloride was prepared by dissolving 14.61 g with deionised water in a 250 mL volumetric flask. For preparing the samples, the same stock solution (1.0 M) was used.

7.3.1.2.4.1 Preparing 0.015 M Sodium Chloride

For preparing the samples of SDS to estimate the CMC in the presence 0.015 M sodium chloride, the following concentrations 1, 1.8, 2.2, 2.4, 2.6, 2.8, 3, 3.2, 3.6, 3.8, 4, 5, 6, 8, 10, and 12 mM were used with volume 320, 576, 704, 768, 832,

896, 960, 1024, 1152, 1216, 280, 1600, 1920, 2560, 3200, and 3840 µL. Then, 120 µL (0.015 M) sodium chloride was added.

7.3.1.2.4.2 Preparing 0.025 M Sodium Chloride

For preparing the samples of SDS to estimate the CMC in the presence 0.025 M sodium chloride, the following concentrations 1, 1.5, 2, 2.3, 2.6, 2.8, 3, 3.2, 3.4, 3.6, 4, 5, 7, 9, 11, and 15 mM with were used volume 320, 480, 640, 736, 832, 896, 960, 1024, 1088, 1152, 1280, 1600, 2240, 2880, 3520, and 4800 µL. Then, 200 µL (0.025 M) sodium chloride was added.

7.3.1.2.4.3 Preparing 0.04 M Sodium Chloride

For preparing the samples of SDS to estimate the CMC in the presence 0.04 M sodium chloride, the following concentrations 1, 1.5, 1.7, 1.9, 2, 2.1, 2.2, 2.3, 2.6, 2.8, 3, 4, 5, 7, 9, 11, and 15 mM were used with volume 320, 480, 544, 608, 640, 672, 704, 736, 832, 896, 960, 1280, 1600, 2240, 2880, 3520, and 4800 µL. Then, 320 µL (0.04 M) sodium chloride was added.

7.3.1.2.4.4 Preparing 0.05 M Sodium Chloride

For preparing the samples of SDS to estimate the CMC in the presence 0.05 M sodium chloride, the following concentrations 0.3, 0.4, 0.5, 0.6, 0.7, 0.8, 0.9, 1, 1.2, 1.6, 2, 4, 6, 8, 10, and 12 mM were used with volume 96, 128, 160, 192, 224, 256, 288, 320, 384, 512, 640, 1280, 1920, 2560, 3200, and 3840 µL. Then, 400 µL (0.05 M) sodium chloride was added.

7.3.1.2.4.5 Preparing 0.1 M Sodium Chloride

For preparing the samples of SDS to estimate the CMC in the presence 0.1 M sodium chloride, the following concentrations 0.4, 0.6, 0.7, 0.8, 0.9, 1, 1.2, 1.4, 1.6, 1.8, 2, 4, 6, 8, 10, and 12 mM were used with volume 128, 192, 224, 256, 288, 320, 384, 448, 512, 576, 640, 1280, 1920, 2560, 3200, and 3840 µL. Then, 800 µL (0.1 M) sodium chloride was added.

7.3.1.2.4.6 Preparing 0.15 M Sodium Chloride

For preparing the samples of SDS to estimate the CMC in the presence 0.15 M sodium chloride, the following concentrations 0.4, 0.5, 0.6, 0.7, 0.8, 0.9, 1, 1.2, 1.6, 2, 3, 4, 6, and 8 mM were used with volume 128, 160,192, 224, 256, 288,

320, 384, 512, 640, 960, 1280, 1920, and 2560 µL. Then, 1200 µL (0.15 M) sodium chloride was added.

7.3.1.2.4.7 Preparing 0.2 M Sodium Chloride

For preparing the samples of SDS to estimate the CMC in the presence 0.2 M sodium chloride, the following concentrations 0.4, 0.5, 0.6, 0.7, 0.8, 0.9, 1, 1.2, 1.6, 2, 3, 4, 6, and 8 mM were used with volume 128, 160, 192, 224, 256, 288, 320, 384, 512, 640, 960, 1280, 1920, and 2560 µL. Then, 1600 µL (0.2 M) sodium chloride was added.

7.3.1.2.4.8 Preparing 0.25 M Sodium Chloride

For preparing the samples of SDS to estimate the CMC in the presence 0.25 M sodium chloride, the following concentrations 0.4, 0.5, 0.6, 0.7, 0.75, 0.8, 0.85, 0.9, 1, 1.2, 1.6, 2, 4, and 6 mM were used with volume 128, 160, 192, 224, 240, 256, 272, 288, 320, 384, 512, 640, 1280, and 1920 µL. Then, 2000 µL (0.25 M) sodium chloride was added.

7.3.1.2.4.9 Preparing 0.35 M Sodium Chloride

For preparing the samples of SDS to estimate the CMC in the presence 0.35 M sodium chloride, the following concentrations 0.2, 0.3, 0.4, 0.5, 0.6, 0.7, 0.8, 0.9, 1, 1.6, 2, 4, and 6 mM were used with volume 64, 96, 128, 60, 192, 224, 256, 288, 320, 512, 640, 1280, and 1920 µL. Then, 2800 µL (0.35 M) sodium chloride was added.

7.3.1.2.4.10 Preparing 0.5 M Sodium Chloride

For preparing the samples of SDS to estimate the CMC in the presence 0.5 M sodium chloride, the following concentrations 0.15, 0.2, 0.35, 0.5, 0.55, 0.6, 0.7, 0.8, 0.9, 1, 1.6, 2, 4, 5, and 6 mM were used with volume 48, 64, 112, 160, 176, 192, 224, 256, 288, 320, 512, 640, 1280, 1600, and 1920 µL. Then, 4000 µL (0.5 M) sodium chloride was added.

7.3.1.2.5 In the Presence of Disodium Phosphate Salts

Stock solution of 1.0 M disodium phosphate was prepared with two different concentrations of 0.5 and 0.8 M. For preparing 0.5 M of phosphate, 17.745 g of sodium phosphate was dissolved with deionized water in a 250 mL volumetric

flask. For preparing 0.8 M of phosphate, 28.392 g of disodium phosphate it was dissolved with deionised water in a 250 mL volumetric flask.

7.3.1.2.5.1 Preparing 0.015 M Disodium Phosphate

For preparing the samples of SDS to estimate the CMC in the presence 0.015 M from 0.5 M stock solution disodium phosphate, the following concentrations 1, 1.5, 1.8, 2, 2.3, 2.5, 2.8, 3, 3.4, 4, 5, 6, 8, 10, and 12 mM were used with volume 320, 480, 576, 640, 736, 800, 896, 960, 1088, 1280, 1600, 1920, 2560, 3200, and 3840 µL. Then, 240 µL (0.015 M) disodium phosphate was added.

7.3.1.2.5.2 Preparing 0.025 M Disodium Phosphate

For preparing the samples of SDS to estimate the CMC in the presence 0.025 M from 0.5 M stock solution disodium phosphate, the following concentrations 1, 1.5, 1.8, 2, 2.3, 2.5, 2.8, 3, 3.4, 4, 5, 8, 10, and 12 mM were used with volume 320, 480, 576, 640, 736, 800, 896, 960, 1088, 1280, 1600, 2560, 3200, and 3840 µL. Then, 400 µL (0.025 M) disodium phosphate was added.

7.3.1.2.5.3 Preparing 0.04 M Disodium Phosphate

For preparing the samples of SDS to estimate the CMC in the presence 0.04M from 0.5 M stock solution disodium phosphate, the following concentrations 0.5, 0.7, 1, 1.1, 1.3, 1.5, 1.7, 1.9, 2.2, 2.5, 3, 4, 5, 8, 10, and 12 mM were used with volume 160, 224, 320, 352, 416, 480, 544, 608, 704, 800, 960, 1280, 1600, 2560, 3200, and 3840 µL. Then, 640 µL (0.04 M) disodium phosphate was added.

7.3.1.2.5.4 Preparing 0.05 M Disodium Phosphate

For preparing the samples of SDS to estimate the CMC in the presence 0.05M from 0.5 M stock solution disodium phosphate, the following concentrations 0.5, 0.7, 0.9, 1.1, 1.3, 1.5, 1.7, 1.8, 2.1, 2.3, 2.5, 4, 5, and 8 mM were used with volume 160, 224, 288, 352, 416, 480, 544, 576, 672, 736, 800, 1280, 1600, and 2560 µL. Then, 800 µL (0.05 M) disodium phosphate was added.

7.3.1.2.5.5 Preparing 0.1 M Disodium Phosphate

For preparing the samples of SDS to estimate the CMC in the presence 0.1M from 0.5 M stock solution disodium phosphate, the following concentrations 0.4, 0.5, 0.6, 0.7, 0.8, 0.9, 1, 1.2 1.5, 1.7, 2.1, 2.3, 3, 4, 6, and 8 mM were used with

volume 128, 160, 192, 224, 256, 288, 320, 384, 480, 544, 672, 736, 960, 1280, 1920, and 2560 µL. Then, 1600 µL (0.1 M) disodium phosphate was added.

7.3.1.2.5.6 Preparing 0.15 M Disodium Phosphate

For preparing the samples of SDS to estimate the CMC in the presence 0.15 M from 0.5 M stock solution disodium phosphate, the following concentrations 0.4, 0.5, 0.6, 0.7, 0.8, 0.9, 1, 1.1, 1.2, 1.5, 1.7, 2.1, 2.3, 3, 4, 6, and 8 mM were used with volume 128, 160, 192, 224, 256, 288, 320, 352, 384, 480, 544, 672, 736, 960, 1280, 1920, and 2560 µL. Then, 2400 µL (0.15 M) disodium phosphate was added.

7.3.1.2.5.7 Preparing 0.2 M Disodium Phosphate

For preparing the samples of SDS to estimate the CMC in the presence 0.2 M from 0.5 M stock solution disodium phosphate, the following concentrations 0.2, 0.3, 0.4, 0.5, 0.6, 0.7, 0.8, 0.9, 1, 1.1, 1.2, 1.3, 1.4, 1.5, 3, 6, and 8 mM were used with volume 64, 96, 128, 160, 192, 224, 256, 288, 320, 352, 384, 416, 448, 480, 960, 1920, and 2560 µL. Then, 3200 µL (0.2 M) disodium phosphate was added.

7.3.1.2.5.8 Preparing 0.25 M Disodium Phosphate

For preparing the samples of SDS to estimate the CMC in the presence 0.25 M from 0.5 M stock solution disodium phosphate, the following concentrations 0.2, 0.3, 0.4, 0.5, 0.6, 0.7, 0.8, 0.9, 1, 1.1, 1.2, 1.3, 1.4, 1.5, 3, 6, and 8 mM were used with volume 64, 96, 128, 160, 192, 224, 256, 288, 320, 352, 384, 416, 448, 480, 960, 1920, and 2560 µL. Then, 4000 µL (0.25 M) disodium phosphate was added.

7.3.1.2.5.9 Preparing 0.35 M Disodium Phosphate

For preparing the samples of SDS to estimate the CMC in the presence 0.35 M from 0.8 M stock solution disodium phosphate, the following concentrations 0.1, 0.2, 0.3, 0.4, 0.5, 0.6, 0.7, 0.8, 0.9, 1, 1.1, 1.2, 1.5, 3, 5, and 7 mM were used with volume 32, 64, 96, 128, 160, 192, 224, 256, 288, 320, 352, 384, 480, 960, 1600, and 2240 µL. Then, 3500 µL (0.35 M) disodium phosphate was added.

7.3.1.2.5.10 Preparing 0.5 M Disodium Phosphate

For preparing the samples of SDS to estimate the CMC in the presence 0.5 M from 0.8 M stock solution disodium phosphate, the following concentrations 0.05,

0.1, 0.2, 0.3, 0.4, 0.5, 0.6, 0.7, 0.8, 0.9, 1, 1.1, 1.3, 1.5, 3, 5, and 7 mM were used with volume 16, 32, 64, 96, 128, 160, 192, 224, 256, 288, 320, 352, 416, 480, 960, 1600, and 2240 µL. Then, 5000 µL (0.5 M) disodium phosphate was added.

7.3.1.2.6 In the Presence of Magnesium Chloride Salts

Stock solution of magnesium chloride was prepared by dissolving 4.066 g of magnesium chloride with deionised water in a 100 mL volumetric flask for stock solution with 0.1 M.

7.3.1.2.6.1 Preparing 0.5 mM Magnesium Chloride

For preparing the samples of SDS to estimate the CMC in the presence 0.5 mM magnesium chloride, it was used the following concentrations 1, 2, 2.4, 2.6, 2.8, 3, 3.1, 3.2, 3.4, 3.6, 3.8, 4, 6, 8, 10, and 12 mM with volume 320, 640, 768, 832, 896, 960, 992, 1024, 1088, 1152, 1216, 1280, 1920, 2560, 3200, and 3840 µL. Then it was added 20 µL (0.5 mM) magnesium chloride.

7.3.1.2.7 Measuring the CMC of Simulated Seawater in Aqueous Media.

Simulated seawater was prepared according to Table 7-4 artificial seawater solution [138].

Table 7-4 The main content of artificial seawater.

Salt	Mass g/L
NaCl	23.926
Na_2SO_4	4.008
KCl	0.677
$NaHCO_3$	0.196
KBr	0.098
H_3BO_4	0.026
$SrCl_2$	0.0025
NaF	0.003
$CaCl_2$	1.16
$MgCl_2$	5.2

Stock solution of seawater was prepared by dissolving the salts mentioned in the table with deionised water in a 1L volumetric flask. To measure the CMC of SDS in aqueous phase in the presence of seawater, two different volume ratios were prepared including 1:10, and 1:5 with total volume of 8000 µL. The same procedure in section 7.3.1.2 of selected salts was followed.

7.3.1.2.7.1 Simulated Seawater with the Ratio 1: 10

For preparing the samples of SDS to estimate the CMC in the presence 1:10 seawater the following concentrations 0.4, 0.6, 0.8, 1, 1.1, 1.2, 1.3, 1.4, 1.6, 1.8, 2.5, 4, 6, 7, 8, 9, 10, 14, and 15 mM were used with volume 128, 192, 256, 320, 352, 384, 416, 448, 512, 576, 800, 1280, 1920, 2240, 2560, 2880,3200, 4480,and 4800 µL, then, 800 µL seawater was added.

7.3.1.2.7.2 Simulated Seawater with the Ratio 1: 5

For preparing the samples of SDS to estimate the CMC in the presence 1:5 seawater, the following concentrations 0.4, 0.6, 0.7, 0.8, 0.9, 1, 2, 3, 4, 5, 6, 7, 8, 9, 10, 13, 14, and 15 mM were used with volume 128, 192, 224, 256, 288, 320, 640, 960, 1280, 1600, 1920, 2240, 2560, 2880, 3200, 4160, 4480, and 4800 µL, then, 1600 µL seawater was added.

7.3.1.2.8 In the presence low and high concentration of PIC

The same stock solution of PIC with different concentrations including lower and higher than used concentrations was used.

7.3.1.2.8.1 The low concentration of PIC is 1×10^{-6} M (8 µL)

For preparing the samples of SDS to estimate the CMC, the following concentrations 2, 4, 5, 5.5, 5.8, 6, 6.2, 6.4, 6.6, 6.8, 7, 10, 12, 14, 16, 18, and 20 mM were used with volume 640, 1280, 1600, 1760, 1856, 1920, 1984, 2048, 2112, 2176, 2240, 3200, 3840, 4480, 5120, 5760, and 6400 µL.

7.3.1.2.8.2 The high concentration of PIC is 1×10^{-5} M (80 µL)

For preparing the samples of SDS to estimate the CMC, the following concentration 2, 3, 4, 5, 5.6, 6, 6.4, 6.8, 7.1, 7.4, 7.8, 8, 10, 13, 16,19, and 20 mM were used with volume 640, 960, 1280, 1600, 1792, 1920, 2048, 2176, 2272, 2368, 2496, 2560, 3200, 4160, 5120, and 6080 µL.

7.3.2 Measuring the CMC of SDS in 0.5 M SHG in the Presence of Selected Salts

The same experimental procedure as in the aqueous phase was followed with some expectation. For providing SHG phase to measure the critical micelle concentrations, 2.0 M of sodium silicate was prepared, an aliquot of 32.05 mL of

sodium silicate solution; contains (≥ 27% of silicate; ≥10 sodium hydroxide, density = 1.39 g cm^{-3}), was mixed with deionised water up to a volume of 100 mL in a volumetric flask. This stock solution of sodium silicate was used to prepare 0.5 M SHG by mixing it with the acid.

To prepare every particular concentration of SDS in SHG phase, the following materials was added: specific quantity of SDS solution, specific quantity of deionised water was needed to reach 8000 µL, specific quantity of selected salts, 40 µL pinacyanol chloride, 180 µL glacier acetic acid and finally 2000 µL sodium silicate in sample vail. Then, the quantity of the solution in this vail was distributed to four cuvettes (Fig. 7.6). and left for 24 h to complete their gelation process.

Figure 7-6: Preparing samples in the 0.5 M SHG.

In the hydrogel phase, the procedure consisted of measuring the absorbance at the wavelength of maximum absorbance (λ_{max}) (identified as 609 nm) by using 0.5 M silica hydrogel without adding salt as a reference. To make base line, deionized water was used as a blank and reference.

7.3.2.1 In the 0.5 M SHG

For preparing the samples of SDS to estimate the CMC in 0.5 M SHG, i the following concentrations 0.1, 0.2, 0.3, 0.4, 0.5, 0.6, 0.7, 0.8, 0.9, 1, 1.5, 3, 3.5, 4, 5, 6, 8, 10, and 12 mM were used with volume 32, 64, 96, 128, 160, 192, 224, 256, 288, 320, 480, 960, 1120, 1280, 1600, 1920, 2560, 3200, and 3840 µL.

7.3.2.2 In the Presence of Selected Salts

7.3.2.2.1 In the Presence of Carbonate

the same stock solution with 1.0 M of sodium carbonate (section 7.3.1.2.2) that used in the aqueous solution was used in the SHG phase. Also, the same different concentrations of SDS (section 7.3.2.1) that used in 0.5 M SHG was

used. For every concentration of sodium carbonate including 0.015, 0.025, 0.4, 0.05 and 0.1 M, it used 120, 200, 320, 400 and 800 µL respectively.

7.3.2.2.2 In the Presence of Sodium Sulphate

The same stock solution with 1.0 M of sodium sulfate (section 7.3.1.2.3) that used in the aqueous solution was used in the SHG phase. Also, the same different concentrations of SDS (section 7.3.2.1) used in 0.5 M SHG was used. For every concentration of sodium carbonate including 0.015, 0.025 M, it used 120 and 200 µL respectively.

7.3.2.2.3 In the Presence of Sodium Chloride

The same stock solution with 1.0 M of sodium chloride (section 7.3.1.2.4) that used in the aqueous solution was used in the SHG phase. Also, the concentrations of SDS that used includes 0.3, 0.4, 0.5, 0.6, 0.7, 0.8, 0.9, 1, 1.5, 3, 3.5, 4, 5, 6, 8, 10, and 12 mM with volume 96, 128, 160, 192, 224, 256, 288, 320, 480, 960, 1120, 1280, 1600, 1920, 2560, 3200, and 3840 µL.

For every concentration of sodium chloride includes 0.015, 0.025, 0.4, 0.05 and 0.1 M, 120, 200, 320, 400, 800, 1200, 1600 and 2000 µL were used respectively.

7.3.2.2.4 In the Presence of Disodium Phosphate

The same stock solution with 0.5 M of disodium phosphate (section 7.3.1.2.5) that used in the aqueous solution was used in the SHG phase. Also, the same different concentrations of SDS (section 7.3.2.1) that used in 0.5 M SHG was used. For every concentration of disodium phosphate including 0.015, 0.025 M, it used 240 and 400 µL respectively.

7.3.2.2.5 In the Presence of Magnesium Chloride

the same stock solution with 0.2 M of disodium phosphate (section 7.3.1.2.6) that used in the aqueous solution was used in the SHG phase. Also, the same different concentrations of SDS (section 7.3.2.1) that used in 0.5 M SHG was used. For every concentration of disodium phosphate including 0.5 M, it used 20 µL.

7.3.2.2.6 In the Presence of Simulated Seawater

Stock solution of seawater in the aqueous phase was used (section 7.3.1.2.7). To measure the CMC of SDS in SHG phase in the presence of seawater, the same volume ratios in aqueous phase was used including 1:10, and 1:5 with total volume of 8000 µL. The same procedure in section 7.3.1.2 of selected salts was followed.

7.3.2.2.6.1 Simulated Seawater with the Ratio 1: 10

For preparing the samples of SDS to estimate the CMC in the presence 1:10 seawater, the following concentrations 0.4, 0.5, 0.6, 0.7, 0.8, 0.9, 1, 1.2, 1.4, 1.6, 2, 4, 6, 8, 10, 12, and 14 mM were used with volume 128, 160, 192, 224, 256, 288, 320, 384, 448, 512, 640, 1280, 1920, 2560, 3200, 3840, and 4480 µL, then, 800 µL seawater was added.

7.3.2.2.6.2 Simulated Seawater with the Ratio 1: 5

For preparing the samples of SDS to estimate the CMC in the presence 1:10 seawater, following concentrations 0.1, 0.2, 0.3, 0.4, 0.6, 0.7, 0.8, 0.9, 1, 2, 4, 6, 7, 8, 10, 11, and 12 mM were used with volume 32, 64, 96, 128, 192, 224, 256, 288, 320, 640, 1280, 1920, 2240, 2560, 3200, 3520, and 3840 µL, then, 600 µL seawater was added.

7.3.3 Measuring the CMC of SDS in the Presence of Alcohol in Aqueous Phase

The same preparation method of essential material includes SDS, and PIC was used as mentioned (section 7.3.1) to measure the CMC of SDS in the presence of alcohol including ethanol, hexanol, octanol, decanol and dodecanol.

Because of the solubility problem, it was used the concentration of 1 mM as a high concentration of alcohol to measure the CMC of alcohol-SDS compared to the concentration that used in selected salts. Also, ethanol solution was used instead of deionized water to make the stock solution. In addition to that, the mixture of SDS and alcohol was heated to get a clear solution which is essential for UV/Vis measurement.

This procedure was modified from the method reported in the literature [192]. It was mixed 1:1 molar ratio of fatty alcohol and sorbitan mono stearate with 2 mL ethanol, then heated at 40-50 C° for 10-15 min and finally added 23 mL water.

This procedure offers an easy and simple way to prepare a set of samples with different concentrations of SDS compared to others with adding buffer solution or heating for a long time. Gentle heating (40°C) and ethanol as a solvent can help make alcohol soluble in the aqueous phase. The heating step is used to increase the kinetics of the dissolution of alcohol [256].

To make the samples of this study, the stock solution of SDS, 25 mM, and PIC were prepared as mentioned (section 7.3.1). Then the stock solution of alcohol, 125 mM for each was prepared. In the vial sample, particular concentration of SDS and a specific concentration of alcohol were mixed then heated to 40 °C for 15 min. Then, deionized water was added to reach the final volume with 8000 µL. Finally, PIC was added and left for 30 min before starting measurement.

Every experiment was repeated three times in aqueous phase and the mean and standard deviation, fitting line with confidence 95% are presented for each data set.

7.3.3.1 Measuring the CMC of SDS in the Presence of Ethanol

Ethanol it used as an additive as it is without diluting, the molarity of ethanol is calculated as below by using ethanol ‘density (0.79 g/cm3) and purity (99.5%).

Molarity of ethanol = 0.79 × 99.5 × 10 / 46.07 = 17.1 M

It was used with five different concentrations including 0.14, 0.4, 0.6, 0.9, 1.1 and 1.3 M with volumes 64, 200, 300, 400, 500, and 600 µL respectively, with total volume of 8000 µL as usual for each.

7.3.3.1.1 Preparing 0.14 M Ethanol

For preparing the samples of SDS to estimate the CMC of 0.14 M, it was used the following concentrations 2, 3, 4, 5, 5.5, 5.8, 6, 6.2, 6.4, 6.5, 7, 10, 12,14, and 17 mM were used with volume 640, 960, 1280, 1600, 1760, 1856, 1920, 1984, 2048, 2080, 2240, 3200, 3840, 4480, and 5440 µL, then, 64 µL ethanol was added.

7.3.3.1.2 Preparing 0.4 M Ethanol

For preparing the samples of SDS to estimate the CMC of 0.4 M, the following concentrations 1, 2, 3, 4, 4.5, 5, 5.3, 5.6, 5.8, 6, 6.2, 6.4, 6.8, 7, 8, 10, 12, and

14 mM were used with volume 320, 640, 960, 1280, 1440, 1600, 1696, 1792, 1856, 1920, 1984, 2048, 2176, 2240, 2560, 3200, 3840, and 4480 µL, then, 200 µL ethanol was added.

7.3.3.1.3 Preparing 0.6 M Ethanol

The same concentrations of section 7.3.3.1.2, then, 300 µL ethanol was added.

7.3.3.1.4 Preparing 0.9 M Ethanol

The same concentrations of section 7.3.3.1.2, then, 400 µL ethanol was added.

7.3.3.1.5 Preparing 1.1 M Ethanol

The same concentrations of section 7.3.3.1.2, then, 500 µL ethanol was added.

7.3.3.1.6 Preparing 1.3 M Ethanol

For preparing the samples of SDS to estimate the CMC 1.3 M, the following concentrations 1, 2, 3, 4, 5, 6, 6.2, 6.3, 6.4, 6.5, 6.8, 7, 8, 10, 12, 14, and 16 mM were used with volume 320, 640, 960, 1280, 1600, 1920, 1984, 2016, 2048, 2080, 2176, 2240, 2560, 3200, 3840, 4480, and 5120 µL, then, 600 µL ethanol was added.

The order of adding solution was SDS solution, then ethanol, then water, and finally PIC.

7.3.3.2 Measuring the CMC of SDS in the Presence of Hexanol

Hexanol was dissolved in ethanol solution, the molarity of hexanol is calculated as below by using hexanol ’density (0.82 g / cm3) and purity (98.0%).

Molarity of hexanol = 0.82 × 98.0 × 10 / 102.177 = 7.9 M. The dilution factor 0.016

Hexanol requires diluting 1582 µL, of this stock solution to 50 mL; dilution factors of 0.016, this contains hexanol concentration at 0.125 M

7.3.3.2.1 0.0625 mM Hexanol, (4 µL)

For preparing the samples of SDS to estimate the CMC, the following concentrations 1, 2, 3, 4, 4.8, 5, 5.2, 5.4, 5.6, 5.8, 6, 6.2, 8, 10, 12, 14, 17, 20,

and 24 mM were used with volume 320, 640, 960, 1280, 1536, 1600, 1664, 1728, 1792, 1856, 1920, 1984, 2560, 3200, 3840, 4480, 5440, 6400, and 7680 µL.

7.3.3.2.2 0.125 mM Hexanol (8 µL)

For preparing the samples of SDS to estimate the CMC, the following concentrations 1, 2, 3, 4, 5, 5.6, 5.7, 5.8, 5.9, 6, 6.2, 8, 10, 12, 14, 17, 20, and 24 mM were used with volume 320, 640, 960, 1280, 1600, 1792, 1824, 1856, 1888, 1920, 1984, 2560, 3200, 3840, 4480, 5440, 6400, and 7680 µL.

7.3.3.2.3 0.25 mM Hexanol (16 µL)

For preparing the samples of SDS to estimate the CMC, the following concentrations 1, 2, 3, 4, 5, 5.6, 5.7, 5.8, 6.2, 8, 10, 12, 14, 17, 20, and 24 mM were used with volume 320, 640, 960, 1280, 1600, 1792, 1824, 1856, 1984, 2560, 3200, 3840, 4480, 5440, 6400, and 7680 µL.

7.3.3.2.4 0.5 mM Hexanol (32 µL)

For preparing the samples of SDS to estimate the CMC, the following concentrations 1, 2, 3, 4, 5, 5.4, 5.6, 5.8, 6, 6.2, 8, 10, 12, 14, 17, 20, and 24 mM were used with volume 320, 640, 960, 1280, 1600, 1728, 1792, 1856, 1920, 1984, 2560, 3200, 3840, 4480, 5440, 6400, and 7680 µL.

7.3.3.2.5 1.0 mM Hexanol (64 µL)

For preparing the samples of SDS to estimate the CMC, the following concentrations 1, 2, 3, 4, 5, 5.6, 5.7, 5.8, 6.2, 8, 10, 12, 14, 17, 20, and 24 mM were used with volume 320, 640, 960, 1280, 1600, 1792, 1824, 1856, 1984, 2560, 3200, 3840, 4480, 5440, 6400, and 7680 µL.

7.3.3.3 Measuring the CMC of SDS in the Presence of Octanol

Octanol was dissolved in ethanol solution, the molarity of octanol is calculated as below by using octanol ’density (0.83 g / cm3) and purity (99.0%).

Molarity of octanol = 0.82 × 99.0 × 10 / 130.23 = 6.3 M.

Octanol requires diluting 992 µL, of this stock solution to 50 mL; dilution factors of 0.019, this contains octanol concentration at 0.125 M.

7.3.3.3.1 0.0625 mM Octanol, (4 µL)

For preparing the samples of SDS to estimate the CMC, the following concentrations 2, 3, 4, 5, 5.7, 5.8, 6, 6.2, 8, 10, 12, 14, 17, 20, and 24 mM were used with volume 640, 960, 1280, 1600, 1824, 1856, 1920, 1984, 2560, 3200, 3840, 4480, 5440, 6400, and 7680 µL.

7.3.3.3.2 0.125 mM Octanol (8 µL)

For preparing the samples of SDS to estimate the CMC, the following concentrations1, 2, 3, 4, 5, 5.7, 5.8, 6, 6.2, 7, 8, 10, 12, 14, 20, and 24 mM were used with volume 320, 640, 960, 1280, 1600, 1824, 1856, 1920, 1984, 2240, 2560, 3200, 3840, 4480, 6400, and 7680 µL.

7.3.3.3.3 0.25 mM Octanol (16 µL)

For preparing the samples of SDS to estimate the CMC, the following concentrations 1, 2, 3, 4, 5, 5.4, 5.5, 5.6, 5.7, 5.8, 6, 6.2, 8, 10, 12, 14, 17, 20, and 24 mM were used with volume 320, 640, 960, 1280, 1600, 1728, 1760, 1792, 1824, 1856, 1920, 1984, 2560, 3200, 3840, 4480, 5440, 6400, and 7680 µL.

7.3.3.3.4 0.5 mM Octanol (32 µL)

For preparing the samples of SDS to estimate the CMC, the following concentrations 1, 2, 3, 4, 5, 5.2, 5.4, 5.5, 5.7, 5.8, 6, 6.2, 8, 10, 12, 14, 17, 20,and 24 mM were used with volume 320, 640, 960, 1280, 1600, 1664, 1728, 1760, 1824, 1856, 1920, 1984, 2560, 3200, 3840, 4480, 5440, 6400, and 7680 µL.

7.3.3.3.5 1 mM Octanol (64 µL)

For preparing the samples of SDS to estimate the CMC, the following concentrations 1, 2, 3, 4, 5, 5.2, 5.4, 5.8, 6, 8, 10, 12, 14, 17, 20, and 24 mM were used with volume 320, 640, 960, 1280, 1600, 1664, 1728, 1856, 1920, 2560, 3200, 3840, 4480, 5440, 6400, and 7680 µL.

7.3.3.4 Measuring the CMC of SDS in the Presence of Decanol

Decanol was dissolved in ethanol solution, the molarity of decanol is calculated as below by using decanol ’density (0.8297 g / cm3) and purity (99.0%).

Molarity of decanol = 0.8297 × 99.0 × 10 / 158.28 = 5.19 M.

Decanol requires diluting 1200 µL, of this stock solution to 50 mL; dilution factors of 0.024, this contains decanol concentration at 0.125 M

7.3.3.4.1 0.0625 mM Decanol, (4 µL)

For preparing the samples of SDS to estimate the CMC, the following concentrations 2, 3, 4, 5, 5.4, 5.6, 5.8, 6, 8, 10, 12, 14, 17, 20, and 24 mM were used with volume 640, 960, 1280, 1600, 1728, 1792, 1856, 1920, 2560, 3200, 3840, 4480, 5440, 6400,and 7680 µL.

7.3.3.4.2 0.125 mM Decanol (8 µL)

For preparing the samples of SDS to estimate the CMC, the following concentrations 2, 3, 3.5, 4, 5, 5.2, 5.4, 5.5, 5.6, 5.8, 6, 6.2, 8, 10, 12, 14, 17, 20, and 24 mM were used with volume 640, 960, 1120, 1280, 1600, 1664, 1728, 1760, 1792, 1856, 1920, 1984, 2560, 3200, 3840, 4480, 5440, 6400, and 7680 µL.

7.3.3.4.3 0.25 mM Decanol (16 µL)

For preparing the samples of SDS to estimate the CMC, the following concentrations 2, 3, 3.5, 4, 5, 5.3, 5.4, 5.5, 6.6, 5.8, 6, 6.2, 8, 10, 12, 14, 17, 20, and 24 mM were used with volume 640, 960, 1120, 1280, 1600, 1696, 1728, 1760, 2112, 1856, 1920, 1984, 2560, 3200, 3840, 4480, 5440, 6400, and 7680 µL.

7.3.3.4.4 0.5 mM Decanol (32 µL)

For preparing the samples of SDS to estimate the CMC, the following concentrations 2, 3, 3.5, 4, 5.5, 5.7, 5.8, 6, 6.2, 6.4, 6.5, 8, 10, 12, 14, 17, 20, and 24 mM were used with volume 640, 960, 1120, 1280, 1760, 1824, 1856, 1920, 1984, 2048, 2080, 2560, 3200, 3840, 4480, 5440, 6400, and 7680 µL.

7.3.3.4.5 1 mM Decanol (64 µL)

For preparing the samples of SDS to estimate the CMC, the following concentrations 1, 2, 3, 4, 5, 5.4, 5.7, 5.8, 5.9, 6, 6.2, 6.5, 8, 10, 12, 14, 17, 20, and 24 mM were used with volume 320, 640, 960, 1280, 1600, 1728, 1824, 1856, 1888, 1920, 1984, 2080, 2560, 3200, 3840, 4480, 5440, 6400, and 7680 µL.

7.3.3.5 Measuring the CMC of SDS in the Presence of Dodecanol

Dodecanol was dissolved in ethanol solution, the molarity of dodecanol is calculated as below by using dodecanol ’density (0.83 g / cm3) and purity (98.0%).

Molarity of dodecanol = 0.83 × 98.0 × 10 / 186.34 = 4.4 M.

Dodecanol requires diluting 1420 µL, of this stock solution to 50 mL; dilution factors of 0.028, this contains decanol concentration at 0.125 M

7.3.3.5.1 0.0625 mM Dodecanol, (4 µL)

For preparing the samples of SDS to estimate the CMC, the following concentrations 2, 3, 4, 5, 5.5, 5.7, 5.8, 6, 6.2, 6.5, 6.8, 7, 8, 10, 12, 14, 17, 20, and 24 mM were used with volume 640, 960, 1280, 1600, 1760, 1824, 1856, 1920, 1984, 2080, 2176, 2240, 2560, 3200, 3840, 4480, 5440, 6400, and 7680 µL.

7.3.3.5.2 0.125 mM Dodecanol (8 µL)

The same concentration of SDS that used with 0.0625 mM dodecanol.

7.3.3.5.3 0.25 mM Dodecanol (16 µL)

For preparing the samples of SDS to estimate the CMC, the following concentrations 2, 3, 4, 5, 5.5, 5.8, 6, 6.2, 6.5, 6.8, 7, 8, 10, 12, 14, 17, 20, and 24 mM were used with volume 640, 960, 280, 1600, 1760, 1856, 192, 1984, 2080, 2176, 2240, 2560, 3200, 3840, 4480, 5440, 6400, and 7680 µL.

7.3.3.5.4 0.5 mM Dodecanol (32 µL)

For preparing the samples of SDS to estimate the CMC, the following concentrations 2,3, 4, 5, 5.5, 5.8, 6, 6.2, 6.4, 6.5, 7, 10, 12, 14, 17, 20, and 24 mM were used with volume 640, 960, 1280, 1600, 1760, 1856, 1920, 1984, 2048, 2080, 2240, 3200, 3840, 4480, 5440, 6400, and 7680 µL.

7.3.3.5.5 1 mM Dodecanol (64 µL)

For preparing the samples of SDS to estimate the CMC, the following concentrations 1, 2, 3, 4, 5, 5.6, 5.8, 6, 6.2, 6.35, 6.5, 8, 10, 11, 12, 14, 17, 20,

and 24 mM were used with volume 320, 640, 960, 1280, 1600, 1792, 1856, 1920, 1984, 2032, 2080, 2560, 3200, 3520, 3840, 4480, 5440, 6400, and 7680 µL.

7.3.4 Measuring the CMC of SDS in the Presence of Alcohol in SHG Phase

The same preparation method of essential material includes SDS, and PIC was used as mentioned (section present selected salt in SHG) to measure the CMC of SDS in the presence of alcohol including ethanol, hexanol, octanol, decanol and dodecanol in SHG phase.

The same problem with solubility was faced especially with decanol and dodecanol. There is a try to overcome this issue by dissolving mentioned alcohol with ethanol instead of using deionised water to make the stock solutions of all alcohol. Also, the mixture of SDS and alcohol was heated to get a clear solution which is essential for UV/Vis measurement as it mentioned (section 7.3.1)

To make the samples of this study, the stock solution of SDS (25 Mm), and PIC were prepared as mentioned. Then the stock solution of alcohol, 125 mM for each, was prepared. In the vial sample, particular concentration of SDS and a specific concentration of alcohol were mixed then heated to 40°C for 15 min. Then, deionized water was added to reach the final volume with 8000 µL, following by adding PIC. To make silica hydrogels media, 180 µL of glacier acetic acid was added into the sample vail with gentle shaking, and finally, adding 2000 µL of sodium silicate also with gentle shaking to make homogenous phase and prevent formation of bubbles. This sample amount was divided into four volumes in each cuvette and left them for 24 hours before starting measurement.

Every experiment was repeated four times in SHG phase and the mean and standard deviation, fitting line with confidence 95% are presented for each data set.

The same five different concentrations of alcohol in aqueous phase with the same total volume of 8000 µL were used as usual for each with one exception. Ethanol was done with two different concentration in SHG phase as it will be mentioned.

7.3.4.1 Measuring the CMC of SDS in the Presence of Ethanol

Two different concentrations including 0.4, and 1.1 M with volumes 200, and 500 µL respectively were used, with the same total volume of 8000 µL as usual for each.

For preparing the samples of SDS to estimate the CMC for both mentioned concentrations, the following concentrations 0.3, 0.4, 0.5, 0.6, 0.7, 0.8, 0.9, 1, 1.5, 3, 3.5, 4, 6, 7, 8, 9, 10, 11, and 12 mM were used with volume 96, 128, 160, 192, 224, 256, 288, 320, 480, 960, 1120, 1280, 1920, 2240, 2560, 2880, 3200, 3520, and 3840 µL .

7.3.4.2 Measuring the CMC of SDS in the Presence of Hexanol

7.3.4.2.1 0.0625 mM Hexanol (4 µL)

For preparing the samples of SDS to estimate the CMC, the following concentrations 0.2, 0.3, 0.4, 0.5, 0.6, 0.7, 0.8, 0.9, 1, 1.1, 1.2, 1.5, 3, 5, 6, 8, 10, 12, and 14 mM were used with volume 64, 96, 128, 160, 192, 224, 256, 288, 320, 352, 384, 480, 960, 1600, 1920, 2560, 3200, 3840, and 4480 µL.

7.3.4.2.2 0.125 mM Hexanol (8 µL)

For preparing the samples of SDS to estimate the CMC, the following concentrations 0.1, 0.2, 0.3, 0.4, 0.5, 0.6, 0.7, 0.8, 0.9, 1, 1.5, 3, 4, 5, 6, 8, 10, 12, and 14 mM were used with volume 32, 64, 96, 128, 160, 192, 224, 256, 288, 320, 480, 960, 1280, 1600, 1920, 2560, 3200, 3840, and 4480 µL.

7.3.4.2.3 0. 25 mM Hexanol (16 µL)

For preparing the samples of SDS to estimate the CMC, the following concentrations 0.2, 0.3, 0.4, 0.5, 0.6, 0.7, 0.8, 0.9, 1, 1.1, 3, 4, 5, 6, 8, 10, 12, and 14 mM were used with volume 64, 96, 128, 160, 192, 224, 256, 288, 320, 352, 960, 1280, 1600, 1920, 2560, 3200, 3840, 4480, and 4480 µL.

7.3.4.2.4 0.5 mM Hexanol (32 µL)

For preparing the samples of SDS to estimate the CMC, the following concentrations 0.2, 0.3, 0.4, 0.5, 0.6, 0.7, 0.8, 0.9, 1, 1.5, 3, 4, 5, 6, 8, 10, 12, and 14 mM were used with volume 64, 96, 128, 160, 192, 224, 256, 288, 320, 480, 960, 1280, 1600, 1920, 2560, 3200, 3840, and 4480 µL.

7.3.4.2.5 1.0 mM Hexanol (64 µL)

For preparing the samples of SDS to estimate the CMC, the following concentrations 0.2, 0.3, 0.4, 0.5, 0.6, 0.7, 0.8, 0.9, 1, 1.1, 1.2, 1.5, 3, 5, 6, 8, 10 12, and 14 mM were used with volume 64, 96, 128, 160, 192, 224, 256, 288, 320, 352, 384, 480, 960, 1600, 1920, 2560, 3200, 3840, and 4480 µL.

7.3.4.3 Measuring the CMC of SDS in the Presence of Octanol

7.3.4.3.1 0.0625 mM Octanol (4 µL)

The same preparing with 0.125 mM hexanol

7.3.4.3.2 0.125 mM Octanol (8 µL)

For preparing the samples of SDS to estimate the CMC, the following concentrations 0.2, 0.3, 0.4, 0.5, 0.6, 0.7, 0.8, 0.9, 1, 1.1, 1.5, 3, 5, 6, 8, 10, 12, and 14 mM were used with volume 64, 96, 128, 160, 192, 224, 256, 288, 320, 352, 480, 960, 1600, 1920, 2560, 3200, 3840, and 4480 µL.

7.3.4.3.3 0.25 mM Octanol (16 µL)

For preparing the samples of SDS to estimate the CMC, the following concentrations 0.2, 0.3, 0.4, 0.5, 0.6, 0.7, 0.8, 0.9, 1, 1.1, 3, 5, 6, 8, 10, 12, and 14 mM with volume 64, 96, 128, 160, 192, 224, 256, 288, 320, 352, 960, 1600, 1920, 2560, 3200, 3840 and 4480 µL.

7.3.4.3.4 0.5 mM Octanol (32 µL)

For preparing the samples of SDS to estimate the CMC, the following concentrations 0.2, 0.3, 0.4, 0.5, 0.6, 0.7, 0.8, 0.9, 1, 1.1, 1.2, 1.5, 3, 5, 6, 8, 10, 12, and 14 mM were used with volume 64, 96, 128, 160, 192, 224, 256, 288, 320, 352, 384, 480, 960, 1600, 1920, 2560, 3200, 3840, and 4480 µL.

7.3.4.3.5 1.0 mM Octanol (64 µL)

The same preparing with 0.125 mM octanol was followed.

7.3.4.4 Measuring the CMC of SDS in the Presence of Decanol

7.3.4.4.1 0.0625 mM Decanol (4 µL)

The same preparing with 0.125 mM hexanol was followed.

7.3.4.4.2 0.125 mM Decanol (8 µL)

The same preparing with 0.125 mM hexanol was followed.

7.3.4.4.3 0.125 mM Decanol (16 µL)

The same preparing with 0.5 mM octanol was followed.

7.3.4.5 Measuring the CMC of SDS in the Presence of Dodecanol

7.3.4.5.1 0.0625 mM Dodecanol (4 µL)

The same preparing with 0.125 mM hexanol was followed.

7.3.4.5.2 0.125 mM Dodecanol (8 µL)

The same preparing with 0.125 mM hexanol was followed.

7.4 Examining Vesicle Formation of SDS-Alcoholic Composites in Aqueous and Silica Hydrogels by Fluorescent Microscopy Technique

7.4.1 Preparing the glass slide

It is important to passivate the surface of glass slides allows for long-term observation [257]. Using Bovine Serum Albumin (BSA) as surface covering can prevent interacting with the surface. It was dissolved 50 mg in 10 mL of deionized water. It was dissolved 50 mg of BSA in 10 mL of deionised water, and then it is simply applied to the glass surface for one hour (Fig. 7-7), then rinsed with copious water and dried under a stream of N_2 (deionized water getting into the sample might burst the vesicles).

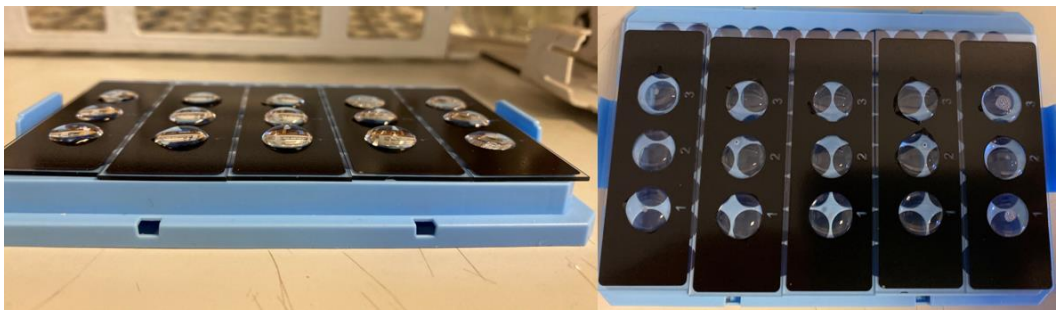

Figure 7-7: Covering the wells of glass slide with BSA for one hour.

For preparing 0.625 M of Nile Red, 0.005 g was dissolved with ehanol in a 25 mL volumetric flask.

Different concentrations of a mixture of SDS/Dodecanol and SDS/ Decanol in the presence of Na_2CO_3 and without were selected for visualisation test.

For preparing the mixture, the same concentration of the stock solution of SDS (25 mM) that prepared freshly with vortex mixing in deionized water, was used.

The same previous (7.3.3.4 and 7.3.3.5) stock solution of decanol and dodecanol, respectively, (125 Mm for each) that dissolved in ethanol were used with different concentrations.

The procedure that used to prepare vesicle solution was modified from [178]. All samples were performed in 25 mL plastic centrifuge tubes. To prepare the mixture, the particular volume of the SDS and alcohol then Na_2CO_3 if there is any were mixed, followed by water to complete 8 mL. Then, the samples were sonicated for 25 min on a bath sonicator and left them to equilibrate for 30 min. Finally, 7 µL Nile Red dye was added into the mixture just before visualizing. Repeating experiments three times to check reproducibility.

It is worth to mentioned that preparation method such as stirring or such as sonication or stirring can help fatty molecules to assebmled to produce stable components like vesicle when they are dissolved in aqueous solutions [258].

7.4.2 Epifluorescence Microscopy

The mixture of 10 µL (with a total volume of 8000 µL) was applied to a microscope slide then covered with a coverslip. The slide then was placed into the specimen holder of a Nikon, Japan, epifluorescence microscope (Leeds University).

Figure 7-8: Epifluorescence Microscopy. University of Leeds, Chemistry department.

The mixture was imaged using a Plan Fluor with magnification 20x/0.50 objective. Excitation was achieved using a Mercury Lamp Power and emission was filtered through a ND filter. Images were obtained in NIS-Elements software and captured as png images.

7.4.2.1 Preparing Mixture of SDS/Decanol in Aqueous phase

It was prepared several solutions with two constant concentrations of SDS/ Decanol in the presence of different concentrations of sodium carbonate as in the following tables:

7.4.2.1.1 Mixtures 1.5 mM SDS and 1.0 mM Decanol with Different Concentrations of Sodium Carbonate

Table 7-5 Preparing mixtures 1.5 mM SDS (480 µL) and 1.0 mM decanol (64 µL) with different concentration of sodium carbonate.

[Na_2CO_3] M	V µL (Na_2CO_3)	V µL water
0.0	0.0	7456
0.015	120	7336
0.025	200	7256
0.04	320	7136
0.05	400	7056
0.1	800	6656

7.4.2.1.2 Mixtures 1.0 mM SDS and 0.04 mM Decanol with Different Concentration of Sodium Carbonate

Table 7-6 Preparing mixtures 1.0 mM SDS (320 µL) and 0.04 mM decanol (3.20 µL) with different concentration of sodium carbonate.

[Na_2CO_3] M	V µL (Na_2CO_3)	V µL Water
0.0	0.0	7676.8
0.04	320	7356.8
0.05	400	7276.8
0.6	480	6996.8

7.4.2.2 Preparing Mixtures of SDS/Dodecanol/Na_2CO_3 in Aqueous Phase

It was prepared several solutions with different concentrations of SDS with constant concentrations dodecanol 0.25 mM (16 µL) in the presence constant concentrations of sodium carbonate as in the following tables:

7.4.2.2.1 Mixtures of Different Concentrations of SDS and 0.25 mM Dodecanol with of 0.04 M Sodium Carbonate.

Table 7-7 Preparing mixtures of different concentrations of SDS and 0.25 mM dodecanol (16.0 µL) with of 0.04 M sodium carbonate (320 µL).

[SDS] mM	V µL $_{(SDS)}$	V µL $_{(Water)}$
0.5	160	7504
1.0	320	7344
1.5	480	7184
2.0	640	7024

7.4.2.2.2 Mixtures 0.125 mM SDS and 0.0625 mM Dodecanol with Different Concentrations of Sodium Carbonate.

Table 7-8 Preparing mixtures 0.125 mM SDS (40 µL) and 0.0625 mM dodecanol (4.0 µL) with different concentrations of sodium carbonate.

[Na_2CO_3] M	V µL (Na_2CO_3)	V µL Water
0.0	0.0	7456
0.015	120	7336
0.025	200	7256
0.04	320	7136
0.05	400	7056
0.1	800	6656

7.4.2.2.3 Mixtures 1.0 mM SDS and 0.04 mM Dodecanol with Different Concentrations of Sodium Carbonate.

Table 7-9 Preparing mixtures 1.0 mM SDS (320 µL) and 0.04 mM dodecanol (3.20 µL) with different concentrations of sodium carbonate.

[Na_2CO_3] M	V µL (Na_2CO_3)	V µL water
0.0	0.0	7676.8
0.04	320	7356.8
0.05	400	7276.8

0.06	480	6996.8

7.4.2.3 Visualisation of the Composite SDS/Decanol by Epifluorescence Microscopy in SHG Phase

7.4.2.3.1 Mixtures 1.0 mM SDS and 0.04 mM Decanol with Different Concentrations of Sodium Carbonate after Four Hours

Table 7-10 Preparing mixtures 1.0 mM SDS (320 µL) and 0.04 mM decanol (3.20 µL) with and without sodium carbonate in 0.5 M SHG phase by adding 2000 µL sodium silicate and 180 µL GAA.

$[Na_2CO_3]$ M	V µL (Na_2CO_3)	V µL water
0.0	0.0	7676.8
0.06	480	6996.8

7.4.3 Confocal Florescent Microscopy

Candidate mixtures that were obtained with epifluorescence microscopy, were chosen to visualise by confocal florescent microscopy in both aqueous and SHG phase.

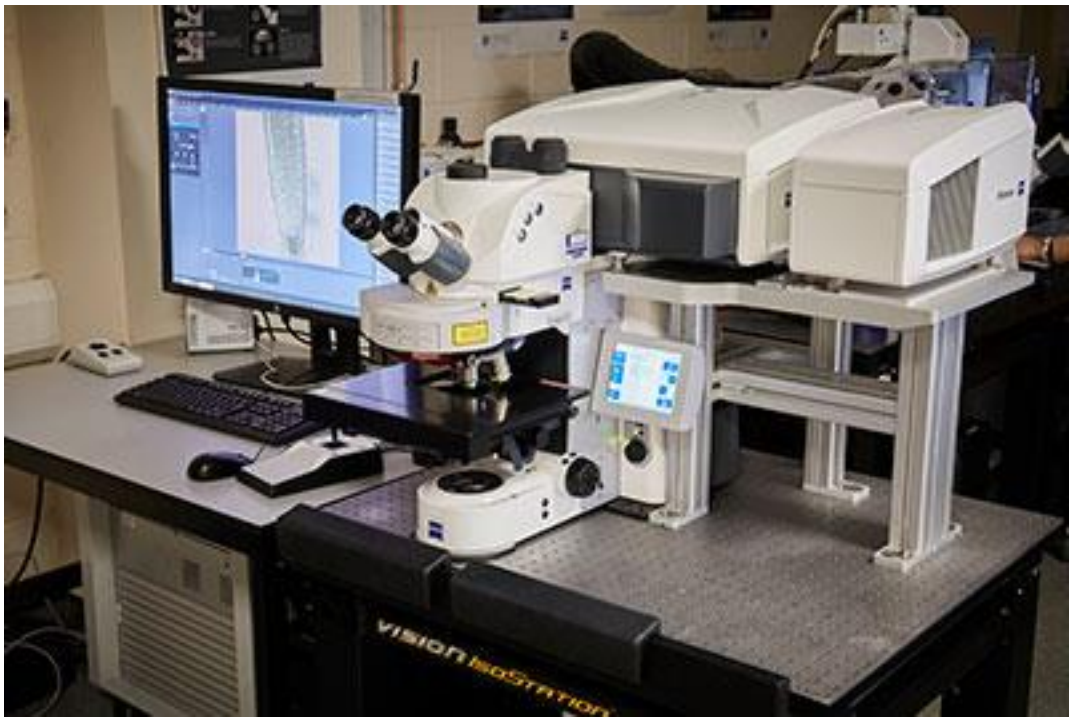

Figure 7-9: Confocal florescent microscopy, Faculty of Biological Sciences, University of Leeds.

The images were acquired the LSM880 upright confocal microscope, using both the 20x/0.8A and 63x/1.4NA oil objectives for brightifeld and NR**.**

7.4.3.1.1 Mixtures of 1.0 mM SDS and 0.04 mM Decanol with and without Sodium Carbonate in the Aqueous Phase.

Table 7-11 Preparing mixtures 1.0 mM SDS (320 µL) and 0.04 mM decanol (3.20 µL) with and without sodium carbonate.

$[Na_2CO_3]$ M	V µL (Na_2CO_3)	V µL water
0.0	0.0	7676.8
0.04	320	7356.8
0.05	400	7276.8
0.06	480	6996.8

7.4.3.1.2 Mixtures of 1.0 mM SDS and 0.04 mM Decanol with and without Sodium Carbonate in the SHG Phase.

Table 7-12 Preparing mixtures 1.0 mM SDS (320 µL) and 0.04 mM decanol (3.20 µL) with and without sodium carbonate in 0.5 M SHG phase by adding 2000 µL sodium silicate and 180 µL GAA.

$[Na_2CO_3]$ M	V µL (Na_2CO_3)	V µL water
0.0	0.0	7676.8
0.06	480	6996.8

7.5 Determination of the Gelation Time by Light Scattering

To determine the gelation time, which refers to the time required to convert from sol-gel to hydrogels phase, it was used two different methods using UV/Vis and turbidity meter.

7.5.1 By Using UV/Vis

2000 µL volume of silica hydrogel with three different concentrations were prepared, including 0.5 M (500 µL from 2 M stock solution), 0.7 M (350 µL from 4 M stock solution), 0.9 M (2000 µL from 4 M stock solution) separately with SDS using different concentration including 0.0, 3.0, 10.0, 18.0 mM in the polystyrene cuvette. To monitor light scattering changes along the gelation process, absorbance was measured at three different wavelengths, including 400, 500, and 600 nm, recorded data from 400 to 800 nm of wavelength to monitor scanning kinetic mode at room temperature at predefined time intervals which were selected depending on the observation of gelation time by the naked eye. It was chosen 900 min for 0.5 M, run every 10 min, and 240 min for 0.7 and 0.9 M of SHG, run every 3 min using water as a reference for all. Measurements were recorded on a Cary 100 (Australia) instrument from Agilent Technology (University of Leeds) with the 4.20 version software and using disposal polystyrene cuvettes. Control in each case was deionized water. All experiments

were conducted in triplicate for each concentration. The result is given as a mean with an error bar of standard deviation using Origin lab software to treat the data. The data average reduces experimental uncertainties, avoids random data, and makes the results more realistic.

7.5.1.1 Determination of the Gelation Time of 0.5 M SHG in the Presence of Different Concentrations of SDS

Table 7-13 Preparing the mixture of silica hydrogel with 500 µL of sodium silicate and 45 µL acetic acid with different concentrations of SDS for each cuvette to determining the gelation time during 900 min.

[SDS] mM	SDS µL	Water
0	0	1455
3	240	1215
10	800	655
18	1440	15

7.5.1.2 Determination of the gelation time of 0.7 M SHG in the Presence of Different Concentration of SDS

Table 7-14 Preparing the mixture of silica hydrogel with 350 µL of sodium silicate and 45 µL acetic acid with different concentrations of SDS for each cuvette to determining the gelation time during 240 min.

[SDS] mM	SDS µL	water
0	0	1605
3	240	1365
10	800	805
18	1440	165

7.5.1.3 Determination of the gelation time of 0.9 M SHG in the Presence of Different Concentration of SDS

Table 7-15 Preparing the mixture of silica hydrogel with 450 µL of sodium silicate and 45 µL acetic acid with different concentrations of SDS for each cuvette to determining the gelation time during 240 min.

[SDS] mM	SDS µL	water
0	0	1505
3	240	1265
10	800	705
18	1440	65

7.5.1.4 Determination Gelation Time of 0.5 M SHG in the Presence of Salts

To estimate the gelation time in the presence of salt (sodium chloride, sodium carbonate, and their effect on 0.5 M silica hydrogel, the same procedure was used in the previous Section 7.5.1, but without SDS, using salts instead. The concentrations of the salts were mentioned in every table.

7.5.1.4.1 In the Presence of Sodium Chloride

Table 7-16 Preparing the mixture of silica hydrogel with 500 µL of sodium silicate and 45 µL acetic acid with two different concentration of NaCl for each cuvette during 900 min.

[NaCl] M	Sodium Chloride µL	Water µL
0.1	200	1255
0.2	400	1055

7.5.1.4.2 In the Presence of Sodium Carbonate

Table 7-17 Preparing the mixture of silica hydrogel with 500 µL of sodium silicate and 45 µL acetic acid during 900 min.

[Na_2CO_3] M	Sodium Carbonate µL	Water µL
0.1	200	1255

7.5.2 By Turbidity Meter

The TN-100 turbid meter (Fig. 7-10) was used to monitor the turbidity during the gelation process of 0.5 M SHG in the presence of salts.

Figure 7-10: Turbidity meter.

It is very important to check the turbidimeter to ensure it is operating correctly. To achieve that, the device was calibrated with each used concentration. The calibration process was performed using four standard solutions with gradual decreasing Nephelometric Turbidity Units (i.e., 800, 100, 20, and 0.02). After calibration process was done , the vial of the aqueous phase of the silica hydrogel was added to the turbidity meter, ensuring no air bubbles were present in the sample. A reading was then taken at 0 minutes and every following 10 minutes of the gelation process for 180 minutes with avoiding shaking of the standard

solutions during calibration because the air can intrude on the sample, which causes degrade the measurement accuracy. Storage of the solutions should be kept at room temperature to prevent reductions in the volume of the particles if they are frozen. The point of calibration is to make sure the treatment process works effectively.

The volume used in this method is on a large scale compared with UV/Vis. 16 mL of the mixture is required to fill the vial in the turbidity meter. To prepare the solution of 0.5 M SHG, all specific amount of all component were mixed gently (Section 7.2) with salt, and recorded the reading immediately at room temperature. The data was collected each 10 min or less depending on the observation by naked eye. It is worth mentioning that the volume of salt was added to the silicate first solution then mixed with the acid.

7.5.2.1 Determination of the Gelation Time of Silica Hydrogel in the Presence of Salts

Table 7-18 Preparing the mixture of silica hydrogel with 4000 µL of sodium silicate and 360 µL acetic acid in 7960 µL to determine the gelation time.

Salt	[Salt]	Volume µL $_{(salt)}$	water µL	Duration
No salt	0.0 M	0.0	4040	every 10 min for 900 min
NaCl	0.1 M	1600	2080	every 10 min for 900 min
NaCl	0.2 M	3200	480	every 10 min for 900 min
Na_2CO_3	0.1 M	1600	2080	every 4 min for 300 min

Chapter 8 Summary, Conclusion and Future Work

Below is a brief summary of significant key findings from the work presented in this thesis, chapter-by-chapter:

8.1 Chapter 2

Silica hydrogels (SHG's) were prepared using the Barge method (104) with three different concentrations, 0.5, 0.7, and 1.0 M by mixing two solutions. The first one is with a specific calculated concentration of sodium silicate solution, and the other with a specific amount of GAA solution.

For surface analysis, the samples were examined by SEM or cryo-SEM to visualize the surface morphologies, EDX to detect salts present in the matrix structure, and BET for porosity measurements.

For 0.75 M SHG, the matrices were prepared by critical point drying (CPD) prior to surface analysis examinations to preserve the integrity of the structure and to visualise the growth of the silica matrix structure. SEM images at different magnifications revealed a fractured surficial material, a rough surface, great porosity, and granularity structure. EDX analysis revealed the presence of silicon, oxygen, and sodium. In addition to that, the presence of unexpected phosphorus was revealed, which possibly have been introduced via a contaminated syringe being used by another member of the group. To remove undesired present salts, dialysis was performed for 48 hrs and 96 hrs respectively, followed by freeze-drying for each of them prior to analysis. After 48 hrs of dialysis, and freeze-drying, the sample was visualised again, the images of matrix structure and morphology revealed a significant changed from that observed post CPD which is supported by BET studies where surface area is almost triple the pre-dialysed values. EDX analysis revealed that there was still some sodium freeze-drying although it appeared significantly reduced in the post CPD sample. Another analysis was conducted after 96 hrs of dialysis and then freeze-drying, this decision is because of the presence of sodium, and the sample was visualised again. EDX analysis revealed a very low levels of sodium and no phosphorus remaining in the matrix. Morphologically too, there was little change in the structural integrity of the silica matrix. However, there were not enough SHG matrices for BET measurement.

For 0.5 M SHG sample was examined using cryo-SEM which did not require having to remove water prior to microscopic examination. This allowed us to provide an additional view of the silica matrix without any water-removal methodology having to be applied. After preparing the sample, the sample was characterised in cryo-SEM because of its ability for mapping the water distribution within the matrix and preserving its structural integrity. The images revealed a porous surficial material and the presence of ice hexagonal with different magnifications, especially, when increasing the magnification to 1 μm, the greater porosity and the crosslinking of the sample were revealed. It is worth mentioning that the analysis of EDX and BET were carried out on matrices prepared by freeze-drying. EDX analysis (done by a Master's degree student, Amy Nicholls) revealed the presence of Si and O from the silica hydrogel matrix as expected. Also, the sample included minor (trace) levels of salt which was expected due to the sodium hydroxide present in the silicate solution used to produce the SHG. In addition to that, the EDX shows a signal for carbon, and boron signal whose presence is less obvious because of the presence of carbonate in the stock solution. The porous surface area of the 0.5 M SHG sample was determined by BET which supports the presence of great porosity by cryo-SEM. To remove undesired salts, dialysis for four days and lyophilised were conducted, then examined by SEM, EDX, and BET measurement. The resulting images revealed more porosity of the morphology which can explain the BET measurement with a very high surface area, the EDX analysis indicated that the elemental composition of the materials was O and Si with no Na.

The conclusion of the second chapter:

1. The Barge method is a good procedure for preparing an optical and homogenous SHG, especially with 0.5 M.
2. Cryo-SEM is a valuable technique to visualise the morphology and structure of SHG without removing water.
3. For surface analysis of SHG, EDX is a suitable method to detect the presence of salts in the silica matrices and BET for porosity measurements.

8.2 Chapter 3

This chapter focuses on measurements of the CMC of SDS surfactant in the aqueous and SHG phase in the presence of inorganic electrolyte.

The CMCs of SDS surfactant were estimated by using UV-Vis spectrophotometry technique and PIC dye as a probe to measure the absorbance of different concentrations of SDS between 500 and 650 nm. It was found that the wavelength of maximum absorbance (λ_{max}) was 608 and 609 nm in the aqueous phase and in the SHG phase respectively. Each absorbance at λ_{max} of 608 nm or 609 nm was plotted against the concentration of the SDS surfactant and from the plots of absorbance vs. the concentration of SDS, there are discontinuities that represent the transition line from molecular amphiphiles to micelle formation, which indicated that intercalation of the pinacyanol cation into the self-assembled structure of the SDS. In both aqueous and SHG phases many different experiments were conducted in the presence of salts, dye, and seawater.

First, CMC of SDS in deionised water was examined, then, the influence of salts on the CMC of SDS (magnesium chloride, sodium silicates, sodium carbonates, sodium chlorides, sodium sulphates, and sodium diphosphates), simulated seawater with two different ratios, and finally, the PIC dye with lower and higher concentrations of used concentration was examined.

The result of the CMCs mM of SDS in the aqueous phase is shown in the following tables:

i. Deionised Water and Salts

Table 8-1 CMC of SDS in deionised water and salts

[Salt]	[Na_2SiO_3] M	[Na_2CO_3] M	[Na_2SO_4] M	[NaCl] M	[HNa_2PO_3] M	[$MgCl_2$] mM
0	6.7 ± 0.3	6.7 ± 0.3	6.7 ± 0.3	6.7 ± 0.3	6.7 ± 0.3	6.7 ± 0.3
0.5	-	-	-	-	-	3.3 ± 0.1
0.015	4.5 ± 0.5	2.8 ± 0.1	3.1 ± 0.5	3.7 ± 0.3	2.8 ± 0.1	
0.025	4.0 ± 0.5	2.0 ± 0.0	2.1 ± 0.0	3.0 ± 0.1	2.2 ± 0.5	
0.04	3.4 ± 0.2	1.7 ± 0.3	1.8 ± 0.2	2.3 ± 0.1	2.0 ± 0.7	
0.05	3.0 ± 0.4	1.6 ± 0.1	1.5 ± 0.2	2.1 ± 0.0	1.6 ± 0.4	
0.1	2.0 ± 0.5	1.0 ± 0.3	1.1 ± 0.1	1.4 ± 0.1	1.1 ± 0.3	
0.15	1.6 ± 0.1	0.8 ± 0.1	0.9 ± 0.2	1.1 ± 0.3	0.8 ± 0.2	
0.2	1.3 ± 0.2	0.7 ± 0.3	0.7 ± 0.1	1.1 ± 0.2	0.8 ± 0.0	
0.25	1.2 ± 0.1	0.6 ± 0.1	0.7 ± 0.1	0.8 ± 0.2	0.7 ± 0.2	
0.35	1.1 ± 0.5	0.5 ± 0.2	0.6 ± 0.1	0.8 ± 0.0	0.6 ± 0.2	
0.5	0.9 ± 0.3	0.4 ± 0.0	0.5 ± 0.0	0.7 ± 0.2	0.5 ± 0.1	
0.7	0.7 ± 0.2	0.4 ± 0.1	-	-	-	
0.9	0.7 ± 0.4	0.4 ± 0.0	-	-	-	
1.2	0.5 ± 0.2	0.4 ± 0.1	-	-	-	
1.4	0.5 ± 0.3	-	-	-	-	

ii. Simulated Seawater:

Table 8-2 CMC of SDS in Simulated Seawater

The ratio of seawater	CMC mM of SDS
1: 10	1.3 ± 0.0
1: 5	1.0 ± 0.3

iii. PIC Dye:

Table 8-3 CMC of SDS of PIC dye

[PIC] M	CMC mM of SDS
1×10^{-6}	6.4 ± 0.6
1×10^{-5}	6.9 ± 0.4

The result of the CMCs mM of SDS in the SHG phase is in the following tables:

i. For Deionised Water and Salts

Table 8-4 CMC of SDS in SHG For deionised water and salts

[Salt]	[Na_2CO_3] M	[Na_2SO_4] M	[NaCl] M	[HNa_2PO_3] M	$MgCl_2$ mM
0	1.2 ± 0.3	1.2 ± 0.3	1.2 ± 0.3	1.2 ± 0.3	1.2 ± 0.3
0.5	-	-	-	-	1.0 ± 0.4
0.015	1.1 ± 0.2	1.3 ± 0.3	1.2 ± 0.1	1.2 ± 0.3	-
0.025	1.1 ± 0.2	-	1.3 ± 0.4	-	-
0.04	1.0 ± 0.4	-	1.3 ± 0.3	-	-
0.05	1.1 ± 0.2	-	1.2 ± 0.3	-	-
0.1	-	-	1.2 ± 0.1	-	-
0.15	-	-	1.3 ± 0.2	-	-
0.2	-	-	1.3 ± 0.3	-	-

ii. Simulated Seawater:

Table 8-5 CMC of SDS in simulated seawater:

The ratio of seawater	CMC mM of SDS
1: 10	1.2 ± 0.1
1: 5	1.3 ± 0.3

The conclusion of the third chapter:

1. The colorimetric method, by using UV-Vis spectrophotometry, in the presence of salts, offers a good technique for measurements of CMC of SDS amphiphile within both aqueous and the SHG phases.
2. In the aqueous phase, as the salt concentration increases, the CMC values decrease.

3. In the SHG phase, no significant change in the CMC of SDS was observed.

8.3 Chapter 4

This chapter focuses on measurements of the CMC of SDS surfactant in the aqueous and SHG phase in the presence of organic compounds.

The same way used in the previous chapter was used for estimating the CMCs of SDS surfactant in the presence of 1-Alcohol (C_2, C_6 - C_{12}) with only the even number of the Carbon. It was found that the wavelength of maximum absorbance (λ_{max}) was 607 and 608 nm in the aqueous phase and in the SHG phase respectively.

The result of the CMCs mM of SDS in the aqueous phase is shown in the following tables:

i. CMC of SDS with Ethanol:

Table 8-6 CMC of SDS in ethanol

[Ethanol] M	CMC mM of SDS
0	6.7 ± 0.3
0.14	6.7 ± 0.0
0.4	6.3 ± 0.5
0.6	6.0 ± 0.4
0.9	6.0 ± 0.2
1.1	5.8 ± 0.3
1.3	7.1 ± 0.2

ii. CMC of SDS with Other Alcohols:

Table 8-7 CMC of SDS in used alcohol

[Alcohol] mM	[Hexanol] mM	[Octanol] mM	[Decanol] mM	[Dodecanol] mM
0	6.7 ± 0.3	6.7 ± 0.3	6.7 ± 0.3	6.7 ± 0.3
0.0625	6.9 ± 0.2	6.7 ± 0.2	5.6 ± 0.2	6.3 ± 0.3
0.125	6.8 ± 0.2	6.7 ± 0.3	5.6 ± 0.1	6.3 ± 0.0
0.25	6.8 ± 0.3	6.7 ± 0.3	5.7 ± 0.3	6.6 ± 0.2
0.5	6.8 ± 0.1	6.0 ± 0.1	5.9 ± 0.0	6.7 ± 0.2
1	6.3 ± 0.2	5.5 ± 0.3	6.1 ± 0.2	6.8 ± 0.0

The result of the CMCs mM of SDS in the SHG phase is shown in the following table:

Table 8-8 CMC of SDS with alcohol in the SHG phase

[Alcohol]	[Ethanol] M	[Hexanol] mM	[Octanol] mM	[Decanol] mM	[Dodecanol] mM
0	-	1.2 ± 0.3	1.2 ± 0.3	1.2 ± 0.3	1.2 ± 0.3
0.0625	-	1.2 ± 0.3	1.3 ± 0.2	1.2 ± 0.3	1.3 ± 0.1
0.125	-	1.1 ± 0.1	1.2 ± 0.2	1.4 ± 0.2	1.3 ± 0.3
0.25	-	1.2 ± 0.1	1.3 ± 0.3	1.3 ± 0.2	-
0.4	1.2 ± 0.3	-	-	-	-
0.5	-	1.1 ± 0.4	1.3 ± 0.2	-	-
1	-	1.1 ± 0.3	1.4 ± 0.5	-	-
1.1	1.4 ± 0.2	-	-	-	-

The conclusion of the fourth chapter:

1. The colorimetric method, by using UV-Vis spectrophotometry, in the presence of alcohol offers a good technique for measurements of CMC of SDS amphiphile within both aqueous and the SHG phases.
2. In the aqueous phase, the CMC of SDS in the presence of hexanol and octanol follow the role of adding alcohol compound; as the concentration and the length of the chain increase, the CMC values decrease. In the case of decanol and dodecanol, only lower concentration follow the role because of the lack of solubility.
3. In the SHG phase, no significant change in the CMC of SDS was observed.

8.4 Chapter 5

This section focuses on the visualising the self-assembly between fatty alcohol (decanol and dodecanol), with a low concentration in the presence and absence of salt (sodium carbonate) in the aqueous and SHG phase by using two types of fluorescent microscopy with Nile red as a probe including epifluorescent microscopy and confocal fluorescent microscopy.

In this chapter, SDS is mixed with fatty alcohol to see if there is any vesicle formation or not, that was obtained by changing some conditions of the used procedure (sonicator, adding salt).

The images obtained by epifluorescence microscopy of SDS with decanol and dodecanol indicated the formation of some structures like oil droplets or vesicles in the aqueous phase and crystals in the SHG phase. However, the images obtained by confocal microscopy of SDS with decanol also revealed oil droplet structures in both phases.

To sum up, for the morphology structure, looking for vesicle formation, the images have been visualised under the impact of the mixing method, and added alcohols of SDS and with/without salt.

To summarise, we have performed a preliminary examination of the self-assembly of SDS-long chain alcohols in both the aqueous salt phase and silica hydrogel phase, also salt-rich. Our initial studies using epifluorescence microscopy led to only limited success as the technique does not allow much depth control nor structural resolution. However, confocal microscopy has provided us some more informative images. In terms of summarising the key points from this chapter, we can make the following points concerning structures visualised from mixtures of SDS-decanol in the presence of Na_2CO_3 salts in both aqueous and silica hydrogel media:

i. The images obtained using epifluorescence are not clear enough to see the structures that were formed.
ii. Confocal microscopy images revealed what appear to be the formation of oil droplets and vesicles with different concentrations that are much smaller than the CMCs of SDS/alcohol mixtures in the previous chapter.
iii. SDS-decanol mixtures of 1.0 mM SDS, 0.04 mM decanol in aqueous phase, in the absence of salt, appeared to show LUV (ca 2 µm), MVV (ca 2 µm), and oil droplet, and in the presence of salt (0.06 M Na_2CO_3) appeared to show oil droplet,
iv. SDS-decanol mixtures of 1.0 mM SDS, 0.04 mM decanol in SHG phase in the absence of salt appeared to show GUV (ca 10 µm), MVV (ca 5 µm) and oil droplet, and in the presence of salt (0.06 M Na_2CO_3) appeared to show oil droplet.

8.5 Chapter 6

The gelation time of different concentrations of SHG in the presence of different concentrations of SDS, and 0.5 M SHG in the presence of salts was estimated by light scattering methods (UV/Vis spectrophotometry, turbidity meter).

By using UV-VIS spectrophotometry, the attenuation of light intensity by silica hydrogel was determined. The detector in this device recorded the transmitted light through the sample. Thus transmitted light is related directly to isotropic scattering effects. To monitor light scattering changes along the gelation process,

the process was monitored by recording scans of the entire spectra (the baseline shifted in the kinetics scan from 400 to 800 nm and analysing by Origin. The 400, 500, and 600 nm (at which no silica absorb) wavelengths were chosen to follow the kinetics studies after baseline correction. Then, the first derivative was applied to intensity vs. time reaching zero, which is a point at which no further change is observed.

0.5, 0.7, and 0.9 M SHG were examined at four different concentrations of SDS (0.3, 10.0, 18.0 mM). The spectra obtained from the mentioned concentrations were featureless showing only a general rise in apparent absorbance rise during data acquirement due to light scattering for suspended particulates as the gel formed. A slow rise in absorption was observed at the early stage of 0.5 M SHG, whereas a quick rise was noticed with both 0.7 and 0.9 M SHG. Then, the absorption of all of them, at the final stage became almost steady which means that there was no significant change in spectra. The light scattering has a strong influence on the shorter wavelength (400 nm) compared to the longer wavelength (600 nm) with all concentrations depending on the light scattering theory.

Then, the light scattering was plotted as a function of time at the fixed wavelength (400, 500, and 600 nm) to help determine the gelation time more clearly by using the first derivatives.

The results obtained by this method indicated that the gelation time decreased as the concentration of sodium silicate increased; the gelation time for 0.5, 0.7, and 0.9 M were 447, 87, and 55 min, respectively. However, the presence of SDS in all of the used concentrations did not show any significant change in the gelation time.

0.5 M SHG with different concentrations of (i) 0.1 M NaCl, (ii) 0.2 M NaCl, and (iii) 0.1 M Na_2CO_3 were examined to determine their effects on the silica gelation time by using the same procedure in previous experiments (UV-Vis light scattering). The figures indicated the transition behaviour from sol to gel phase with increasing absorbance. Similarly with 0.5 M SHG, for all concentrations of salts in 0.5 M SHG, the light scattering has a strong influence on the shorter wavelength (400 nm light scattering). A quick rise in absorption is observed at the early stage in the presence of sodium carbonate, compared to sodium chloride with both concentrations. Then, the absorption at the final stage became almost steady. Then, the gradient of the scatter vs. time at the fixed wavelength of 400,

500, and 600 nm was plotted to allow determine the gelation time clearly by obtaining the first derivatives. The results show that the gelation process of 0.1 M Na_2CO_3 happened faster than others. The gelation time was 345 min for both concentrations of sodium chloride, and 185 min for sodium carbonate. These experiments demonstrate a relationship between gelation time and the salts concentration, namely that gelation time decreases with the increase of salts concentration.

The other method to estimate the gelation time was using the turbidity meter to monitor the turbidity for 0.5 M SHG in the presence of salts, following the same procedure to form 0.5 M SHG with 16 mL, including salts. The measuring of gelation time started after mixing the silicate solution with GAA solution immediately, then, the first reading with the time of zero was recorded, and finally data were collected every 10 min for 900 min. This method plots the rate of change of the light scatting versus time then the first derivative was applied.

0.5 M SHG in the absence and presence of salts, including 0.5 M SHG, 0.5 M SHG/0.1 M NaCl, 0.5 M SHG/0.2 M NaCl, 0.5 M SHG/0.1M Na_2CO_3, were examined. The change in the turbidity as gelation continued, particularly with adding sodium carbonate, which had rapidly changed the turbidity, whereas 0.5 M with/without sodium chloride have slight changes.

Overall, this section can be concluded by:

1. By using UV/Vis spectrophotometry with kinetic mode, at all the selected wavelength:
    a. The gelation time decreases as the content of silicate increases.
    b. No significant change in the presence of different concentration of SDS.
    c. Adding monovalent salts can affect the gelation time.

2. Turbidimetry experiments also show that light scattering can be influenced by this salt presence, and more significant change in the case of sodium carbonate.

8.6 Future Works

As indicated in the aims and objectives section of this thesis, certain fundamental aspects of molecular behaviour in both the aqueous and silica hydrogel phases

have been examined here, principally involving single-chain amphiphiles. The hydrogel phase could have been a very important environmental condition in terms of the emergence of biological cells because the aqueous-based environment (the cytoplasm) of a biological cell is better designated as a hydrogel. Therefore, in order to more closely align our work with questions in this field, molecular behaviours of self-assembly of sodium dodecyl sulphate as a representative (but not necessarily prebiotically available) amphiphile SDS in the presence of organic and inorganic materials was examined. The results obtained revealed differences in self-assembly behaviour in gel-phase media from those conducted in purely aqueous media. Silica hydrogels (SHGs) in this project showed their ability to maintain the critical micelle concentration in the presence of salt and some of the long chains of alcohol, which is expected to be important from the perspective of abiogenesis.

Some investigation questions need to be answered in this project, which could be followed in greater detail for possibly another project. Some of these questions are collected below:

Question 1. Is it possible to change the CMC of the SHG?

The CMC of SDS depends on the SHG concentration, which was confirmed by this work in the presence of different materials. The presence of too many salts can destroy the vesicle structure. One could try lowering concentrations of the SHGs and examine the vesicle formation (because it is formed below the CMC) by using fluorescent microscopy.

Question 2. Is it possible to form a vesicle structure using SDS and a long chain alcohol?

Most of the images obtained from confocal fluorescent microscopy revealed the formation of oil droplets because of the high concentration of used alcohol. One could try lower concentrations on a μM scale [90] and examine different ratios of both.

Question 3. Is it possible to visualise vesicles in the SHG environment by another method?

Fluorescent microscopy depends on the stain of the sample by the fluorescent compound. It was suggested that examination of the vesicle formation within SHG environments can use cryo-TEM [259, 260], for which the stain of the sample is

not required. TEM is considered the most used approach to determine the morphology and the size of the vesicle formation. This method uses electrons that transmit through the vesicle, which can form 2D images. TEM images are based on the power of an electron beam that can provide inner structure information about the structure [261].

Question 4. Is the gelation time influenced by the natural pH of used salt?

Adding monovalent salts did not show significant change in the gelation time by using turbidity meter. However, there is a change on the gelation time in the case of sodium carbonate which could be due to the presence of two atoms in the structure of carbonate or high pH. One can use phosphate (high pH), and sulphate (natural pH) to compare.

Question 5. Is the micellar structure in the 0.5 M SHG effected by the increasing SDS concentration?

The micelle formation was examined in the 0.5 M SHG by the colorimetric method using PIC as a probe with a series of different concentrations of SDS, with the highest concentrations of SDS being at 24 mM. However, in the case of increasing the SDS concentration, can the SHGs maintain the micellar structure? Is there a limited concentration of SDS to keep the micellar formation?

Chapter 9 Appendix

9.1 Chapter 3

9.1.1 Spectrophotometric Investigation of the Critical Micelle Concentration (CMC) of Sodium Dodecyl Sulphate (SDS) in Aqueous Phase

9.1.1.1 In the Presence of Sodium Silicate Solution

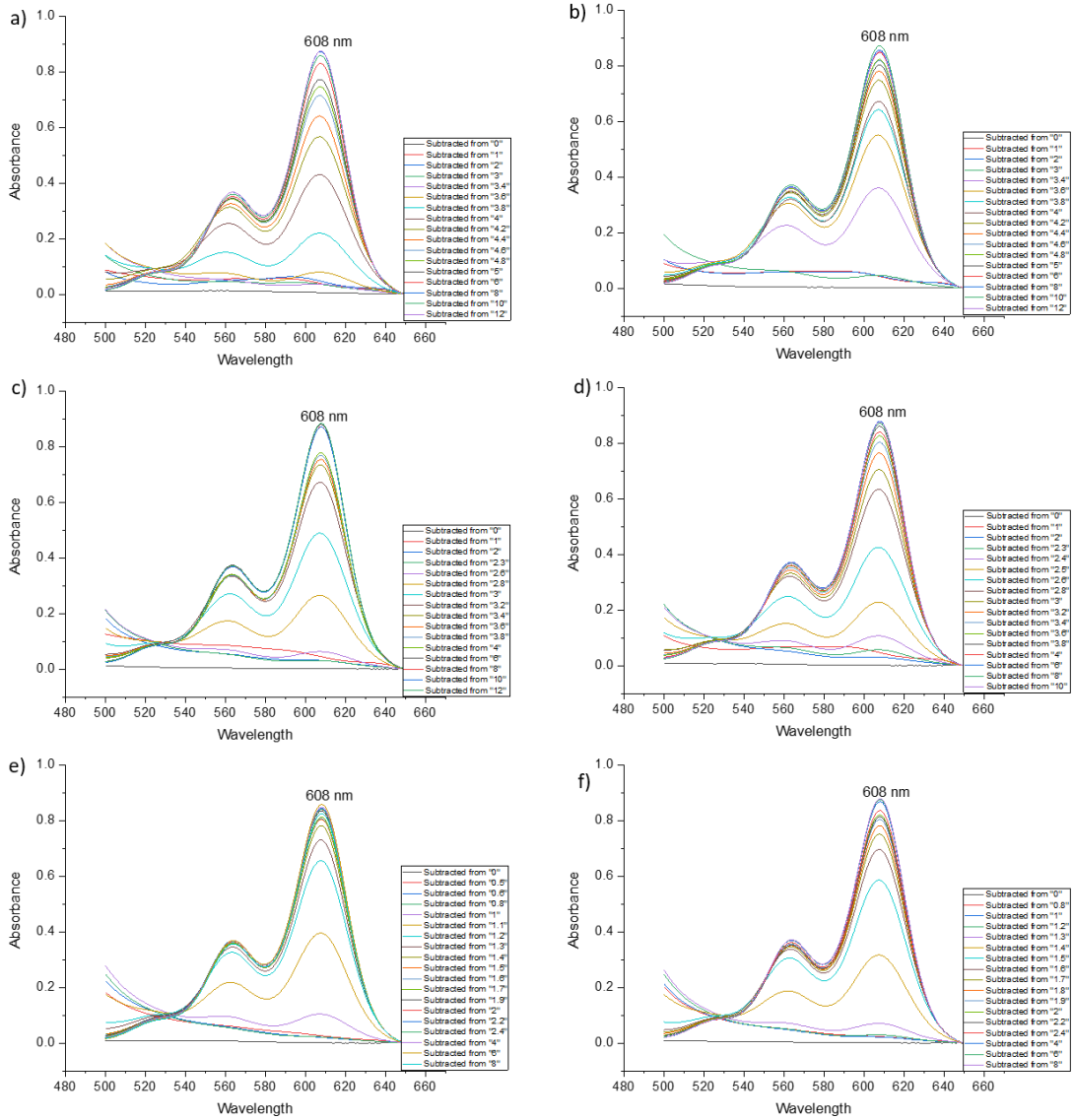

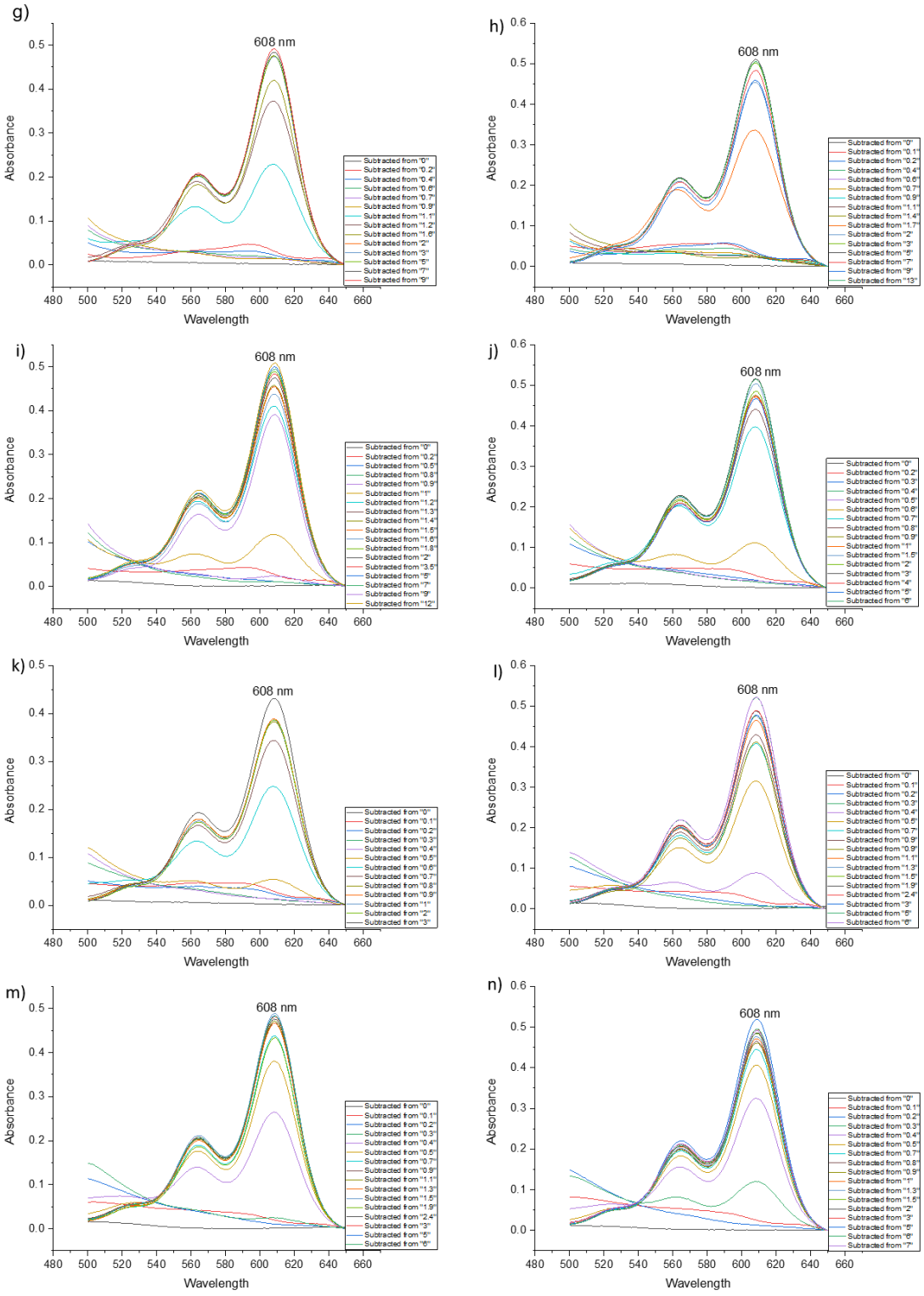

Figure 9-1: Determination of the (λmax) of pinacyanol chloride silicate solution in the presence of a range of SDS concentrations: a) 0.015 M, b) 0.025 M, c) 0.04 M, d) 0.05 M, e) 0.1 M, f) 0.15 M, g) 0.2 M, h) 0.25 M, i) 0.35 M, j) 0.5 M, k) 0.7 M, l) 0.9 M, m) 1.2 M, n) 1.4 M of sodium silicate solutions.

9.1.1.2 In the Presence of Sodium Carbonate Solution

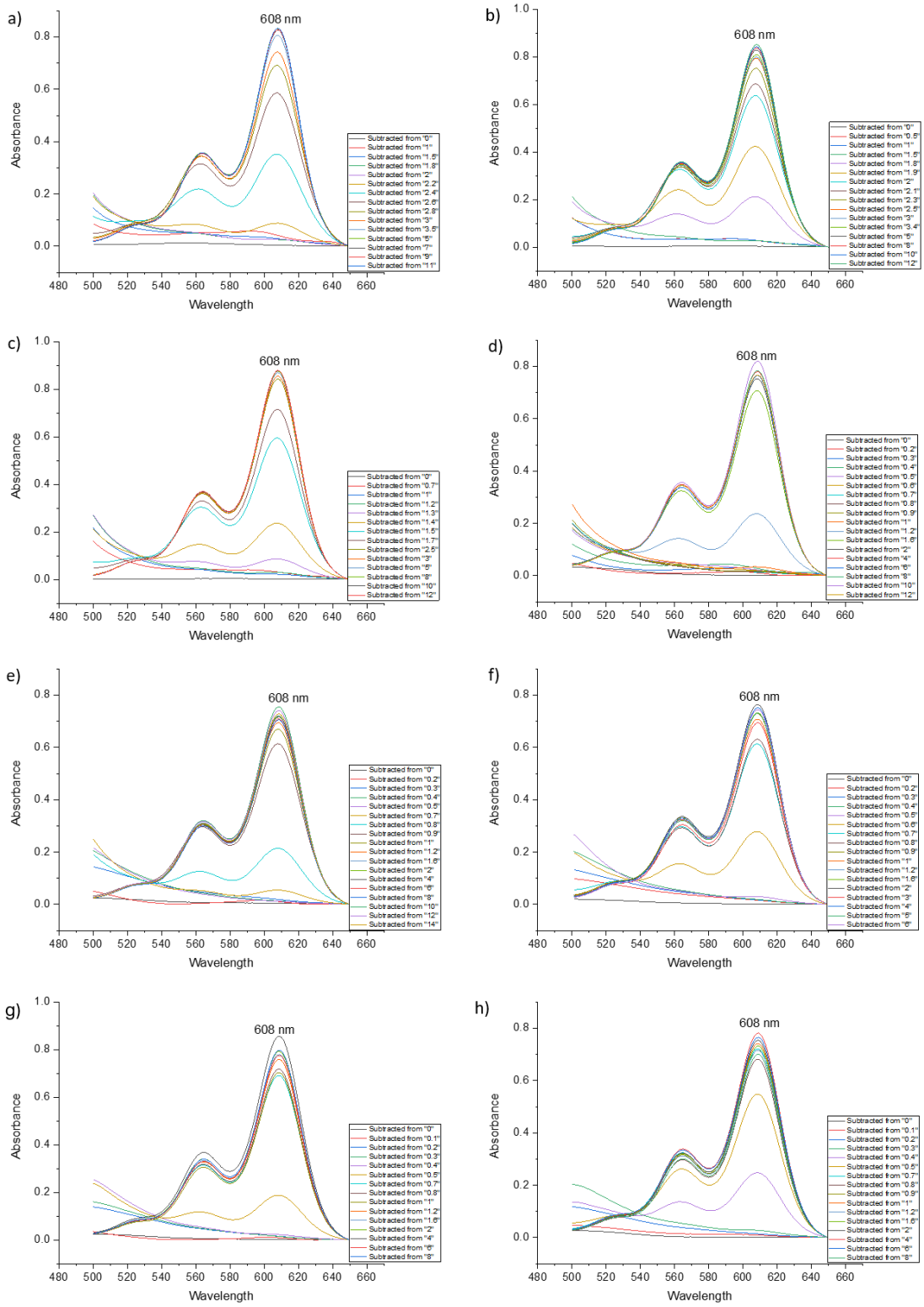

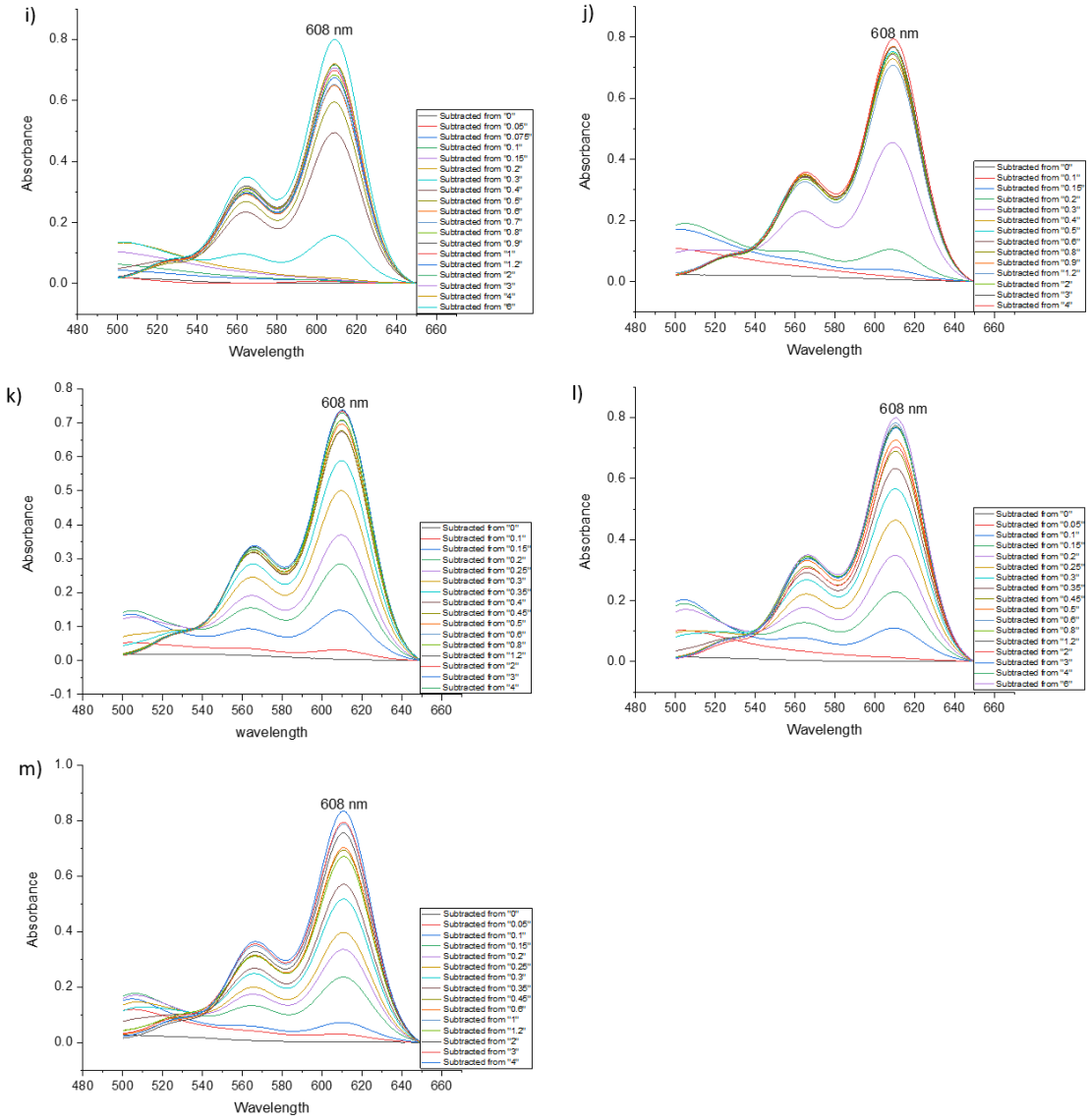

Figure 9-2: Determination of the (λ_{max}) of pinacyanol chloride in the presence of a range of SDS concentrations: a) 0.015 M, b) 0.025 M, c) 0.04 M, d) 0.05 M, e) 0.1 M, f) 0.15 M, g) 0.2 M, h) 0.25 M, i) 0.35 M, j) 0.5 M, k) 0.7 M, l) 0.9 M, and m) 1.2 M of sodium carbonate solutions

9.1.1.3 In the Presence of Sodium Sulphate Solution

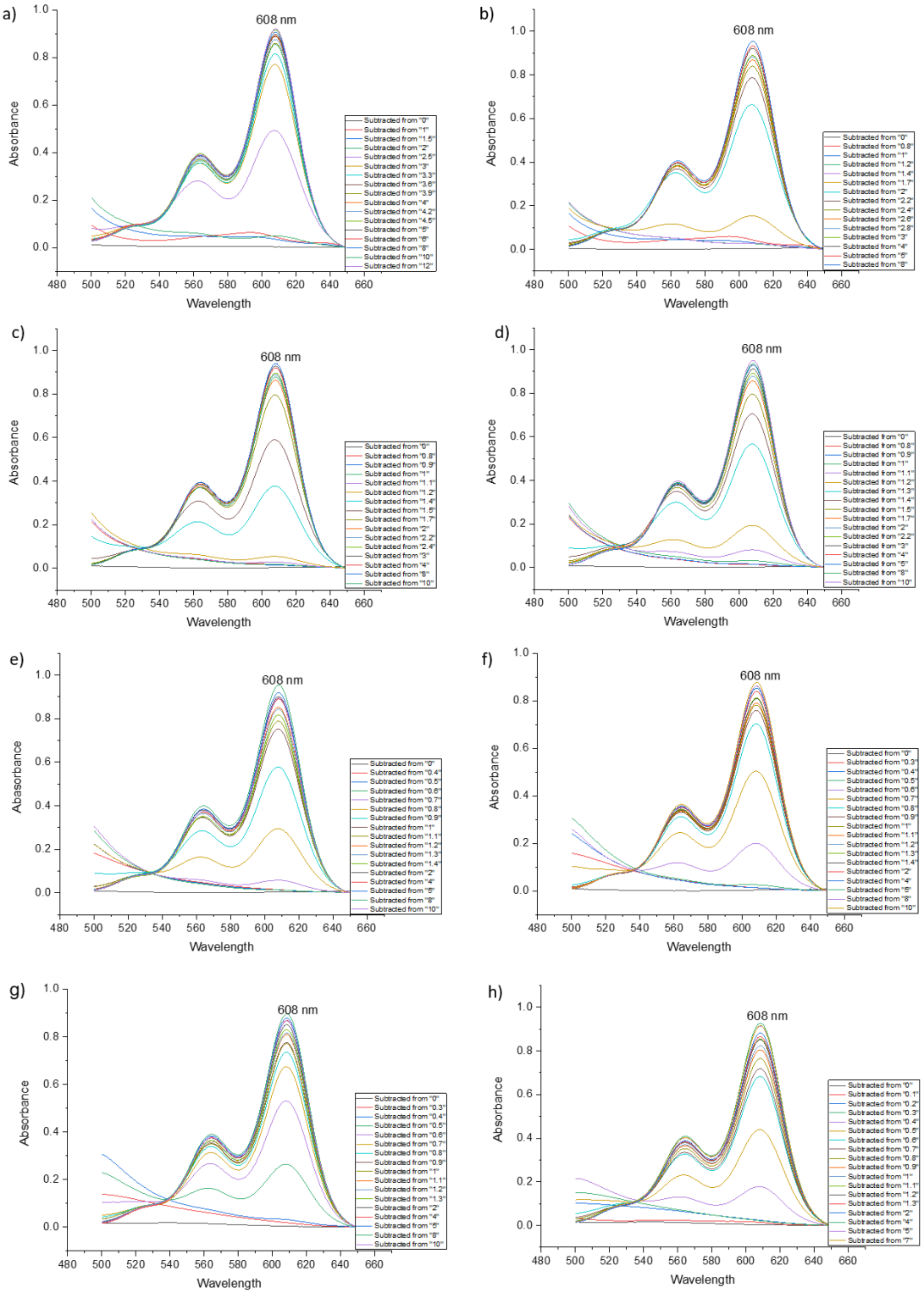

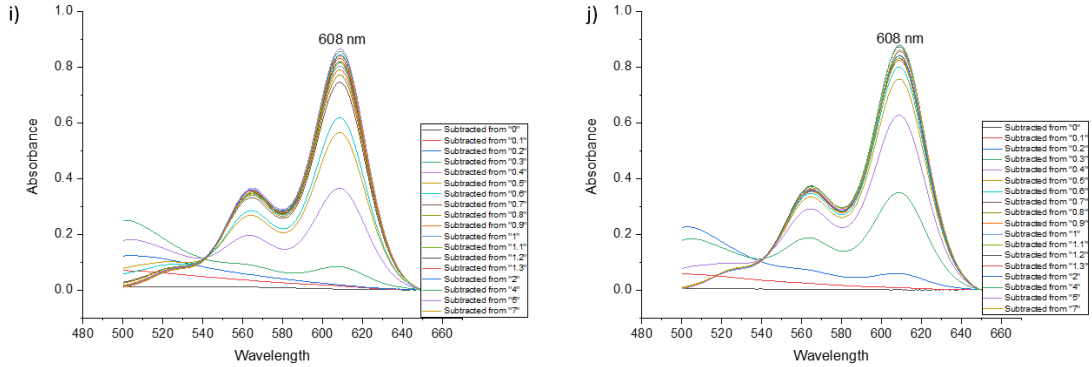

Figure 9-3: Determination of the (λ_{max}) of pinacyanol chloride in the presence of a range of SDS concentrations: a) 0.015 M, b) 0.025 M, c) 0.04 M, d) 0.05 M, e) 0.1 M, f) 0.15 M, g) 0.2 M, h) 0.25 M, i) 0.35 M, j) 0.5 M of sulphate solutions.

9.1.1.4 In the Presence of Sodium Chloride Solution

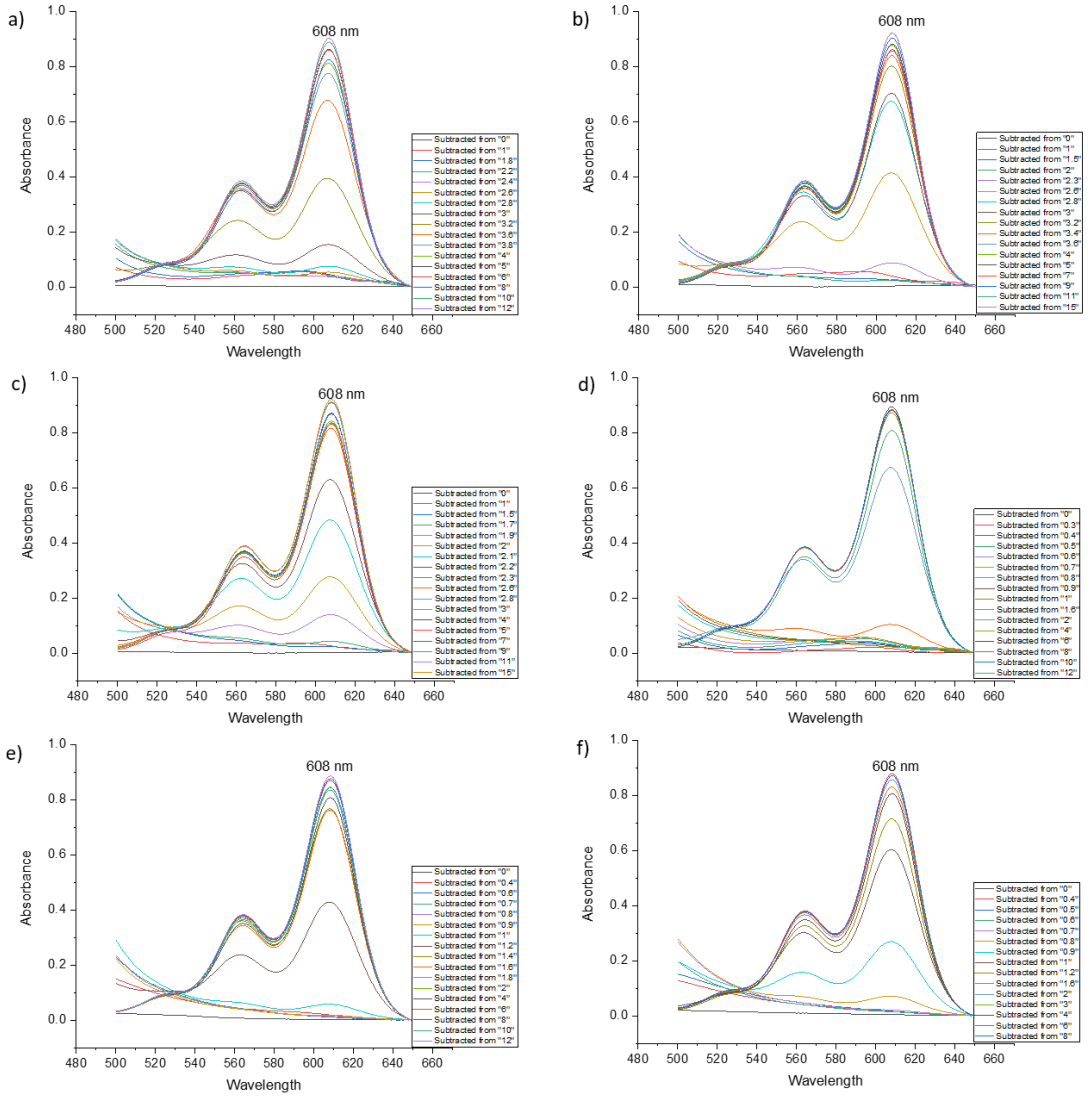

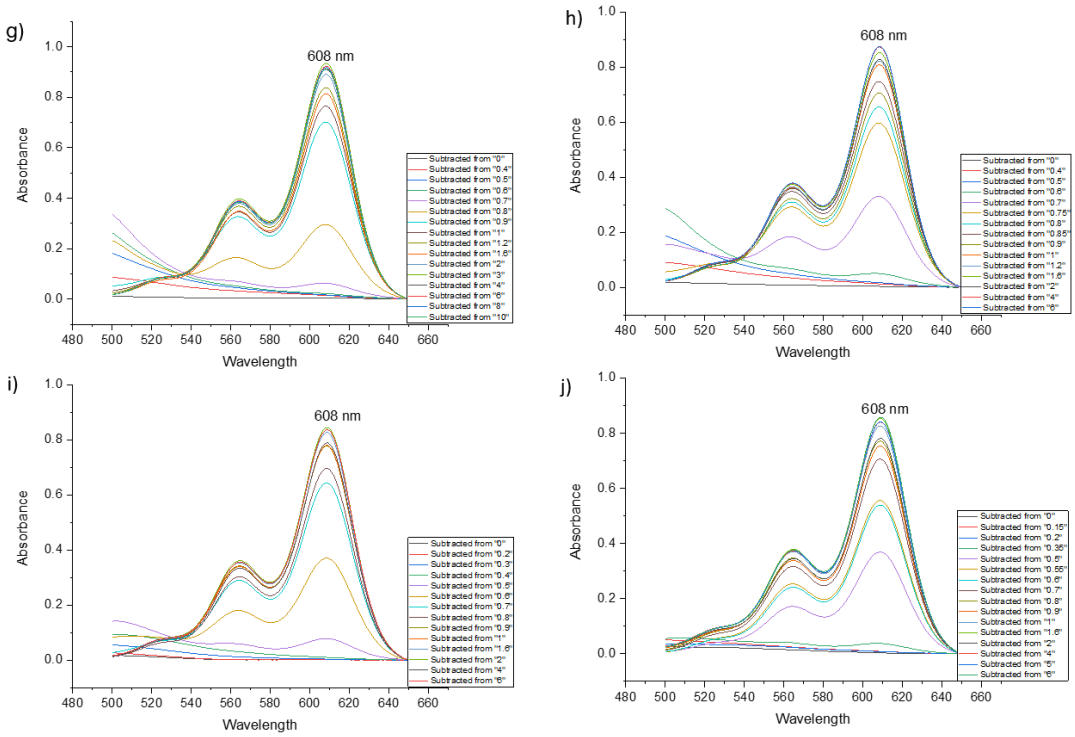

Figure 9-4: Determination of the (λ_{max}) of pinacyanol chloride in the presence of a range of SDS concentrations: a) 0.015 M, b) 0.025 M, c) 0.04 M, d) 0.05 M, e) 0.1 M, f) 0.15 M, g) 0.2 M, h) 0.25 M, i) 0.35 M, j) 0.5 M of sodium chloride solutions.

9.1.1.5 In the Presence of Sodium Phosphate Solution

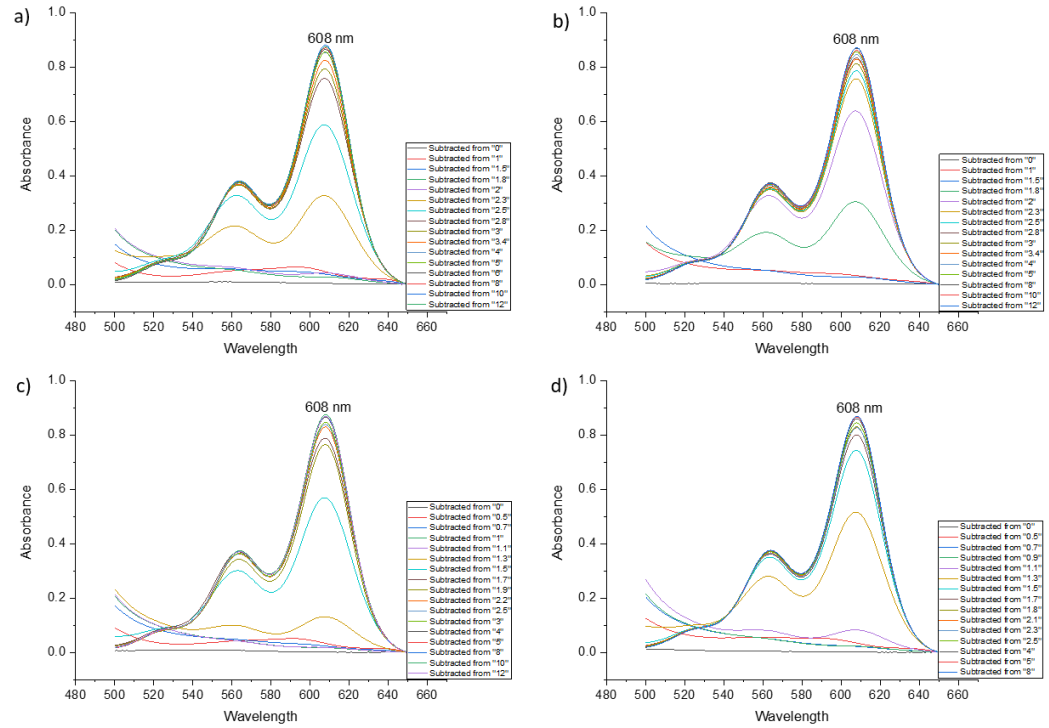

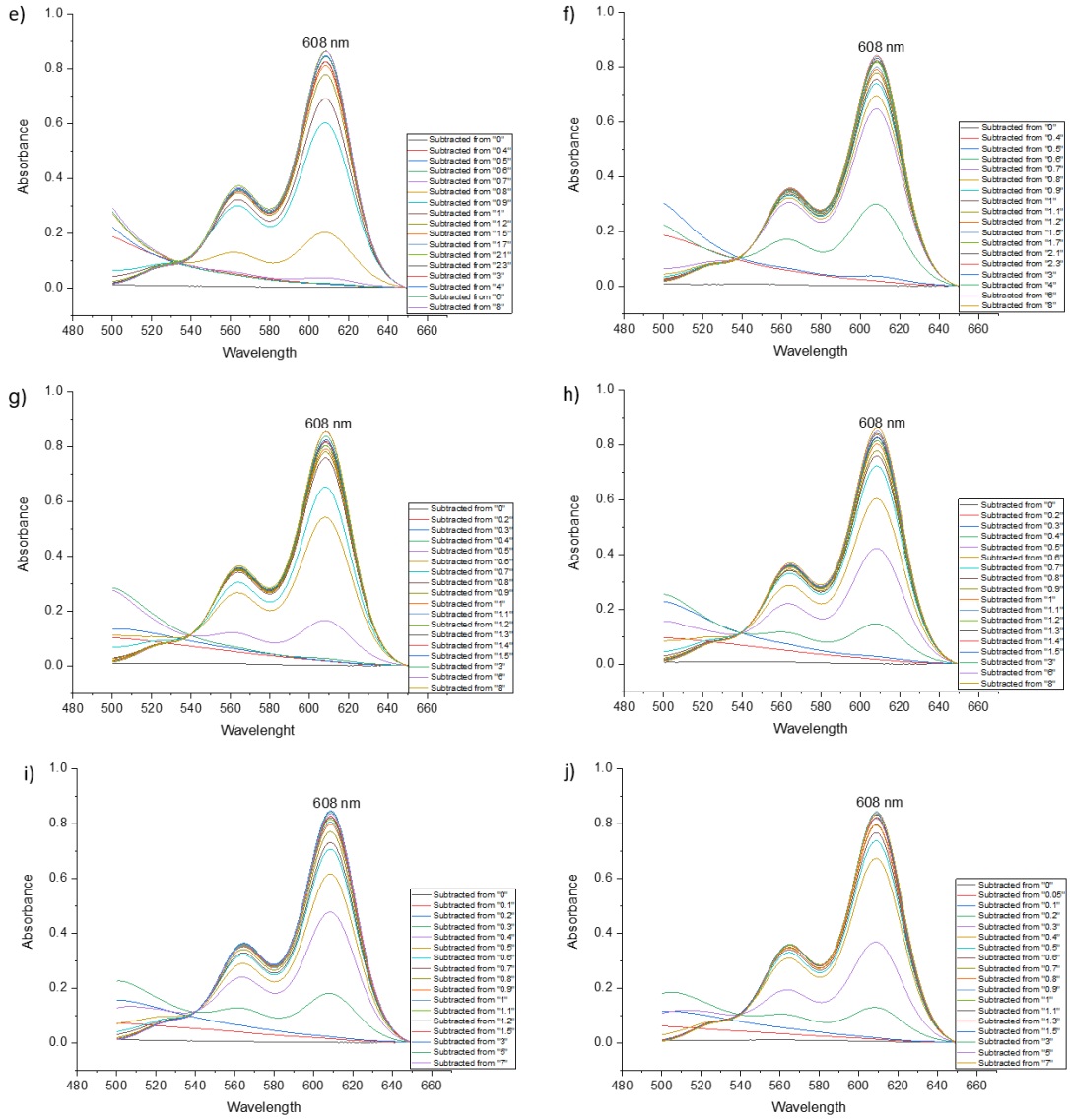

Figure 9-5: Determination of the (λ_{max}) of pinacyanol chloride in the presence of a range of SDS concentrations: a) 0.015 M, b) 0.025 M, c) 0.04 M, d) 0.05 M, e) 0.1 M, f) 0.15 M, g) 0.2 M, h) 0.25 M, i) 0.35 M, j) 0.5 M of disodium phosphate solutions.

9.1.1.6 In the Presence of Magnesium Chloride Solution

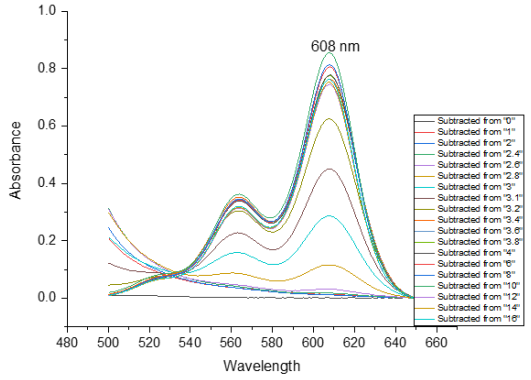

Figure 9-6: Determination of the (λ_{max}) of pinacyanol chloride in the presence of a range of SDS concentrations in 0.5 mM of magnesium chloride solutions.

9.1.1.7 In the Presence of Seawater Solution

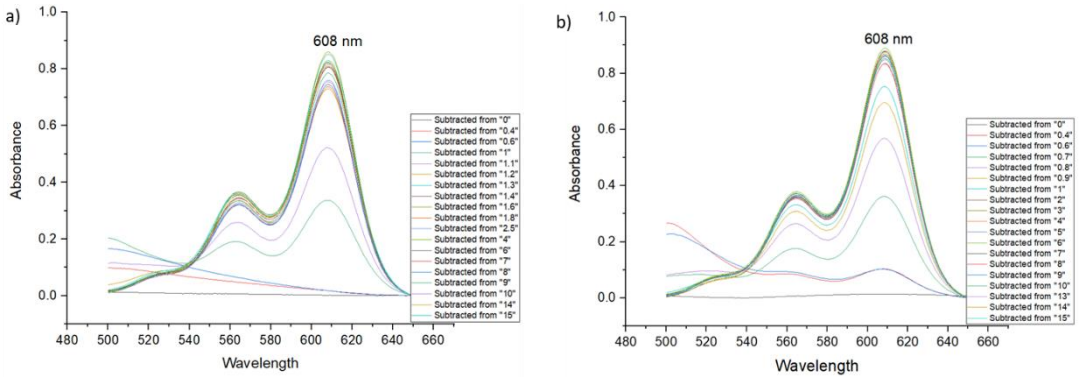

Figure 9-7: Determination of the (λ_{max}) of pinacyanol chloride in the presence of a range of SDS concentrations in seawater with a)1:10, and b) 1:5 in total volume of 8000 µL.

9.1.1.8 In the Presence Different Concentrations of PIC Dye

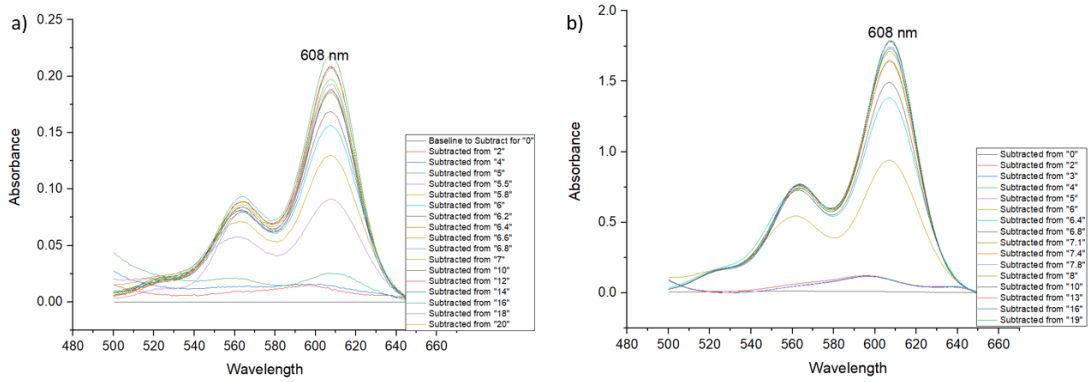

Figure 9-8: Determination of the (λ_{max}) of pinacyanol chloride with conc. a) 1×10^{-6} M, b) 1×10^{-5} M in the presence of a range of SDS concentrations.

9.1.2 Spectrophotometric investigation of the critical micelle concentration (CMC) of sodium dodecyl sulphate (SDS) with Salts in SHG Phase

9.1.2.1 In the 0.5 M SHG

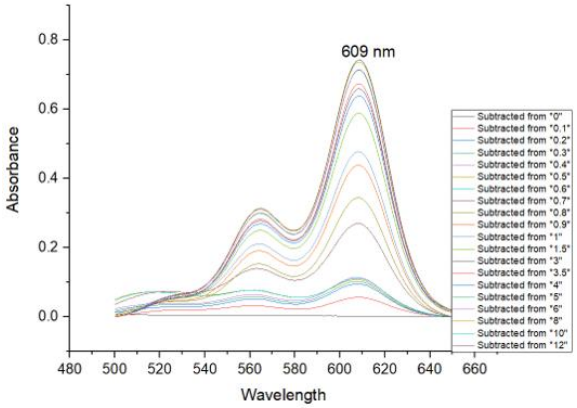

Figure 9-9: Determination of the (λ_{max}) of pinacyanol chloride in the presence of a range of SDS concentrations in 0.5 M SHG with total volume of 8000 µL.

9.1.2.2 In the Presence of Sodium Carbonate Salts

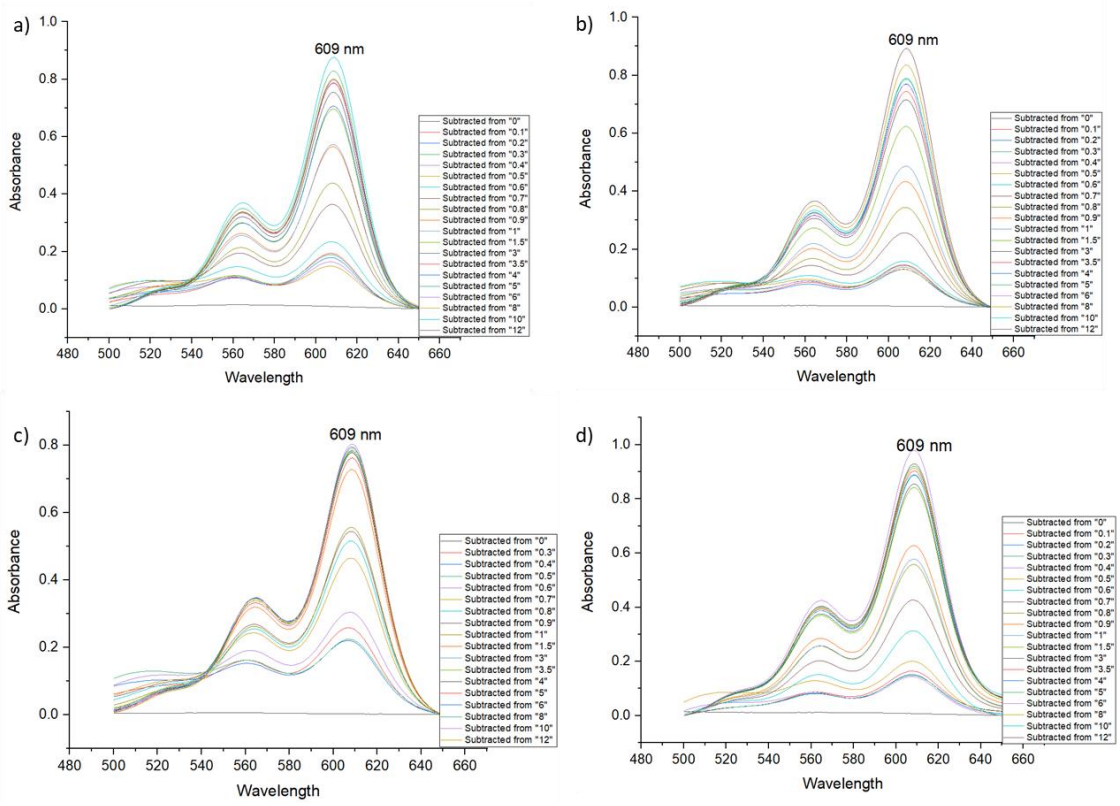

Figure 9-10: Determination of the (λ_{max}) of pinacyanol chloride in the presence of a range of SDS concentrations: a) 0.015 M, b) 0.025 M, c) 0.04 M, d) 0.05 M of sodium carbonate solutions.

9.1.2.3 In the Presence of Sodium Sulphate

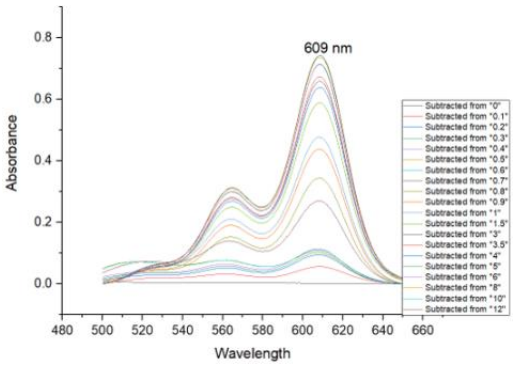

Figure 9-11: Determination of the (λ_{max}) of pinacyanol chloride in the presence of a range of SDS concentrations 0.015 M sodium sulfate solutions.

9.1.2.4 In the Presence of Sodium Chloride

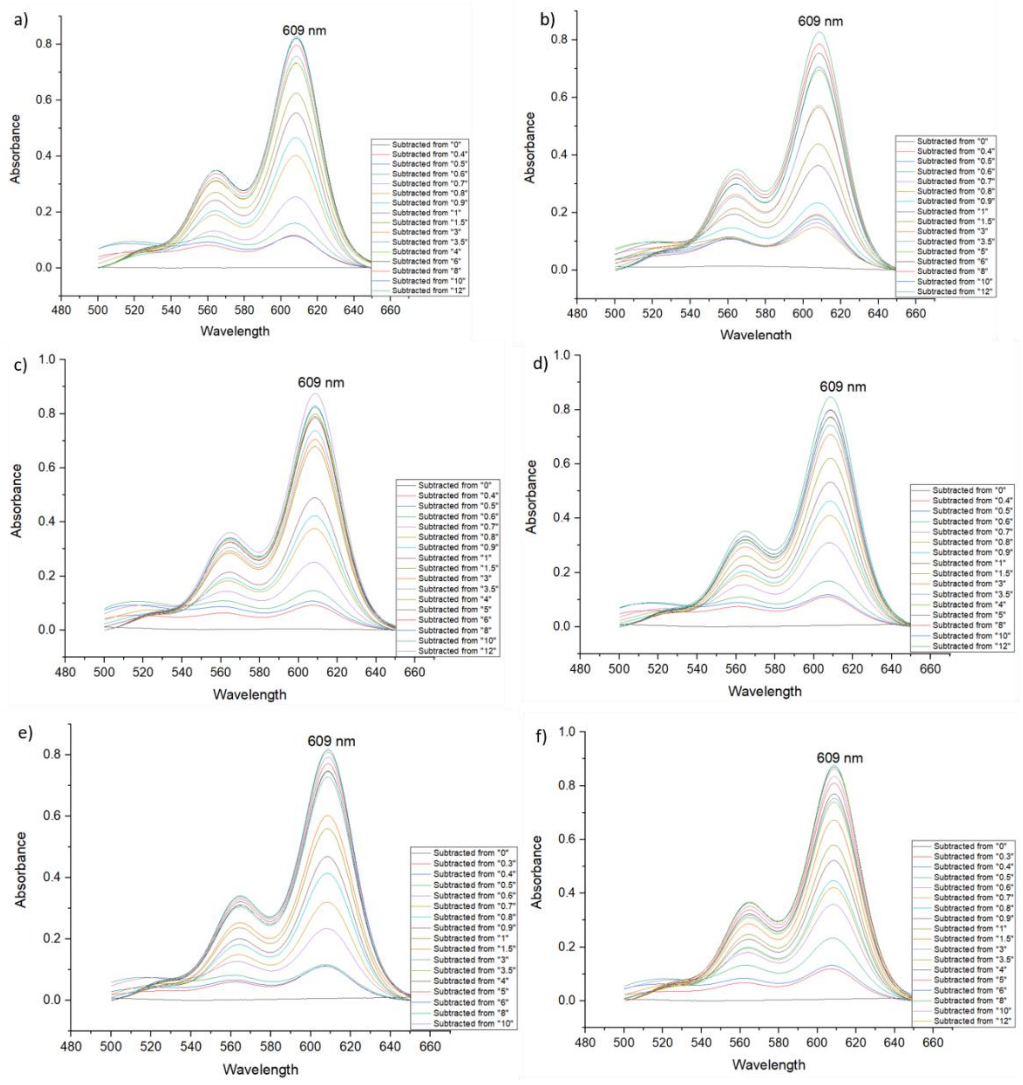

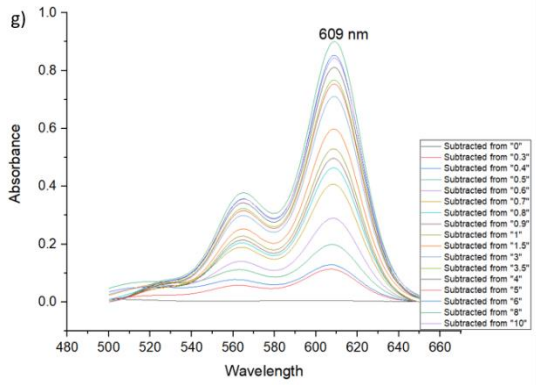

Figure 9-12: Determination of the (λ_{max}) of pinacyanol chloride in the presence of a range of SDS concentrations: a) 0.015 M, b) 0.025 M, c) 0.04 M, d) 0.05 M, e) 0.1 M, f) 0.1 M, g) 0.1 M of sodium chloride solutions.

9.1.2.5 In the Presence of Disodium Phosphates

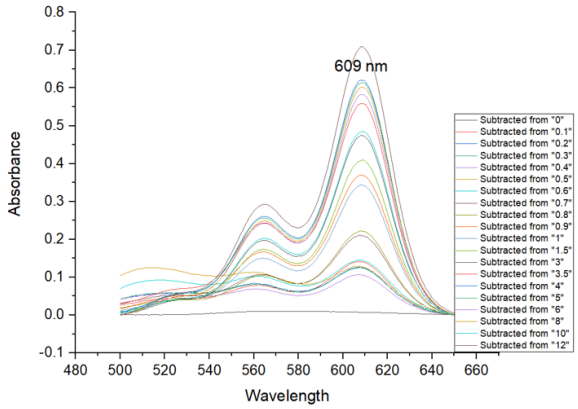

Figure 9-13: Determination of the (λ_{max}) of pinacyanol chloride in the presence of a range of SDS concentrations in 0.015 M, disodium phosphate solutions.

9.1.2.6 In the Presence of Magnesium Chloride

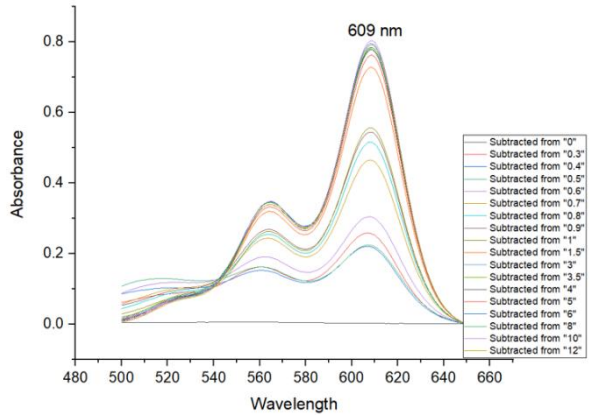

Figure 9-14: Determination of the (λ_{max}) of pinacyanol chloride in the presence of a range of SDS concentrations in magnesium chloride a)1:10, and b) 1:5 in total volume of 8000 µL.

9.1.2.7 In the Presence of simulated seawater

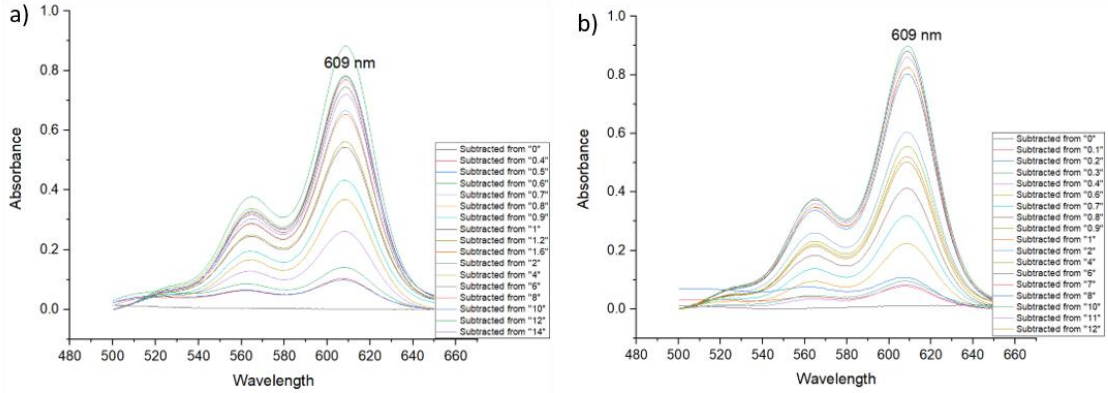

Figure 9-15: Determination of the (λ_{max}) of pinacyanol chloride in the presence of a range of SDS concentrations in seawater with a)1:10, and b) 1:5 in total volume of 8000 µL.

9.1.3 Fitting Equations for CMC Measurements of all Media in the Presence of Salts (Left cell represent vertical fitted line, right cell represent horizontal fitted line) for each Concentration.

1. Deionized Water

Equation	y = a + b*x
Plot	B
Weight	Instrumental (=1/ei^2)
Intercept	-4.93104 ± 0.54195
Slope	0.94263 ± 0.09575
Residual Sum of Squares	44.30363
Pearson's r	0.99488
R-Square (COD)	0.98979
Adj. R-Square	0.97958

Equation	y = a + b*x
Plot	B
Weight	Instrumental (=1/ei^2)
Intercept	0.99601 ± 0.00994
Slope	9.71183E-5 ± 6.61132E-4
Residual Sum of Squares	0.13002
Pearson's r	0.10332
R-Square (COD)	0.01067
Adj. R-Square	-0.48399

2. 0.015 M Sodium Silicate

Equation	y = a + b*x
Plot	B
Weight	Instrumental (=1/ei^2)
Intercept	-2.82812 ± 0.36957
Slope	0.80672 ± 0.10052
Residual Sum of Squares	0.65043
Pearson's r	0.99233
R-Square (COD)	0.98471
Adj. R-Square	0.96942

Equation	y = a + b*x
Plot	B
Weight	Instrumental (=1/ei^2)
Intercept	0.83591 ± 0.04104
Slope	0.00287 ± 0.00409
Residual Sum of Squares	11.41881
Pearson's r	0.44479
R-Square (COD)	0.19784
Adj. R-Square	-0.20324

3. 0.025 M Sodium Silicate

Equation	y = a + b*x
Plot	B
Weight	Instrumental (=1/ei^2)
Intercept	-2.41942 ± 0.07804
Slope	0.8219 ± 0.02591
Residual Sum of Squares	0.09834
Pearson's r	0.9995
R-Square (COD)	0.99901
Adj. R-Square	0.99801

Equation	y = a + b*x
Plot	B
Weight	Instrumental (=1/ei^2)
Intercept	0.84751 ± 0.02274
Slope	8.92774E-4 ± 0.00241
Residual Sum of Squares	1.53298
Pearson's r	0.25325
R-Square (COD)	0.06414
Adj. R-Square	-0.40379

4. 0.04 M Sodium Silicate

Equation	y = a + b*x
Plot	B
Weight	Instrumental (=1/ei^2)
Intercept	-2.6542 ± 0.0647
Slope	1.04509 ± 0.02483
Residual Sum of Squares	0.05352
Pearson's r	0.99972
R-Square (COD)	0.99944
Adj. R-Square	0.99887

Equation	y = a + b*x
Plot	B
Weight	Instrumental (=1/ei^2)
Intercept	0.85858 ± 0.01168
Slope	0.00209 ± 0.00107
Residual Sum of Squares	0.29189
Pearson's r	0.8115
R-Square (COD)	0.65853
Adj. R-Square	0.4878

5. 0.05 M Sodium Silicate

Equation	y = a + b*x
Plot	B
Weight	Instrumental (=1/ei^2)
Intercept	-3.02039 ± 0.50282
Slope	1.29677 ± 0.20734
Residual Sum of Squares	0.19263
Pearson's r	0.98746
R-Square (COD)	0.97507
Adj. R-Square	0.95015

Equation	y = a + b*x
Plot	B
Weight	Instrumental (=1/ei^2)
Intercept	0.82376 ± 0.00762
Slope	0.0056 ± 0.00128
Residual Sum of Squares	0.29176
Pearson's r	0.92997
R-Square (COD)	0.86484
Adj. R-Square	0.81979

6. 0.1 M Sodium Silicate

Equation	y = a + b*x
Plot	B
Weight	Instrumental (=1/ei^2)
Intercept	-0.99355 ± 0.09709
Slope	0.72739 ± 0.06399
Residual Sum of Squares	23.2924
Pearson's r	0.99615
R-Square (COD)	0.99232
Adj. R-Square	0.98464

Equation	y = a + b*x
Plot	B
Weight	Instrumental (=1/ei^2)
Intercept	0.5086 ± 0.01168
Slope	-0.00192 ± 0.0023
Residual Sum of Squares	1.92747
Pearson's r	-0.43397
R-Square (COD)	0.18833
Adj. R-Square	-0.08222

7. 0.15 M Sodium Silicate

Equation	y = a + b*x
Plot	B
Weight	Instrumental (=1/ei^2)
Intercept	-3.22412 ± 0.07616
Slope	2.53447 ± 0.05809
Residual Sum of Squares	0.08464
Pearson's r	0.99974
R-Square (COD)	0.99947
Adj. R-Square	0.99895

Equation	y = a + b*x
Plot	B
Weight	Instrumental (=1/ei^2)
Intercept	0.85356 ± 0.00818
Slope	0.00345 ± 0.00139
Residual Sum of Squares	2.61684
Pearson's r	0.86816
R-Square (COD)	0.75371
Adj. R-Square	0.63057

8. 0.2 M Sodium Silicate

Equation	y = a + b*x
Plot	B
Weight	Instrumental (=1/ei^2)
Intercept	-0.98587 ± 0.05293
Slope	1.11191 ± 0.05823
Residual Sum of Squares	0.85625
Pearson's r	0.99863
R-Square (COD)	0.99726
Adj. R-Square	0.99453

Equation	y = a + b*x
Plot	B
Weight	Instrumental (=1/ei^2)
Intercept	0.467 ± 0.00252
Slope	0.00234 ± 5.74502E-4
Residual Sum of Squares	0.08146
Pearson's r	0.92021
R-Square (COD)	0.84678
Adj. R-Square	0.79571

9. 0.25 M Sodium silicate

Equation	y = a + b*x
Plot	B
Weight	Instrumental (=1/ei^2)
Intercept	-2.78309 ± 0.07434
Slope	2.88812 ± 0.06979
Residual Sum of Squares	0.34267
Pearson's r	0.99971
R-Square (COD)	0.99942
Adj. R-Square	0.99883

Equation	y = a + b*x
Plot	B
Weight	Instrumental (=1/ei^2)
Intercept	0.83457 ± 0.00939
Slope	0.00352 ± 0.00193
Residual Sum of Squares	0.71018
Pearson's r	0.72532
R-Square (COD)	0.52608
Adj. R-Square	0.36811

10. 0.35 M Sodium Silicate

Equation	y = a + b*x
Plot	B
Weight	Instrumental (=1/ei^2)
Intercept	-1.10671 ± 0.09297
Slope	1.25578 ± 0.10242
Residual Sum of Squares	13.98652
Pearson's r	0.99669
R-Square (COD)	0.99339
Adj. R-Square	0.98678

Equation	y = a + b*x
Plot	B
Weight	Instrumental (=1/ei^2)
Intercept	0.47733 ± 0.00353
Slope	0.00253 ± 2.98068E-4
Residual Sum of Squares	0.5529
Pearson's r	0.97335
R-Square (COD)	0.94742
Adj. R-Square	0.93427

11. 0.5 M Sodium Silicate

Equation	y = a + b*x
Plot	B
Weight	Instrumental (=1/ei^2)
Intercept	-0.66726 ± 0.26346
Slope	1.36617 ± 0.5076
Residual Sum of Squares	107.49562
Pearson's r	0.93739
R-Square (COD)	0.8787
Adj. R-Square	0.75739

Equation	y = a + b*x
Plot	B
Weight	Instrumental (=1/ei^2)
Intercept	0.51674 ± 0.0252
Slope	-0.00494 ± 0.00738
Residual Sum of Squares	7.807
Pearson's r	-0.31744
R-Square (COD)	0.10077
Adj. R-Square	-0.12404

12. 0.7 M Sodium Silicate

Equation	y = a + b*x
Plot	B
Weight	Instrumental (=1/ei^2)
Intercept	-0.77375 ± 0.13456
Slope	1.65794 ± 0.25959
Residual Sum of Squares	6.09876
Pearson's r	0.98796
R-Square (COD)	0.97607
Adj. R-Square	0.95214

Equation	y = a + b*x
Plot	B
Weight	Instrumental (=1/ei^2)
Intercept	0.36851 ± 0.00947
Slope	0.01751 ± 0.0061
Residual Sum of Squares	0.47987
Pearson's r	0.85627
R-Square (COD)	0.73319
Adj. R-Square	0.64426

13. 0.9 M Sodium Silicate

Equation	y = a + b*x
Plot	B
Weight	Instrumental (=1/ei^2)
Intercept	-0.27934 ± 0.08601
Slope	0.95779 ± 0.28422
Residual Sum of Squares	22.64775
Pearson's r	0.95868
R-Square (COD)	0.91907
Adj. R-Square	0.83814

Equation	y = a + b*x
Plot	B
Weight	Instrumental (=1/ei^2)
Intercept	0.46739 ± 0.00696
Slope	0.0095 ± 0.00191
Residual Sum of Squares	4.42124
Pearson's r	0.91197
R-Square (COD)	0.83168
Adj. R-Square	0.79802

14. 1.2 M Sodium Silicate

Equation	y = a + b*x
Plot	B
Weight	Instrumental (=1/ei^2)
Intercept	-0.55162 ± 0.09043
Slope	1.92824 ± 0.28436
Residual Sum of Squares	5.89352
Pearson's r	0.9893
R-Square (COD)	0.97872
Adj. R-Square	0.95743

Equation	y = a + b*x
Plot	B
Weight	Instrumental (=1/ei^2)
Intercept	0.46828 ± 0.01482
Slope	0.00284 ± 0.00374
Residual Sum of Squares	49.19845
Pearson's r	0.35563
R-Square (COD)	0.12647
Adj. R-Square	-0.09191

15. 1.4 M Sodium Silicate

Equation	y = a + b*x
Plot	B
Weight	Instrumental (=1/ei^2)
Intercept	-0.21384 ± 0.0381
Slope	1.1367 ± 0.17707
Residual Sum of Squares	10.5445
Pearson's r	0.98808
R-Square (COD)	0.97631
Adj. R-Square	0.95262

Equation	y = a + b*x
Plot	B
Weight	Instrumental (=1/ei^2)
Intercept	0.47787 ± 0.00475
Slope	0.00385 ± 0.00182
Residual Sum of Squares	6.49706
Pearson's r	0.68698
R-Square (COD)	0.47194
Adj. R-Square	0.36632

16. 0.015 M Sodium Carbonate

Equation	y = a + b*x
Plot	B
Weight	Instrumental (=1/ei^2)
Intercept	-2.69035 ± 0.08579
Slope	1.26333 ± 0.03794
Residual Sum of Squares	0.19165
Pearson's r	0.99955
R-Square (COD)	0.9991
Adj. R-Square	0.9982

Equation	y = a + b*x
Plot	B
Weight	Instrumental (=1/ei^2)
Intercept	0.81748 ± 0.01441
Slope	0.00177 ± 0.00233
Residual Sum of Squares	1.02444
Pearson's r	0.40264
R-Square (COD)	0.16212
Adj. R-Square	-0.11717

17. 0.025 M Sodium Carbonate

Equation	y = a + b*x
Plot	B
Weight	Instrumental (=1/ei^2)
Intercept	-3.60423 ± 0.00997
Slope	2.11995 ± 0.00539
Residual Sum of Squares	5.5133E-4
Pearson's r	1
R-Square (COD)	0.99999
Adj. R-Square	0.99999

Equation	y = a + b*x
Plot	B
Weight	Instrumental (=1/ei^2)
Intercept	0.78655 ± 0.00604
Slope	0.00611 ± 9.01445E-4
Residual Sum of Squares	0.22086
Pearson's r	0.94965
R-Square (COD)	0.90184
Adj. R-Square	0.8822

18. 0.04 M Sodium Carbonate

Equation	y = a + b*x
Plot	B
Weight	Instrumental (=1/ei^2)
Intercept	-2.6591 ± 0.7785
Slope	2.10631 ± 0.5842
Residual Sum of Squares	16.30125
Pearson's r	0.96362
R-Square (COD)	0.92857
Adj. R-Square	0.85714

Equation	y = a + b*x
Plot	B
Weight	Instrumental (=1/ei^2)
Intercept	0.85818 ± 0.00507
Slope	0.00214 ± 8.59103E-4
Residual Sum of Squares	0.3091
Pearson's r	0.82112
R-Square (COD)	0.67424
Adj. R-Square	0.56566

19. 0.05 M Sodium Carbonate

Equation	y = a + b*x
Plot	B
Weight	Instrumental (=1/ei^2)
Intercept	-1.0736 ± 0.0392
Slope	1.10719 ± 0.03872
Residual Sum of Squares	4.45049
Pearson's r	0.99939
R-Square (COD)	0.99878
Adj. R-Square	0.99756

Equation	y = a + b*x
Plot	B
Weight	Instrumental (=1/ei^2)
Intercept	0.74212 ± 0.00603
Slope	0.00514 ± 0.00124
Residual Sum of Squares	1.60023
Pearson's r	0.9001
R-Square (COD)	0.81018
Adj. R-Square	0.76272

20. 0.1 M Sodium Carbonate

Equation	y = a + b*x
Plot	B
Weight	Instrumental (=1/ei^2)
Intercept	-1.72469 ± 0.50267
Slope	2.52027 ± 0.66541
Residual Sum of Squares	184.91469
Pearson's r	0.96687
R-Square (COD)	0.93483
Adj. R-Square	0.86967

Equation	y = a + b*x
Plot	B
Weight	Instrumental (=1/ei^2)
Intercept	0.70096 ± 0.01381
Slope	0.00199 ± 0.00144
Residual Sum of Squares	2.95078
Pearson's r	0.52598
R-Square (COD)	0.27666
Adj. R-Square	0.13199

21. 0.15 M Sodium Carbonate

Equation	y = a + b*x
Plot	B
Weight	Instrumental (=1/ei^2)
Intercept	-1.30878 ± 0.17267
Slope	2.65876 ± 0.2986
Residual Sum of Squares	23.97998
Pearson's r	0.99375
R-Square (COD)	0.98754
Adj. R-Square	0.97509

Equation	y = a + b*x
Plot	B
Weight	Instrumental (=1/ei^2)
Intercept	0.72592 ± 0.02097
Slope	0.0019 ± 0.00475
Residual Sum of Squares	25.77475
Pearson's r	0.17612
R-Square (COD)	0.03102
Adj. R-Square	-0.16278

22. 0.2 M Sodium Carbonate

Equation	y = a + b*x
Plot	B
Weight	Instrumental (=1/ei^2)
Intercept	-0.39906 ± 0.22335
Slope	1.21773 ± 0.35234
Residual Sum of Squares	4492.30127
Pearson's r	0.92552
R-Square (COD)	0.85658
Adj. R-Square	0.78487

Equation	y = a + b*x
Plot	B
Weight	Instrumental (=1/ei^2)
Intercept	0.76848 ± 0.01343
Slope	0.00304 ± 0.00195
Residual Sum of Squares	89.93658
Pearson's r	0.67016
R-Square (COD)	0.44912
Adj. R-Square	0.26549

23. 0.25 M Sodium Carbonate

Equation	y = a + b*x
Plot	B
Weight	Instrumental (=1/ei^2)
Intercept	-0.65408 ± 0.05362
Slope	2.2709 ± 0.16525
Residual Sum of Squares	41.79913
Pearson's r	0.99736
R-Square (COD)	0.99473
Adj. R-Square	0.98947

Equation	y = a + b*x
Plot	B
Weight	Instrumental (=1/ei^2)
Intercept	0.75389 ± 0.02741
Slope	-0.00177 ± 0.00591
Residual Sum of Squares	21.23025
Pearson's r	-0.17046
R-Square (COD)	0.02906
Adj. R-Square	-0.29459

42. 0.35 M Sodium Carbonate

Equation	y = a + b*x
Plot	B
Weight	Instrumental (=1/ei^2)
Intercept	-0.501 ± 0.07892
Slope	2.20062 ± 0.21112
Residual Sum of Squares	64.51855
Pearson's r	0.99543
R-Square (COD)	0.99088
Adj. R-Square	0.98176

Equation	y = a + b*x
Plot	B
Weight	Instrumental (=1/ei^2)
Intercept	0.63532 ± 0.04175
Slope	0.02453 ± 0.00969
Residual Sum of Squares	1.72958
Pearson's r	0.87306
R-Square (COD)	0.76224
Adj. R-Square	0.64336

25. 0.5 M Sodium Carbonate

Equation	y = a + b*x
Plot	B
Weight	Instrumental (=1/ei^2)
Intercept	-0.56319 ± 0.03845
Slope	3.34266 ± 0.18837
Residual Sum of Squares	14.53211
Pearson's r	0.99842
R-Square (COD)	0.99683
Adj. R-Square	0.99367

Equation	y = a + b*x
Plot	B
Weight	Instrumental (=1/ei^2)
Intercept	0.73168 ± 0.02125
Slope	0.01187 ± 0.00901
Residual Sum of Squares	12.49649
Pearson's r	0.55029
R-Square (COD)	0.30282
Adj. R-Square	0.12852

26. 0.7 M Sodium Carbonate

Equation	y = a + b*x
Plot	B
Weight	Instrumental (=1/ei^2)
Intercept	-0.20782 ± 0.0116
Slope	2.39914 ± 0.09709
Residual Sum of Squares	53.81401
Pearson's r	0.99837
R-Square (COD)	0.99674
Adj. R-Square	0.9951

Equation	y = a + b*x
Plot	B
Weight	Instrumental (=1/ei^2)
Intercept	0.70879 ± 0.01142
Slope	0.00624 ± 0.00563
Residual Sum of Squares	1.35722
Pearson's r	0.53856
R-Square (COD)	0.29005
Adj. R-Square	0.05339

27. 0.9 M Sodium Carbonate

Equation	y = a + b*x
Plot	B
Weight	Instrumental (=1/ei^2)
Intercept	-0.125 ± 2.84723E-4
Slope	2.34485 ± 0.00216
Residual Sum of Squares	0.00886
Pearson's r	1
R-Square (COD)	1
Adj. R-Square	1

Equation	y = a + b*x
Plot	B
Weight	Instrumental (=1/ei^2)
Intercept	0.71551 ± 0.02715
Slope	0.011 ± 0.00779
Residual Sum of Squares	45.1833
Pearson's r	0.57687
R-Square (COD)	0.33278
Adj. R-Square	0.16597

28. 1.2 M Sodium Carbonate

Equation	y = a + b*x
Plot	B
Weight	Instrumental (=1/ei^2)
Intercept	-0.02371 ± 0.02994
Slope	1.71135 ± 0.14345
Residual Sum of Squares	8.27132
Pearson's r	0.99305
R-Square (COD)	0.98614
Adj. R-Square	0.97921

Equation	y = a + b*x
Plot	B
Weight	Instrumental (=1/ei^2)
Intercept	0.7295 ± 0.03517
Slope	0.01263 ± 0.01687
Residual Sum of Squares	50.45865
Pearson's r	0.39672
R-Square (COD)	0.15739
Adj. R-Square	-0.12348

29. 0.015 M Sodium Sulphate

Equation	y = a + b*x
Plot	B
Weight	Instrumental (=1/ei^2)
Intercept	-1.43564 ± 0.12521
Slope	0.74324 ± 0.05994
Residual Sum of Squares	1.47988
Pearson's r	0.99676
R-Square (COD)	0.99354
Adj. R-Square	0.98707

Equation	y = a + b*x
Plot	B
Weight	Instrumental (=1/ei^2)
Intercept	0.85253 ± 0.06502
Slope	0.00502 ± 0.00589
Residual Sum of Squares	280.97586
Pearson's r	0.3917
R-Square (COD)	0.15343
Adj. R-Square	-0.05821

30. 0.025 M Sodium Sulphate

Equation	y = a + b*x
Plot	B
Weight	Instrumental (=1/ei^2)
Intercept	-2.72636 ± --
Slope	1.69431 ± --
Residual Sum of Squares	0
Pearson's r	1
R-Square (COD)	1
Adj. R-Square	--

Equation	y = a + b*x
Plot	B
Weight	Instrumental (=1/ei^2)
Intercept	0.87608 ± 0.01293
Slope	0.00981 ± 0.00172
Residual Sum of Squares	6.16895
Pearson's r	0.95692
R-Square (COD)	0.9157
Adj. R-Square	0.8876

31. 0.04 M Sodium Sulphate

Equation	y = a + b*x
Plot	B
Weight	Instrumental (=1/ei^2)
Intercept	-2.02349 ± 0.13477
Slope	1.72938 ± 0.10378
Residual Sum of Squares	2.10602
Pearson's r	0.9982
R-Square (COD)	0.99641
Adj. R-Square	0.99282

Equation	y = a + b*x
Plot	B
Weight	Instrumental (=1/ei^2)
Intercept	0.9393 ± 0.0126
Slope	-0.00368 ± 0.00334
Residual Sum of Squares	33.75499
Pearson's r	-0.61519
R-Square (COD)	0.37845
Adj. R-Square	0.06768

32. 0.05 M Sodium Sulphate

Equation	y = a + b*x
Plot	B
Weight	Instrumental (=1/ei^2)
Intercept	-2.24006 ± 0.89855
Slope	2.09137 ± 0.77508
Residual Sum of Squares	27.97306
Pearson's r	0.93768
R-Square (COD)	0.87924
Adj. R-Square	0.75847

Equation	y = a + b*x
Plot	B
Weight	Instrumental (=1/ei^2)
Intercept	0.90818 ± 0.00683
Slope	0.00406 ± 0.00102
Residual Sum of Squares	1.63887
Pearson's r	0.91723
R-Square (COD)	0.84131
Adj. R-Square	0.78841

33. 0.1 M Sodium Sulphate

Equation	y = a + b*x
Plot	B
Weight	Instrumental (=1/ei^2)
Intercept	-1.67656 ± 0.11147
Slope	2.47425 ± 0.14789
Residual Sum of Squares	1.29269
Pearson's r	0.99822
R-Square (COD)	0.99644
Adj. R-Square	0.99288

Equation	y = a + b*x
Plot	B
Weight	Instrumental (=1/ei^2)
Intercept	0.91106 ± 0.01989
Slope	-8.93066E-4 ± 0.00278
Residual Sum of Squares	194.33745
Pearson's r	-0.18237
R-Square (COD)	0.03326
Adj. R-Square	-0.28899

34. 0.15 M Sodium Sulphate

Equation	y = a + b*x
Plot	B
Weight	Instrumental (=1/ei^2)
Intercept	-0.88218 ± 0.12274
Slope	1.81296 ± 0.22936
Residual Sum of Squares	87.6268
Pearson's r	0.99209
R-Square (COD)	0.98425
Adj. R-Square	0.96849

Equation	y = a + b*x
Plot	B
Weight	Instrumental (=1/ei^2)
Intercept	0.83234 ± 0.00441
Slope	0.00464 ± 8.53347E-4
Residual Sum of Squares	10.29378
Pearson's r	0.95279
R-Square (COD)	0.90781
Adj. R-Square	0.87708

35. 0.2 M Sodium Sulphate

Equation	y = a + b*x
Plot	B
Weight	Instrumental (=1/ei^2)
Intercept	-0.89952 ± 0.01442
Slope	2.32889 ± 0.03546
Residual Sum of Squares	1.10342
Pearson's r	0.99988
R-Square (COD)	0.99977
Adj. R-Square	0.99954

Equation	y = a + b*x
Plot	B
Weight	Instrumental (=1/ei^2)
Intercept	0.8448 ± 0.01021
Slope	0.00588 ± 0.00203
Residual Sum of Squares	12.33935
Pearson's r	0.85869
R-Square (COD)	0.73735
Adj. R-Square	0.6498

36. 0.25 M Sodium Sulphate

Equation	y = a + b*x
Plot	B
Weight	Instrumental (=1/ei^2)
Intercept	-0.84636 ± 0.01788
Slope	2.5609 ± 0.04438
Residual Sum of Squares	0.1412
Pearson's r	0.99985
R-Square (COD)	0.9997
Adj. R-Square	0.9994

Equation	y = a + b*x
Plot	B
Weight	Instrumental (=1/ei^2)
Intercept	0.8904 ± 0.02568
Slope	0.00427 ± 0.0048
Residual Sum of Squares	28.98014
Pearson's r	0.53211
R-Square (COD)	0.28314
Adj. R-Square	-0.0753

37. 0.35 M Sodium Sulphate

Equation	y = a + b*x
Plot	B
Weight	Instrumental (=1/ei^2)
Intercept	-0.72804 ± 0.06576
Slope	2.71302 ± 0.19347
Residual Sum of Squares	5.3568
Pearson's r	0.99747
R-Square (COD)	0.99494
Adj. R-Square	0.98988

Equation	y = a + b*x
Plot	B
Weight	Instrumental (=1/ei^2)
Intercept	0.83614 ± 0.0115
Slope	0.00261 ± 0.00299
Residual Sum of Squares	8.97298
Pearson's r	0.44994
R-Square (COD)	0.20244
Adj. R-Square	-0.06341

38. 0.5 M Sodium Sulphate

Equation	y = a + b*x
Plot	B
Weight	Instrumental (=1/ei^2)
Intercept	-0.51686 ± 0.01
Slope	2.88391 ± 0.03941
Residual Sum of Squares	1.27607
Pearson's r	0.99991
R-Square (COD)	0.99981
Adj. R-Square	0.99963

Equation	y = a + b*x
Plot	B
Weight	Instrumental (=1/ei^2)
Intercept	0.84319 ± 0.01823
Slope	0.0025 ± 0.00393
Residual Sum of Squares	11.79338
Pearson's r	0.34519
R-Square (COD)	0.11915
Adj. R-Square	-0.17446

39. 0.015 M Sodium Chloride

Equation	y = a + b*x
Plot	B
Weight	Instrumental (=1/ei^2)
Intercept	-2.48936 ± 0.21535
Slope	0.88161 ± 0.07015
Residual Sum of Squares	10.28546
Pearson's r	0.99685
R-Square (COD)	0.99371
Adj. R-Square	0.98742

Equation	y = a + b*x
Plot	B
Weight	Instrumental (=1/ei^2)
Intercept	0.82012 ± 0.01745
Slope	0.00675 ± 0.00192
Residual Sum of Squares	14.3211
Pearson's r	0.89649
R-Square (COD)	0.8037
Adj. R-Square	0.73827

40. 0.025 M Sodium Chloride

Equation	y = a + b*x
Plot	B
Weight	Instrumental (=1/ei^2)
Intercept	-2.58833 ± 0.10346
Slope	1.16241 ± 0.04147
Residual Sum of Squares	5.54725
Pearson's r	0.99936
R-Square (COD)	0.99873
Adj. R-Square	0.99746

Equation	y = a + b*x
Plot	B
Weight	Instrumental (=1/ei^2)
Intercept	0.85745 ± 0.01138
Slope	0.00468 ± 0.00123
Residual Sum of Squares	30.07822
Pearson's r	0.88549
R-Square (COD)	0.78409
Adj. R-Square	0.73011

41. 0.04 M Sodium Chloride

Equation	y = a + b*x
Plot	B
Weight	Instrumental (=1/ei^2)
Intercept	-3.00946 ± 0.1388
Slope	1.65479 ± 0.06725
Residual Sum of Squares	0.36907
Pearson's r	0.99835
R-Square (COD)	0.99671
Adj. R-Square	0.99506

Equation	y = a + b*x
Plot	B
Weight	Instrumental (=1/ei^2)
Intercept	0.81335 ± 0.02938
Slope	0.00892 ± 0.00313
Residual Sum of Squares	102.45178
Pearson's r	0.81879
R-Square (COD)	0.67042
Adj. R-Square	0.58802

42. 0.05 M Sodium Chloride

Equation	y = a + b*x
Plot	B
Weight	Instrumental (=1/ei^2)
Intercept	-2.17655 ± --
Slope	1.42499 ± --
Residual Sum of Squares	0
Pearson's r	1
R-Square (COD)	1
Adj. R-Square	--

Equation	y = a + b*x
Plot	B
Weight	Instrumental (=1/ei^2)
Intercept	0.90397 ± 0.03061
Slope	-0.00483 ± 0.00432
Residual Sum of Squares	104.11189
Pearson's r	-0.54195
R-Square (COD)	0.29371
Adj. R-Square	0.05828

43. 0.1 M Sodium Chloride

Equation	y = a + b*x
Plot	B
Weight	Instrumental (=1/ei^2)
Intercept	-1.68895 ± 0.05238
Slope	1.7559 ± 0.03946
Residual Sum of Squares	6.20885
Pearson's r	0.99975
R-Square (COD)	0.9995
Adj. R-Square	0.99899

Equation	y = a + b*x
Plot	B
Weight	Instrumental (=1/ei^2)
Intercept	0.832 ± 0.01555
Slope	0.0039 ± 0.00246
Residual Sum of Squares	85.07744
Pearson's r	0.62047
R-Square (COD)	0.38498
Adj. R-Square	0.23122

44. 0.15 M Sodium Chloride

Equation	y = a + b*x
Plot	B
Weight	Instrumental (=1/ei^2)
Intercept	-2.13595 ± 0.20046
Slope	2.73912 ± 0.20173
Residual Sum of Squares	65.98511
Pearson's r	0.9973
R-Square (COD)	0.99461
Adj. R-Square	0.98921

Equation	y = a + b*x
Plot	B
Weight	Instrumental (=1/ei^2)
Intercept	0.84658 ± 0.0161
Slope	0.00378 ± 0.00225
Residual Sum of Squares	188.79095
Pearson's r	0.69607
R-Square (COD)	0.48451
Adj. R-Square	0.31268

45. 0.2 M Sodium Chloride

Equation	y = a + b*x
Plot	B
Weight	Instrumental (=1/ei^2)
Intercept	-1.78375 ± 0.39947
Slope	2.61996 ± 0.52098
Residual Sum of Squares	24.05305
Pearson's r	0.9808
R-Square (COD)	0.96196
Adj. R-Square	0.92393

Equation	y = a + b*x
Plot	B
Weight	Instrumental (=1/ei^2)
Intercept	0.89553 ± 0.01265
Slope	0.00288 ± 0.00258
Residual Sum of Squares	45.28088
Pearson's r	0.48735
R-Square (COD)	0.23751
Adj. R-Square	0.04689

46. 0.25 M Sodium Chloride

Equation	y = a + b*x
Plot	B
Weight	Instrumental (=1/ei^2)
Intercept	-2.10971 ± 0.12664
Slope	3.59921 ± 0.20645
Residual Sum of Squares	162.24268
Pearson's r	0.99836
R-Square (COD)	0.99672
Adj. R-Square	0.99344

Equation	y = a + b*x
Plot	B
Weight	Instrumental (=1/ei^2)
Intercept	0.81773 ± 0.01853
Slope	0.01043 ± 0.00459
Residual Sum of Squares	46.87765
Pearson's r	0.84908
R-Square (COD)	0.72094
Adj. R-Square	0.58141

47. 0.35 M Sodium Chloride

Equation	y = a + b*x
Plot	B
Weight	Instrumental (=1/ei^2)
Intercept	-1.33911 ± 0.01556
Slope	2.83403 ± 0.02883
Residual Sum of Squares	0.40199
Pearson's r	0.99995
R-Square (COD)	0.9999
Adj. R-Square	0.99979

Equation	y = a + b*x
Plot	B
Weight	Instrumental (=1/ei^2)
Intercept	0.82837 ± 0.03388
Slope	-0.00202 ± 0.00887
Residual Sum of Squares	1.06776
Pearson's r	-0.15877
R-Square (COD)	0.02521
Adj. R-Square	-0.46219

48. 0.5 M Sodium Chloride

Equation	y = a + b*x
Plot	B
Weight	Instrumental (=1/ei^2)
Intercept	-0.80386 ± 0.06986
Slope	2.40442 ± 0.19466
Residual Sum of Squares	70.67918
Pearson's r	0.99674
R-Square (COD)	0.99349
Adj. R-Square	0.98698

Equation	y = a + b*x
Plot	B
Weight	Instrumental (=1/ei^2)
Intercept	0.82511 ± 0.01699
Slope	0.00486 ± 0.00428
Residual Sum of Squares	24.27233
Pearson's r	0.49348
R-Square (COD)	0.24353
Adj. R-Square	0.05441

49. 0.015 M Sodium Diphosphate

Equation	y = a + b*x
Plot	B
Weight	Instrumental (=1/ei^2)
Intercept	-2.06964 ± 0.13892
Slope	1.05526 ± 0.06731
Residual Sum of Squares	0.83407
Pearson's r	0.99797
R-Square (COD)	0.99595
Adj. R-Square	0.9919

Equation	y = a + b*x
Plot	B
Weight	Instrumental (=1/ei^2)
Intercept	0.85138 ± 0.00845
Slope	0.0023 ± 8.61455E-4
Residual Sum of Squares	8.32888
Pearson's r	0.80011
R-Square (COD)	0.64018
Adj. R-Square	0.55022

50. 0.025 M Sodium Diphosphate

Equation	y = a + b*x
Plot	B
Weight	Instrumental (=1/ei^2)
Intercept	-1.65872 ± 0.21075
Slope	1.12412 ± 0.14014
Residual Sum of Squares	7.3466
Pearson's r	0.99232
R-Square (COD)	0.9847
Adj. R-Square	0.96939

Equation	y = a + b*x
Plot	B
Weight	Instrumental (=1/ei^2)
Intercept	0.83778 ± 0.0075
Slope	0.00279 ± 8.83575E-4
Residual Sum of Squares	4.59495
Pearson's r	0.87641
R-Square (COD)	0.7681
Adj. R-Square	0.69079

51. 0.04 M Sodium Diphosphate

Equation	y = a + b*x
Plot	B
Weight	Instrumental (=1/ei^2)
Intercept	-1.00637 ± 0.45599
Slope	0.93085 ± 0.41104
Residual Sum of Squares	153.86278
Pearson's r	0.91479
R-Square (COD)	0.83683
Adj. R-Square	0.67367

Equation	y = a + b*x
Plot	B
Weight	Instrumental (=1/ei^2)
Intercept	0.86803 ± 0.00399
Slope	1.45085E-4 ± 3.82839E-4
Residual Sum of Squares	1.27509
Pearson's r	0.21374
R-Square (COD)	0.04569
Adj. R-Square	-0.27242

52. 0.05 M Sodium Diphosphate

Equation	y = a + b*x
Plot	B
Weight	Instrumental (=1/ei^2)
Intercept	-1.7603 ± 0.19654
Slope	1.67983 ± 0.16105
Residual Sum of Squares	7.60734
Pearson's r	0.99544
R-Square (COD)	0.99089
Adj. R-Square	0.98178

Equation	y = a + b*x
Plot	B
Weight	Instrumental (=1/ei^2)
Intercept	0.83477 ± 0.00944
Slope	0.00565 ± 0.00216
Residual Sum of Squares	2.24807
Pearson's r	0.87997
R-Square (COD)	0.77434
Adj. R-Square	0.66151

53. 0.1 M Sodium Diphosphate

Equation	y = a + b*x
Plot	B
Weight	Instrumental (=1/ei^2)
Intercept	-1.31993 ± 0.35836
Slope	1.93818 ± 0.50926
Residual Sum of Squares	55.7101
Pearson's r	0.96717
R-Square (COD)	0.93542
Adj. R-Square	0.87084

Equation	y = a + b*x
Plot	B
Weight	Instrumental (=1/ei^2)
Intercept	0.83317 ± 0.01023
Slope	0.00353 ± 0.00246
Residual Sum of Squares	39.12004
Pearson's r	0.63806
R-Square (COD)	0.40712
Adj. R-Square	0.2095

54. 0.15 M Sodium Diphosphate

Equation	y = a + b*x
Plot	B
Weight	Instrumental (=1/ei^2)
Intercept	-1.30588 ± 0.0755
Slope	2.68605 ± 0.15091
Residual Sum of Squares	4.73619
Pearson's r	0.99843
R-Square (COD)	0.99685
Adj. R-Square	0.99371

Equation	y = a + b*x
Plot	B
Weight	Instrumental (=1/ei^2)
Intercept	0.81631 ± 0.00199
Slope	0.00293 ± 7.80065E-4
Residual Sum of Squares	4.54851
Pearson's r	0.859
R-Square (COD)	0.73788
Adj. R-Square	0.68545

55. 0.2 M Sodium Diphosphate

Equation	y = a + b*x
Plot	B
Weight	Instrumental (=1/ei^2)
Intercept	-1.19768 ± 0.28052
Slope	2.72666 ± 0.5574
Residual Sum of Squares	6.2321
Pearson's r	0.97974
R-Square (COD)	0.95989
Adj. R-Square	0.91977

Equation	y = a + b*x
Plot	B
Weight	Instrumental (=1/ei^2)
Intercept	0.81575 ± 0.00121
Slope	0.00496 ± 2.7652E-4
Residual Sum of Squares	0.35482
Pearson's r	0.99691
R-Square (COD)	0.99382
Adj. R-Square	0.99074

56. 0.25 M Sodium Diphosphate

Equation	y = a + b*x
Plot	B
Weight	Instrumental (=1/ei^2)
Intercept	-0.8441 ± 0.0936
Slope	2.4761 ± 0.2322
Residual Sum of Squares	0.76796
Pearson's r	0.99563
R-Square (COD)	0.99128
Adj. R-Square	0.98257

Equation	y = a + b*x
Plot	B
Weight	Instrumental (=1/ei^2)
Intercept	0.82631 ± 0.00491
Slope	0.00412 ± 0.00183
Residual Sum of Squares	31.43846
Pearson's r	0.7924
R-Square (COD)	0.62789
Adj. R-Square	0.50386

57. 0.35 M Sodium Diphosphate

Equation	y = a + b*x
Plot	B
Weight	Instrumental (=1/ei^2)
Intercept	-0.50501 ± 0.09574
Slope	2.28984 ± 0.29742
Residual Sum of Squares	1.72508
Pearson's r	0.99167
R-Square (COD)	0.98341
Adj. R-Square	0.96682

Equation	y = a + b*x
Plot	B
Weight	Instrumental (=1/ei^2)
Intercept	0.83005 ± 0.0079
Slope	0.00112 ± 0.00154
Residual Sum of Squares	7.21195
Pearson's r	0.38611
R-Square (COD)	0.14908
Adj. R-Square	-0.13456

58. 0.5 M Sodium Diphosphate

Equation	y = a + b*x
Plot	B
Weight	Instrumental (=1/ei^2)
Intercept	-0.41106 ± 0.04237
Slope	2.68145 ± 0.15296
Residual Sum of Squares	31.18434
Pearson's r	0.99838
R-Square (COD)	0.99676
Adj. R-Square	0.99351

Equation	y = a + b*x
Plot	B
Weight	Instrumental (=1/ei^2)
Intercept	0.82727 ± 0.00782
Slope	0.0013 ± 0.00153
Residual Sum of Squares	2.35497
Pearson's r	0.43978
R-Square (COD)	0.19341
Adj. R-Square	-0.07546

59. 0.5 mM Magnesium chloride

Equation	y = a + b*x
Plot	B
Weight	Instrumental (=1/ei^2)
Intercept	-3.37209 ± 0.45971
Slope	1.2477 ± 0.14836
Residual Sum of Squares	13.49404
Pearson's r	0.98615
R-Square (COD)	0.9725
Adj. R-Square	0.95875

Equation	y = a + b*x
Plot	B
Weight	Instrumental (=1/ei^2)
Intercept	0.83274 ± 0.02621
Slope	-0.00112 ± 0.00207
Residual Sum of Squares	2.99186
Pearson's r	-0.29764
R-Square (COD)	0.08859
Adj. R-Square	-0.21521

60. 1:10 Seawater

Equation	y = a + b*x
Plot	B
Weight	Instrumental (=1/ei^2)
Intercept	-1.65319 ± 0.02231
Slope	1.98716 ± 0.02058
Residual Sum of Squares	0.51816
Pearson's r	0.99995
R-Square (COD)	0.99989
Adj. R-Square	0.99979

Equation	y = a + b*x
Plot	B
Weight	Instrumental (=1/ei^2)
Intercept	0.83281 ± 0.02023
Slope	0.00193 ± 0.00173
Residual Sum of Squares	2.63661
Pearson's r	0.38819
R-Square (COD)	0.15069
Adj. R-Square	0.02936

61. 1:5 Seawater

Equation	y = a + b*x
Plot	B
Weight	Instrumental (=1/ei^2)
Intercept	-0.76449 ± 0.07247
Slope	1.61646 ± 0.09141
Residual Sum of Squares	7.00496
Pearson's r	0.9984
R-Square (COD)	0.99681
Adj. R-Square	0.99362

Equation	y = a + b*x
Plot	B
Weight	Instrumental (=1/ei^2)
Intercept	0.85328 ± 0.00535
Slope	7.29236E-4 ± 5.28428E-4
Residual Sum of Squares	14.87965
Pearson's r	0.41791
R-Square (COD)	0.17465
Adj. R-Square	0.08294

62. Low Conc.PIC

Equation	y = a + b*x
Plot	B
Weight	Instrumental (=1/ei^2)
Intercept	-0.66904 ± 0.05168
Slope	0.1387 ± 0.0087
Residual Sum of Squares	0.75074
Pearson's r	0.99804
R-Square (COD)	0.99608
Adj. R-Square	0.99216

Equation	y = a + b*x
Plot	B
Weight	Instrumental (=1/ei^2)
Intercept	0.20997 ± 0.00698
Slope	4.10835E-4 ± 4.60587E-4
Residual Sum of Squares	6.27758
Pearson's r	0.45784
R-Square (COD)	0.20962
Adj. R-Square	-0.05384

63. High Conc. PIC

Equation	y = a + b*x
Plot	abs
Weight	Instrumental (=1/ei^2)
Intercept	-3.27339 ± 0.96756
Slope	0.70136 ± 0.14702
Residual Sum of Squares	1.18892
Pearson's r	0.97873
R-Square (COD)	0.95791
Adj. R-Square	0.91582

Equation	y = a + b*x
Plot	abs
Weight	Instrumental (=1/ei^2)
Intercept	1.73119 ± 0.00875
Slope	9.73297E-4 ± 7.04819E-4
Residual Sum of Squares	0.00446
Pearson's r	0.69863
R-Square (COD)	0.48809
Adj. R-Square	0.23213

64. 0.5 M SHG

Equation	y = a + b*x
Plot	B
Weight	Instrumental (=1/ei^2)
Intercept	-0.40834 ± 0.10897
Slope	0.93294 ± 0.14399
Residual Sum of Squares	87.72174
Pearson's r	0.96608
R-Square (COD)	0.9333
Adj. R-Square	0.91107

Equation	y = a + b*x
Plot	B
Weight	Instrumental (=1/ei^2)
Intercept	0.68864 ± 0.01332
Slope	0.00555 ± 0.0016
Residual Sum of Squares	2.5805
Pearson's r	0.89461
R-Square (COD)	0.80033
Adj. R-Square	0.73378

65. 0.015 M Sodium Carbonate (SHG)

Equation	y = a + b*x
Plot	B
Weight	Instrumental (=1/ei^2)
Intercept	-0.32974 ± 0.10953
Slope	0.98222 ± 0.14024
Residual Sum of Squares	1.40631
Pearson's r	0.98996
R-Square (COD)	0.98002
Adj. R-Square	0.96004

Equation	y = a + b*x
Plot	B
Weight	Instrumental (=1/ei^2)
Intercept	0.77194 ± 0.05576
Slope	0.00354 ± 0.0059
Residual Sum of Squares	1.91353
Pearson's r	0.28716
R-Square (COD)	0.08246
Adj. R-Square	-0.14692

66. 0.025 M Sodium Carbonate (SHG)

Equation	y = a + b*x
Plot	B
Weight	Instrumental (=1/ei^2)
Intercept	-0.41312 ± 0.01573
Slope	0.95107 ± 0.02544
Residual Sum of Squares	0.02239
Pearson's r	0.99964
R-Square (COD)	0.99929
Adj. R-Square	0.99857

Equation	y = a + b*x
Plot	B
Weight	Instrumental (=1/ei^2)
Intercept	0.75097 ± 0.02173
Slope	0.0048 ± 0.00316
Residual Sum of Squares	2.25118
Pearson's r	0.60478
R-Square (COD)	0.36576
Adj. R-Square	0.2072

67. 0.04 M Sodium Carbonate (SHG)

Equation	y = a + b*x
Plot	B
Weight	Instrumental (=1/ei^2)
Intercept	-0.52018 ± 0.1722
Slope	1.37393 ± 0.28233
Residual Sum of Squares	6.58105
Pearson's r	0.97953
R-Square (COD)	0.95949
Adj. R-Square	0.91897

Equation	y = a + b*x
Plot	B
Weight	Instrumental (=1/ei^2)
Intercept	0.76634 ± 0.01384
Slope	0.0024 ± 0.00174
Residual Sum of Squares	0.16467
Pearson's r	0.5673
R-Square (COD)	0.32183
Adj. R-Square	0.15229

68. 0.05 M Sodium Carbonate (SHG)

Equation	y = a + b*x
Plot	B
Weight	Instrumental (=1/ei^2)
Intercept	-0.41319 ± 0.03105
Slope	1.20837 ± 0.04725
Residual Sum of Squares	0.01167
Pearson's r	0.99924
R-Square (COD)	0.99847
Adj. R-Square	0.99695

Equation	y = a + b*x
Plot	B
Weight	Instrumental (=1/ei^2)
Intercept	0.88892 ± 0.03085
Slope	0.00361 ± 0.00398
Residual Sum of Squares	1.28812
Pearson's r	0.41342
R-Square (COD)	0.17092
Adj. R-Square	-0.03635

69. 0.015 M Sodium Sulphate (SHG)

Equation	y = a + b*x
Plot	B
Weight	Instrumental (=1/ei^2)
Intercept	-0.36744 ± 0.06699
Slope	0.86869 ± 0.09009
Residual Sum of Squares	3.01346
Pearson's r	0.98425
R-Square (COD)	0.96875
Adj. R-Square	0.95833

Equation	y = a + b*x
Plot	B
Weight	Instrumental (=1/ei^2)
Intercept	0.76529 ± 0.02321
Slope	-6.1229E-5 ± 0.00385
Residual Sum of Squares	2.59642
Pearson's r	-0.00711
R-Square (COD)	5.05255E-5
Adj. R-Square	-0.19994

70. 0.015 M Sodium Chloride (SHG)

Equation	y = a + b*x
Plot	B
Weight	Instrumental (=1/ei^2)
Intercept	-0.43675 ± 0.05665
Slope	1.00967 ± 0.0709
Residual Sum of Squares	0.90915
Pearson's r	0.99268
R-Square (COD)	0.98542
Adj. R-Square	0.98056

Equation	y = a + b*x
Plot	B
Weight	Instrumental (=1/ei^2)
Intercept	0.71618 ± 0.02603
Slope	0.01089 ± 0.0028
Residual Sum of Squares	0.76059
Pearson's r	0.88942
R-Square (COD)	0.79107
Adj. R-Square	0.73883

71. 0.025 M Sodium Chloride (SHG)

Equation	y = a + b*x
Plot	B
Weight	Instrumental (=1/ei^2)
Intercept	-0.18404 ± 0.11251
Slope	0.74019 ± 0.14463
Residual Sum of Squares	0.87809
Pearson's r	0.96388
R-Square (COD)	0.92906
Adj. R-Square	0.89359

Equation	y = a + b*x
Plot	B
Weight	Instrumental (=1/ei^2)
Intercept	0.76465 ± 0.02734
Slope	0.00407 ± 0.00475
Residual Sum of Squares	2.51311
Pearson's r	0.44383
R-Square (COD)	0.19699
Adj. R-Square	-0.07068

72. 0.04 M Sodium Chloride (SHG)

Equation	y = a + b*x
Plot	B
Weight	Instrumental (=1/ei^2)
Intercept	-0.41785 ± 0.08014
Slope	0.95491 ± 0.10997
Residual Sum of Squares	1.13954
Pearson's r	0.98699
R-Square (COD)	0.97416
Adj. R-Square	0.96124

Equation	y = a + b*x
Plot	B
Weight	Instrumental (=1/ei^2)
Intercept	0.7698 ± 0.01217
Slope	0.00681 ± 0.00223
Residual Sum of Squares	0.4803
Pearson's r	0.83692
R-Square (COD)	0.70043
Adj. R-Square	0.62554

73. 0.05 M Sodium Chloride (SHG)

Equation	y = a + b*x
Plot	B
Weight	Instrumental (=1/ei^2)
Intercept	-0.36606 ± 0.10241
Slope	0.94921 ± 0.1442
Residual Sum of Squares	24.62951
Pearson's r	0.96708
R-Square (COD)	0.93525
Adj. R-Square	0.91366

Equation	y = a + b*x
Plot	B
Weight	Instrumental (=1/ei^2)
Intercept	0.73034 ± 0.00996
Slope	0.00854 ± 0.00153
Residual Sum of Squares	0.50334
Pearson's r	0.955
R-Square (COD)	0.91203
Adj. R-Square	0.8827

74. 0.1 M Sodium Chloride (SHG)

Equation	y = a + b*x
Plot	B
Weight	Instrumental (=1/ei^2)
Intercept	-0.28505 ± 0.01835
Slope	0.86964 ± 0.02919
Residual Sum of Squares	0.16318
Pearson's r	0.99888
R-Square (COD)	0.99775
Adj. R-Square	0.99663

Equation	y = a + b*x
Plot	B
Weight	Instrumental (=1/ei^2)
Intercept	0.77538 ± 0.03911
Slope	-0.00116 ± 0.00561
Residual Sum of Squares	2.10056
Pearson's r	-0.11807
R-Square (COD)	0.01394
Adj. R-Square	-0.31475

75. 0.15 M Sodium Chloride (SHG)

Equation	y = a + b*x
Plot	B
Weight	Instrumental (=1/ei^2)
Intercept	-0.1218 ± 0.04163
Slope	0.72187 ± 0.06432
Residual Sum of Squares	1.46027
Pearson's r	0.9883
R-Square (COD)	0.97674
Adj. R-Square	0.96898

Equation	y = a + b*x
Plot	B
Weight	Instrumental (=1/ei^2)
Intercept	0.76996 ± 0.03791
Slope	0.0079 ± 0.00423
Residual Sum of Squares	0.83018
Pearson's r	0.68232
R-Square (COD)	0.46556
Adj. R-Square	0.33195

76. 0.2 M Sodium Chloride (SHG)

Equation	y = a + b*x
Plot	B
Weight	Instrumental (=1/ei^2)
Intercept	-0.11053 ± 0.10418
Slope	0.7051 ± 0.13706
Residual Sum of Squares	0.79429
Pearson's r	0.96423
R-Square (COD)	0.92974
Adj. R-Square	0.89461

Equation	y = a + b*x
Plot	B
Weight	Instrumental (=1/ei^2)
Intercept	0.76002 ± 0.10394
Slope	0.01651 ± 0.01305
Residual Sum of Squares	6.27544
Pearson's r	0.53471
R-Square (COD)	0.28591
Adj. R-Square	0.10739

77. 0.015 M Sodium Diphosphate (SHG)

Equation	y = a + b*x
Plot	B
Weight	Instrumental (=1/ei^2)
Intercept	-0.39171 ± 0.06314
Slope	0.87336 ± 0.1011
Residual Sum of Squares	0.81705
Pearson's r	0.98686
R-Square (COD)	0.9739
Adj. R-Square	0.96085

Equation	y = a + b*x
Plot	B
Weight	Instrumental (=1/ei^2)
Intercept	0.63074 ± 0.04389
Slope	0.00389 ± 0.00447
Residual Sum of Squares	1.89576
Pearson's r	0.39882
R-Square (COD)	0.15906
Adj. R-Square	-0.05118

78. 0.5 mM Magnesium Chloride (SHG)

Equation	y = a + b*x
Plot	B
Weight	Instrumental (=1/ei^2)
Intercept	-0.52018 ± 0.1722
Slope	1.37393 ± 0.28233
Residual Sum of Squares	6.58105
Pearson's r	0.97953
R-Square (COD)	0.95949
Adj. R-Square	0.91897

Equation	y = a + b*x
Plot	B
Weight	Instrumental (=1/ei^2)
Intercept	0.76634 ± 0.01384
Slope	0.0024 ± 0.00174
Residual Sum of Squares	0.16467
Pearson's r	0.5673
R-Square (COD)	0.32183
Adj. R-Square	0.15229

79. 1:10 Seawater (SHG)

Equation	y = a + b*x
Plot	B
Weight	Instrumental (=1/ei^2)
Intercept	-0.39862 ± 0.06085
Slope	0.95285 ± 0.08343
Residual Sum of Squares	3.98437
Pearson's r	0.98869
R-Square (COD)	0.97752
Adj. R-Square	0.97002

Equation	y = a + b*x
Plot	B
Weight	Instrumental (=1/ei^2)
Intercept	0.69719 ± 0.02142
Slope	0.01025 ± 0.00282
Residual Sum of Squares	0.64964
Pearson's r	0.87581
R-Square (COD)	0.76704
Adj. R-Square	0.70881

80. 1:5 Seawater (SHG)

Equation	y = a + b*x
Plot	B
Weight	Instrumental (=1/ei^2)
Intercept	-0.19328 ± 0.06472
Slope	0.70375 ± 0.08049
Residual Sum of Squares	0.94548
Pearson's r	0.98094
R-Square (COD)	0.96224
Adj. R-Square	0.94965

Equation	y = a + b*x
Plot	B
Weight	Instrumental (=1/ei^2)
Intercept	0.72651 ± 0.04132
Slope	0.00811 ± 0.00362
Residual Sum of Squares	2.2267
Pearson's r	0.70781
R-Square (COD)	0.501
Adj. R-Square	0.4012

9.1.4 Tables of pH Measurement to Determine the pH Values of Salts Solutions in the Presence of a Range of SDS Concentrations and Pinacyanol Chloride.

9.1.4.1 Tables of pH Measurement in Sodium Silicate Solutions with 0.015, 0.025, 0.04, 0.05, 0.15, 0.25, 0.35, 0.5 M.

Table 9-1: 0.015 M Silicate

[SDS] mM	pH of 0.015 M silicate
1	10.5
2	10.5
3	10.5
3.4	10.5
3.6	10.5
3.8	10.5
4	10.5
4.2	10.5
4.4	10.5
4.6	10.5
4.8	10.6
5	10.5
6	10.5
8	10.5
10	10.5
12	10.6

Table 9-2: 0.025 M Silicate

[SDS] mM	pH of 0.025 M silicate
1	10.7
2	10.7
3	10.7
3.4	10.7
3.6	10.7
3.8	10.7
4	10.7
4.2	10.7
4.4	10.7
4.6	10.7
4.8	10.7
5	10.7
6	10.7
8	10.7
10	10.7
12	10.7

Table 9-3: 0.04 M Silicate

[SDS] mM	pH of 0.04 M silicate
1	10.7
2	10.7
2.3	10.7
2.6	10.7
2.8	10.7
3	10.7
3.2	10.7
3.4	10.7
3.6	10.7
3.8	10.7
4	10.7
6	10.7
8	10.8
10	10.7
12	10.7

Table 9-4: 0.05 M Silicate

[SDS] mM	pH of 0.05 M silicate
1	10.8
2	10.8
2.3	10.8
2.4	10.8
2.5	10.8
2.6	10.8
2.8	10.8
3	10.8
3.2	10.8
3.4	10.8
3.6	10.8
3.8	10.8
4	10.8
6	10.8
8	10.8
10	10.8

Table 9-5: 0.1 M Silicate

[SDS] mM	pH of 0.1 M silicate
0	11.0
0.1	11.0
0.2	11.0
0.4	11.0
0.6	11.0
0.7	11.0
0.9	11.0
1.1	11.0
1.4	11.0
1.7	11.0
2	11.0
3	11.0
5	11.0
7	11.0
9	11.0
13	11.0

Table 9-6: 0.15 M Silicate

[SDS] mM	pH of 0.15 M silicate
0.5	11.1
0.6	11.1
0.8	11.1
1	11.1
1.1	11.2
1.2	11.1
1.3	11.1
1.4	11.1
1.5	11.1
1.6	11.1
1.7	11.1
1.9	11.1
2	11.1
2.2	11.1
2.4	11.1
4	11.1
6	11.1
8	11.1

Table 9-7: 0.2 M Silicate

[SDS] mM	pH of 0.2 M silicate
0	11.2
0.2	11.2
0.4	11.3
0.6	11.2
0.7	11.2
0.9	11.2
1.1	11.2
1.2	11.2
1.6	11.2
2	11.2
3	11.2
5	11.2
7	11.2
9	11.2

Table 9-8: 0.25 M Silicate

[SDS] mM	pH of 0.2 M silicate
0.5	11.3
0.6	11.3
0.8	11.3
1	11.3
1.1	11.3
1.2	11.3
1.3	11.3
1.4	11.3
1.5	11.3
1.6	11.3
1.7	11.3
1.9	11.3
2	11.3
2.2	11.3
2.4	11.3
4	11.3
6	11.3
8	11.3

Table 9-9: 0.35 M Silicate

[SDS] mM	pH of 0.35 M silicate
0.2	11.4
0.5	11.4
0.8	11.4
0.9	11.4
1	11.4
1.2	11.3

Table 9-10: 0.5 M Silicate

[SDS] mM	pH of 0.5 M silicate
0.2	11.5
0.3	11.5
0.4	11.5
0.5	11.5
0.6	11.5
0.7	11.5

1.3	11.4
1.4	11.4
1.5	11.4
1.6	11.4
1.8	11.4
2	11.4
3.5	11.4
5	11.4
7	11.4
9	11.4
12	11.4

0.8	11.5
0.9	11.5
1	11.4
1.5	11.5
2	11.5
3	11.5
4	11.5
5	11.5
6	11.4

9.1.4.2 pH measurement in Sodium Carbonate Solutions with 0.015, 0.025, 0.04, 0.05, 0.1, 0.15, 0.2, 0.25, 0.35, 0.5 M.

Table 9-11: 0.015 M carbonate

[SDS] mM	pH of 0.015 M carbonate
1	10.2
1.5	10.2
1.8	10.2
2	10.2
2.2	10.2
2.4	10.3
2.6	10.4
2.8	10.3
3	10.4
3.5	10.4
5	10.2
7	10.3
9	10.3
11	10.4

Table 9-12: 0.025 M carbonate

[SDS] mM	pH of 0.025 M carbonate
0.5	10.8
1	10.8
1.5	10.9
1.8	10.8
1.9	10.9
2	10.9
2.1	10.9
2.3	10.9
2.5	10.9
3	10.9
3.4	10.9
5	10.9
8	10.9
10	10.9
12	10.9

Table 9-13: 0.04 M carbonate

[SDS] Mm	pH of 0.04 M carbonate
0.2	11.4
0.3	11.4
0.4	11.4
0.5	11.4
0.6	11.4
0.7	11.4
0.8	11.4
0.9	11.4
1	11.4
1.2	11.4
1.6	11.4
2	11.4
3	11.4
4	11.4
5	11.4
6	11.4

Table 9-14: 0.05 M carbonate

[SDS] mM	pH of 0.05 M carbonate
0.1	11.5
0.2	11.5
0.3	11.5
0.4	11.5
0.5	11.5
0.7	11.5
0.8	11.5
0.9	11.5
1	11.5
1.2	11.5
1.6	11.5
2	11.5
4	11.5
6	11.5
8	11.5
10	11.5
12	11.5
14	11.5

Table 9-15: 0.1 M carbonate

[SDS] Mm	pH of 0.1 M carbonate
0.1	11.5
0.2	11.6
0.3	11.6
0.4	11.6
0.5	11.6
0.7	11.6
0.8	11.6
0.9	11.6
1	11.6
1.2	11.6
1.6	11.6
2	11.6
4	11.6
6	11.6

Table 9-16: 0.15 M carbonate

[SDS] Mm	pH of 0.15 M carbonate
0.05	11.7
0.075	11.7
0.1	11.7
0.15	11.7
0.2	11.7
0.3	11.7
0.4	11.7
0.5	11.7
0.6	11.7
0.7	11.7
0.8	11.7
0.9	11.7
1	11.7
1.2	11.7
2	11.7
3	11.7
4	11.7
6	11.7

Table 9-17: 0.2 M carbonate

[SDS] Mm	pH of 0.2 M carbonate
0.1	11.8
0.15	11.8
0.2	11.8
0.3	11.8
0.4	11.8
0.5	11.8
0.6	11.8
0.8	11.8
0.9	11.8
1.2	11.8
2	11.8
3	11.8
4	11.8

Table 9-18: 0.25 M carbonate

[SDS] Mm	pH of 0.25 M carbonate
0.1	12.0
0.15	12.0
0.2	12.0
0.25	12.0
0.3	12.0
0.35	12.0
0.4	12.0
0.45	12.1
0.5	12.0
0.6	12.0
0.8	12.0
1.2	12.0
2	12.0
3	12.0
4	12.1

9.1.4.3 Tables of pH Measurement in Sodium Sulphate Solutions with 0.015 ,0.025, 0.04, 0.05, 0.1, 0.25, 0.35 and 0.5 M.

Table 9-19: 0.015 M Sulphate

[SDS] mM	pH of 0.015 M sulphate
1	6.4
1.5	6.3
2	6.3
2.5	6.2
3	6.3
3.3	6.1
3.6	6.4
3.9	6.4
4	6.5
4.2	6.3
4.5	6.2
5	6.2
6	6.2
8	6.1
10	6.3
12	6.2

Table 9-20: 0.025 M Sulphate

[SDS] mM	pH of 0.025 M sulphate
0.8	6.5
1	6.5
1.2	6.5
1.4	6.5
1.7	6.4
2	6.4
2.2	6.4
2.4	6.5
2.6	6.4
2.8	6.4
3	6.4
4	6.4
5	6.4
8	6.4

Table 9-21: 0.04 M Sulphate

[SDS] mM	pH of 0.04 M sulphate
0.8	6.6
0.9	6.7
1	6.6
1.1	6.5
1.2	6.5
1.4	6.5
1.5	6.5
1.7	6.5
2	6.5
2.2	6.5
2.4	6.5
3	6.5
4	6.5
8	6.5
10	6.5

Table 9-22: 0.05 Sulphate

[SDS] mM	pH of 0.05 M sulphate
0.8	6.6
0.9	6.5
1	6.5
1.1	6.5
1.2	6.6
1.3	6.6
1.4	6.6
1.5	6.6
1.7	6.6
2	6.6
2.2	6.5
3	6.5
4	6.5
5	6.5
8	6.5
10	5.6

Table 9-23: 0.1 Sulphate

[SDS] mM	pH of 0.1 M sulphate
0.4	6.5
0.5	6.6
0.6	6.5
0.7	6.5
0.8	6.6
0.9	6.6
1	6.6
1.1	6.6
1.2	6.6
1.3	6.5
1.4	6.6
2	6.6
4	6.6
5	6.6
8	6.6
10	6.6

Table 9-24: 0.15 M Sulphate

[SDS] mM	pH of 0.15 M sulphate
0.3	6.6
0.4	6.6
0.5	6.6
0.6	6.6
0.7	6.6
0.8	6.6
0.9	6.6
1	6.6
1.1	6.5
1.2	6.6
1.3	6.6
1.4	6.6
2	6.6
4	6.6
5	6.6
8	6.6
10	6.6

Table 9-25: 0.2 M Sulphate

[SDS] mM	pH of 0.2 M sulphate
0.3	6.4
0.4	6.4
0.5	6.4
0.6	6.4
0.7	6.4
0.8	6.4
0.9	6.4
1	6.4
1.1	6.4
1.2	6.4
1.3	6.4
2	6.4
4	6.4
5	6.4
8	6.4
10	6.4

Table 9-26: 0.25 M Sulphate

[SDS] mM	pH of 0.25 M sulphate
0.1	6.5
0.2	6.5
0.3	6.5
0.4	6.5
0.5	6.5
0.6	6.5
0.7	6.5
0.8	6.5
0.9	6.5
1	6.5
1.1	6.5
1.2	6.5
1.3	6.5
2	6.5
4	6.6
5	6.5
7	6.5

Table 9-27: 0.35 M Sulphate

[SDS] mM	pH of 0.35 M sulphate
0.1	6.6
0.2	6.6
0.3	6.6
0.4	6.6
0.5	6.6
0.6	6.6
0.7	6.6
0.8	6.6
0.9	6.6
1	6.6
1.1	6.6
1.2	6.6
1.3	6.6
2	6.6
4	6.6
5	6.6
7	6.6

Table 9-28: 0.5 M Sulphate

[SDS] mM	pH of 0.5 M sulphate
0.1	6.6
0.2	6.5
0.3	6.6
0.4	6.6
0.5	6.6
0.6	6.6
0.7	6.6
0.8	6.6
0.9	6.6
1	6.6
1.1	6.6
1.2	6.6
1.3	6.6
2	6.6
4	6.6
5	6.6
7	6.6

9.1.4.4 Tables of pH Measurement in Sodium Chloride Solutions with 0.015 ,0.025, 0.04, 0.05, 0.1, 0.25, 0.35 and 0.5 M.

Table 9-29: 0.015 M Chloride

[SDS] mM	pH of 0.015 M chloride
1	6.9
1.8	6.9
2.2	6.9
2.4	6.9
2.6	6.9
2.8	6.9
3	6.9
3.2	6.9
3.6	6.9
3.8	6.9
4	6.9
5	6.9
6	6.9
8	6.9
10	6.9
12	6.9

Table 9-30: 0.025 M Chloride

[SDS] mM	pH of 0.025 M chloride
1	6.9
1.5	6.9
2	6.9
2.3	6.9
2.6	6.9
2.8	6.9
3	6.9
3.2	6.9
3.4	6.9
3.6	6.9
4	6.9
5	6.9
7	6.9
9	6.9
11	6.9
15	6.9

Table 9-31: 0.04 M Chloride

[SDS] mM	pH of 0.04 M chloride
1	6.9
1.5	6.9
1.7	6.9
1.9	6.9
2	6.9
2.1	6.9
2.2	6.8
2.3	6.8
2.6	6.9
2.8	6.9
3	6.9
4	6.9
5	6.9
7	6.9
9	6.9
11	6.9
15	6.9

Table 9-32: 0.05 M Chloride

[SDS] mM	pH of 0.05 M chloride
0.3	7.0
0.4	7.0
0.5	7.0
0.6	7.1
0.7	7.0
0.8	7.1
0.9	7.1
1	7.1
1.6	7.1
2	7.1
4	7.1
6	7.1
8	7.1
10	7.1
12	7.1

Table 9-33:0.1 M Chloride

[SDS] mM	pH of 0.1 M chloride
0.4	7.1
0.6	7.1
0.7	7.1
0.8	7.1
0.9	7.1
1	7.1
1.2	7.1
1.4	7.1
1.6	7.1
1.8	7.1
2	7.1
4	7. 1
6	7.1
8	7.1
10	7.1
12	7.2

Table 9-34: 0.15 Chloride

[SDS] mM	pH of 0.15 M chloride
0.4	7.2
0.5	7.2
0.6	7.2
0.7	7.2
0.8	4.2
0.9	7.2
1	7.2
1.2	7.3
1.6	7.2
2	7.3
3	7.2
4	7.2
6	7.3
8	7.2

Table 9-35: 0.2 M Chloride

[SDS] mM	pH of 0.2 M chloride
0.4	7.3
0.5	7.3
0.6	7.3
0.7	7.3
0.8	7.3
0.9	7.3
1	7.3
1.2	7.3
1.6	7.3
2	7.3
3	7.3
4	7.3
6	7.3
8	7.3

Table 9-36: 0.25 M Chloride

[SDS] mM	pH of 0.25 M chloride
0.4	7.3
0.5	7.3
0.6	7.3
0.7	7.3
0.75	7.3
0.8	7.3
0.85	7.3
0.9	7.3
1	7.3
1.2	7.3
1.6	7.3
2	7.3
4	7.3
6	7.3

Table 9-37: 0.35 M Chloride

[SDS] mM	pH of 0.35 M chloride
0.2	7.3
0.3	7.3
0.4	7.3
0.5	7.3
0.6	7.3
0.7	7.3
0.8	7.3
0.9	7.3
1	7.3
1.6	7.3

Table 9-38: 0.5 M Chloride

[SDS] mM	pH of 0.5 M chloride
0.15	7.3
0.2	7.3
0.35	7.3
0.5	7.3
0.55	7.3
0.6	7.3
0.7	7.3
0.8	7.3
0.9	7.3
1	7.3
1.6	7.3

2	7.3
4	7.3
6	7.3

2	7.3
4	7.3
5	7.3
6	7.3

9.1.4.5 Tables of pH Measurement in Sodium Phosphate Solutions with 0.015 ,0.025, 0.04, 0.05, 0.1, 0.25, 0.35 and 0.5 M.

Table 9-39: 0.015 M Phosphate

[SDS] mM	pH of 0.015 M phosphate
1	9.0
1.5	9.0
1.8	9.0
2	9.0
2.3	9.0
2.5	9.0
2.8	9.0
3	9.0
3.4	9.0
4	9.0
5	9.0
6	9.0
8	9.0
10	9.0
12	9.0

Table 9-40: 0.025 M Phosphate

[SDS] mM	pH of 0.025 M phosphate
1	9.0
1.5	9.1
1.8	9.1
2	9.1
2.3	9.1
2.5	9.1
2.8	9.0
3	9.1
3.4	9.0
4	9.1
5	9.1
8	9.1
10	9.1
12	9.1

Table 9-41: 0.04 M Phosphate

[SDS] mM	pH of 0.04 M phosphate
0.5	9.1
0.7	9.1
1	9.1
1.1	9.1
1.3	9.1
1.5	9.2
1.7	9.1
1.9	9.1
2.2	9.1
2.5	9.1
3	9.1
4	9.1
5	9.1
8	9.2
10	9.1
12	9.2

Table 9-42: 0.05 M Phosphate

[SDS] mM	pH of 0.05 M phosphate
0.5	9.1
0.7	9.1
0.9	9.2
1.1	9.2
1.3	9.1
1.5	9.2
1.7	9.2
1.8	9.2
2.1	9.2
2.3	9.1
2.5	9.2
4	9.1
5	9.2
8	9.2

Table 9-43: 0.1 M Phosphate

[SDS] mM	pH of 0.1 M phosphate
0.4	9.2
0.5	9.2
0.6	9.2
0.7	9.2
0.8	9.2
0.9	9.2
1	9.2
1.2	9.2
1.5	9.2
1.7	9.2
2.1	9.2
2.3	9.2
3	9.2
4	9.2
6	9.2
8	9.2

Table 9-44: 0.15 M Phosphate

[SDS] mM	pH of 0.15 M phosphate
0.4	9.2
0.5	9.3
0.6	9.3
0.7	9.3
0.8	9.2
0.9	9.2
1	9.3
1.1	9.3
1.2	9.3
1.5	9.3
1.7	9.3
2.1	9.2
2.3	9.2
3	9.3
4	9.3
6	9.3
8	9.3

Table 9-45: 0.2 M Phosphate

[SDS] mM	PH of 0.2 M phosphate
0.2	9.3
0.3	9.3
0.4	9.3
0.5	9.3
0.6	9.3
0.7	9.3
0.8	9.3
0.9	9.2
1	9.3
1.1	9.2
1.2	9.3
1.3	9.3
1.4	9.3
1.5	9.3
3	9.3
6	9.3
8	9.3

Table 9-46: 0.25 M Phosphate

[SDS] mM	pH of 0.25 M phosphate
0.1	9.3
0.2	9.4
0.3	9.4
0.4	9.4
0.5	9.4
0.6	9.4
0.7	9.4
0.8	9.4
0.9	9.4
1	9.4
1.1	9.4
1.2	9.4
1.5	9.4
3	9.4
5	9.4
7	9.4

Table 9-47: 0.35 M Phosphate

[SDS] mM	pH of 0.35 M phosphate
0.1	9.4
0.2	9.4
0.3	9.5
0.4	9.5
0.5	9.5
0.6	9.5
0.7	9.5
0.8	9.5
0.9	9.5
1	9.5
1.1	9.5
1.3	9.5
1.5	9.4
3	9.4
5	9.5
7	9.5

Table 9-48: 0.5 M Phosphate

[SDS] mM	pH of 0.5 M phosphate
0.05	9.5
0.1	9.5
0.2	9.5
0.3	9.5
0.4	9.5
0.5	9.5
0.6	9.5
0.7	9.5
0.8	9.5
0.9	9.5
1	9.5
1.1	9.5
1.3	9.5
1.5	9.5
3	9.5
5	9.5
7	9.5

9.2 Chapter 4 Appendix

9.2.1 Spectrophotometric Investigation of the Critical Micelle Concentration (CMC) of Sodium Dodecyl Sulphate (SDS) with Alcohol in Aqueous Phase

9.2.1.1 In the Presence of Ethanol

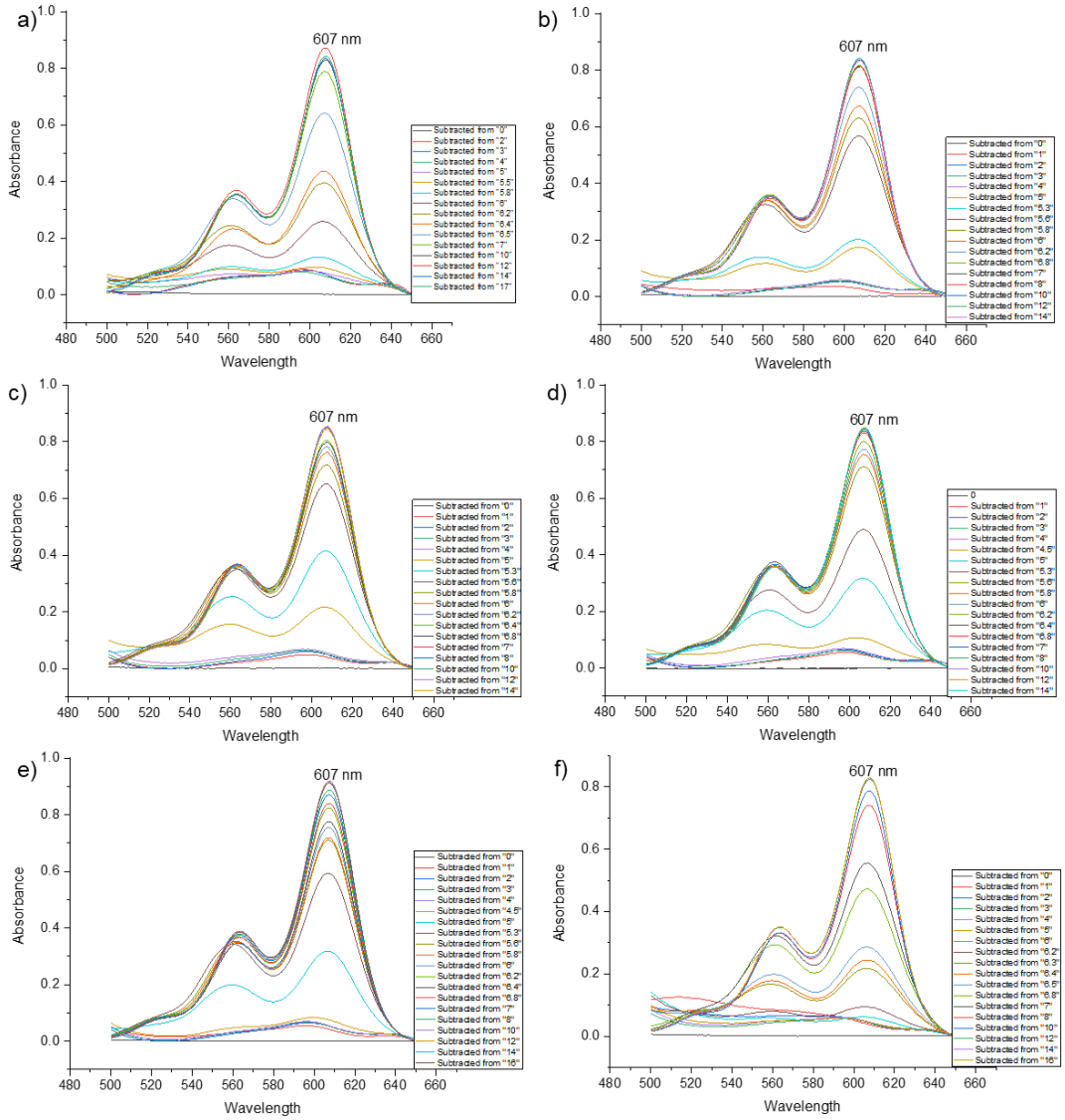

Figure 9-16: Determination of the (λ_{max}) of pinacyanol chloride in the presence of a range of SDS concentrations: a) 0.14 M, b) 0.4 M, c) 0.6 M, d) 0.9 M, e) 1.1 M, f) 1.3 M of ethanol solutions.

9.2.1.2 In the Presence of Hexanol

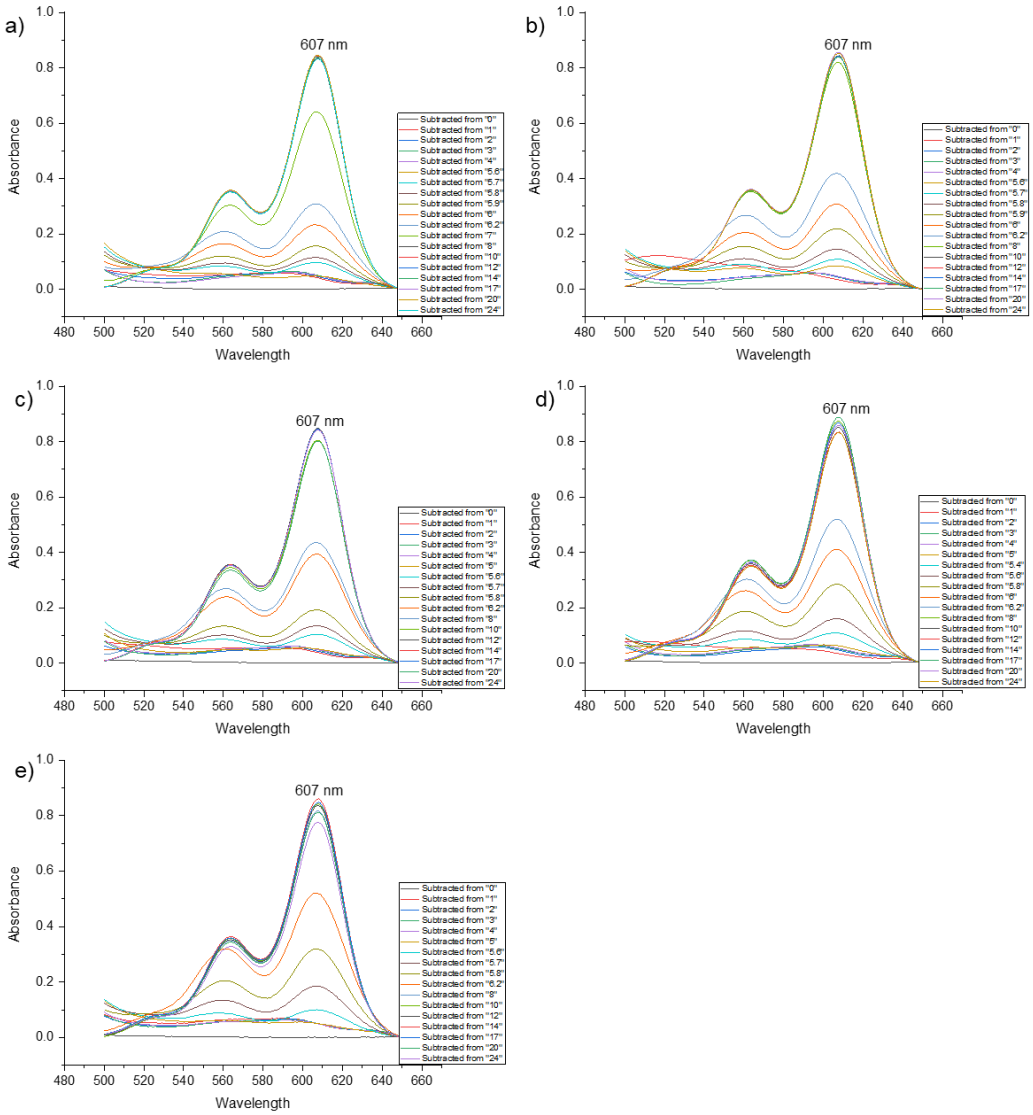

Figure 9-17: Determination of the (λ_{max}) of pinacyanol chloride in the presence of a range of SDS concentrations: a) 0.0625 mM, b) 0.125 mM, c) 0.25 mM, d) 0.5 mM, e)1.0 mM of hexanol solutions.

9.2.1.3 In the Presence of Octanol

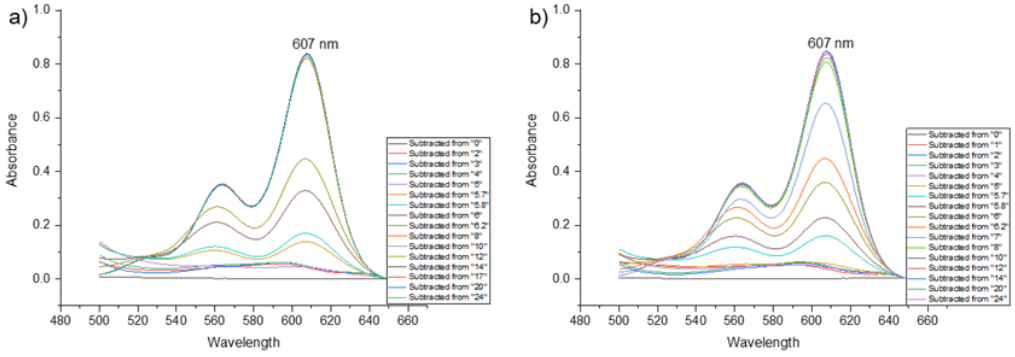

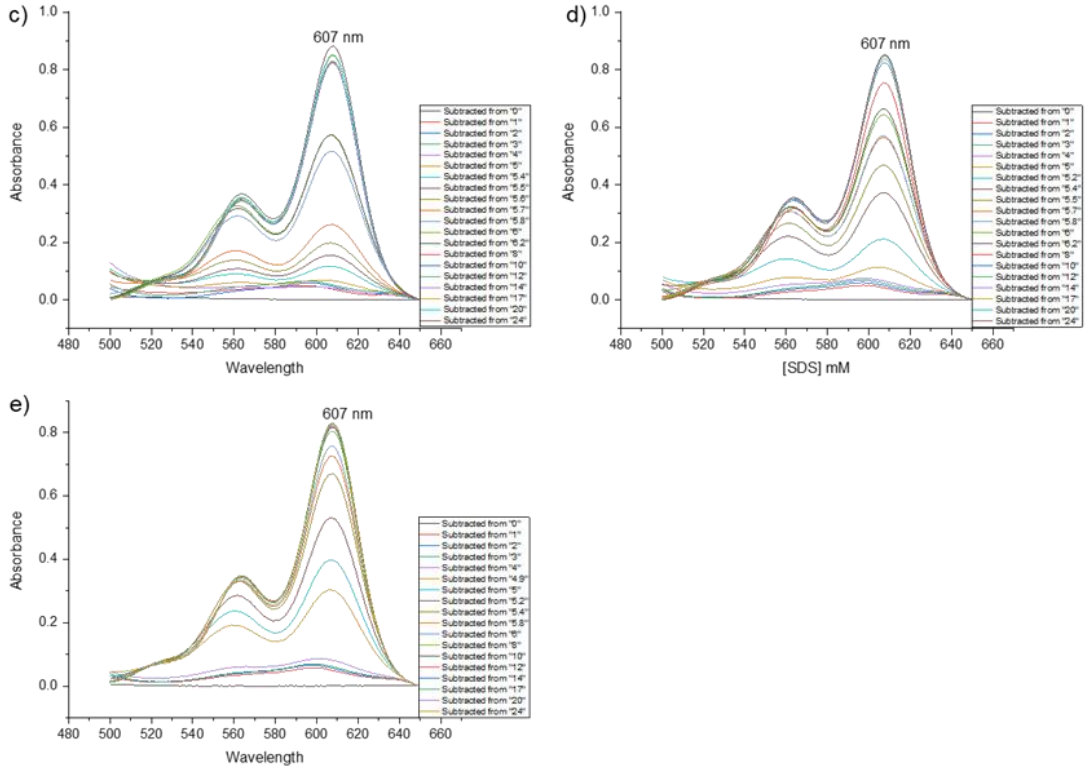

Figure 9-18: Determination of the (λ_{max}) of pinacyanol chloride in the presence of a range of SDS concentrations: a) 0.0625 mM, b) 0.125 mM, c) 0.25 mM, d) 0.5 mM, e)1.0 mM of octanol solutions.

9.2.1.4 In the Presence of Decanol

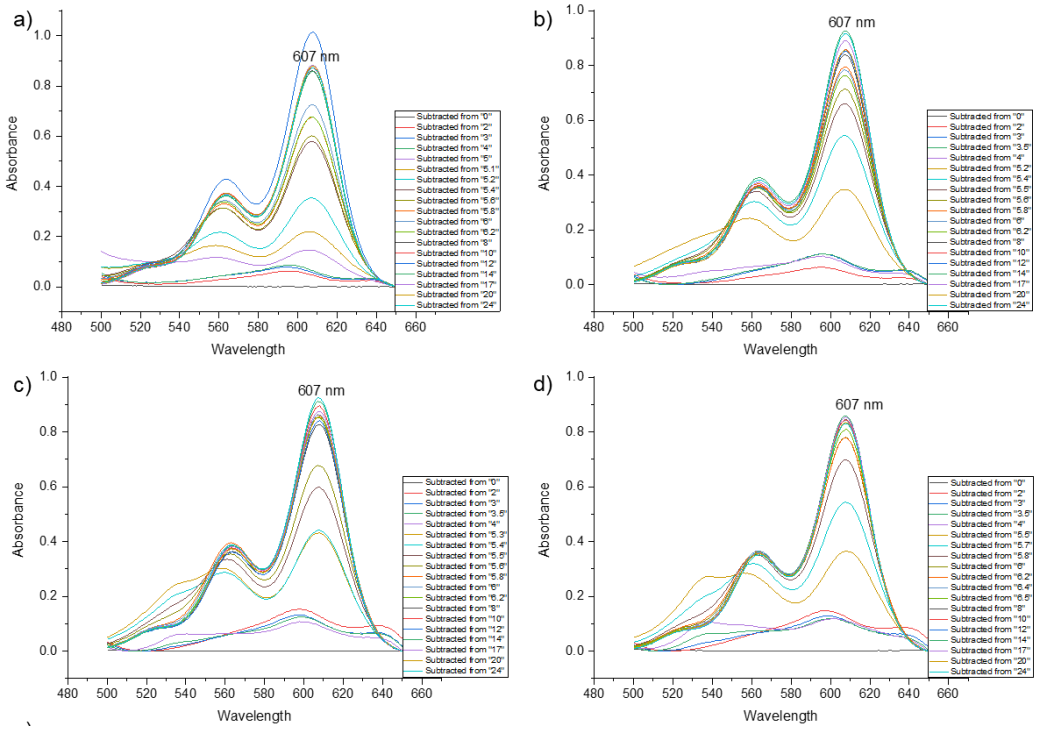

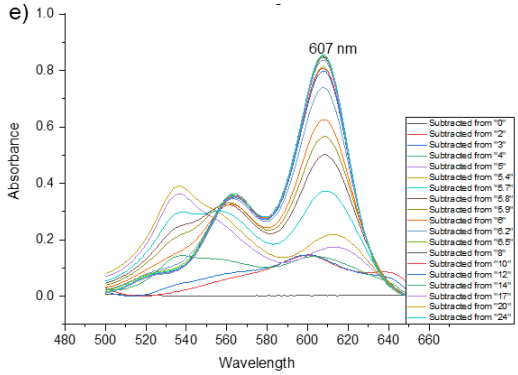

Figure 9-19: Determination of the (λ_{max}) of pinacyanol chloride in the presence of a range of SDS concentrations: a) 0.0625 mM, b) 0.125 mM, c) 0.25 mM, d) 0.5 mM, e)1.0 mM of decanol solutions.

9.2.1.5 In the Presence of Dodecanol

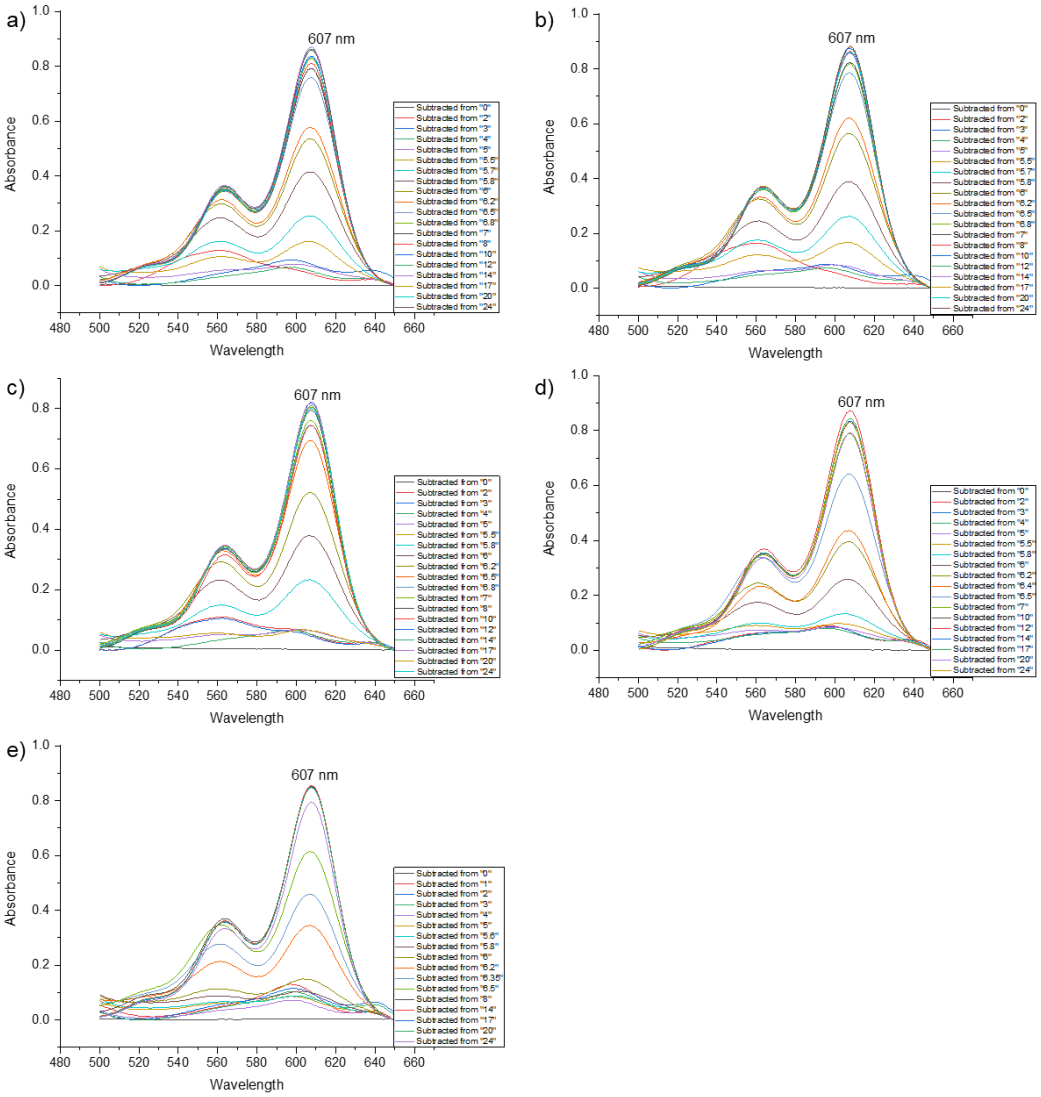

Figure 9-20: Determination of the (λ_{max}) of pinacyanol chloride in the presence of a range of SDS concentrations: a) 0.0625 mM, b) 0.125 mM, c) 0.25 mM, d) 0.5 mM, e)1.0 mM of dodecanol solutions.

9.2.2 Spectrophotometric Investigation of the Critical Micelle Concentration (CMC) of Sodium Dodecyl Sulphate (SDS) with Alcohol in SHG Phase

9.2.2.1 In the Presence of Ethanol

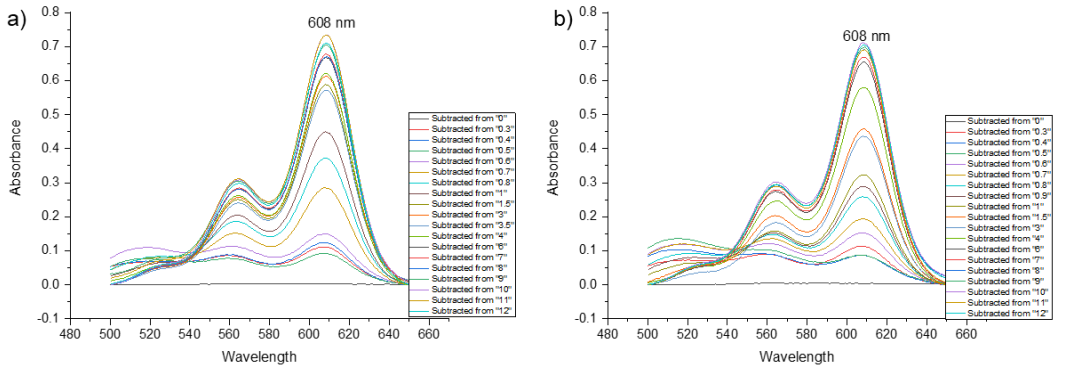

Figure 9-21: Determination of the (λ_{max}) of pinacyanol chloride in the presence of a range of SDS concentrations: a) 0.14 M, b) 1.1 M of ethanol solutions.

9.2.2.2 In the Presence of Hexanol

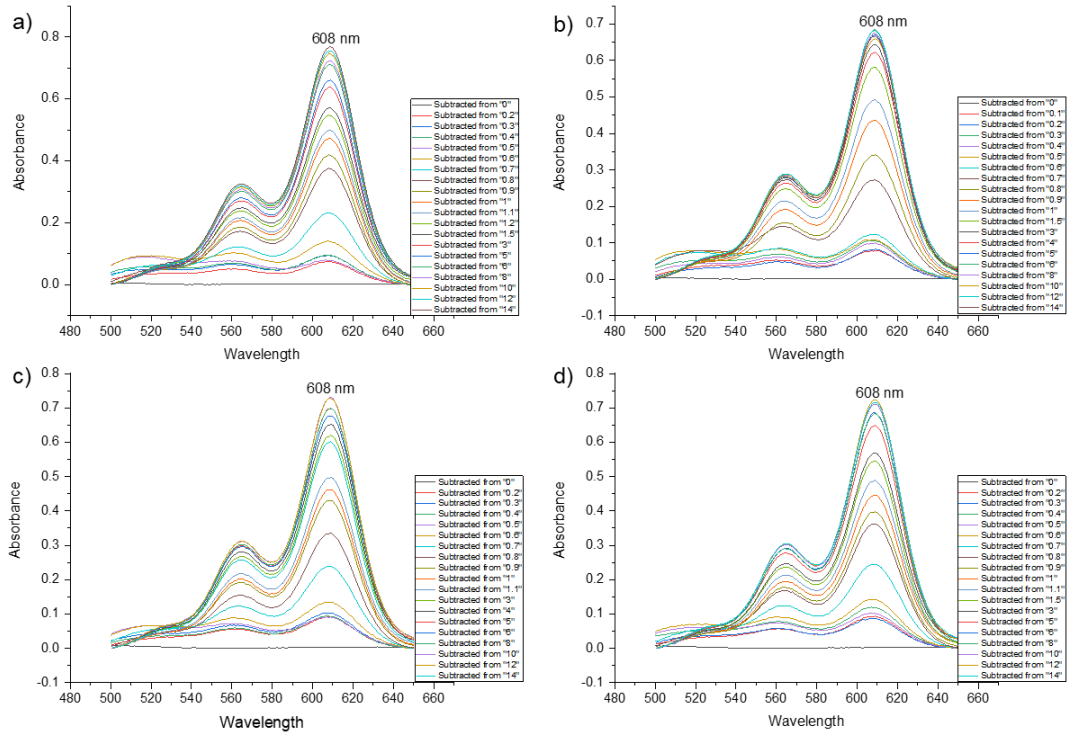

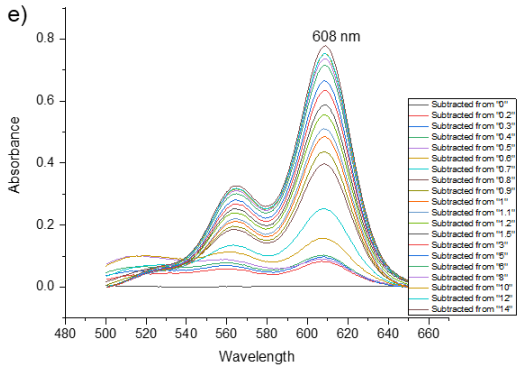

Figure 9-22: Determination of the (λ_{max}) of pinacyanol chloride in the presence of a range of SDS concentrations: a) 0.0625 mM, b) 0.125 mM, c) 0.25 mM, d) 0.5 mM, e)1.0 mM of hexanol solutions.

9.2.2.3 In the Presence of Octanol

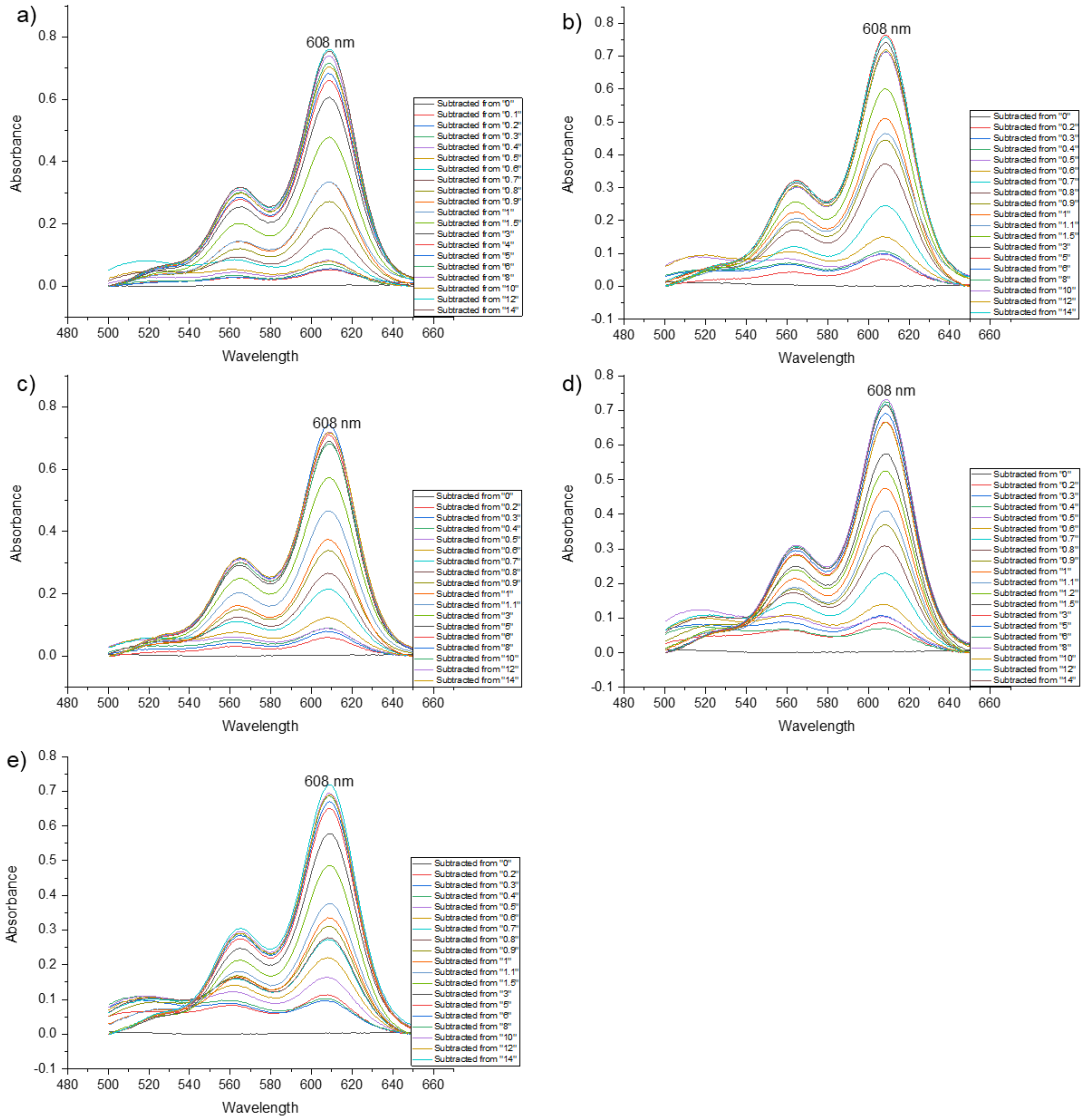

Figure 9-23: Determination of the (λ_{max}) of pinacyanol chloride in the presence of a range of SDS concentrations: a) 0.0625 mM, b) 0.125 mM, c) 0.25 mM, d) 0.5 mM, e)1.0 mM of octanol solutions.

9.2.2.4 In the Presence of Decanol

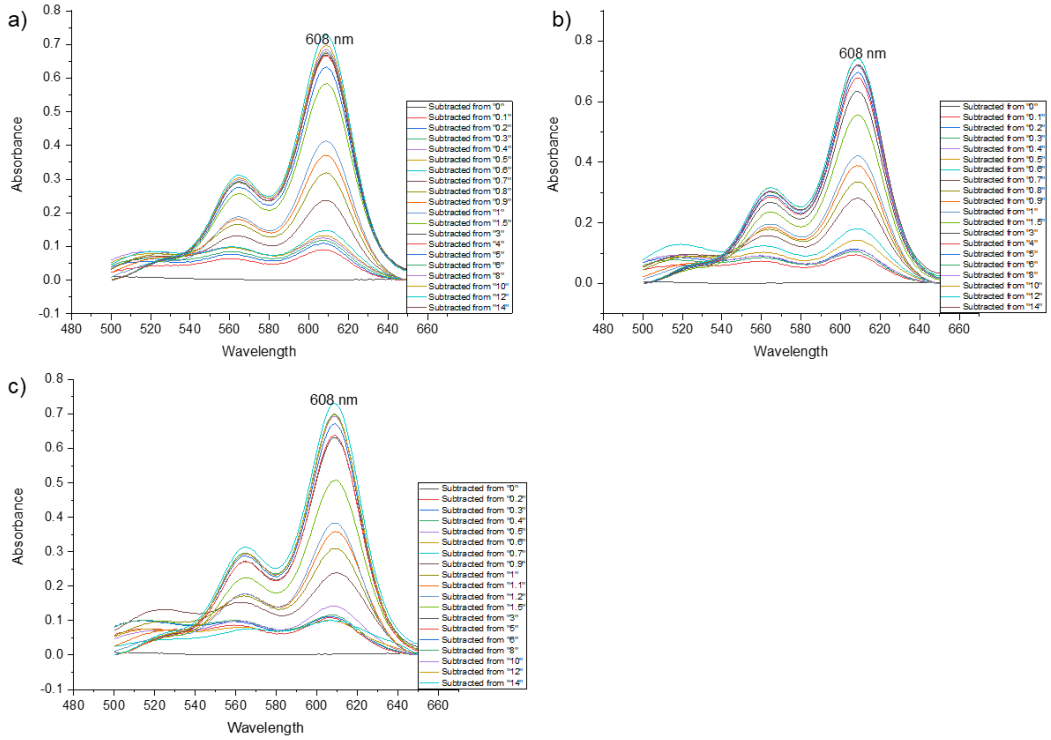

Figure 9-24: Determination of the (λ_{max}) of pinacyanol chloride in the presence of a range of SDS concentrations: a) 0.0625 mM, b) 0.125 mM, c) 0.25 mM of decanol solutions.

9.2.2.5 In the Presence of Dodecanol

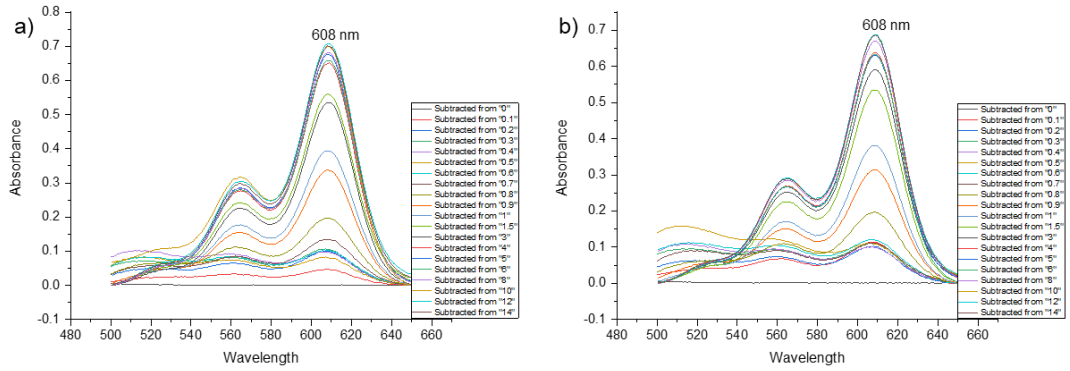

Figure 9-25: Determination of the (λ_{max}) of pinacyanol chloride in the presence of a range of SDS concentrations: a) 0.0625 mM, b) 0.125 mM, of dodecanol solutions.

9.2.3 Fitting Equations for CMC Measurements of Alcohols (Left cell represent vertical fitted line, right cell represent horizontal fitted line) for each concentration.

1. 0.14 M Ethanol

Equation	y = a + b*x
Plot	B
Weight	Instrumental (=1/ei^2)
Intercept	-3.98802 ± 0.17891
Slope	0.71232 ± 0.02781
Residual Sum of Squares	6.32366
Pearson's r	0.99772
R-Square (COD)	0.99545
Adj. R-Square	0.99393

Equation	y = a + b*x
Plot	B
Weight	Instrumental (=1/ei^2)
Intercept	0.81412 ± 0.01227
Slope	0.00112 ± 9.17804E-4
Residual Sum of Squares	1.33855
Pearson's r	0.65495
R-Square (COD)	0.42896
Adj. R-Square	0.14344

2. 0.4 M Ethanol

Equation	y = a + b*x
Plot	B
Weight	Instrumental (=1/ei^2)
Intercept	-2.24518 ± 0.21905
Slope	0.48709 ± 0.03938
Residual Sum of Squares	772.96551
Pearson's r	0.98718
R-Square (COD)	0.97452
Adj. R-Square	0.96815

Equation	y = a + b*x
Plot	B
Weight	Instrumental (=1/ei^2)
Intercept	0.78219 ± 0.01119
Slope	0.00442 ± 0.00125
Residual Sum of Squares	3.24272
Pearson's r	0.87047
R-Square (COD)	0.75771
Adj. R-Square	0.69714

3. 0.6 M Ethanol

Equation	y = a + b*x
Plot	B
Weight	Instrumental (=1/ei^2)
Intercept	-3.19121 ± 0.24612
Slope	0.68165 ± 0.04778
Residual Sum of Squares	18.70061
Pearson's r	0.99755
R-Square (COD)	0.99511
Adj. R-Square	0.99022

Equation	y = a + b*x
Plot	B
Weight	Instrumental (=1/ei^2)
Intercept	0.85447 ± 0.01307
Slope	-5.19656E-4 ± 0.00115
Residual Sum of Squares	8.97114
Pearson's r	-0.25259
R-Square (COD)	0.0638
Adj. R-Square	-0.24826

4. 0.9 M Ethanol

Equation	y = a + b*x
Plot	B
Weight	Instrumental (=1/ei^2)
Intercept	-2.51663 ± 0.50255
Slope	0.56863 ± 0.09481
Residual Sum of Squares	31.44233
Pearson's r	0.97331
R-Square (COD)	0.94733
Adj. R-Square	0.921

Equation	y = a + b*x
Plot	B
Weight	Instrumental (=1/ei^2)
Intercept	0.83462 ± 0.01546
Slope	0.00103 ± 0.00125
Residual Sum of Squares	1.51244
Pearson's r	0.42963
R-Square (COD)	0.18458
Adj. R-Square	-0.08722

5. 1.1 M Ethanol

Equation	y = a + b*x
Plot	B
Weight	Instrumental (=1/ei^2)
Intercept	-2.52853 ± 0.48129
Slope	0.58525 ± 0.09259
Residual Sum of Squares	14.77898
Pearson's r	0.97587
R-Square (COD)	0.95233
Adj. R-Square	0.92849

Equation	y = a + b*x
Plot	B
Weight	Instrumental (=1/ei^2)
Intercept	0.88166 ± 0.01786
Slope	0.00327 ± 0.00136
Residual Sum of Squares	0.44429
Pearson's r	0.81168
R-Square (COD)	0.65882
Adj. R-Square	0.54509

6. 1.3 M Ethanol

Equation	y = a + b*x
Plot	B
Weight	Instrumental (=1/ei^2)
Intercept	-3.77266 ± 0.49507
Slope	0.62214 ± 0.07849
Residual Sum of Squares	0.56587
Pearson's r	0.98445
R-Square (COD)	0.96914
Adj. R-Square	0.95372

Equation	y = a + b*x
Plot	B
Weight	Instrumental (=1/ei^2)
Intercept	0.68307 ± 0.02336
Slope	0.00867 ± 0.00146
Residual Sum of Squares	0.48122
Pearson's r	0.95988
R-Square (COD)	0.92137
Adj. R-Square	0.89516

7. 0.0625 mM Hexanol

Equation	y = a + b*x
Plot	B
Weight	Instrumental (=1/ei^2)
Intercept	-2.38142 ± 0.08697
Slope	0.43423 ± 0.01491
Residual Sum of Squares	0.42016
Pearson's r	0.99824
R-Square (COD)	0.99648
Adj. R-Square	0.9953

Equation	y = a + b*x
Plot	B
Weight	Instrumental (=1/ei^2)
Intercept	0.83672 ± 0.00532
Slope	3.24117E-4 ± 3.52622E-4
Residual Sum of Squares	5.60178
Pearson's r	0.38019
R-Square (COD)	0.14455
Adj. R-Square	-0.02654

8. 0.125 mM Hexanol

Equation	y = a + b*x
Plot	B
Weight	Instrumental (=1/ei^2)
Intercept	-3.39549 ± 0.19419
Slope	0.62039 ± 0.03202
Residual Sum of Squares	24.64508
Pearson's r	0.99471
R-Square (COD)	0.98945
Adj. R-Square	0.98682

Equation	y = a + b*x
Plot	B
Weight	Instrumental (=1/ei^2)
Intercept	0.83037 ± 0.00441
Slope	9.24559E-4 ± 2.95635E-4
Residual Sum of Squares	4.10578
Pearson's r	0.84246
R-Square (COD)	0.70973
Adj. R-Square	0.63717

9. 0.25 mM Hexanol

Equation	y = a + b*x
Plot	B
Weight	Instrumental (=1/ei^2)
Intercept	-2.81129 ± 0.14608
Slope	0.52028 ± 0.02546
Residual Sum of Squares	0.19785
Pearson's r	0.99761
R-Square (COD)	0.99524
Adj. R-Square	0.99285

Equation	y = a + b*x
Plot	B
Weight	Instrumental (=1/ei^2)
Intercept	0.8236 ± 0.02511
Slope	8.10156E-4 ± 0.00135
Residual Sum of Squares	3.35649
Pearson's r	0.28645
R-Square (COD)	0.08205
Adj. R-Square	-0.14743

10. 0.5 mM Hexanol

Equation	y = a + b*x
Plot	B
Weight	Instrumental (=1/ei^2)
Intercept	-2.46401 ± 0.06688
Slope	0.48044 ± 0.01156
Residual Sum of Squares	0.24653
Pearson's r	0.99913
R-Square (COD)	0.99827
Adj. R-Square	0.99769

Equation	y = a + b*x
Plot	B
Weight	Instrumental (=1/ei^2)
Intercept	0.84964 ± 0.02238
Slope	0.00104 ± 0.00155
Residual Sum of Squares	15.62905
Pearson's r	0.35949
R-Square (COD)	0.12923
Adj. R-Square	-0.16102

11. 1.0 mM Hexanol

Equation	y = a + b*x
Plot	B
Weight	Instrumental (=1/ei^2)
Intercept	-6.03028 ± 0.55527
Slope	1.0955 ± 0.09659
Residual Sum of Squares	3.05409
Pearson's r	0.99614
R-Square (COD)	0.99229
Adj. R-Square	0.98457

Equation	y = a + b*x
Plot	B
Weight	Instrumental (=1/ei^2)
Intercept	0.84126 ± 0.00789
Slope	2.08427E-4 ± 6.40784E-4
Residual Sum of Squares	0.26154
Pearson's r	0.14395
R-Square (COD)	0.02072
Adj. R-Square	-0.17513

12. 0.0625 mM Octanol

Equation	y = a + b*x
Plot	B
Weight	Instrumental (=1/ei^2)
Intercept	-3.44527 ± 0.20614
Slope	0.63009 ± 0.03445
Residual Sum of Squares	0.35268
Pearson's r	0.99702
R-Square (COD)	0.99406
Adj. R-Square	0.99108

Equation	y = a + b*x
Plot	B
Weight	Instrumental (=1/ei^2)
Intercept	0.82275 ± 0.00728
Slope	5.37357E-4 ± 4.35254E-4
Residual Sum of Squares	62.06502
Pearson's r	0.48334
R-Square (COD)	0.23362
Adj. R-Square	0.08035

13. 0.125 mM Octanol

Equation	y = a + b*x
Plot	B
Weight	Instrumental (=1/ei^2)
Intercept	-3.19001 ± 0.30484
Slope	0.5934 ± 0.0529
Residual Sum of Squares	6.56695
Pearson's r	0.99215
R-Square (COD)	0.98436
Adj. R-Square	0.97653

Equation	y = a + b*x
Plot	B
Weight	Instrumental (=1/ei^2)
Intercept	0.831 ± 0.01056
Slope	7.29794E-4 ± 7.94809E-4
Residual Sum of Squares	6.13573
Pearson's r	0.46838
R-Square (COD)	0.21938
Adj. R-Square	-0.04083

14. 0.25 mM Octanol

Equation	y = a + b*x
Plot	B
Weight	Instrumental (=1/ei^2)
Intercept	-2.48455 ± 0.28541
Slope	0.49248 ± 0.05127
Residual Sum of Squares	0.28824
Pearson's r	0.98934
R-Square (COD)	0.97879
Adj. R-Square	0.96818

Equation	y = a + b*x
Plot	B
Weight	Instrumental (=1/ei^2)
Intercept	0.79552 ± 0.00883
Slope	0.0032 ± 6.39911E-4
Residual Sum of Squares	13.08108
Pearson's r	0.91292
R-Square (COD)	0.83342
Adj. R-Square	0.8001

15. 0.5 mM Octanol

Equation	y = a + b*x
Plot	B
Weight	Instrumental (=1/ei^2)
Intercept	-2.90442 ± 0.19073
Slope	0.62358 ± 0.03468
Residual Sum of Squares	0.83391
Pearson's r	0.99692
R-Square (COD)	0.99385
Adj. R-Square	0.99078

Equation	y = a + b*x
Plot	B
Weight	Instrumental (=1/ei^2)
Intercept	0.81691 ± 0.00714
Slope	0.00165 ± 4.40467E-4
Residual Sum of Squares	4.69975
Pearson's r	0.85865
R-Square (COD)	0.73728
Adj. R-Square	0.68473

16. 1.0 mM Octanol

Equation	y = a + b*x
Plot	B
Weight	Instrumental (=1/ei^2)
Intercept	-3.10165 ± 0.3074
Slope	0.70864 ± 0.06003
Residual Sum of Squares	0.69061
Pearson's r	0.9929
R-Square (COD)	0.98585
Adj. R-Square	0.97878

Equation	y = a + b*x
Plot	B
Weight	Instrumental (=1/ei^2)
Intercept	0.85175 ± 0.01607
Slope	-5.59168E-4 ± 8.80364E-4
Residual Sum of Squares	1.46213
Pearson's r	-0.27324
R-Square (COD)	0.07466
Adj. R-Square	-0.11041

17. 0.0625 mM Decanol

Equation	y = a + b*x
Plot	B
Weight	Instrumental (=1/ei^2)
Intercept	-6.34331 ± 0.68034
Slope	1.28831 ± 0.13079
Residual Sum of Squares	2.98308
Pearson's r	0.99489
R-Square (COD)	0.9898
Adj. R-Square	0.9796

Equation	y = a + b*x
Plot	B
Weight	Instrumental (=1/ei^2)
Intercept	0.85406 ± 0.00655
Slope	8.79991E-4 ± 3.91343E-4
Residual Sum of Squares	3.97552
Pearson's r	0.70909
R-Square (COD)	0.5028
Adj. R-Square	0.40337

18. 0.125 mM Decanol

Equation	y = a + b*x
Plot	B
Weight	Instrumental (=1/ei^2)
Intercept	-5.01297 ± 0.06685
Slope	1.03316 ± 0.01232
Residual Sum of Squares	0.06862
Pearson's r	0.99993
R-Square (COD)	0.99986
Adj. R-Square	0.99972

Equation	y = a + b*x
Plot	B
Weight	Instrumental (=1/ei^2)
Intercept	0.79362 ± 0.03022
Slope	0.0044 ± 0.00157
Residual Sum of Squares	199.67625
Pearson's r	0.81448
R-Square (COD)	0.66338
Adj. R-Square	0.57923

19. 0.25 mM Decanol

Equation	y = a + b*x
Plot	B
Weight	Instrumental (=1/ei^2)
Intercept	-6.53408 ± 1.46708
Slope	1.29416 ± 0.27067
Residual Sum of Squares	23.51153
Pearson's r	0.95893
R-Square (COD)	0.91955
Adj. R-Square	0.87933

Equation	y = a + b*x
Plot	B
Weight	Instrumental (=1/ei^2)
Intercept	0.87144 ± 0.01308
Slope	0.00216 ± 9.09641E-4
Residual Sum of Squares	13.70086
Pearson's r	0.72725
R-Square (COD)	0.52889
Adj. R-Square	0.43466

20. 0.5 mM Decanol

Equation	y = a + b*x
Plot	B
Weight	Instrumental (=1/ei^2)
Intercept	-5.44506 ± 0.19971
Slope	1.05697 ± 0.03553
Residual Sum of Squares	0.36613
Pearson's r	0.99944
R-Square (COD)	0.99887
Adj. R-Square	0.99774

Equation	y = a + b*x
Plot	B
Weight	Instrumental (=1/ei^2)
Intercept	0.84896 ± 0.0119
Slope	3.33043E-4 ± 7.34768E-4
Residual Sum of Squares	2.18078
Pearson's r	0.19866
R-Square (COD)	0.03947
Adj. R-Square	-0.15264

21. 1.0 mM Decanol

Equation	y = a + b*x
Plot	B
Weight	Instrumental (=1/ei^2)
Intercept	-6.64948 ± 1.09619
Slope	1.23109 ± 0.19216
Residual Sum of Squares	4.00798
Pearson's r	0.98804
R-Square (COD)	0.97622
Adj. R-Square	0.95243

Equation	y = a + b*x
Plot	B
Weight	Instrumental (=1/ei^2)
Intercept	0.85285 ± 0.00432
Slope	-6.92144E-5 ± 3.27807E-4
Residual Sum of Squares	4.91848
Pearson's r	-0.09401
R-Square (COD)	0.00884
Adj. R-Square	-0.18939

22. 0.0625 mM Dodecanol

Equation	y = a + b*x
Plot	B
Weight	Instrumental (=1/ei^2)
Intercept	-4.42655 ± 0.64711
Slope	0.82548 ± 0.11156
Residual Sum of Squares	58.05796
Pearson's r	0.98222
R-Square (COD)	0.96476
Adj. R-Square	0.94714

Equation	y = a + b*x
Plot	B
Weight	Instrumental (=1/ei^2)
Intercept	0.82253 ± 0.01943
Slope	0.00161 ± 0.00132
Residual Sum of Squares	3369.99734
Pearson's r	0.47858
R-Square (COD)	0.22904
Adj. R-Square	0.07485

23. 0.125 mM Dodecanol

Equation	y = a + b*x
Plot	aBSORBANCE
Weight	Instrumental (=1/ei^2)
Intercept	-5.05314 ± 0.8707
Slope	0.93453 ± 0.15183
Residual Sum of Squares	275.08679
Pearson's r	0.9746
R-Square (COD)	0.94985
Adj. R-Square	0.92478

Equation	y = a + b*x
Plot	aBSORBANCE
Weight	Instrumental (=1/ei^2)
Intercept	0.82802 ± 0.0248
Slope	0.00221 ± 0.00174
Residual Sum of Squares	271.9377
Pearson's r	0.49351
R-Square (COD)	0.24355
Adj. R-Square	0.09226

24. 0.25 mM Dodecanol

Equation	y = a + b*x
Plot	B
Weight	Instrumental (=1/ei^2)
Intercept	-3.50526 ± 0.08912
Slope	0.64917 ± 0.01619
Residual Sum of Squares	10.91014
Pearson's r	0.99938
R-Square (COD)	0.99876
Adj. R-Square	0.99814

Equation	y = a + b*x
Plot	B
Weight	Instrumental (=1/ei^2)
Intercept	0.79468 ± 0.01891
Slope	0.00119 ± 0.00147
Residual Sum of Squares	457.34428
Pearson's r	0.37461
R-Square (COD)	0.14033
Adj. R-Square	-0.07458

25. 0.5 mM Dodecanol

Equation	y = a + b*x
Plot	B
Weight	Instrumental (=1/ei^2)
Intercept	-4.10669 ± 0.44479
Slope	0.7306 ± 0.06866
Residual Sum of Squares	6.04359
Pearson's r	0.99128
R-Square (COD)	0.98264
Adj. R-Square	0.97396

Equation	y = a + b*x
Plot	B
Weight	Instrumental (=1/ei^2)
Intercept	0.83368 ± 0.0098
Slope	-3.0959E-4 ± 5.99362E-4
Residual Sum of Squares	2.06817
Pearson's r	-0.34308
R-Square (COD)	0.1177
Adj. R-Square	-0.32345

26. 1.0 mM Dodecanol

Equation	y = a + b*x
Plot	B
Weight	Instrumental (=1/ei^2)
Intercept	0.91203 ± 0.01411
Slope	-0.004 ± 9.99558E-4
Residual Sum of Squares	1.17734
Pearson's r	-0.94298
R-Square (COD)	0.88921
Adj. R-Square	0.83382

Equation	y = a + b*x
Plot	B
Weight	Instrumental (=1/ei^2)
Intercept	0.8507 ± 0.01047
Slope	3.16905E-4 ± 7.90946E-4
Residual Sum of Squares	13.18902
Pearson's r	0.22537
R-Square (COD)	0.05079
Adj. R-Square	-0.26561

27. 0.4 M Ethanol

Equation	y = a + b*x
Plot	B
Weight	Instrumental (=1/ei^2)
Intercept	-0.24168 ± 0.10419
Slope	0.69736 ± 0.12629
Residual Sum of Squares	54.26652
Pearson's r	0.96873
R-Square (COD)	0.93844
Adj. R-Square	0.90766

Equation	y = a + b*x
Plot	B
Weight	Instrumental (=1/ei^2)
Intercept	0.5702 ± 0.02638
Slope	0.01388 ± 0.00319
Residual Sum of Squares	24.91432
Pearson's r	0.87171
R-Square (COD)	0.75988
Adj. R-Square	0.71986

28. 1.1 M Ethanol

Equation	y = a + b*x
Plot	B
Weight	Instrumental (=1/ei^2)
Intercept	-0.14073 ± 0.03073
Slope	0.47481 ± 0.03884
Residual Sum of Squares	2.08033
Pearson's r	0.99338
R-Square (COD)	0.9868
Adj. R-Square	0.9802

Equation	y = a + b*x
Plot	B
Weight	Instrumental (=1/ei^2)
Intercept	0.63796 ± 0.01299
Slope	0.00555 ± 0.00127
Residual Sum of Squares	31.51806
Pearson's r	0.89045
R-Square (COD)	0.79291
Adj. R-Square	0.75149

29. 0.0625 mM Hexanol (SHG)

Equation	y = a + b*x
Plot	B
Weight	Instrumental (=1/ei^2)
Intercept	-0.37008 ± 0.09314
Slope	0.86536 ± 0.11915
Residual Sum of Squares	107.68283
Pearson's r	0.97272
R-Square (COD)	0.94619
Adj. R-Square	0.92825

Equation	y = a + b*x
Plot	B
Weight	Instrumental (=1/ei^2)
Intercept	0.66388 ± 0.00106
Slope	0.00741 ± 1.03146E-4
Residual Sum of Squares	0.80051
Pearson's r	0.99971
R-Square (COD)	0.99942
Adj. R-Square	0.99923

30. 0.125 mM Hexanol (SHG)

Equation	y = a + b*x
Plot	B
Weight	Instrumental (=1/ei^2)
Intercept	-0.43665 ± 0.04993
Slope	0.96221 ± 0.06193
Residual Sum of Squares	22.63653
Pearson's r	0.99384
R-Square (COD)	0.98772
Adj. R-Square	0.98363

Equation	y = a + b*x
Plot	B
Weight	Instrumental (=1/ei^2)
Intercept	0.62126 ± 0.00577
Slope	0.00526 ± 0.00107
Residual Sum of Squares	8.14309
Pearson's r	0.8949
R-Square (COD)	0.80085
Adj. R-Square	0.76766

31. mM Hexanol (SHG)

Equation	y = a + b*x
Plot	B
Weight	Instrumental (=1/ei^2)
Intercept	-0.40817 ± 0.05533
Slope	0.91551 ± 0.07229
Residual Sum of Squares	62.88472
Pearson's r	0.99078
R-Square (COD)	0.98164
Adj. R-Square	0.97552

Equation	y = a + b*x
Plot	B
Weight	Instrumental (=1/ei^2)
Intercept	0.65673 ± 0.0115
Slope	0.00462 ± 0.0015
Residual Sum of Squares	1.68011
Pearson's r	0.8088
R-Square (COD)	0.65416
Adj. R-Square	0.585

32. 0.5 mM Hexanol (SHG)

Equation	y = a + b*x
Plot	B
Weight	Instrumental (=1/ei^2)
Intercept	-0.47466 ± 0.03197
Slope	1.02796 ± 0.0508
Residual Sum of Squares	1.62924
Pearson's r	0.99878
R-Square (COD)	0.99756
Adj. R-Square	0.99513

Equation	y = a + b*x
Plot	B
Weight	Instrumental (=1/ei^2)
Intercept	0.65725 ± 0.00417
Slope	0.00424 ± 3.40319E-4
Residual Sum of Squares	1.11328
Pearson's r	0.99048
R-Square (COD)	0.98105
Adj. R-Square	0.97474

33. 1.0 mM Hexanol (SHG)

Equation	y = a + b*x
Plot	B
Weight	Instrumental (=1/ei^2)
Intercept	-0.44328 ± 0.10154
Slope	0.99729 ± 0.13985
Residual Sum of Squares	43.57752
Pearson's r	0.9809
R-Square (COD)	0.96216
Adj. R-Square	0.94324

Equation	y = a + b*x
Plot	B
Weight	Instrumental (=1/ei^2)
Intercept	0.68103 ± 0.01092
Slope	0.0063 ± 0.001
Residual Sum of Squares	4.68709
Pearson's r	0.96416
R-Square (COD)	0.9296
Adj. R-Square	0.90613

34.0.0625 mM Octanol (SHG)

Equation	y = a + b*x
Plot	B
Weight	Instrumental (=1/ei^2)
Intercept	-0.32896 ± 0.03951
Slope	0.739 ± 0.04542
Residual Sum of Squares	5.32178
Pearson's r	0.99624
R-Square (COD)	0.9925
Adj. R-Square	0.98875

Equation	y = a + b*x
Plot	B
Weight	Instrumental (=1/ei^2)
Intercept	0.6463 ± 0.01681
Slope	0.00806 ± 0.00208
Residual Sum of Squares	33.50497
Pearson's r	0.86663
R-Square (COD)	0.75105
Adj. R-Square	0.70126

35. 0.125 mM Octanol (SHG)

Equation	y = a + b*x
Plot	B
Weight	Instrumental (=1/ei^2)
Intercept	-0.46845 ± 0.05433
Slope	1.02263 ± 0.07381
Residual Sum of Squares	4.89438
Pearson's r	0.99483
R-Square (COD)	0.98969
Adj. R-Square	0.98453

Equation	y = a + b*x
Plot	B
Weight	Instrumental (=1/ei^2)
Intercept	0.72347 ± 0.04168
Slope	-3.99367E-4 ± 0.00659
Residual Sum of Squares	31.78308
Pearson's r	-0.03027
R-Square (COD)	9.16362E-4
Adj. R-Square	-0.24885

36. 0.25 mM Octanol (SHG)

Equation	y = a + b*x
Plot	B
Weight	Instrumental (=1/ei^2)
Intercept	-0.31641 ± 0.05163
Slope	0.72573 ± 0.07242
Residual Sum of Squares	1.95821
Pearson's r	0.99506
R-Square (COD)	0.99014
Adj. R-Square	0.98028

Equation	y = a + b*x
Plot	B
Weight	Instrumental (=1/ei^2)
Intercept	0.64896 ± 0.01457
Slope	0.00757 ± 0.00196
Residual Sum of Squares	3.32803
Pearson's r	0.88782
R-Square (COD)	0.78822
Adj. R-Square	0.73528

37. 0.5 mM Octanol (SHG)

Equation	y = a + b*x
Plot	B
Weight	Instrumental (=1/ei^2)
Intercept	-0.32328 ± 0.02081
Slope	0.75863 ± 0.02984
Residual Sum of Squares	0.93269
Pearson's r	0.99846
R-Square (COD)	0.99691
Adj. R-Square	0.99537

Equation	y = a + b*x
Plot	B
Weight	Instrumental (=1/ei^2)
Intercept	0.68714 ± 0.0189
Slope	0.00174 ± 0.00192
Residual Sum of Squares	16.94842
Pearson's r	0.46325
R-Square (COD)	0.2146
Adj. R-Square	-0.0472

38. 1.0 mM Octanol (SHG)

Equation	y = a + b*x
Plot	B
Weight	Instrumental (=1/ei^2)
Intercept	-0.09105 ± 0.05577
Slope	0.50131 ± 0.09243
Residual Sum of Squares	1.01195
Pearson's r	0.98342
R-Square (COD)	0.96712
Adj. R-Square	0.93425

Equation	y = a + b*x
Plot	B
Weight	Instrumental (=1/ei^2)
Intercept	0.61716 ± 0.00975
Slope	0.0072 ± 0.00103
Residual Sum of Squares	9.64111
Pearson's r	0.96152
R-Square (COD)	0.92452
Adj. R-Square	0.90565

39. 0.0625 mM Decanol (SHG)

Equation	y = a + b*x
Plot	B
Weight	Instrumental (=1/ei^2)
Intercept	-0.36053 ± 0.0339
Slope	0.84027 ± 0.05236
Residual Sum of Squares	1.98951
Pearson's r	0.99806
R-Square (COD)	0.99613
Adj. R-Square	0.99227

Equation	y = a + b*x
Plot	B
Weight	Instrumental (=1/ei^2)
Intercept	0.67274 ± 0.04468
Slope	0.00412 ± 0.00378
Residual Sum of Squares	66.57531
Pearson's r	0.43785
R-Square (COD)	0.19171
Adj. R-Square	0.03005

40. 0.125 mM Decanol (SHG)

Equation	y = a + b*x
Plot	B
Weight	Instrumental (=1/ei^2)
Intercept	-0.08375 ± 0.02554
Slope	0.51681 ± 0.03098
Residual Sum of Squares	0.70927
Pearson's r	0.99821
R-Square (COD)	0.99642
Adj. R-Square	0.99284

Equation	y = a + b*x
Plot	B
Weight	Instrumental (=1/ei^2)
Intercept	0.66784 ± 0.01109
Slope	0.0062 ± 0.00145
Residual Sum of Squares	56.26022
Pearson's r	0.8866
R-Square (COD)	0.78605
Adj. R-Square	0.74326

41. 0.25 mM Decanol (SHG)

Equation	y = a + b*x
Plot	B
Weight	Instrumental (=1/ei^2)
Intercept	0.60835 ± 0.024
Slope	0.00829 ± 0.00251
Residual Sum of Squares	23.1976
Pearson's r	0.85568
R-Square (COD)	0.73219
Adj. R-Square	0.66524

Equation	y = a + b*x
Plot	B
Weight	Instrumental (=1/ei^2)
Intercept	-0.41198 ± 0.02501
Slope	0.71443 ± 0.02878
Residual Sum of Squares	0.33204
Pearson's r	0.99919
R-Square (COD)	0.99838
Adj. R-Square	0.99676

42. 0.0625 mM Dodecanol (SHG)

Equation	y = a + b*x
Plot	B
Weight	Instrumental (=1/ei^2)
Intercept	-0.51687 ± 0.08041
Slope	0.91188 ± 0.09244
Residual Sum of Squares	15.24483
Pearson's r	0.98988
R-Square (COD)	0.97986
Adj. R-Square	0.96979

Equation	y = a + b*x
Plot	B
Weight	Instrumental (=1/ei^2)
Intercept	0.64153 ± 0.01078
Slope	0.00452 ± 0.00132
Residual Sum of Squares	12.29969
Pearson's r	0.83678
R-Square (COD)	0.7002
Adj. R-Square	0.64024

43. 0.125 mM Dodecanol (SHG)

Equation	y = a + b*x
Plot	B
Weight	Instrumental (=1/ei^2)
Intercept	-0.60448 ± 0.10007
Slope	0.97072 ± 0.10845
Residual Sum of Squares	0.1841
Pearson's r	0.99382
R-Square (COD)	0.98767
Adj. R-Square	0.97535

Equation	y = a + b*x
Plot	B
Weight	Instrumental (=1/ei^2)
Intercept	0.61191 ± 0.01141
Slope	0.00677 ± 0.00131
Residual Sum of Squares	2.23251
Pearson's r	0.91811
R-Square (COD)	0.84292
Adj. R-Square	0.81151

9.3 Chapter 7 appendix

9.3.1 The Spectra of Light Scattering of 0.5 M SHG in the Presence of Different Concentration of SDS after Baseline Correction

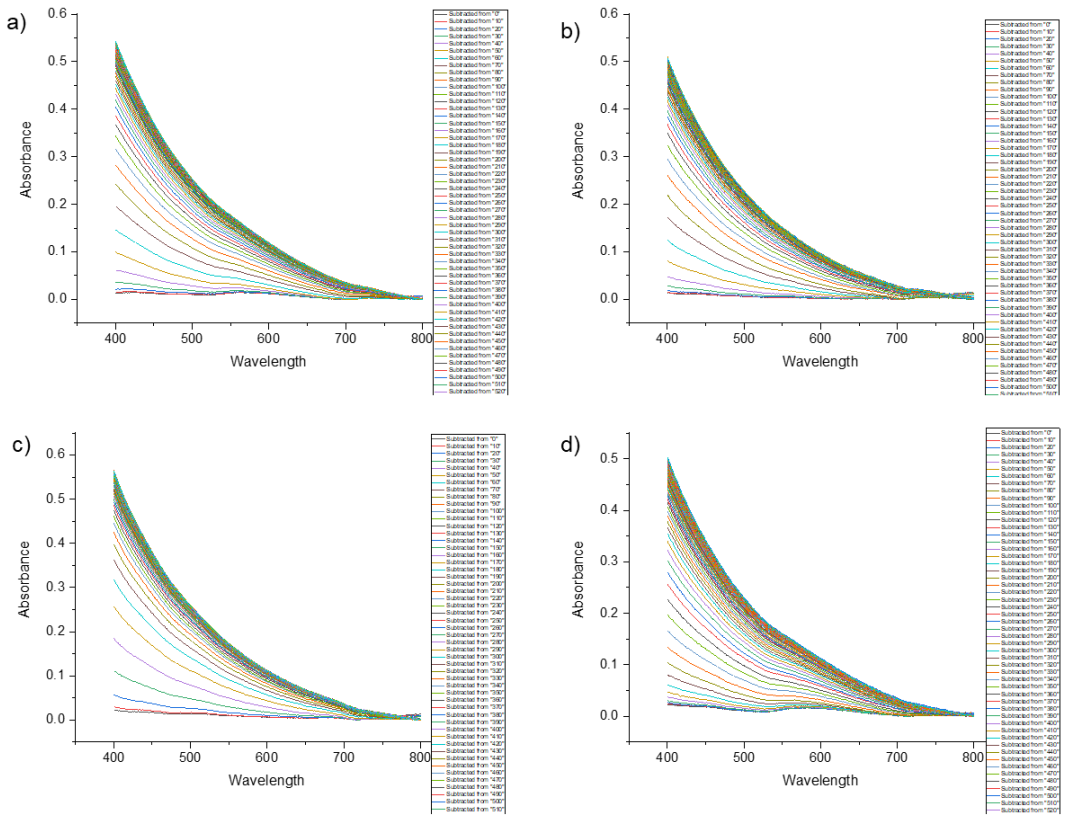

Figure 9-26: Spectra for determining gelation time of 0.5 M SHG in the presence: a) 0.0, b) 3.0 mM, c) 10.0 mM, and d) 18.0 mM SDS.

9.3.2 Error Bar of the UV-Vis Spectre of 0.5 M SHG in the Presence of Different Concentration of SDS for Determining Gelation Time

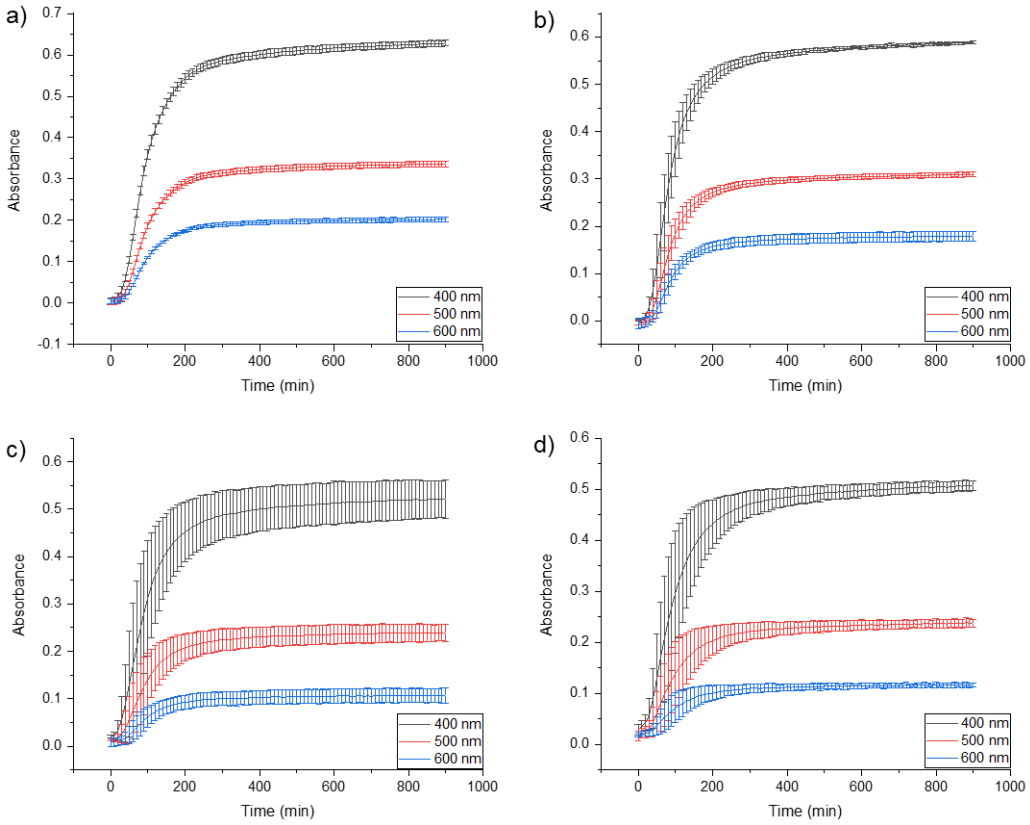

Figure 9-27: Error bar of the UV-Vis spectre at 400, 500, 600 nm for determining gelation time of 0.5 M SHG in the presence of a) 0.0, b) 3.0 mM, c) 10.0 mM, and d) 18.0 mM SDS.

9.3.3 The Spectra of Light Scattering of 0.7 M SHG in the Presence of Different Concentration of SDS after Baseline Correction

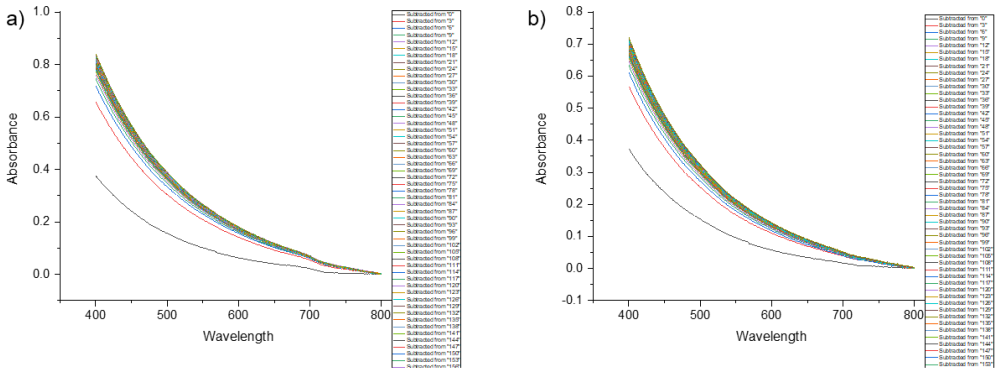

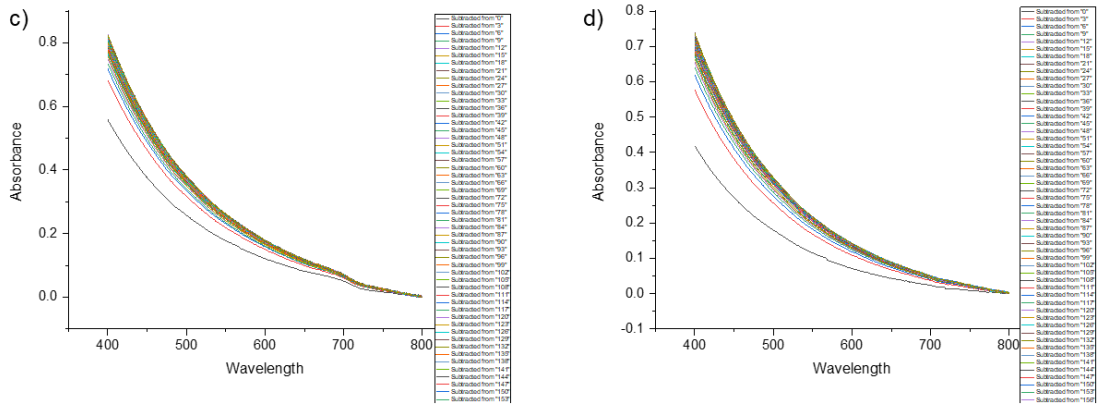

Figure 9-28: Spectra for determining gelation time of 0.7 M SHG in the presence: a) 0.0, b) 3.0 mM, c) 10.0 mM, and d) 18.0 mM SDS.

9.3.4 Error Bar of the UV-Vis Spectre of 0.7 M SHG in the Presence of Different Concentration of SDS for Determining Gelation Time

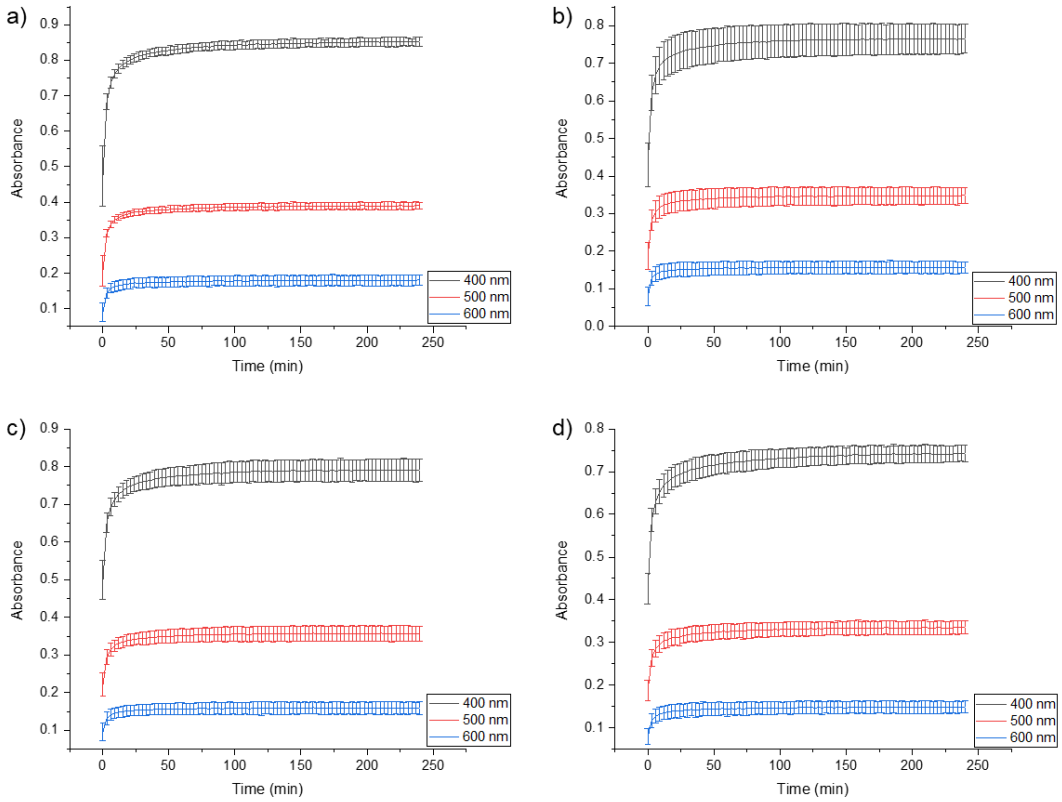

Figure 9-29: Error bar of the UV-Vis spectre at 400, 500, 600 nm for determining gelation time of 0.7 M SHG in the presence of a) 0.0, b) 3.0 mM, c) 10.0 mM, and d) 18.0 mM SDS.

9.3.5 The Spectra of Light scattering of 0.9 M SHG in the Presence of Different Concentration of SDS after Baseline Correction

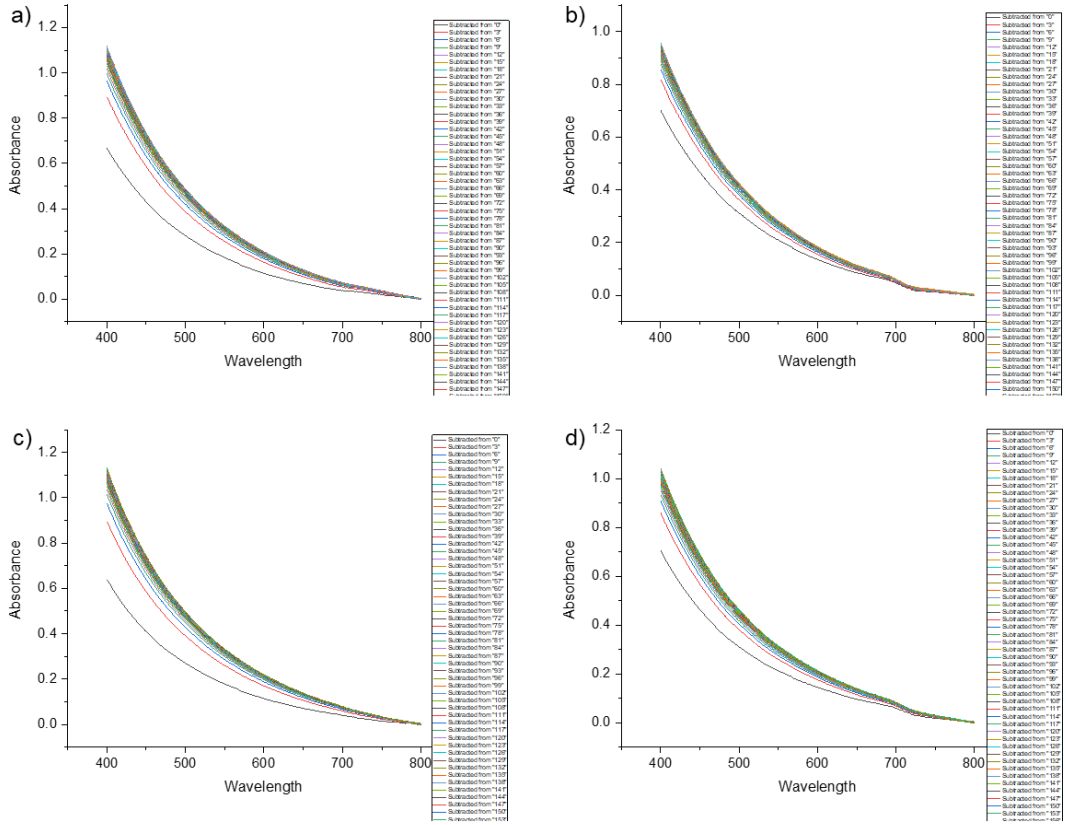

Figure 9-30: Spectra for determining gelation time of 0.9 M SHG in the presence: a) 0.0, b) 3.0 mM, c) 10.0 mM, and d) 18.0 mM SDS.

9.3.6 Error Bar of the UV-vis Spectre of 0.9 M SHG in the Presence of Different Concentration of SDS for Determining Gelation Time

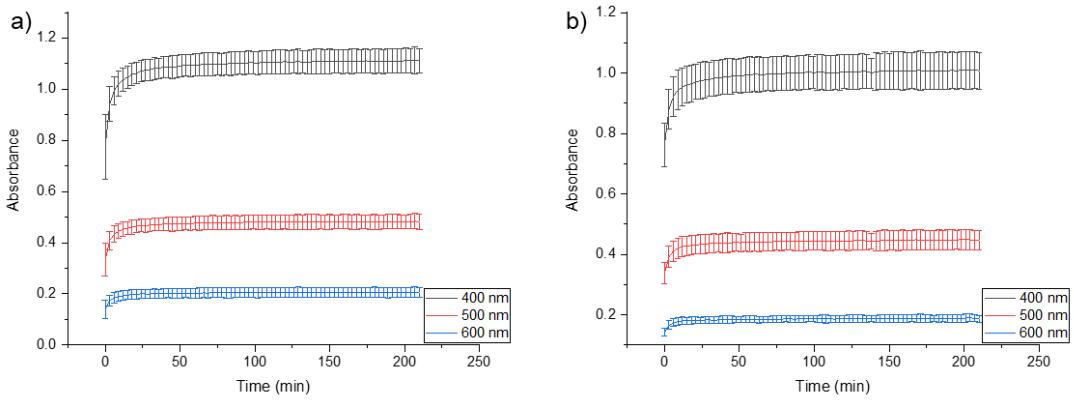

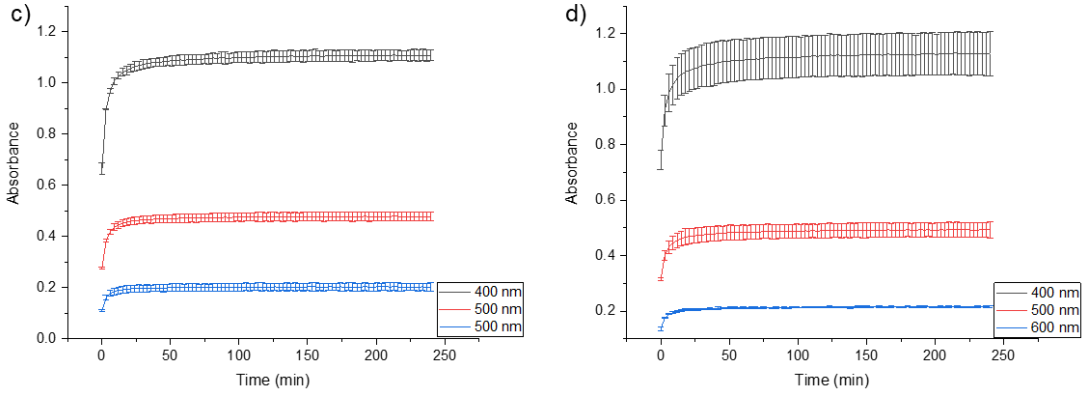

Figure 9-31: Error bar of the UV-Vis spectre at 400, 500, 600 nm for determining gelation time of 0.9 M SHG in the presence of a) 0.0, b) 3.0 mM, c) 10.0 mM, and d) 18.0 mM SDS.

9.3.7 The Spectra of Light scattering of 0.5 M SHG in the Presence of Salts after Baseline Correction

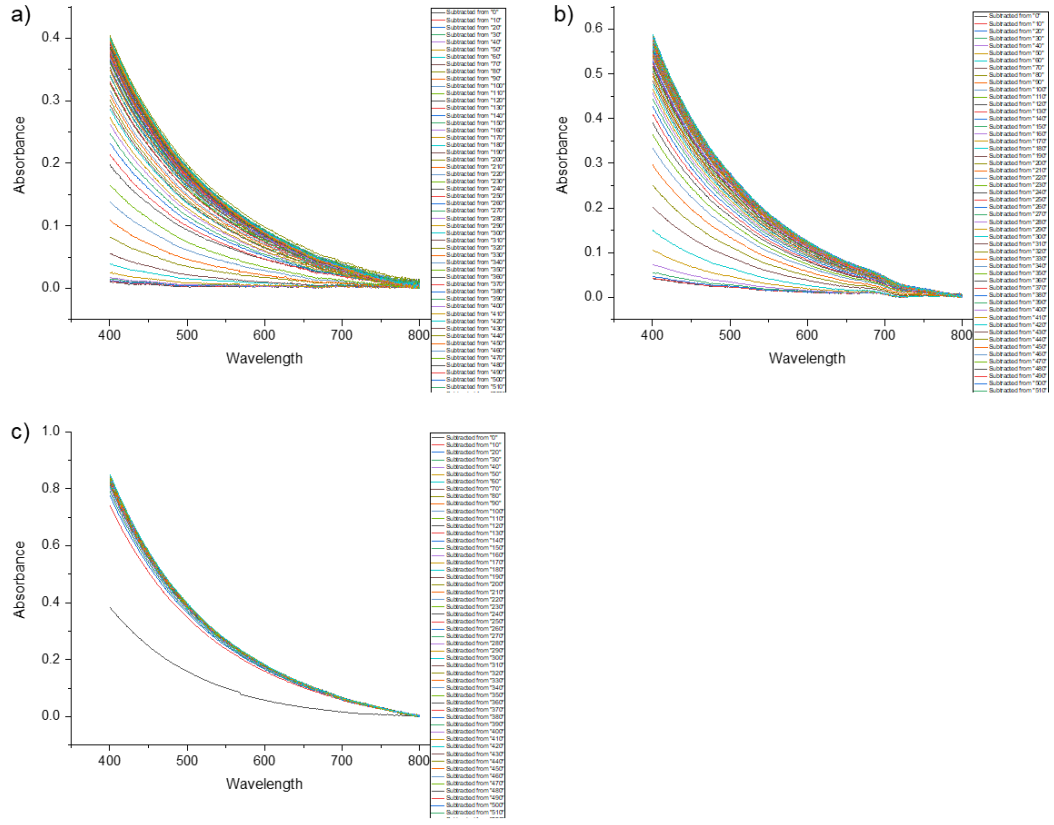

Figure 9-32: Spectra for determining gelation time of 0.5 M SHG in the presence: a) 0.1 M NaCl , b) 0.2 M NaCl, and c) 0.1 M Na_2CO_3.

9.3.8 Error Bar of the UV-Vis Spectre of 0.9 M SHG in the Presence of Different Concentration of SDS for Determining Gelation Time

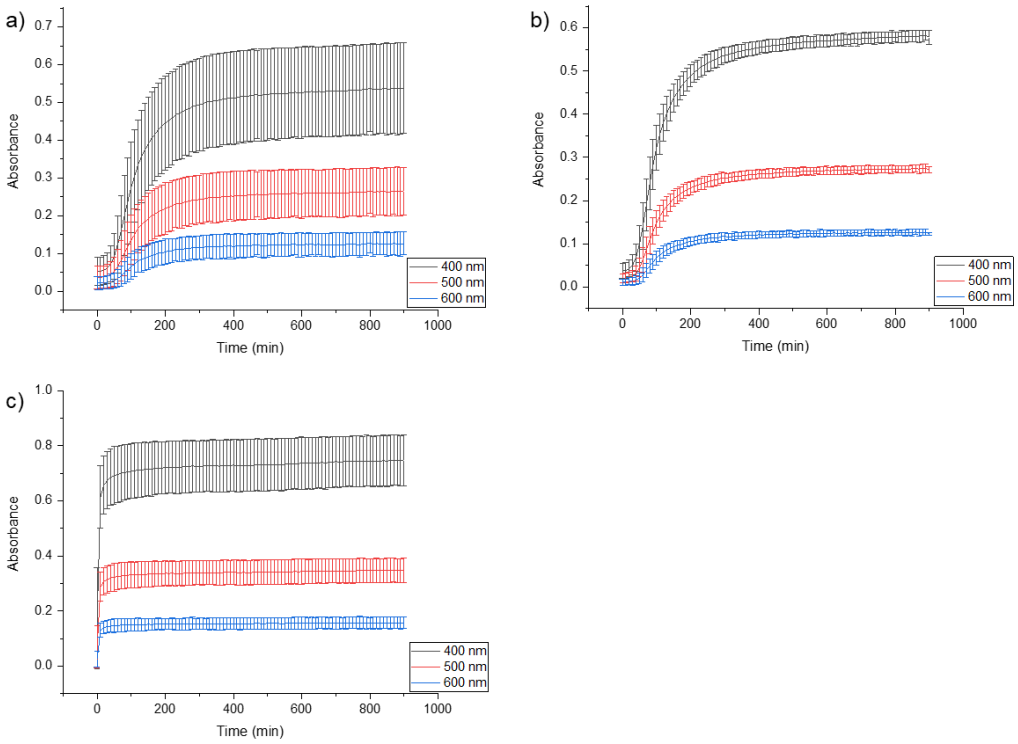

Figure 9-33: Error bar of the UV-Vis spectre at 400, 500, 600 nm for determining gelation time of 0.5 M SHG in the presence: a) 0.1 M NaCl, b) 0.2 M NaCl, and c) 0.1 M Na_2CO_3.

Chapter 10 References

1. Ullah, F., Othman, M.B.H., Javed, F., Ahmad, Z. and Akil, H.M *Classification, processing and application of hydrogels: A review.* Materials Science and Engineering: C, 2015. **57**: pp. 414-433.
2. Chai, Q., Y. Jiao, and X.J.G. Yu, *Hydrogels for biomedical applications: their characteristics and the mechanisms behind them.* 2017. **3**(1): p. 6.
3. Caló, E. and V.V. Khutoryanskiy, *Biomedical applications of hydrogels: A review of patents and commercial products.* European Polymer Journal, 2015. **65**: pp. 252-267.
4. Gorrell, I.B., Henderson, T.W., Albdeery, K., Savage, P.M. and Kee, T.P., *Chemical transformations in proto-cytoplasmic media. Phosphorus coupling in the silica hydrogel phase.* 2017. **7**(4): p. 45.
5. Khan, A., Othman, M.B.H., Razak, K.A. and Akil, H.M., *Synthesis and physicochemical investigation of chitosan-PMAA-based dual-responsive hydrogels.* Journal of Polymer Research, 2013. **20**(10): p. 273.
6. Hamidi, M., A. Azadi, and P. Rafiei, *Hydrogel nanoparticles in drug delivery.* Advanced drug delivery reviews, 2008. **60**(15): pp. 1638-1649.
7. Li, J. and D.J.J.N.R.M. Mooney, *Designing hydrogels for controlled drug delivery.* 2016. **1**(12): pp. 1-17.
8. Donshik, P., Weinstock, F.J., Wechsler, S., Asbell, P., Atwood, J., Davis, H., Farkas, B., Farris, R.L., Gruber, E. and Hartstein, J., *Disposable hydrogel contact lenses for extended wear.* The CLAO journal: official publication of the Contact Lens Association of Ophthalmologists, Inc, 1988. **14**(4): pp. 191-194.
9. Alvarez-Lorenzo, C., Anguiano-Igea, S., Varela-García, A., Vivero-Lopez, M. and Concheiro, A., *Bioinspired hydrogels for drug-eluting contact lenses.* 2019. **84**: pp. 49-62.
10. Saxena, A.K., *Synthetic biodegradable hydrogel (PleuraSeal) sealant for sealing of lung tissue after thoracoscopic resection.* The Journal of thoracic and cardiovascular surgery, 2010. **139**(2): pp. 496-497.
11. Kaihara, S., S. Matsumura, and J.P. Fisher, *Synthesis and characterization of cyclic acetal based degradable hydrogels.* European Journal of Pharmaceutics and Biopharmaceutics, 2008. **68**(1): pp. 67-73.
12. Zhang, L., Li, K., Xiao, W., Zheng, L., Xiao, Y., Fan, H. and Zhang, X., *Preparation of collagen–chondroitin sulfate–hyaluronic acid hybrid hydrogel scaffolds and cell compatibility in vitro.* Carbohydrate polymers, 2011. **84**(1): pp. 118-125.
13. Drury, J.L. and D.J.J.B. Mooney, *Hydrogels for tissue engineering: scaffold design variables and applications.* 2003. **24**(24): pp. 4337-4351.
14. Chen, X., Martin, B.D., Neubauer, T.K., Linhardt, R.J., Dordick, J.S. and Rethwisch, D.G., *Enzymatic and chemoenzymatic approaches to synthesis of sugar-based polymer and hydrogels.* Carbohydrate Polymers, 1995. **28**(1): pp. 15-21.
15. Kashyap, N., N. Kumar, and M.R. Kumar, *Hydrogels for pharmaceutical and biomedical applications.* Critical Reviews™ in Therapeutic Drug Carrier Systems, 2005. **22**(2).
16. Nishida, K., Yamato, M., Hayashida, Y., Watanabe, K., Yamamoto, K., Adachi, E., Nagai, S., Kikuchi, A., Maeda, N., Watanabe, H. and Okano, T., *Corneal reconstruction with tissue-engineered cell sheets composed of autologous oral mucosal epithelium.* New England Journal of Medicine, 2004. **351**(12): pp. 1187-1196.

17. Sikareepaisan, P., U. Ruktanonchai, and P. Supaphol, *Preparation and characterization of asiaticoside-loaded alginate films and their potential for use as effectual wound dressings.* Carbohydrate Polymers, 2011. **83**(4): pp. 1457-1469.
18. Kamoun, E.A., E.-R.S. Kenawy, and X.J.J.o.a.r. Chen, *A review on polymeric hydrogel membranes for wound dressing applications: PVA-based hydrogel dressings.* 2017. **8**(3): pp. 217-233.
19. Wang, F., Li, Z., Khan, M., Tamama, K., Kuppusamy, P., Wagner, W.R., Sen, C.K. and Guan, J., *Injectable, rapid gelling and highly flexible hydrogel composites as growth factor and cell carriers.* Acta biomaterialia, 2010. **6**(6): pp. 1978-1991.
20. Raafat, A.I., M. Eid, and M.B. El-Arnaouty, *Radiation synthesis of superabsorbent CMC based hydrogels for agriculture applications.* Nuclear Instruments and Methods in Physics Research Section B: Beam Interactions with Materials and Atoms, 2012. **283**: pp. 71-76.
21. Krsko, P., McCann, T.E., Thach, T.T., Laabs, T.L., Geller, H.M. and Libera, M.R., *Length-scale mediated adhesion and directed growth of neural cells by surface-patterned poly (ethylene glycol) hydrogels.* Biomaterials, 2009. **30**(5): pp. 721-729.
22. Russell, R.J., Pishko, M.V., Gefrides, C.C., McShane, M.J. and Cote, G.L., *A fluorescence-based glucose biosensor using concanavalin A and dextran encapsulated in a poly (ethylene glycol) hydrogel.* Analytical Chemistry, 1999. **71**(15): pp. 3126-3132.
23. Jena, K.K., Rout, T.K., Narayan, R. and Raju, K.V., *Novel organic–inorganic hybrid coatings prepared by the sol–gel process: corrosion and mechanical properties.* Polymer international, 2012. **61**(7): pp. 1101-1106.
24. Trevors, J.T. and G.H. Pollack, *Hypothesis: the origin of life in a hydrogel environment.* Progress in biophysics and molecular biology, 2005. **89**(1): pp. 1-8.
25. Trevors, J.T. and D.L. Abel, *Chance and necessity do not explain the origin of life.* Cell Biology International, 2004. **28**(11): pp. 729-739.
26. Bashkin, V.N. and R.W. Howarth, *Modern biogeochemistry*. 2002: Springer Science & Business Media.
27. Bebié, J. and M.A. Schoonen, *Pyrite and phosphate in anoxia and an origin-of-life hypothesis.* Earth and Planetary Science Letters, 1999. **171**(1): pp. 1-5.
28. Segré, D., Ben-Eli, D., Deamer, D.W. and Lancet, D., *The lipid world.* Origins of Life and Evolution of the Biosphere, 2001. **31**(1-2): pp. 119-145.
29. Ingber, D.E., *The origin of cellular life.* Bioessays, 2000. **22**(12): pp. 1160-1170.
30. Trevors, J., *The subsurface origin of microbial life on the Earth.* Research in microbiology, 2002. **153**(8): p. 487-491.
31. Ling, G.N., *Life at the cell and below-cell level: The hidden history of a fundamental revolution in biology*. 2001: Pacific Press New York, NY, USA:.
32. Yang, D., Peng, S., Hartman, M.R., Gupton-Campolongo, T., Rice, E.J., Chang, A.K., Gu, Z., Lu, G.Q. and Luo, D., *Enhanced transcription and translation in clay hydrogel and implications for early life evolution.* Scientific reports, 2013. **3**: p. 3165.

33. Golmohamadi, M. and K.J.J.C.p. Wilkinson, *Diffusion of ions in a calcium alginate hydrogel-structure is the primary factor controlling diffusion.* 2013. **94**(1): pp. 82-87.
34. Barge, L.M., Hammond, D.E., Chan, M.A., Potter, S., Petruska, J. and Nealson, K.H., *Precipitation patterns formed by self‐organizing processes in porous media.* Geofluids, 2011. **11**(2): pp. 124-133.
35. Lu, C., Zahedi, P., Forman, A. and Allen, C., *Multi‐arm PEG/Silica Hydrogel for Sustained Ocular Drug Delivery.* Journal of pharmaceutical sciences, 2014. **103**(1): pp. 216-226.
36. Lowenstam, H.A. and S. Weiner, *On biomineralization*. 1989: Oxford University Press on Demand.
37. Peppas, N.A., Bures, P., Leobandung, W.S. and Ichikawa, H., *Hydrogels in pharmaceutical formulations.* European journal of pharmaceutics and biopharmaceutics, 2000. **50**(1): pp. 27-46.
38. Pohorille, A. and D. Deamer, *Self-assembly and function of primitive cell membranes.* Research in microbiology, 2009. **160**(7): pp. 449-456.
39. Sarkar, S., Das, S., Dagar, S., Joshi, M.P., Mungi, C.V., Sawant, A.A., Patki, G.M. and Rajamani, S., *Prebiological membranes and their role in the emergence of early cellular life.* 2020. **253**(6): pp. 589-608.
40. Brinker, C.J. and G.W. Scherer, *Sol-gel science: the physics and chemistry of sol-gel processing*. 2013: Academic press.
41. Yin, Z., Wu, F., Xing, T., Yadavalli, V.K., Kundu, S.C. and Lu, S., *A silk fibroin hydrogel with reversible sol–gel transition.* 2017. **7**(39): pp. 24085-24096.
42. Saeed, S., Al Soubaihi, R.M., White, L.S., Bertino, M.F. and Saoud, K.M., *Rapid fabrication of cross-linked silica aerogel by laser induced gelation.* 2016. **221**: pp. 245-252.
43. Huck-Iriart, C., et al., *Micro to mesoporous SiO2xerogels: the effect of acid catalyst type in sol–gel process.* 2021: pp. 1-11.
44. Aegerter, M.A. and M. Mennig, *Sol-gel technologies for glass producers and users*. 2013: Springer Science & Business Media.
45. Nedelčev, T., Krupa, I., Lath, D. and Špirková, M., *The leaching of Rhodamine B, Naphthol Blue Black, Metanil Yellow and Bismarck Brown R from silica deposits on polyester and viscose textiles.* Journal of Sol-Gel Science and Technology, 2008. **46**(1): pp. 47-56.
46. Nedelčev, T., Krupa, I., Hrdlovič, P., Kollár, J., Chorvát, D. and Lacik, I., *Silica hydrogel formation and aging monitored by pyrene-based fluorescence probes.* Journal of sol-gel science and technology, 2010. **55**(2): pp. 143-150.
47. Cammarata, M., Levantino, M., Cupane, A., Longo, A., Martorana, A. and Bruni, F., *Structure and dynamics of water confined in silica hydrogels: X-ray scattering and dielectric spectroscopy studies.* The European Physical Journal E, 2003. **12**(1): pp. 63-66.
48. Ferri, F., B. Frisken, and D.S. Cannell, *Structure of silica gels.* Physical review letters, 1991. **67**(25): p. 3626.
49. Peri, J. and A. Hensley Jr, *The surface structure of silica gel.* The Journal of Physical Chemistry, 1968. **72**(8): pp. 2926-2933.
50. Stadtländer, C.J.M.r. and e.t.i. microscopy, *Scanning electron microscopy and transmission electron microscopy of mollicutes: challenges and opportunities.* 2007. **1**: pp. 122-131.
51. Rahman, I.A. and V. Padavettan, *Synthesis of silica nanoparticles by sol-gel: size-dependent properties, surface modification, and applications in*

silica-polymer nanocomposites—a review. Journal of Nanomaterials, 2012. **2012**: p. 8.

52. Anderson, T.F., *Techniques for the preservaation of three-dimensional structure in preparing specimens for the electron microscope.* Transactions of the New York Academy of Sciences, 1951. **13**(4 Series II): pp. 130-134.
53. Suleimenova, A., Bake, K.D., Ozkan, A., Valenza II, J.J., Kleinberg, R.L., Burnham, A.K., Ferralis, N. and Pomerantz, A.E., *Acid demineralization with critical point drying: A method for kerogen isolation that preserves microstructure.* Fuel, 2014. **135**: pp. 492-497.
54. Gurav, J.L., Jung, I.K., Park, H.H., Kang, E.S. and Nadargi, D.Y., *Silica aerogel: synthesis and applications.* Journal of Nanomaterials, 2010. **2010**: p. 23.
55. Pathan, A., J. Bond, and R. Gaskin, *Sample preparation for scanning electron microscopy of plant surfaces—horses for courses.* Micron, 2008. **39**(8): pp. 1049-1061.
56. Pierre, A.C. and G.M.J.C.R. Pajonk, *Chemistry of aerogels and their applications.* 2002. **102**(11): pp. 4243-4266.
57. Nireesha, G.R., Divya, L., Sowmya, C., Venkateshan, N.N.B.M. and Lavakumar, V., *Lyophilization/freeze drying-an review.* International journal of novel trends in pharmaceutical sciences, 2013. **3**(4): pp. 87-98.
58. do Vale Morais, A.R., et al., *Freeze-drying of emulsified systems: A review.* International journal of pharmaceutics, 2016. **503**(1-2): pp. 102-114.
59. Remington, J.P., *Remington: the science and practice of pharmacy*. Vol. 1. 2006: Lippincott Williams & Wilkins.
60. Franks, F., *Freeze-drying of bioproducts: putting principles into practice.* European Journal of Pharmaceutics and Biopharmaceutics, 1998. **45**(3): pp. 221-229.
61. Rajeevani, K., K. Mahalakshmi, and V.U.M. Rao, *International journal of trends in pharmacy and life sciences (ijtpls).*
62. Bellows, R.J. and C.J. King, *Freeze-drying of aqueous solutions: Maximum allowable operating temperature.* Cryobiology, 1972. **9**(6): pp. 559-561.
63. Chen, M., C.T.J.S. Jafvert, and P. Technology, *Application of cross-linked stearic acid nanoparticles with dialysis membranes for methylene blue recovery.* 2018. **204**: pp. 21-29.
64. Hwang, S.-T., *Fundamentals of membrane transport.* Korean Journal of Chemical Engineering, 2011. **28**(1): pp. 1-15.
65. Emmanuel, K., Cheng, C., Erigene, B., Mondal, A.N., Hossain, M.M., Khan, M.I., Afsar, N.U., Liang, G., Wu, L. and Xu, T., *Imidazolium functionalized anion exchange membrane blended with PVA for acid recovery via diffusion dialysis process.* Journal of Membrane Science, 2016. **497**: pp. 209-215.
66. Luo, J., Wu, C., Xu, T. and Wu, Y., *Diffusion dialysis-concept, principle and applications.* Journal of Membrane Science, 2011. **366**(1-2): pp. 1-16.
67. Welton, J.E., *SEM petrology atlas.* 1984.
68. Chimupala, Y., *Synthesis and characterization of the TiO2 (B) phase*. 2015, University of Leeds.

69. Chang, K.-S., H.-C. Wang, and T.-W. Chung, *Effect of regeneration conditions on the adsorption dehumidification process in packed silica gel beds.* Applied Thermal Engineering, 2004. **24**(5-6): p. 735-742.
70. Li, X., Li, Z., Xia, Q. and Xi, H., *Effects of pore sizes of porous silica gels on desorption activation energy of water vapour.* Applied thermal engineering, 2007. **27**(5-6): pp. 869-876.
71. Liang, J., et al., *Characterization of Complex Drug Formulations Using Cryogenic Scanning Electron Microscopy (Cryo-SEM).* 2022. **2**(4): p. e406.
72. Dubochet, J.J.B.j., *A reminiscence about early times of vitreous water in electron cryomicroscopy.* 2016. **110**(4): p. 756.
73. Aston, R., Sewell, K., Klein, T., Lawrie, G. and Grøndahl, L., *Evaluation of the impact of freezing preparation techniques on the characterisation of alginate hydrogels by cryo-SEM.* 2016. **82**: pp. 1-15.
74. Lombardo, D., Kiselev, M.A., Magazù, S. and Calandra, P., *Amphiphiles self-assembly: basic concepts and future perspectives of supramolecular approaches.* Advances in Condensed Matter Physics, 2015. **2015**.
75. Holmberg, K., Jönsson, B., Kronberg, B. and Lindman, B., *Surfactants and polymers in aqueous solution*. Vol. 2. 2003: Wiley Online Library.
76. Whitesides, G.M., J.P. Mathias, and C.T. Seto, *Molecular self-assembly and nanochemistry: a chemical strategy for the synthesis of nanostructures.* Science, 1991. **254**(5036): pp. 1312-1319.
77. Lindman, B., Medronho, B., Alves, L., Norgren, M. and Nordenskiöld, L., *Hydrophobic interactions control the self-assembly of DNA and cellulose.* 2021. **54**.
78. Subramaniam, K., Butkus, M., Strevett, K. and Bergendahl, J., *A review of non-DLVO interactions in environmental colloidal systems.* Reviews in Environmental Science and Biotechnology, 2002. **1**(1): pp. 17-38.
79. Ikkala, O., *Hydrogen Bonding Directed Colloidal Self-Assembly of Nanoparticles into 2D Crystals, Capsids, and Supracolloidal Assemblies.* Advanced Functional Materials, 2018. **28**(27): p. 1704328.
80. Groß, R. and M. Dorigo, *Self-assembly at the macroscopic scale.* Proceedings of the IEEE, 2008. **96**(9): pp. 1490-1508.
81. Domb, C., *Phase transitions and critical phenomena*. Vol. 19. 2000: Elsevier.
82. Maurer, S.E., G.J. Nguyen, and E.o. Biospheres, *Prebiotic vesicle formation and the necessity of salts.* 2016. **46**(2-3): pp. 215-222.
83. Deamer, D.W.J.O.o.L. and E.o.t. Biosphere, *Role of amphiphilic compounds in the evolution of membrane structure on the early Earth.* 1986. **17**(1): pp. 3-25.
84. Dutt, S., P.F. Siril, and S.J.R.a. Remita, *Swollen liquid crystals (SLCs): a versatile template for the synthesis of nano structured materials.* 2017. **7**(10): pp. 5733-5750.
85. Patist, A., Kanicky, J.R., Shukla, P.K. and Shah, D.O., *Importance of micellar kinetics in relation to technological processes.* Journal of colloid and interface science, 2002. **245**(1): pp. 1-15.
86. Jafari, M., Mehrnejad, F., Rahimi, F. and Asghari, S.M., *The molecular basis of the sodium dodecyl sulfate effect on human ubiquitin structure: a molecular dynamics simulation study.* 2018. **8**(1): pp. 1-15.
87. Maurer, S.J.L., *The impact of salts on single chain amphiphile membranes and implications for the location of the origin of life.* 2017. **7**(4): p. 44.

88. Guida, V.J.A.i.c. and i. science, *Thermodynamics and kinetics of vesicles formation processes.* 2010. **161**(1-2): pp. 77-88.
89. Luisi, P.L., Walde, P. and Oberholzer, T., *Lipid vesicles as possible intermediates in the origin of life.* 1999. **4**(1): pp. 33-39.
90. Jordan, S.F., Rammu, H., Zheludev, I.N., Hartley, A.M., Maréchal, A. and Lane, N., *Promotion of protocell self-assembly from mixed amphiphiles at the origin of life.* 2019. **3**(12): pp. 1705-1714.
91. Maurer, S.E., Tølbøl Sørensen, K., Iqbal, Z., Nicholas, J., Quirion, K., Gioia, M., Monnard, P.A. and Hanczyc, M.M., *Vesicle self-assembly of monoalkyl amphiphiles under the effects of high ionic strength, extreme pH, and high temperature environments.* 2018. **34**(50): pp. 15560-15568.
92. Apel, C.L., D.W. Deamer, and M.N.J.B.e.B.A.-B. Mautner, *Self-assembled vesicles of monocarboxylic acids and alcohols: conditions for stability and for the encapsulation of biopolymers.* 2002. **1559**(1): pp. 1-9.
93. Garidel, P., Hildebrand, A., Neubert, R. and Blume, A., *Thermodynamic characterization of bile salt aggregation as a function of temperature and ionic strength using isothermal titration calorimetry.* Langmuir, 2000. **16**(12): pp. 5267-5275.
94. Carey, M.C. and D.M. Small, *Micellar properties of dihydroxy and trihydroxy bile salts: effects of counterion and temperature.* Journal of colloid and interface science, 1969. **31**(3): pp. 382-396.
95. Lin, C.-E., W.-C. Lin, and W.-C. Chiou, *Migration behaviour and selectivity of dichlorophenols in micellar electrokinetic capillary chromatography Influence of micelle concentration and buffer pH.* Journal of Chromatography A, 1996. **722**(1-2): pp. 333-343.
96. Fuguet, E., Ràfols, C., Rosés, M. and Bosch, E., *Critical micelle concentration of surfactants in aqueous buffered and unbuffered systems.* Analytica Chimica Acta, 2005. **548**(1-2): pp. 95-100.
97. Benito, I., Garcia, M.A., Monge, C., Saz, J.M. and Marina, M.L., *Spectrophotometric and conductimetric determination of the critical micellar concentration of sodium dodecyl sulfate and cetyltrimethylammonium bromide micellar systems modified by alcohols and salts.* Colloids and Surfaces A: Physicochemical and Engineering Aspects, 1997. **125**(2-3): pp. 221-224.
98. Niraula, T.P., S.K. Chatterjee, and A. Bhattarai, *Micellization of sodium dodecyl sulphate in presence and absence of alkali metal halides at different temperatures in water and methanol-water mixtures.* Journal of Molecular Liquids, 2018. **250**: pp. 287-294.
99. Dutkiewicz, E. and A. Jakubowska, *Effect of electrolytes on the physicochemical behaviour of sodium dodecyl sulphate micelles.* Colloid and Polymer Science, 2002. **280**(11): p. 1009-1014.
100. Ren, Z.H.J.I. and E.C. Research, *Mechanism of the salt effect on micellization of an aminosulfonate amphoteric surfactant.* 2015. **54**(40): pp. 9683-9688.
101. Sarkar, M. and S. Poddar, *Studies on the interaction of surfactants with cationic dye by absorption spectroscopy.* Journal of colloid and interface science, 2000. **221**(2): pp. 181-185.
102. Chattopadhyay, A. and E. London, *Fluorimetric determination of critical micelle concentration avoiding interference from detergent charge.* Analytical biochemistry, 1984. **139**(2): pp. 408-412.
103. Banipal, T.S., R. Kaur, and P.K. Banipal, *Effect of sodium chloride on the interactions of ciprofloxacin hydrochloride with sodium dodecyl sulfate*

and hexadecyl trimethylammonium bromide: Conductometric and spectroscopic approach. Journal of Molecular Liquids, 2018. **255**: pp. 113-121.
104. Niraula, T.P., Shah, S.K., Chatterjee, S.K. and Bhattarai, A., *Effect of methanol on the surface tension and viscosity of sodiumdodecyl sulfate (SDS) in aqueous medium at 298.15–323.15 K.* 2018. **4**(1): pp. 26-34.
105. Perkampus, H.-H., *UV-VIS Spectroscopy and its Applications*. 2013: Springer Science & Business Media.
106. Sommer, L., *Analytical absorption spectrophotometry in the visible and ultraviolet: the principles*. Vol. 8. 2012: Elsevier.
107. Pedraza, A., Sicilia, M.D., Rubio, S. and Pérez-Bendito, D., *Surfactant–dye binding degree method for the determination of amphiphilic drugs.* Analytica chimica acta, 2004. **522**(1): pp. 89-97.
108. Chibisov, A.K., V.I. Prokhorenko, and H. Görner, *Effects of surfactants on the aggregation behaviour of thiacarbocyanine dyes.* Chemical Physics, 1999. **250**(1): pp. 47-60.
109. Sarkar, M. and S. Poddar, *Spectral studies of methyl violet in aqueous solutions of different surfactants in supermicellar concentration region.* Spectrochimica Acta Part A: Molecular and Biomolecular Spectroscopy, 1999. **55**(9): pp. 1737-1742.
110. Sa'ib, J.K. and V. Buss, *UV/Vis Spectral Study of the Self-aggregation of Pinacyanol Chloride in Ethanol–Water Solutions.* Journal of solution chemistry, 2010. **39**(1): pp. 121-130.
111. Calcabrini, M. and D.J.E. Onna, *Exploring the gel state: optical determination of gelation times and transport properties of gels with an inexpensive 3D-printed spectrophotometer.* 2018. **96**(1): pp. 116-123.
112. Zare, R.N., Spencer, B.H., Springer, D.S. and Jacobson, M.P., *Laser experiments for beginners*. 1995: University Science Books.
113. Dallas, P., *Generation of Polymers and Nanomaterials at Liquid-Liquid Interfaces: Application to Crystalline, Light Emitting and Energy Materials*. 2020: Elsevier.
114. Lichtman, J.W. and J.-A.J.N.m. Conchello, *Fluorescence microscopy.* 2005. **2**(12): pp. 910-919.
115. Rumin, J., Bonnefond, H., Saint-Jean, B., Rouxel, C., Sciandra, A., Bernard, O., Cadoret, J.P. and Bougaran, G., *The use of fluorescent Nile red and BODIPY for lipid measurement in microalgae.* 2015. **8**(1): pp. 1-16.
116. Lee, S.J., B.-D. Yoon, and H.-M.J.B.t. Oh, *Rapid method for the determination of lipid from the green alga Botryococcus braunii.* 1998. **12**(7): pp. 553-556.
117. Borst, J.W., A.J.J.M.S. Visser, and Technology, *Fluorescence lifetime imaging microscopy in life sciences.* 2010. **21**(10): p. 102002.
118. Huang, G.-H., et al., *Rapid screening method for lipid production in alga based on Nile red fluorescence.* 2009. **33**(10): pp. 1386-1392.
119. Pandey, S.J.J.o.d.s. and technology, *Solvation Environment Provided by Self-Assembling Aqueous Sodium Oleate+ 1-Octanol Small Unilamellar Vesicles.* 2005. **26**(3): pp. 381-387.
120. Stewart, C. and J. Giannini, *Inexpensive, open source epifluorescence microscopes*. 2016, ACS Publications.
121. Mei, E., Fomitchov, P.A., Graves, R. and Campion, M., *A line scanning confocal fluorescent microscope using a CMOS rolling shutter as an adjustable aperture.* 2012. **247**(3): pp. 269-276.

122. Ahn, M., Kim, T., Yoo, H., Song, I. and Gweon, D. *Simultaneous imaging of confocal fluorescence and raman spectrum*. in *European Conference on Biomedical Optics*. 2007. Optical Society of America.
123. Nwaneshiudu, A., Kuschal, C., Sakamoto, F.H., Anderson, R.R., Schwarzenberger, K. and Young, R.C., *Introduction to confocal microscopy.* 2012. **132**(12): pp. 1-5.
124. Albdeery, K.G.S., *Abiogenically relevant self-assembly processes within silica hydrogels*. 2019, University of Leeds.
125. Thompson, R.F., Walker, M., Siebert, C.A., Muench, S.P. and Ranson, N.A., *An introduction to sample preparation and imaging by cryo-electron microscopy for structural biology.* 2016. **100**: pp. 3-15.
126. Deamer, D.W.J.M. and M.B. Reviews, *The first living systems: a bioenergetic perspective.* 1997. **61**(2): pp. 239-261.
127. Kundu, N., D. Mondal, and N.J.B.R. Sarkar, *Dynamics of the vesicles composed of fatty acids and other amphiphile mixtures: unveiling the role of fatty acids as a model protocell membrane.* 2020. **12**(5): pp. 1117-1131.
128. Dzieciol, A.J. and S.J.C.S.R. Mann, *Designs for life: protocell models in the laboratory.* 2012. **41**(1): pp. 79-85.
129. Hanczyc, M.M., S.M. Fujikawa, and J.W.J.S. Szostak, *Experimental models of primitive cellular compartments: encapsulation, growth, and division.* 2003. **302**(5645): pp. 618-622.
130. Bachmann, P.A., P.L. Luisi, and J.J.N. Lang, *Autocatalytic self-replicating micelles as models for prebiotic structures.* 1992. **357**(6373): p. 57-59.
131. Jakab, K., Norotte, C., Damon, B., Marga, F., Neagu, A., Besch-Williford, C.L., Kachurin, A., Church, K.H., Park, H., Mironov, V. and Markwald, R., *Tissue engineering by self-assembly of cells printed into topologically defined structures.* 2008. **14**(3): pp. 413-421.
132. Namani, T., D.W.J.O.o.L. Deamer, and E.o. Biospheres, *Stability of model membranes in extreme environments.* 2008. **38**(4): pp. 329-341.
133. Lukanov, B. and A. Firoozabadi, *Specific ion effects on the self-assembly of ionic surfactants: a molecular thermodynamic theory of micellization with dispersion forces.* Langmuir, 2014. **30**(22): pp. 6373-6383.
134. Chattopadhyay, A. and K. Harikumar, *Dependence of critical micelle concentration of a zwitterionic detergent on ionic strength: implications in receptor solubilization.* Febs Letters, 1996. **391**(1-2): pp. 199-202.
135. Neves, A.C.S., Valente, A.J.M., Burrows, H.D., Ribeiro, A.C.F. and Lobo, V.M.M., *Effect of terbium (III) chloride on the micellization properties of sodium decyl-and dodecyl-sulfate solutions.* Journal of colloid and interface science, 2007. **306**(1): pp. 166-174.
136. Arutchelvi, J., Sangeetha, J., Philip, J. and Doble, M., *Self-assembly of surfactin in aqueous solution: Role of divalent counterions.* Colloids and Surfaces B: Biointerfaces, 2014. **116**: pp. 396-402.
137. Naderi Miqan, S., Farshchi Tabrizi, F., Abedini, H. and Atashy Kashi, H., *Estimation of Micellization Parameters of SDS in the Presence of Some Electrolytes for Emulsion Polymerization Systems.* Journal of Surfactants and Detergents, 2013. **16**(2): pp. 271-278.
138. Kester, D.R., Duedall, I.W., Connors, D.N. and Pytkowicz, R.M., *Preparation of artificial seawater 1.* Limnology and oceanography, 1967. **12**(1): pp. 176-179.

139. Smith, R. and C.J.P.o.t.N.A.o.S. Tanford, *Hydrophobicity of long chain n-alkyl carboxylic acids, as measured by their distribution between heptane and aqueous solutions.* 1973. **70**(2): pp. 289-293.
140. Monnard, P.-A. and D.W. Deamer, *Preparation of vesicles from nonphospholipid amphiphiles*, in *Methods in enzymology*. 2003, Elsevier. pp. 133-151.
141. Tanford, C., *The hydrophobic effect: formation of micelles and biological membranes 2d ed*. 1980: J. Wiley.
142. Madenci, D., S.J.C.O.i.C. Egelhaaf, and I. Science, *Self-assembly in aqueous bile salt solutions.* 2010. **15**(1-2): pp. 109-115.
143. Naskar, B., A. Dey, and S.P. Moulik, *Counter-ion Effect on Micellization of Ionic Surfactants: A Comprehensive Understanding with Two Representatives, Sodium Dodecyl Sulfate (SDS) and Dodecyltrimethylammonium Bromide (DTAB).* Journal of Surfactants and Detergents, 2013. **16**(5): pp. 785-794.
144. Ábrahám, Á., A. Mezei, and R.J.S.M. Mészáros, *The effect of salt on the association between linear cationic polyelectrolytes and sodium dodecyl sulfate.* 2009. **5**(19): pp. 3718-3726.
145. Mitra, S., S.R.J.J.o.a. Dungan, and f. chemistry, *Micellar properties of Quillaja saponin. 1. Effects of temperature, salt, and pH on solution properties.* 1997. **45**(5): pp. 1587-1595.
146. Rahman, A. and C.J.J.o.A.P.S. Brown, *Effect of pH on the critical micelle concentration of sodium dodecyl sulphate.* 1983. **28**(4): pp. 1331-1334.
147. Moroi, Y., Motomura, K. and Matuura, R., *The critical micelle concentration of sodium dodecyl sulfate-bivalent metal dodecyl sulfate mixtures in aqueous solutions.* 1974. **46**(1): pp. 111-117.
148. Yu, X., Miao, X., Li, H., Qiu, K., Zong, R. and Li, Q., *Influence of Seawater on Interfacial Properties, Foam Performance and Aggregation Behaviour of Fluorocarbon/Hydrocarbon Surfactant Mixtures.* 2022: p. 119297.
149. Upstone, S.L., Theory and Instrumentation, *Ultraviolet/visible light absorption spectrophotometry in clinical chemistry.* 2006.
150. Solomon, T., *The definition and unit of ionic strength.* Journal of Chemical Education, 2001. **78**(12): p. 1691.
151. Mohd, T.A.T. and M.Z. Jaafar, *Influences of Alkaline and Salinity on Adsorption Capacity of Anionic Sodium Dodecyl Sulfate Surfactant.* Asia Proceedings of Social Sciences, 2018. **2**(1): pp. 19-23.
152. Krumrine, P.H., J.S. Falcone Jr, and T.C. Campbell, *Surfactant flooding 1: the effect of alkaline additives on IFT, surfactant adsorption, and recovery efficiency.* Society of Petroleum Engineers Journal, 1982. **22**(04): pp. 503-513.
153. Abe, Y., H. Watanabe, and M. Fujiwara, *Micellar Effects on the Hydrolysis Reaction of an Anionic Surfactant in Aqueous Solution.* Langmuir, 2018. **34**(46): pp. 13979-13992.
154. Hansson, P., B.J.C.o.i.c. Lindman, and i. science, *Surfactant-polymer interactions.* 1996. **1**(5): pp. 604-613.
155. Antunes, F.E., Marques, E.F., Miguel, M.G. and Lindman, B., *Polymer–vesicle association.* 2009. **147**: pp. 18-35.
156. Avalos, M., Babiano, R., Cintas, P., Gómez-Carretero, A., Jiménez, J.L., Lozano, M., Ortiz, A.L., Palacios, J.C. and Pinazo, A., *A Family of Hydrogels Based on Ureido-Linked Aminopolyol-Derived Amphiphiles and Bolaamphiphiles: Synthesis, Gelation under Thermal and*

Sonochemical Stimuli, and Mesomorphic Characterization. Chemistry-A European Journal, 2008. **14**(18): pp. 5656-5669.
157. Liley, J.R., Thomas, R.K., Penfold, J., Tucker, I.M., Petkov, J.T., Stevenson, P. and Webster, J.R., *Impact of Electrolyte on Adsorption at the Air–Water Interface for Ternary Surfactant Mixtures above the Critical Micelle Concentration.* 2017. **33**(17): pp. 4301-4312.
158. Laçin, O., B. Dönmez, and F.J.I.J.o.M.P. Demir, *Dissolution kinetics of natural magnesite in acetic acid solutions.* 2005. **75**(1-2): pp. 91-99.
159. Rangel-Argote, M., Claudio-Rizo, J.A., Castellano, L.E., Vega-González, A., Mata-Mata, J.L. and Mendoza-Novelo, B., et al., *ECM–oligourethene–silica hydrogels as a local drug release system of dexamethasone for stimulating macrophages.* 2017. **7**(17): pp. 10443-10453.
160. Dhara, D. and D.O.J.T.J.o.P.C.B. Shah, *Stability of sodium dodecyl sulfate micelles in the presence of a range of water-soluble polymers: A pressure-jump study.* 2001. **105**(29): pp. 7133-7138.
161. Shen, C. and N.M.J.J.o.t.A.C.S. Kostić, *Kinetics of photoinduced electron-transfer reactions within sol-gel silica glass doped with zinc cytochrome c. Study of electrostatic effects in confined liquids.* 1997. **119**(6): pp. 1304-1312.
162. Ellerby, L.M., Nishida, C.R., Nishida, F., Yamanaka, S.A., Dunn, B., Valentine, J.S. and Zink, J.I., *Encapsulation of proteins in transparent porous silicate glasses prepared by the sol-gel method.* 1992. **255**(5048): pp. 1113-1115.
163. Dave, B.C., Dunn, B., Valentine, J.S. and Zink, J.I., *Sol-gel encapsulation methods for biosensors.* 1994. **66**(22): p. 1120A-1127A.
164. Bryant, C. and D.J.J.o.F.S. McClements, *Influence of NaCl and CaCl2 on cold-set gelation of heat-denatured whey protein.* 2000. **65**(5): pp. 801-804.
165. Rendón, A., Carton, D.G., Sot, J., García-Pacios, M., Montes, L.R., Valle, M., Arrondo, J.L.R., Goni, F.M. and Ruiz-Mirazo, K., *Model systems of precursor cellular membranes: long-chain alcohols stabilize spontaneously formed oleic acid vesicles.* 2012. **102**(2): pp. 278-286.
166. Barrett, W., G %J Psychoanalytic Quarterly, *The Origin of Life: By AI Oparin. New York: The Macmillan Co., 1938. 252 pp.* 1938. **7**: pp. 570-571.
167. Lopez, A. and M.J.L. Fiore, *Investigating prebiotic protocells for a comprehensive understanding of the origins of life: A prebiotic systems chemistry perspective.* 2019. **9**(2): p. 49.
168. McCollom, T.M., et al., *Lipid synthesis under hydrothermal conditions by Fischer-Tropsch-type reactions.* 1999. **29**(2): p. 153-166.
169. Simoneit, B.R., A.I. Rushdi, and D.W.J.A.i.S.R. Deamer, *Abiotic formation of acylglycerols under simulated hydrothermal conditions and self-assembly properties of such lipid products.* 2007. **40**(11): pp. 1649-1656.
170. Chen, I.A., R.W. Roberts, and J.W.J.S. Szostak, *The emergence of competition between model protocells.* 2004. **305**(5689): pp. 1474-1476.
171. Kundu, N., D. Banik, and N.J.L. Sarkar, *Self-assembly of amphiphiles into vesicles and fibrils: investigation of structure and dynamics using spectroscopy and microscopy techniques.* 2018. **34**(39): pp. 11637-11654.
172. Motin, M.A., Mia, M.H., Reza, K.S., Islam, A.N., Yousuf, M.A. and Salam, M.A., *Effect of sodium dodecyl sulfate on viscometric properties of*

methanol, ethanol, n-propanol and iso-propanol at different temperatures. 2012. **25**(2): pp. 110-123.
173. Patist, A., Axelberd, T. and Shah, D.O., *Effect of long chain alcohols on micellar relaxation time and foaming properties of sodium dodecyl sulfate solutions.* 1998. **208**(1): pp. 259-265.
174. Dubey, N.J.J.o.C. and E. Data, *Studies of monohydric alcohols in aqueous sodium dodecyl sulfate solutions at T=(298.15 and 308.15) K.* 2010. **55**(3): pp. 1219-1226.
175. Rao, I., E.J.J.o.c. Ruckenstein, and i. science, *Micellization behavior in the presence of alcohols.* 1986. **113**(2): pp. 375-387.
176. Yatcilla, M.T., Herrington, K.L., Brasher, L.L., Kaler, E.W., Chiruvolu, S. and Zasadzinski, J.A., *Phase behavior of aqueous mixtures of cetyltrimethylammonium bromide (CTAB) and sodium octyl sulfate (SOS).* 1996. **100**(14): pp. 5874-5879.
177. Israelachvili, J.N., Mitchell, D.J. and Ninham, B.W., *Theory of self-assembly of hydrocarbon amphiphiles into micelles and bilayers.* 1976. **72**: pp. 1525-1568.
178. Albertsen, A.N., Duffy, C.D., Sutherland, J.D. and Monnard, P.A., *Self-assembly of phosphate amphiphiles in mixtures of prebiotically plausible surfactants.* 2014. **14**(6): pp. 462-472.
179. Manabe, M., Tokunaga, A., Kawamura, H., Katsuura, H., Shiomi, M. and Hiramatsu, K., *The counterion releasing effect and the partition coefficient of branched alkanols in ionic micellar solution.* 2002. **280**(10): pp. 929-935.
180. Li, D.M., Huang, J., Ren, Z.H., Lu, Y.J., He, Y.J., Liu, S.W. and Huang, J.J., *Interfacial properties and micellization of octadecyltrimethylammonium bromide in aqueous solution containing short chain alcohol and effect of chain length of alcohol.* 2019.
181. Griffiths, P.C., Hirst, N., Paul, A., King, S.M., Heenan, R.K. and Farley, R., *Effect of ethanol on the interaction between poly (vinylpyrrolidone) and sodium dodecyl sulfate.* 2004. **20**(16): pp. 6904-6913.
182. Liu, W., Chen, Y., Hao, H., Zhang, K., Zhang, H. and Teng, H., *The significant effects of linear medium chain fatty alcohols on phase behavior of aqueous solution of mixed cationic–anionic surfactant.* 2019. **40**(2): pp. 299-305.
183. Vierros, S. and M. Sammalkorpi, *Effects of 1-hexanol on C12E10 micelles.* 2018.
184. Zana, R.J.A.i.C. and I. Science, *Aqueous surfactant-alcohol systems: a review.* 1995. **57**: pp. 1-64.
185. Backlund, S., Rundt, K., Birdi, K.S. and Dalsager, S., *Aggregation behavior of ionic surfactant micelles in aqueous alcoholic solutions at different temperatures.* 1981. **79**(2).
186. Safarpour, M.A., Rafati, A.A., Gharibi, H. and Sameti, M.R., *Influence of Short-Chain Alcohols on the Micellization Parameters of Sodium Dodecyl Sulfate (SDS).* 1999. **46**(6): pp. 983-991.
187. Wang, Y.X., Lin, K., Chen, L., Zhou, X.G. and Liu, S.L., *Intermolecular interactions in self-assembly process of sodium dodecyl sulfate by vertically polarized Raman spectra.* 2017. **30**(4): p. 365.
188. Plastinin, I.V., Burikov, S.A., Gofurov, S.P., Ismailova, O.B., Mirgorod, Y.A. and Dolenko, T.A., *Features of self-organization of sodium dodecyl sulfate in water-ethanol solutions: Theory and vibrational spectroscopy.* 2020. **298**: p. 112053.

189. El-Dossoki, F.I., E.A. Gomaa, and O.K.J.S.A.S. Hamza, *Solvation thermodynamic parameters for sodium dodecyl sulfate (SDS) and sodium lauryl ether sulfate (SLES) surfactants in aqueous and alcoholic-aqueous solvents.* 2019. **1**(8): pp. 1-17.
190. Meng, S., Zhang, J., Wu, C., Zhang, Y., Xiao, Q. and Lu, G., *Dissipative particle dynamics simulations of surfactant CTAB in ethanol/water mixture.* 2014. **40**(13): pp. 1052-1058.
191. Aslanzadeh, S., A.J.J.o.S. Yousefi, and Detergents, *The effect of ethanol on nanostructures of mixed cationic and anionic surfactants.* 2014. **17**(4): pp. 709-716.
192. Bandyopadhyay, P., N.J.C. Neeta, and S.B. Biointerfaces, *Evidence for vesicle formation from 1: 1 nonionic surfactant span 60 and fatty alcohol mixtures in aqueous ethanol: Potential delivery vehicle composition.* 2007. **58**(2): pp. 305-308.
193. Oremusová, J., Vitková, Z., Vitko, A., Tárník, M., Miklovičová, E., Ivánková, O., Murgaš, J. and Krchňák, D., *Effect of Molecular Composition of Head Group and Temperature on Micellar Properties of Ionic Surfactants with C12 Alkyl Chain.* 2019. **24**(3): p. 651.
194. Hayase, K., S.J.J.o.C. Hayano, and I. Science, *Effect of alcohols on the critical micelle concentration decrease in the aqueous sodium dodecyl sulfate solution.* 1978. **63**(3): pp. 446-451.
195. Sidim, T., G.J.J.o.S. Acar, and Detergents, *Alcohols effect on critic micelle concentration of polysorbate 20 and cetyl trimethyl ammonium bromine mixed solutions.* 2013. **16**(4): pp. 601-607.
196. Zana, R., Yiv, S., Strazielle, C. and Lianos, P., *Effect of alcohol on the properties of micellar systems: I. Critical micellization concentration, micelle molecular weight and ionization degree, and solubility of alcohols in micellar solutions.* 1981. **80**(1): pp. 208-223.
197. Dubey, N.J.J.o.C. and E. Data, *Micellar properties and related thermodynamic parameters of aqueous anionic surfactants in the presence of monohydric alcohols.* 2011. **56**(8): pp. 3291-3300.
198. Wang, J., et al., *Foamability of sodium dodecyl sulfate solutions: Anomalous effect of dodecanol unexplained by conventional theories.* 2016. **495**: pp. 110-117.
199. Summerton, E., Zimbitas, G., Britton, M. and Bakalis, S., *Crystallisation of sodium dodecyl sulfate and the corresponding effect of 1-dodecanol addition.* 2016. **455**: pp. 111-116.
200. Iler, R.K. and R. Iler, *The chemistry of silica: solubility, polymerization, colloid and surface properties, and biochemistry.* 1979.
201. Coradin, T. and J.J.A.o.c.r. Livage, *Aqueous silicates in biological sol–gel applications: new perspectives for old precursors.* 2007. **40**(9): pp. 819-826.
202. Binana-Limbele, W., R.J.C. Zana, and surfaces, *Interactions between sodium dodecyl sulfate and polycarboxylates and polyethers. Effect of Ca2+ on these interactions.* 1986. **21**: pp. 483-494.
203. Vinot, B., R.S. Schechter, and L.W.J.S.r.e. Lake, *Formation of water-soluble silicate gels by the hydrolysis of a diester of dicarboxylic acid solublized as microemulsions.* 1989. **4**(03): pp. 391-397.
204. Whitsitt, E.A., A.R.J.J.o.C. Barron, and I. Science, *Effect of surfactant on particle morphology for liquid phase deposition of submicron silica.* 2005. **287**(1): pp. 318-325.

205. Peppas, N.A., Hilt, J.Z., Khademhosseini, A. and Langer, R., *Hydrogels in biology and medicine: from molecular principles to bionanotechnology.* 2006. **18**(11): pp. 1345-1360.
206. Yamanaka, S.A., Nishida, F., Ellerby, L.M., Nishida, C.R., Dunn, B., Valentine, J.S. and Zink, J.I., *Enzymatic activity of glucose oxidase encapsulated in transparent glass by the sol-gel method.* 1992. **4**(3): pp. 495-497.
207. Dworkin, J.P., Deamer, D.W., Sandford, S.A. and Allamandola, L.J., *Self-assembling amphiphilic molecules: Synthesis in simulated interstellar/precometary ices.* 2001. **98**(3): pp. 815-819.
208. Deamer, D., Singaram, S., Rajamani, S., Kompanichenko, V. and Guggenheim, S., *Self-assembly processes in the prebiotic environment.* 2006. **361**(1474): pp. 1809-1818.
209. Monnard, P.A. and D.W.J.T.A.R.A.O.P.o.t.A.A.o.A. Deamer, *Membrane self-assembly processes: Steps toward the first cellular life.* 2002. **268**(3): pp. 196-207.
210. Monnard, P.A., Apel, C.L., Kanavarioti, A. and Deamer, D.W., *Influence of ionic inorganic solutes on self-assembly and polymerization processes related to early forms of life: Implications for a prebiotic aqueous medium.* 2002. **2**(2): pp. 139-152.
211. Wang, C., Z. Wang, and X.J.A.o.c.r. Zhang, *Amphiphilic building blocks for self-assembly: from amphiphiles to supra-amphiphiles.* 2012. **45**(4): pp. 608-618.
212. Gao, X., J.J.J.o.c. Chorover, and i. science, *Adsorption of sodium dodecyl sulfate (SDS) at ZnSe and α-Fe2O3 surfaces: Combining infrared spectroscopy and batch uptake studies.* 2010. **348**(1): pp. 167-176.
213. Lu, Y., G. Allegri, and J.J.M.H. Huskens, *Vesicle-based artificial cells: materials, construction methods and applications.* 2022.
214. Tzocheva, S.S., et al., *Solubility limits and phase diagrams for fatty alcohols in anionic (SLES) and zwitterionic (CAPB) micellar surfactant solutions.* 2015. **449**: pp. 46-61.
215. Huang, J.-B., G.-X.J.C. Zhao, and P. Science, *Formation and coexistence of the micelles and vesicles in mixed solution of cationic and anionic surfactant.* 1995. **273**(2): pp. 156-164.
216. Wang, Q., Hu, N., Lei, J., Qing, Q., Huang, J., Tao, K., Zhao, S., Sun, K. and Yang, J., *Formation of Giant Lipid Vesicles in the Presence of Nonelectrolytes—Glucose, Sucrose, Sorbitol and Ethanol.* 2021. **9**(6): p. 945.
217. Hao, J., Liu, W., Xu, G. and Zheng, L., *Vesicles from salt-free cationic and anionic surfactant solutions.* 2003. **19**(26): pp. 10635-10640.
218. Agarwal, V., et al., *Microstructure evolution in aqueous solutions of cetyl trimethylammonium bromide (CTAB) and phenol derivatives.* 2006. **281**(1-3): pp. 246-253.
219. Ghosh, S., Ghatak, C., Banerjee, C., Mandal, S., Kuchlyan, J. and Sarkar, N., *Spontaneous transition of micelle–vesicle–micelle in a mixture of cationic surfactant and anionic surfactant-like ionic liquid: a pure nonlipid small unilamellar vesicular template used for solvent and rotational relaxation study.* 2013. **29**(32): pp. 10066-10076.
220. Khan, A., E.F.J.C.o.i.c. Marques, and i. science, *Synergism and polymorphism in mixed surfactant systems.* 1999. **4**(6): pp. 402-410.

221. Shi, L., Wei, Y., Sun, N. and Zheng, L., *First observation of rich lamellar structures formed by a single-tailed amphiphilic ionic liquid in aqueous solutions.* 2013. **49**(97): pp. 11388-11390.
222. Maurer, S.E., Deamer, D.W., Boncella, J.M. and Monnard, P.A., *Chemical evolution of amphiphiles: glycerol monoacyl derivatives stabilize plausible prebiotic membranes.* 2009. **9**(10): pp. 979-987.
223. Ghoneim, N.J.S.A.P.A.M. and B. Spectroscopy, *Photophysics of Nile red in solution: steady state spectroscopy.* 2000. **56**(5): pp. 1003-1010.
224. Meyers, R.A., *Encyclopedia of analytical chemistry.* 2000.
225. Kimura, K., M. Yamaoka, and Y.J.J.o.m.m. Kamisaka, *Rapid estimation of lipids in oleaginous fungi and yeasts using Nile red fluorescence.* 2004. **56**(3): pp. 331-338.
226. Fowler, S.D., P.J.J.o.H. Greenspan, and Cytochemistry, *Application of Nile red, a fluorescent hydrophobic probe, for the detection of neutral lipid deposits in tissue sections: comparison with oil red O.* 1985. **33**(8): pp. 833-836.
227. Benbouzid, H., Le Floch, S., Stephan, L., Olier, R. and Privat, M., *Combined effects of salinity and temperature on the solubility of organic compounds.* 2012. **48**: pp. 54-64.
228. Deamer, D.J.L., *The role of lipid membranes in life's origin.* 2017. **7**(1): p. 5.
229. Jabbour, J.M., Malik, B.H., Olsovsky, C., Cuenca, R., Cheng, S., Jo, J.A., Cheng, Y.S.L., Wright, J.M. and Maitland, K.C., *Optical axial scanning in confocal microscopy using an electrically tunable lens.* 2014. **5**(2): pp. 645-652.
230. Nie, S., D.T. Chiu, and R.N.J.S. Zare, *Probing individual molecules with confocal fluorescence microscopy.* 1994. **266**(5187): pp. 1018-1021.
231. Robson, A.L., Dastoor, P.C., Flynn, J., Palmer, W., Martin, A., Smith, D.W., Woldu, A. and Hua, S., *Advantages and limitations of current imaging techniques for characterizing liposome morphology.* 2018. **9**: p. 80.
232. Miura, K.J.F., *Bleach correction ImageJ plugin for compensating the photobleaching of time-lapse sequences.* 2020. **9**.
233. Steller, L.H., M.J. Van Kranendonk, and A.J.A.c.s. Wang, *Dehydration Enhances Prebiotic Lipid Remodeling and Vesicle Formation in Acidic Environments.* 2022. **8**(1): pp. 132-139.
234. Fiore, M.J.O. and B. Chemistry, *The synthesis of mono-alkyl phosphates and their derivatives: an overview of their nature, preparation and use, including synthesis under plausible prebiotic conditions.* 2018. **16**(17): pp. 3068-3086.
235. Caschera, F., de la Serna, J.B., Löffler, P.M.G., Rasmussen, T.E., Hanczyc, M.M., Bagatolli, L.A. and Monnard, P.A., *Stable vesicles composed of monocarboxylic or dicarboxylic fatty acids and trimethylammonium amphiphiles.* 2011. **27**(23): pp. 14078-14090.
236. Castañeda-Reyes, E.D., de Jesús Perea-Flores, M., Davila-Ortiz, G., Lee, Y. and de Mejia, E.G., *Development, characterization and use of liposomes as amphipathic transporters of bioactive compounds for melanoma treatment and reduction of skin inflammation: A review.* 2020. **15**: p. 7627.
237. Ciriminna, R., Fidalgo, A., Pandarus, V., Beland, F., Ilharco, L.M. and Pagliaro, M., *The sol–gel route to advanced silica-based materials and recent applications.* Chemical reviews, 2013. **113**(8): pp. 6592-6620.

238. Katoueizadeh, E., Rasouli, M. and Zebarjad, S.M., *A comprehensive study on the gelation process of silica gels from sodium silicate.* 2020. **9**(5): pp. 10157-10165.
239. Dathe, M., Lebek, W., Koslowski, E., Bron, M., Bräuniger, T., Stoessel, I. and Roggendorf, H., *Dissolution of sodium silicate glasses for the production of water glass–part IV: characterisation of reaction layer and glass surface.* 2021. **62**(1): pp. 9-23.
240. Qomariyah, L., Sasmita, F.N., Novaldi, H.R., Widiyastuti, W. and Winardi, S. *Preparation of stable colloidal silica with controlled size nano spheres from sodium silicate solution*. in *IOP Conference Series: Materials Science and Engineering*. 2018. IOP Publishing.
241. Kharlamova, A., C. Chassenieux, and T.J.F.H. Nicolai, *Acid-induced gelation of whey protein aggregates: Kinetics, gel structure and rheological properties.* 2018. **81**: pp. 263-272.
242. Hu, Y., Zhao, D., Qin, Y. and Wang, X., *An order determination method in direct derivative absorption spectroscopy for correction of turbidity effects on COD measurements without baseline required.* 2020. **226**: p. 117646.
243. Metin, C.O., K.M. Rankin, and Q.P.J.A.N. Nguyen, *Phase behavior and rheological characterization of silica nanoparticle gel.* 2014. **4**(1): pp. 93-101.
244. Bohren, C.F.J.A.J.o.P., *Multiple scattering of light and some of its observable consequences.* 1987. **55**(6): pp. 524-533.
245. Hamouda, A.A. and H.A.A.J.E. Amiri, *Factors affecting alkaline sodium silicate gelation for in-depth reservoir profile modification.* 2014. **7**(2): pp. 568-590.
246. Gurav, J.L., Rao, A.V., Rao, A.P., Nadargi, D.Y. and Bhagat, S.D., *Physical properties of sodium silicate based silica aerogels prepared by single step sol–gel process dried at ambient pressure.* 2009. **476**(1-2): pp. 397-402.
247. Besbes, M., N. Fakhfakh, and M.J.P.P. Benzina, *Characterization of silica gel prepared by using sol–gel process.* 2009. **2**(3): pp. 1087-1095.
248. Siouffi, A.-M.J.J.o.C.A., *Silica gel-based monoliths prepared by the sol–gel method: facts and figures.* 2003. **1000**(1-2): pp. 801-818.
249. Osterholtz, F.D. and Pohl, E.R., Pohl, and Technology, *Kinetics of the hydrolysis and condensation of organofunctional alkoxysilanes: a review.* 1992. **6**(1): pp. 127-149.
250. Norisuye, T., Inoue, M., Shibayama, M., Tamaki, R. and Chujo, Y., *Time-resolved dynamic light scattering study on the dynamics of silica gels during gelation process.* 2000. **33**(3): pp. 900-905.
251. Matsui, K., T. Nakazawa, and H.J.T.J.o.P.C. Morisaki, *Micellar formation of sodium dodecyl sulfate in sol-gel glasses probed by pyrene fluorescence.* 1991. **95**(2): pp. 976-979.
252. Jurinak, J.J. and Summers, L.E., *Oilfield applications of colloidal silica gel.* 1991. **6**(04): pp. 406-412.
253. Quarch, K., M.J.C.E. Kind, and T.I.C.P.E.P. Engineering-Biotechnology, *Inorganic precipitated silica gel. Part 1: Gelation kinetics and gel properties.* 2010. **33**(6): pp. 1034-1039.
254. Maiti, S., Fortunati, I., Ferrante, C., Scrimin, P. and Prins, L.J., *Dissipative self-assembly of vesicular nanoreactors.* 2016. **8**(7): pp. 725-731.

255. Trompette, J.L. and Meireles, M., science, *Ion-specific effect on the gelation kinetics of concentrated colloidal silica suspensions.* 2003. **263**(2): pp. 522-527.
256. Bailey, D.J. and J.G.J.J.o.C.A. Dorsey, *Linear solvation energy relationships of mixed micelles of sodium dodecyl sulfate and decanol: towards a better model of octanol/water partitioning.* 2001. **919**(1): pp. 181-194.
257. Chandradoss, S.D., Haagsma, A.C., Lee, Y.K., Hwang, J.H., Nam, J.M. and Joo, C., *Surface passivation for single-molecule protein studies.* 2014(86): p. e50549.
258. Nagle, J.F. and S.J.B.e.B.A.-R.o.B. Tristram-Nagle, *Structure of lipid bilayers.* 2000. **1469**(3): pp. 159-195.
259. Matsuoka, K., Noshiro, N., Kuroki, H., Tsuyuzaki, K. and Hashimoto, G., *Vesicle formation of disodium lauryl sulfosuccinate.* 2022. **348**: p. 118422.
260. Cheng, C.Y., Lai, Y.F., Hsieh, Y.L., Wu, C.H., Chiu, C.C. and Yang, Y.M., *Divergent Effects of Cholesterol on the Structure and Fluidity of Liposome and Catanionic Vesicle Membranes.* 2022.
261. Hartjes, T.A., Mytnyk, S., Jenster, G.W., van Steijn, V. and van Royen, M.E., *Extracellular vesicle quantification and characterization: common methods and emerging approaches.* 2019. **6**(1): p. 7.